Aus dem Institut für Molekularbiologie und Tumorforschung
Geschäftsführender Direktor: Prof. Dr. Alexander Brehm
des Fachbereichs Medizin der Philipps-Universität Marburg

Transcriptional regulators employ chromatin modifiers to coordinate lineage-specific gene expression

Inaugural-Dissertation zur Erlangung des
Doktorgrades der Naturwissenschaften (Dr. rer. nat.)
dem Fachbereich Medizin der Philipps-Universität Marburg vorgelegt
von

Jonathan Lenz
aus Wolzhausen

Marburg, 2021

Angenommen vom Fachbereich Medizin der Philipps-Universität Marburg am:

10.11.2021

Gedruckt mit Genehmigung des Fachbereichs Medizin

Dekanin: Prof. Dr. Denise Hilfiker-Kleiner

Referent: Prof. Dr. Alexander Brehm

1. Korreferent: Prof. Dr. Sven Bogdan

Für meine Eltern.

“Le doute n'est pas une état bien agréable, mais l'assurance est un état ridicule.”

“Doubt is an unpleasant condition, but certainty is absurd.”

- Voltaire

TABLE OF CONTENTS

LIST OF ABBREVIATIONS

3D	Three dimensional
ac	acetyl
ACC	Acetyl coenzyme A carboxylase
Antp	Antennapedia
ATP	Adenosine triphosphate
BCL11B	B-cell leukemia 11A
BHC80	BRAF histone deacetylase complex 80
BRAF35	BRCA2 (Breast cancer type 2 susceptibility protein) associated factor 35
C-	Carboxy-
Cas9	CRISPR-associated endonuclease 9
CDK1	Cyclin-dependent kinase 1
CDK2AP1	Cyclin-dependent kinase 2 associated protein 1
cDNA	coding DNA
CENPB	Centromere protein B
CHD	Chromodomain-helicase-DNA-binding protein
CHES-1	Checkpoint suppressor 1
ChIP	Chromatin immunoprecipitation
ChIP-seq	ChIP sequencing
CoREST	Co-repressor of RE1 silencing transcription factor
CRISPR	Clustered regularly interspaced short palindromic repeats
CROT	Carnitine O-octanoyltransferase
CtBP	C-terminal-binding protein
CZ	Cortical zone
d	Drosophila-
D-mef2	Drosophila Myocyte-specific enhancer factor 2
dCas9	‘Dead’ Cas9 (inactive mutant)
DNA	Deoxyribonucleic acid
DOC1	Deleted in oral cancer 1
ds	Double stranded
dsRNA	Double stranded RNA
E-box	Enhancer box
e.g.	Exempli gratia (for example)
E2F2	E2-promoter binding factor 2
ebd1	Earthbound 1
EBF	Early B-cell factor
Echs1	Enoyl coenzyme A hydratase 1
EGFP	Enhanced green fluorescent protein

ELM2	Egl-27 and MTA1 homology 2 domain
et al.	Et alii (and others)
etc.	Et cetera (and so forth)
fa2h	Fatty acid 2 hydroxylase
FOG	Friend of GATA
G1	Gap 1 phase
G2	Gap 2 phase
G9a	Gene 9a in class III region of human major histocompatibility complex
GAGA	(GA)n motif
GATA	(T/A)GATA(A/G) motif
GATAD2A/B	GATA zinc finger domain-containing 2A/B
Gcm	Glial cells missing
GFP	Green fluorescent protein
GO	Gene Ontology
GST	Glutathione S-transferase
H2A	Histone 2A
H2B	Histone 2B
H3	Histone 3
H4	Histone 4
HA	Hemagglutinin
HDAC	Histone deacetylase
Hh	Hedgehog
hhF4f	Hedgehog enhancer fragment 4f
i.e.	Id est (that is)
ibid.	Ibidem (in the same place)
IP	Immunoprecipitation
JAK	Janus kinase
kDa	Kilodaltons
L(3)mbt	Lethal (3) malignant brain tumor
L2	Second larval instar
L3	Third larval instar
LDB	LIM (Lin-11, Isl-1 and Mec-3) domain-binding protein
LINT	L(3)mbt interacting
Lint-1	L(3)mbt interacting protein 1
LMO2	LIM (Lin-11, Isl-1 and Mec-3) domain only 2
LSD1	Lysin-specific demethylase 1
Luc	Luciferase
Lz	Lozenge
M	Mitosis
MBD	Methyl-CpG-binding domain

MBT	Malignant brain tumor
Mcad	Medium-chain specific acyl coenzyme A dehydrogenase
mCherry	Monomeric Cherry
me	methyl
Mec	MEP-1 complex
MeCP2	Methyl-CpG-binding protein 2
MEP-1	MOG (Masculinization of the germ line) interacting and ectopic P-granules
Mi-2	Mitchell 2
mRNA	Messenger RNA
MSN-C	Misshapen-mCherry
MTA	Metastasis-associated protein
MZ	Medullary zone
N-	Amino-
NuRD	Nucleosome remodeling and deacetylation
OAZ	Olf/EBF-associated zinc finger factor
Olf	Olfactory neuronal transcription factor
p55	Chromatin assembly factor 1 subunit of 55 kDa
p66	Transcriptional repressor of 66 kDa
PCR	Polymerase chain reaction
PHD	Plant homeodomain
PI	Propidium iodide
Pnr	Pannier
pRB	Retinoblastoma protein
PSC	Posterior signaling center
RBAP	Retinoblastoma-associated protein
RE1	Neuron-restrictive silencer element 1
RNA	Ribonucleic acid
RNA-seq	RNA sequencing
RNAi	RNA interference
ROS	Reactive oxygen species
RPD3	Reduced potassium dependency 3
RT-qPCR	Reverse transcriptase quantitative PCR
RUNX	Runt-related transcription factor
S2	Schneider 2
Sall4	Spalt-like 4
SANT	Swi3, ADA2, N-Cor and TFIIIB domain
Sf9	Spodoptera frugiperda cell line clone 9
SFMBT1	Scm (Sex combs on midleg) related gene containing four MBT domains
SIRT1	Silent mating type information regulation 2 homolog 1

SLC	SFMBT, LSD1 and CoREST complex
Srp	Serpent
SSNC	Second site non-complementation
STAT	Signal transducer and activator of transcription
SWI/SNF	Switching defective/Sucrose non-fermenting
TSS	Transcription start site
Ttk88	Tramtrack 88
Ush	U-shaped
Zeb2	Zinc finger E-box binding homeobox 2
ZFP	Zinc finger protein
Zn	Zinc
ZNF	Zinc finger protein

Abbreviations of amino acids and nucleotides follow the standard single-letter code.

1. INTRODUCTION

1.1. Cell identity and transcription

With few exceptions, every somatic cell of a eukaryotic organism contains the same genetic information which is encoded in its DNA. The identity, morphology, and function of a given cell are largely determined by the activation status of its genes, which ultimately constitutes a cell type-specific proteome. A cell's transcriptome, the set and quantity of its expressed genes, even allows to infer its identity (Ye & Sarkar, 2018). In fact, recent advances in single-cell RNA sequencing make it possible to assign cell types solely on the basis of their expression profiles and even to discover novel cell types (examples: Cattenoz et al., 2020, Cho et al., 2020; Fu et al., 2020). Aside from genes that are needed for fundamental cellular functions, so-called housekeeping genes, the genome encodes factors that are required only in certain cell types or during particular processes. The formation of a specialized cell requires both: The activation of cell type-specific genes as well as repression of genes that are not necessary for the respective tissue. During lineage specification these expression patterns are established.

This is facilitated with the help of lineage-specific transcription factors. These DNA-binding proteins repress or activate the transcription of genes that are pivotal in shaping cell identity and function. The presence, absence, amount, and combination of cell type-specific transcription factors thus engineers lineage-appropriate gene expression (Nowic et al., 2010; Kato & Igarashi, 2019).

1.2. Chromatin structure and gene expression

DNA resides tightly packed inside the nucleus and is organized in a condensed structure, called chromatin. At its most basic level, the negatively charged DNA winds around a complex of eight basic histone proteins (two copies of histones H2A, H2B, H3, and H4), assembling the nucleosome core particle (Luger et al., 1997). Interactions between nucleosomes and addition of structural proteins, as well as RNA organize the genome into more compacted structures (Woodcock & Ghosh, 2010; Li & Reinberg, 2011). Cellular processes that operate on DNA, like replication, DNA damage repair, or gene transcription, have to contend with this barrier of packaging. Thus, the efficiency of these processes is influenced by the local chromatin environment (Michael & Thomä, 2021). This becomes especially important in differentiation, during which transcription factors have to overcome and change the chromatin structures that occlude their target genes (Rodrigues et al., 2021).

Chromatin composition and structure can be modulated by different means: Covalent modification of histones and repositioning of nucleosomes are among the best-studied alterations and will be further discussed below. Additional changes comprise the covalent modification of DNA (Greenberg & Bourc'his, 2019), incorporation of non-

canonical nucleosomes that contain histone variants (Henikoff & Smith, 2015), and reorganization of the genome in the 3D nuclear space (Peterson et al., 2021). These structural changes can impinge on gene expression and play a role in regulating developmental processes. Thus, chromatin modifiers exerting these changes are often implicated in differentiation.

1.3. Histone modification and chromatin remodeling

Histone proteins can be covalently modified, mostly on their N- and C-terminal tails that protrude from the nucleosome, but also on the lateral surface of the octamer (Bannister & Kouzarides, 2011; Lawrence et al., 2016). Most prominent are the methylation and acetylation of lysine and arginine residues, the phosphorylation of serine, threonine, and tyrosine residues as well as the ubiquitylation of lysine residues, although there is a plethora of additional covalent modifications known (Zhao et al., 2015). Which histone modifications are present at a given genomic region depends on the genomic element (i.e. promoter, enhancer, gene body, etc.), the activation status of the gene as well as on the general chromatin environment. The following loose classification of selected modifications can be applied: Transcriptionally inactive gene promoters and heterochromatic regions are marked by methylation of H3K9 and H3K27me3. Transcriptionally active regions are associated with H3K4me3 (promoters), H3K36me3 (gene body), or H3K4me1 (enhancers). Histone acetylation generally correlates with relaxed chromatin states and is enriched at active, accessible regions (Bannister & Kouzarides, 2011, Zhao et al., 2015; Morgan & Shilatifard, 2020).

The deposition and removal of histone modifications is facilitated by specialized enzymes (e.g. histone methyltransferases and demethylases, histone acetyltransferases and deacetylases). The specificity towards a particular modification varies: Some enzymes are capable of catalysing the modification of multiple substrates, while others are highly specific for their target residue (Lu, 2013, Marmorstein & Trievel, 2009).

Histone modifications influence chromatin structure directly as well as indirectly. Acetylation and phosphorylation can impact nucleosome integrity by masking the positive charge of histones, thus weakening DNA-histone interactions and increasing DNA accessibility. Modified histone residues can also serve as interaction platforms for chromatin modifiers or even disable their binding (Bannister & Kouzarides, 2011). For example, the N-terminal tail of histone H3 is bound by the mammalian Nucleosome Remodeling and Deacetylation (NuRD) complex. This interaction, however, is impaired upon methylation of H3K4 (Nishioka et al., 2002).

A more direct change in chromatin architecture is achieved by ATP-dependent chromatin remodelers. These enzymes can incorporate, evict, exchange or slide nucleosomes along the genome. Chromatin remodelers actively change the local nucleosome density and thereby restrict or enhance the accessibility of certain DNA loci for the transcriptional machinery and other gene regulatory factors. These processes

consume energy, thus remodeling enzymes are capable of hydrolyzing ATP (Clapier et al., 2017).

1.4. Developmental functions of the chromatin regulator NuRD

Most chromatin modifiers are part of protein complexes. Their mode of action is best evaluated in the context of their interacting subunits. One interesting example is the Nucleosome Remodeling and Deacetylation complex (NuRD), which combines two enzymatic activities: The first one being mediated by the ATP-dependent chromatin remodelers CHD3/Mi-2α, CHD4/Mi-2β or CHD5, the second one exerted by the histone deacetylases HDAC1 and HDAC2. NuRD is highly conserved in eukaryotes. I will mostly focus on the *Drosophila melanogaster* version of the complex (dNuRD), which contains the dMi-2 remodeling ATPase as well as dRPD3, a histone deacetylase. Additional subunits provide structural features and contribute to the interactions of NuRD with chromatin and further proteins. These include GATAD2A/B (*dp66*), CDK2AP1 (*dDOC1*), MTA1/1/3 (*dMTA1-like*), RBAP46/48 (*dp55*) and MBD2/3 (*dMBD-like*). Their *Drosophila* homologs are mentioned in italics. NuRD is primarily associated with transcriptional repression but was also shown to maintain higher levels of gene expression (Basta & Rauchman, 2015; Lai & Wade, 2011; Denslow & Wade, 2007).

CHD4/dMi-2 and NuRD are important regulators of differentiation (Hota & Bruneau, 2016; Basta & Rauchman, 2015). They influence cell fate decisions in a wide number of tissues ranging from the formation of the hair follicle epithelium to differentiation of B-lymphocytes and *Drosophila* spermatogenesis (Kashiwagi et al., 2007; Loughran et al., 2017; Kim et al., 2017). Even during the first steps of lineage diversification, the differentiation of mouse embryonic stem cells (ESCs), NuRD is involved. Here, NuRD seems to enable differentiation by maintaining transcriptional heterogeneity as well as keeping cells committed to a specific lineage once they enter differentiation (Signolet & Hendrich, 2015; Burgold et al., 2019). It emerges that CHD4/NuRD functions to ensure timely and lineage-appropriate gene expression and thereby plays a crucial role in numerous developmental processes.

Neither dMi-2 nor other dNuRD complex subunits are reported to show sequence-specific DNA binding activity. Rather, the complex is recruited to chromatin by other means, specifically by transcription factors. In *Drosophila* testes, the zinc finger protein Kumgang tethers dMi-2 to highly expressed germline genes (Kim et al., 2017). In a macrophage-related cell line treated with the steroid hormone ecdysone the ecdysone receptor recruits dMi-2 to ecdysone-responsive genes and prevents their excessive expression (Kreher et al., 2017). Both examples highlight how the transcriptional regulation of developmental pathways depends on the interplay of transcription factors with the general chromatin modifier dNuRD.

2.

USH REGULATES HEMOCYTE-SPECIFIC GENE EXPRESSION, FATTY ACID METABOLISM AND CELL CYCLE PROGRESSION AND COOPERATES WITH dNuRD TO ORCHESTRATE HEMATOPOIESIS

Jonathan Lenz, Robert Liefke, Julianne Funk, Samuel Shoup, Andrea Nist, Thorsten Stiewe, Robert Schulz, Yumiko Tokusumi, Lea Albert, Hartmann Raifer, Klaus Förstemann, Olalla Vázquez, Tsuyoshi Tokusumi, Nancy Fossett and Alexander Brehm

PLOS Genetics, 2021 Feb, 18;17(2):e1009318, doi: 10.1371/journal.pgen.1009318

2.1. Introduction

2.1.1. Hematopoiesis and immunity in Drosophila melanogaster

Differentiation of progenitor cells into mature specialized cell types is accompanied by changes in their gene expression profiles. During this process, the transcription of genes that maintain multipotency is reduced while simultaneously expression of factors specific for the intended mature cell type has to be established. We used the *Drosophila* hematopoietic system to study the role of a transcriptional regulator that functions during blood cell development.

Drosophila melanogaster harbors three blood cell types that can all originate from a common multipotent precursor and take part in the cellular immune response. The macrophage-like plasmatocytes are capable of phagocytosis, enabling them to clear the organism from infectious material like bacteria and viruses as well as apoptotic bodies during development. Crystal cells, named after their crystal-like inclusions, produce an enzyme that catalyses the production of melanin. This polymeric molecule is used for wound closure and encapsulation of foreign objects that threaten the organism, a process called melanization. Lamellocytes represent a very rare blood cell type that is only produced under extreme stress conditions like parasite infestation (Letourneau et al., 2016; Vlisidou & Wood, 2015; Gold & Brückner, 2014). Recent single-cell transcriptomic analyses of hemocytes have revealed relatively cohesive and uniform populations of crystal cells and lamellocytes. The plasmatocyte lineage, on the other hand, displayed a high degree of diversity. This population can be divided into sub-groups of specialized cells that potentially undertake distinct functions based on their gene expression profiles (Cattenoz et al., 2020, Cho et al., 2020; Fu et al., 2020). These studies even identified novel hemocyte populations, thereby expanding the classical dogma of three distinct *Drosophila* hemocyte lineages.

Hematopoiesis occurs at different stages in *Drosophila* development as well as upon immune challenge. In the embryonic head mesoderm, blood cell progenitors divide and finally commit to the plasmatocyte or crystal cell lineage. Production of lamellocytes does not occur in the embryo. Embryonic plasmatocytes migrate through the organism and are present throughout *Drosophila* life. In the larval stage, embryonic plasmatocytes can still be found in circulation and in sessile pockets as "tissue macrophages" (Gold & Brückner, 2014). Additionally, larvae maintain a central hemocyte-producing organ: the lymph gland. Supervised by the posterior signaling center (PSC), a stem cell-like niche, blood cell precursors in the medullary zone (MZ) are kept in their progenitor state. The cortical zone (CZ) of the lymph gland contains differentiated and differentiating hemocytes. Various triggers, including mechanical, nutritional, and immunogenic stresses can stimulate blood cell differentiation in the lymph gland. Finally, during metamorphosis, the lymph gland disintegrates, thereby releasing its hemocytes into circulation (Grigorian et al., 2011). Thus, adult flies contain hemocytes of both embryonic and larval origin (Cattenoz et al., 2020; Letourneau et al., 2016; Vlisidou & Wood, 2015; Gold & Brückner, 2014).

Parasitic wasps (e.g. of the *Leptopilina* genus) deposit their eggs into *Drosophila* larvae which provide a source of nutrition for the developing wasp (Kim-Jo et al., 2019). This infestation triggers an immune response in the larva: Sessile as well as lymph gland prohemocytes undergo proliferation and differentiation and are released into circulation. Since the parasitic wasp eggs are too big for plasmatocyte-mediated phagocytosis, inactivation of the invader relies on lamellocytes, which envelop the egg. An orchestrated, step-wise process that involves all three blood cell types results in the close encapsulation of the wasp egg with layers of plasmatocytes, lamellocytes, and melanin. Melanization produces reactive oxygen species (ROS) and these radicals are thought to ultimately kill the invader (Letourneau et al., 2016; Vlisidou & Wood, 2015).

2.1.2. U-shaped, a transcriptional regulator of hematopoiesis

The transcriptional mechanisms that underlie hemocyte differentiation during development and upon stress are complex and require the crosstalk of several transcription factors. For instance, hemocytes and hemocyte precursors are characterized by the expression of Serpent (Srp), a GATA-type transcription factor. Subsequent co-expression of Glial cells missing (Gcm) initiates plasmatocyte differentiation, whereas co-expression of the RUNX protein Lozenge (Lz) directs cells towards the crystal cell lineage (Vlisidou & Wood, 2015; Fossett et al., 2001a; Fossett & Schulz, 2001b; Lebestky et al., 2000). The expression and/or activity of these transcription factors is developmentally regulated and also responds to external stimuli, e.g. immune challenge. Many signaling pathways have been identified to transmit cues for progenitor maintenance or differentiation, thereby influencing the transcriptome of developing hemocytes (Le-

tourneau et al., 2016; Fossett, 2013). However, there is limited knowledge about the genomic targets that are regulated by the final effectors of these cascades.

One of these effectors is the transcriptional co-factor U-shaped (Ush). Its name stems from the morphology of Ush loss-of-function embryos (Nüsslein-Volhard & Wieschaus, 1980). The *ush* gene encodes a multi-zinc finger protein (four CCHH and five CCHC type Zn fingers) whose length ranges from 1175 to 1212 amino acids, depending on the isoform (Cubadda et al., 1997; FlyBase 06/2021). The protein interacts with the N-terminal Zn-finger of GATA factors, in particular Pannier (Pnr; Haenlin et al., 1997; Tokusumi et al., 2007) and Srp (Walzer et al., 2002). GATA/Ush complexes are thought to bind GATA motifs in the DNA and influence gene expression (ibid.). Pnr-dependent roles of Ush were observed during cardiogenesis (Fossett et al., 2000; Tokusumi et al., 2007) as well as sensory organ development (Cubadda et al., 1997; Haenlin et al., 1997). Interestingly, in both cases, Pnr and Ush regulate gene expression by influencing the function of specific enhancers (*D-mef2* and *achaete*/*scute*, respectively). However, transcriptional regulation by Ush is best studied in hematopoiesis where it functions together with Srp.

Ush is expressed in embryonic prohemocytes but its expression decreases progressively during lineage specification. In fact, the reduction of Ush levels is required to allow crystal cell differentiation (Fossett et al., 2001a; Fossett & Schulz, 2001b; Muratoglu et al., 2006; Muratoglu et al., 2007; Fossett, 2013). In larval lymph glands, Ush is found in prohemocytes of the medullary zone as well as in differentiating hemocytes in the cortical zone. Crystal cells and plasmatocytes show lower Ush levels, while it is absent in the lamellocyte population. Importantly, Ush is also not expressed in cells of the PSC (Gao et al., 2009; Tokusumi et al., 2010). In the lymph gland, Ush is required to maintain the prohemocyte pool and to prevent progenitors from differentiating.

As a safeguard of differentiation, Ush resides at the vertex of a complex signaling network. Its expression is regulated by pathways such as JAK/STAT (Sorrentino et al., 2007; Gao et al., 2009), Toll (Gao et al., 2016), and Hedgehog (Hh; Baldeosingh et al., 2018). These cascades ensure constant expression of Ush in the MZ to maintain the progenitor state of prohemocytes. The Ush cis-regulatory module contains GATA as well as RUNX motifs and both Srp and Lz, respectively, are required for Ush activation in the lymph gland (Muratoglu et al., 2006). Interestingly, together with Srp, Ush represses its own transcription, creating a negative feedback loop that is counterbalanced by Lz- and Srp-mediated activation (Muratoglu et al., 2007). This complex network illustrates the need for precise regulation of Ush levels in prohemocytes. In fact, different levels of Ush expression influence cell fate decisions of hemocyte progenitors: While a 50% reduction of Ush expression allows generation of plasmatocytes and crystal cells, production of lamellocytes requires a complete loss of Ush expression (Gao et al., 2009; Fossett, 2013).

Aside from regulating its own expression, only few Ush targets have been identified using reporter gene assays and genetic interaction studies in the hematopoietic system. These include the hemocyte genes *croquemort* (Walzer et al., 2002), *lz* (Muratoglu et al., 2007), *hh* (Tokusumi et al., 2010), and *E-cadherin* (Gao et al., 2013). However, we still lack comprehensive information about additional Ush-regulated genes.
Ush does not contain any discernible catalytic domains. To influence transcription and possibly modulate the chromatin environment, it cooperates with additional co-factors. In its cardiogenic function, the Pnr/Ush complex binds to the co-repressor CtBP (C-terminal-binding protein) to inhibit gene expression (Tokusumi et al., 2007). It is currently unclear whether other transcriptional co-factors are required for Ush's function in hematopoiesis.

Thus, the objective of this study was to elucidate the Ush-regulated transcriptome as well as identifying transcriptional regulators that cooperate with Ush during hematopoiesis.

2.2. Synopsis of results

I have studied the molecular function of Ush in *Drosophila* Schneider 2 (S2) cells. This cell line originates from 20-24 hour old embryos (Schneider, 1972) and is considered to resemble a hemocyte precursor population (Rämet et al., 2002). To evaluate the expression of Ush in this cell line I depleted the protein via RNA interference (RNAi). I used Western blot of extracts derived from S2 cells that had been transfected with a double stranded RNA (dsRNA) targeting Ush as well as with a non-targeting dsRNA against EGFP. Lysates of these cells were analyzed using a Ush-specific antibody (Fossett et al., 2001a) (Fig. 1A). The antibody detected several peptides, two of which were not observed in dsUsh-treated cell lysates, indicating that Ush proteins are expressed in S2 cells. Using a CRISPR/Cas9-based approach (Böttcher et al., 2014) we inserted a GFP- and a FLAG-tag sequence in the genome of S2 cells positioned at the 3'-end of the Ush gene (Fig. S1A). Western blot of these lysates again revealed two differentially migrating bands containing GFP- or FLAG-tags (Fig. 1A). I concluded that Ush is expressed in S2 cells and hypothesized that at least two polypeptides can be generated from the Ush locus.

Ush cooperates with GATA transcription factors (Fossett, 2013; Waltzer et al., 2002; Haenlin et al., 1997) and is thought to regulate gene expression. I considered that this might be achieved by Ush binding to chromatin. Therefore I decided to examine the genome-wide occupancy of Ush. To this end, we performed ChIP-seq in a Ush-GFP expressing cell line. We found Ush to preferentially occupy promoters and intronic sequences (Fig. 1B). Histone post-translational modifications marking promoters (H3K4me3 and H3K27ac) or enhancers (H3K4me1 and H3K27ac) were enriched at Ush peaks. Conversely, we found that Ush-bound regions were mostly devoid of

H3K27me3 (Fig. 1C). A metagene analysis revealed that the Ush signal peaks at approximately 135 bp upstream of the TSS of genes and then rapidly decreases within the gene body (Fig. 1D). Thus Ush is most highly enriched over the nucleosome-free region and the -1 nucleosome (Radman-Livaja et al., 2010). Compared to mammalian genomes the *Drosophila* genome is very gene dense which entails that enhancer sequences are often located within introns. The enrichment of Ush at intronic regions and the co-occurrence of enhancer-typical histone marks argues that Ush binds to enhancers. These observations suggest that Ush occupies regulatory sequences (promoters and enhancers) and advocate for a function in gene regulation at the level of transcription. In fact, several transcription factor binding motifs were enriched at Ush-occupied regions (Fig. 1E). These include promoter-associated motifs like GAGA, the Initiator sequence, and E-boxes. Interestingly, the most highly enriched sequence was the GATA-motif that can be recognized by GATA transcription factors. Given that Ush physically and genetically interacts with GATA factors (Waltzer et al., 2002) we proposed a function for Ush in GATA-factor regulated transcription.

To gain insight into Ush-mediated gene regulation we performed transcriptome analysis upon Ush depletion. S2 cells were transfected with dsRNA against Ush and EGFP as a control (see Fig. 1A), RNA was isolated and subjected to RNA sequencing. We detected a large number of genes that were significantly deregulated in Ush-depleted cells. Most of these exhibited higher expression levels (1268), whereas a smaller fraction (560) showed decreased expression upon Ush-depletion (Fig. 2A). At 51.3% percent of the derepressed genes we found one or more regions that were occupied by Ush in our ChIP-seq experiment. 31.3% of genes that showed reduced expression upon Ush depletion were also bound by the Ush protein (Fig. 2B). This suggests that Ush might indeed regulate the expression of a large number of genes by occupying their regulatory regions. Those genes define a set of direct targets. It is noteworthy that Ush seems to act primarily as a transcriptional repressor but can also have activating functions on a subset of genes.

Ush has been implicated in the differentiation of hemocytes in *Drosophila* embryos and larvae (Fossett & Schulz, 2001b; Sorrentino et al., 2007; Tokusumi et al., 2010). To address whether this biological function is reflected in gene networks that Ush regulates I performed Gene Ontology (GO) term analysis (Fig. 2C). In fact Ush-regulated genes associated significantly with the GO term “Innate Immune System” (R-DME-168249) supporting the hypothesis that, also in cultured S2 cells, Ush regulates genes involved in hemocyte function. Importantly, this illustrates that the biological activity of Ush can be evaluated on the basis of its transcriptional activity. I found two other groups of GO terms that were highly enriched among Ush-regulated genes: GO terms that I grouped as “cell cycle” terms (“cell cycle process” (GO:0022402) and “regulation of cell cycle process” (GO:0010564)) and GO terms that I summarized under “lipid metabolism” (“organic acid catabolic process” (GO:0016054), “Metabolism

of lipids" (R-DME-556833) and "beta-Oxidation" (M00087)). Most genes included in the categories "hemocyte-related" and "lipid metabolism" were upregulated upon Ush knockdown (84% and 82% respectively) whereas the expression of most cell cycle related genes seemed to be dependent on Ush (72%) (Fig. 2D). I selected five genes per category and verified their response to Ush depletion using RT-qPCR (Fig. 2E). Some, but not all of these genes were occupied by Ush according to our ChIP-seq data (Table S1), so the results obtained here may reflect direct as well as indirect consequences of Ush RNAi. Genes involved in hemocyte function and differentiation showed medium to strong derepression upon Ush-depletion. Notably, pro-mitotic genes like *Aurora B*, *CDK1*, *polo* and *Cyclin B* showed lower expression in Ush-depleted cells whereas expression of *CHES-1*, an anti-proliferative transcription factor (Huot et al., 2014; Ahmad et al., 2012), increased. This suggests that Ush coordinates a transcriptional program that is required for proliferation. Similarly, genes involved in the catabolism of fatty acids (*Mcad*, *Echs1*, *CROT*, *fa2h*) are mostly repressed by Ush whereas the key enzyme of fatty acid synthesis, *ACC*, requires Ush for appropriate expression. These observations show that Ush regulates gene networks underlying biological processes in a coordinated fashion.

This prompted me to investigate whether these biological processes are indeed affected in Ush-depleted cells. To this end, cells were transfected with control dsRNA (dsLuc) and two different dsRNA constructs targeting Ush (dsUsh #1 & #2). We observed a strong decrease in proliferation of cells that had been depleted of Ush (Fig. 3A). This decrease was not due to cells undergoing cell death since Ush-depleted cells did not display decreased viability (Fig. 3B). Instead, Ush-depleted cells seemed to accumulate in G2/M phase, shown by PI-staining with subsequent flow cytometry (Fig. 3C, 3D, Fig. S7). Their inability to transition through M-phase was accompanied by reduced expression of the mitotic cyclins A and B (Fig. 3E). These results suggest that, although Ush-depleted cells still replicate their DNA, they are not able to enter or transition through mitosis. Taken together with our RNA-seq results I speculate that this dependence on Ush for successful mitosis is in part due to transcriptional regulation of pivotal cell cycle genes.

The previous paragraph has highlighted Ush's ability to modulate transcriptional programs in S2 cells. An analysis of the domain structure, however, revealed no apparent catalytic activities that are frequently found in chromatin regulators (Fig. 4B). It is therefore unlikely that Ush influences gene expression by catalyzing an enzymatic reaction. Ush manipulates gene expression at two different levels: It seems to be a negative as well as a positive regulator of transcription. Moreover, it uses these abilities on distinct gene classes in a coordinated fashion. I hypothesized that for one protein to facilitate these functions it would need to (a) increase its diversity (e.g. by gen-

erating various protein isoforms) and/or (b) employ different epigenetic regulators, like chromatin-modifying enzymes, in different transcriptional contexts.

The Ush gene gives rise to at least three protein products, which are possibly generated by alternative splicing and/or alternative promoter usage (Fig. 4A & 4B). The majority of the sequence (1175 amino acids) is shared between all polypeptides and includes all nine zinc finger domains. The three isoforms only differ in their N-terminal sequences. Ush-D does not possess a unique N-terminus. Ush-A contains 16 and Ush-B 23 amino acids N-terminal to the common sequence. Since Ush-A and Ush-B N-termini also share a 9 amino acid stretch, this results in 7 amino acids unique to Ush-A and 14 amino acids unique to Ush-B (Fig. 4B). Our transcriptomic analysis detected reads emanating from Ush-A as well as Ush-B-specific exons (Fig. S3). The multiple polypeptides that we observed in S2 cells by Western blot therefore likely represent different Ush isoforms.

I hypothesized that the diverse functions of Ush might be mediated by proteins that interact with it and subsequently manipulate transcription. To uncover Ush-associated proteins I analyzed a published dataset of protein-protein interactions (Guruharsha et al., 2011). Here the authors overexpressed almost 5000 HA-tagged proteins in *Drosophila* S2 cells and determined associated factors using mass spectrometry after anti-HA immunoprecipitation. They identified 12 Ush-binding proteins, six of which (namely dDOC-1, dMBD-like, dp66, dMTA1-like, dRPD3, dMi-2) can be found in the *Drosophila* Nucleosome Remodeling and Deacetylation (dNuRD) complex, a chromatin-associated multiprotein assembly that is involved in transcriptional regulation. We have also found Ush in an unbiased proteomic screen for dMi-2 interacting proteins using IP with subsequent mass spectrometry (data not shown). We performed immunoprecipitation of endogenously FLAG-tagged Ush. Subunits of the dNuRD complex indeed coprecipitated with Ush-FLAG, whereas dMEP-1, which forms a separate complex together with dMi-2 (dMec), was not recovered in Ush-FLAG precipitates (Fig. 4C). We therefore concluded that Ush interacts with the dNuRD complex. Anti-FLAG immunoprecipitation of endogenously FLAG-tagged dMi-2 (Fig. S1C-E) confirmed this observation (Fig. 4D). Remarkably, only one of the two Ush-specific bands coprecipitated with dMi-2. Using a RNAi construct targeting the unique 5'-end we identified this band as Ush-B. Upon specific depletion of the Ush-B isoform we did no longer detect a dMi-2/Ush interaction (Fig. 4D). This indicates that dNuRD associates primarily with Ush-B and I speculated that this interaction is likely mediated by the Ush-B-specific N-terminal sequence.

The Ush-B N-terminus contains a short conserved motif. This 9 amino acid long sequence is also found in a group of mammalian transcription factors (Fig. 4E). Most of them, as Ush, contain multiple zinc finger domains and harbor the conserved motif at their N-terminus. The conserved sequence was first identified to be important for the repressive function of the mouse FOG1 protein and was therefore named "FOG

repression motif" (Svensson et al., 2000; Lin et al., 2004). This short peptide directly contacts mammalian NuRD. In fact, many proteins containing this sequence have been shown to associate with the complex (Gao et al., 2010; Wu et al., 2016: Dubuissez et al., 2016; Kloet et al., 2018; Yang et al., 2018). A GST-fusion protein containing the first 45 amino acids of mouse FOG1 was able to bind to dNuRD but not to other chromatin regulators in *Drosophila* cell and embryo nuclear extracts (Fig. 4F), highlighting the conserved nature of this interaction. We generated synthetic peptides derived from FOG1 and Ush N-termini, scrambled versions of these peptides, and peptides where a basic stretch that is crucial for dNuRD binding was mutated (Hong et al., 2005) (Fig. 4G). Titrating these peptides into our GST interaction assay we observed that FOG1 and Ush wild type peptides competed with the Ush/dNuRD interaction whereas mutant and scrambled peptides had no effect (Fig. 4H). Notably, the FOG1 peptide seemed to be a more potent competitor than the Ush peptide. Addition of this peptide to co-immunoprecipitation experiments also efficiently abrogated the interaction of Ush-FLAG with dNuRD in soluble nuclear extract (Fig. 4I). In summary, we have identified the *Drosophila* NuRD complex as an interactor of a distinct Ush isoform, Ush-B. This interaction is mediated by the FOG repression motif residing in the unique Ush-B N-terminus.

In contrast to Ush, the dNuRD complex harbors known enzymatic activities that are able to modulate gene expression: The chromatin remodeling ATPase dMi-2 as well as the histone deacetylase dRDP3. I therefore hypothesized that Ush might, at least partly, exert its gene regulatory function by employing dNuRD. I used a cell line expressing endogenously GFP-tagged dMi-2 to study its genomic distribution via anti-GFP ChIP-seq and compared it to that of Ush. We obtained a dataset with high similarity to published genome-wide dMi-2 ChIP datasets that had been generated using different antibodies (Fig. S4). 53.8% of all identified dMi-2 binding sites also contained a Ush peak, while 64.9% Ush binding sites were co-occupied by dMi-2 (Fig. 5A). Peaks with high enrichment of Ush also showed a tendency for higher dMi-2 signal (Fig. 5B). We also identified regions with exclusive Ush or dMi-2 binding (Fig. 5C). Sites with exclusive Ush occupancy were found at promoters and introns whereas "dMi-2 only" regions were predominantly enriched in promoters. Loci that were bound by both factors showed an enrichment of promoters and intronic sequences (Fig. 5D). "Ush only" peaks showed high H3K4me1 signals but low levels of H3K4me3 and H3K27me3. This argues that these loci contain active enhancers. Sites occupied by dMi-2 only, on the other hand, displayed enrichment of H3K4me3 which is indicative of active promoters. Here, H3K4me1 and H3K27me3 profiles were decreased. Ush and dMi-2 cooccupied regions were decorated with H3K4me1 as well as H3K4me3 containing nucleosomes but devoid of the H3K27me3 mark (Fig. 5E). This suggests that Ush and dMi-2 come together at regulatory elements in the genome and opens up the potential for these factors to cooperate in regulating transcription.

We have identified three groups of Ush-dependent genes: genes encoding cell cycle regulators, genes coding for factors involved in fatty acid metabolism, and hemocyte-related genes. I considered that if dMi-2 contributed to the regulation of Ush-dependent genes, mRNA levels in these groups would also likely respond to depletion of dMi-2. Furthermore, depletion of the dNuRD-interacting Ush isoform, Ush-B, should also affect their expression.

To address this, dMi-2-regulated genes were determined by sequencing the transcriptome of S2 cells upon RNAi-mediated depletion of dMi-2. The expression of 945 genes was significantly changed compared to cells treated with control dsRNA (Fig. 6A). One third of these genes (322 genes, 34.1%) showed decreased mRNA levels whereas two thirds (623 genes, 65.9%) displayed increased expression upon dMi-2 depletion. This suggests that dMi-2 has positive as well as negative effects on gene transcription and is in line with observations made with mammalian CHD4 (de Dieuleveult et al., 2016; Reynolds et al., 2013). I performed Gene Ontology term analysis on dMi-2-regulated genes (Fig. 6B) and identified GO terms associated with development to be enriched ("post-embryonic development" (GO:0009791) and "cell part morphogenesis" (GO:0032990)). This supports a role for dMi-2 in fly development and agrees well with previous reports (Kreher et al., 2017). Strikingly, the term "Innate immune response" (GO:0045087) was among the ten most highly enriched GO terms, indicating that dMi-2 impacts the expression of genes important for hemocyte function. GO terms linked to regulation of cell cycle or lipid metabolism were not found to be enriched.

Depletion of Ush-B had only mild effects on the S2 cell transcriptome: 85 genes were differentially expressed in cells transfected with dsRNA directed against Ush-B. The mRNA levels of 47 Ush-B-responsive genes (55.3%) increased upon depletion (Fig S5). Conversely, 38 genes (44.7%) showed lower expression (Fig. S5). Due to the low number of deregulated genes, algorithmic GO term analysis did not yield meaningful results. However, I was able to associate 18 Ush-B-dependent genes with hemocyte-related functions based on their biological activity and/or expression patterns (Fig. S5-S6 and Table S2). Only very few genes could be linked to functions in lipid metabolism or cell cycle (2 and 4 genes respectively; Table S2).

The expression of representative genes from each group was evaluated by RT-qPCR upon RNAi of dMi-2 or Ush-B (Fig. 6C). I chose the same set of genes that I validated previously to be susceptible to the simultaneous depletion of all Ush isoforms (Fig. 2E). Most of the hemocyte-related genes inspected here responded significantly to depletion of dMi-2 and Ush-B. The cell cycle regulators tested were not affected and expression of genes relevant to lipid metabolism showed only mild alterations upon depletion of Ush-B or dMi-2. I, thus, reasoned that the contribution of dMi-2/dNuRD to Ush-mediated transcriptional regulation is most prominent in the group of

hemocyte-related genes. Cell cycle regulators and lipid metabolism genes, on the other hand, do not seem to rely on dNuRD or Ush-B for their appropriate expression.

Indeed, depletion of Ush-B, dMi-2, or the dNuRD complex subunit dMTA1-like did not lead to alterations in cell cycle (Fig. 3D, Fig. S7A). Also, levels of mitotic cyclins did not change in these cells (Fig. 3E), indicating that Ush-dependent cell cycle effects are not mediated by the Ush-B/dNuRD assembly.

Based on our expression analysis we conjectured that Ush and dNuRD might cooperate in regulating hemocyte-specific functions and/or hematopoiesis in *Drosophila*. We used two complementing approaches to study this relationship *in vivo*.

In the primary lobes of the lymph gland, the main larval hematopoietic organ, cells of the 'posterior signaling centre' (PSC) secrete signaling molecules that keep hemocytes of the medullary zone in a progenitor state (Jung et al., 2005). Thus, the PSC is considered a stem cell niche. The homeotic gene *Antennapedia* (*Antp*) specifies this niche and is frequently used as a marker for cells of the PSC (Mandal et al., 2007). Prohemocytes in the medullary zone of the lymph gland do not produce certain signaling polypeptide ligands themselves but receive them from the PSC. The expression of Hedgehog (Hh), one of the signaling proteins, is regulated by an enhancer residing in its first intron (Tokusumi et al., 2010; Baldeosingh et al., 2018). The enhancer is active in the PSC but repressed in other parts of the lymph gland and this repression requires Ush. Concomitantly Ush is not detectable in the PSC but is expressed in cells of the medullary zone. The *Hh* enhancer activity can be monitored using a reporter gene assay where a minimal enhancer fragment (hhF4f) controls the expression of a GFP transgene (Tokusumi et al., 2010). In lymph glands of larvae carrying the reporter, GFP-positive cells are found exclusively in the PSC and are marked by *Antp* expression (Fig. 7A). Upon RNAi-mediated depletion of Ush or in larvae carrying a homozygous Ush mutation GFP signal is detected in cells located in the medullary zone (Fig. S7). The colocalization of Ush and dMi-2 on regulatory genomic elements that we have identified in S2 cells prompted us to investigate dMi-2's involvement in Hh enhancer function in the lymph gland. We directed the expression of a dMi-2 RNAi construct to the medullary zone in lymph glands of larvae carrying the hhF4f-GFP reporter. We detected expression of GFP in prohemocytes of the medullary zone indicating that dMi-2 is indeed required for proper silencing of the Hh enhancer in these cells (Fig. 7B). Using the same experimental setup we depleted the dNuRD complex subunit dMTA1-like from medullary zone prohemocytes. Also in lymph glands from these larvae, GFP-positive cells were observed outside of the PSC (Fig. 7C). Taken together, these data suggest that the dNuRD complex is implicated in the repression of a Hh enhancer during larval hematopoiesis. Since this enhancer also responds to Ush depletion, we propose that the Ush/dNuRD assembly is required to restrain Hh expression in larval prohemocytes.

Prohemocytes give rise to three distinct blood cell populations: Plasmatocytes, crystal cells, and lamellocytes. The latter are virtually absent in *Drosophila* larvae and are only produced upon parasite infestation or other extreme stress conditions (Sinenko et al., 2012; Tokusumi et al., 2018). Ush prevents the spontaneous differentiation of lamellocytes in unstressed larvae (Gao et al., 2009). Larvae carrying two mutant copies of the *ush* gene display an increased number of circulating lamellocytes (Fig. 7G), while one intact copy of *ush* is sufficient to keep the lamellocyte count close to wild type level (Fig. 7D; Gao et al., 2009). This fact can be exploited to identify genetic interactors, factors that act in the same pathway together with Ush. In a so-called 'second site non-complementation' (SSNC) assay *ush* heterozygotes are used as a sensitized background and crossed with flies carrying a heterozygous mutation in a candidate gene. In case of a genetic interaction, a phenotype is detected in transheterozygotes, while no effect is seen in both single heterozygotes. We crossed flies heterozygous for dNuRD complex subunits with *ush* heterozygotes and examined circulating lamellocytes in transheterozygous progeny. In our experimental setup, these specialized hemocytes are marked by expression of a mCherry transgene which is controlled by a lamellocyte-specific enhancer regulating the *misshapen* gene (Tokusumi et al., 2009). The *misshapen-mCherry* construct (*MSN-C*) is also active in larval muscle which is marked by arrowheads (Fig. 7D-7G). We quantified the phenotype penetrance by counting the number of larvae that displayed a more than 10-fold increase in circulating lamellocytes.

Transheterozygous larvae with only one functional *ush* and one functional *dMTA1-like* allele showed an elevated level of circulating lamellocytes (Fig. 7E). Also, larvae with only one functional *ush* and one functional *dp66* allele produced increased numbers of lamellocytes (Fig. 7F). In this manner we tested four different dNuRD complex subunits for their genetic interaction with Ush. Each factor was evaluated using two different mutant alleles (Fig. 7H and Table S3). We set a routinely used threshold of 40% to count the penetrance of a crossed genotype as robust genetic interaction. The penetrance in *ush*/*dMTA1-like* and *ush*/*dp66* transheterozygous larvae passed this threshold in both tested alleles. In single *dMTA1-like* or *dp66* heterozygotes the penetrance did not exceed background levels. Both *dMi-2* mutant alleles produced increased lamellocyte levels when crossed into a *ush* heterozygous background, though the penetrance was below 40%. Double heterozygotes of *ush* and the *Drosophila* histone deacetylase dRPD3 showed high penetrance levels. However, one mutant allele also led to a phenotype penetrance higher than 40% in single heterozygous larvae. Thus, the genetic interaction of dRPD3 and Ush remains undefined. dRPD3 is part of many gene regulatory complexes. It is, therefore, possible that the effects we observed in heterozygous but also transheterozygous larvae are not emanating from an altered dNuRD function specifically.

Based on the genetic interaction of Ush with the dNuRD-specific factors dMTA1-like and dp66 we concluded that Ush likely cooperates with dNuRD to restrict the spontaneous differentiation of lamellocytes in unstressed larvae.

2.3. Discussion

2.3.1. Transcriptional regulation by Ush

Prior to the work described here, our understanding of Ush's capacity to regulate gene expression was mainly informed by *in vivo* studies in *Drosophila* embryos and larvae (Cubadda et al., 1997; Haenlin et al., 1997; Waltzer et al., 2002; Tokusumi et al., 2010). Using mutation analysis, genetic interaction, and reporter gene assays Ush has been implicated in the transcriptional control of a small number of genes relevant to hemocyte differentiation (Tokusumi et al., 2010; Gao et al., 2013). In part, this effect in gene expression has been assigned to Ush cooperating with GATA factors, such as Serpent and Pannier (Haenlin et al., 1997; Waltzer et al., 2002). Our data significantly expands this notion. We uncover Ush-regulated genes in hemocyte-derived S2 cells on a genome-wide scale and show that Ush impinges on the expression of more than 1700 genes (Fig. 2A). Among the Ush-regulated transcriptome we find classical hemocyte genes, like *Lozenge* and *atilla* (Cattenoz et al., 2020), whose expression depends on Ush (Fig. 2E). This is in line with observations during hematopoietic differentiation in the embryo. Here, Ush levels gradually decrease, thereby allowing the expression of hemocyte-specific factors (Gao et al., 2009; Fossett, 2013). Derepression of these genes upon reduction of Ush expression can be simulated in our RNAi approach in cell culture.

Beyond that, Ush regulates genes involved in other biological processes, particularly genes encoding for cell cycle regulators and enzymes involved in fatty acid metabolism (Fig. 2C). It is noteworthy that Ush does not only have repressive potential but also enables transcription. This finding becomes especially apparent in the regulation of crucial cell cycle genes, such as *Cyclin B*, or the mitotic kinases *Aurora B*, *CDK1*, and *polo* (Fig. 2D-2E).

Ush binds to more than 7000 sites in the *Drosophila* genome which are associated with regulatory regions, such as promoters and enhancers. On these sites, the GATA motif is highly enriched (Fig. 1). This observation provides unbiased and genome wide evidence that Ush associates with regions that are potentially bound by GATA factors. So far, this concept was based on biochemical and genetic interaction data of Ush and GATA factors as well as reporter gene assays (Haenlin et al., 1997; Fossett et al., 2000; Waltzer et al., 2002). In mammalian genomes the GATA sequence often occurs together with E-boxes generating a composite site. This sequence combination can provide a platform to assemble LMO2/LDB complexes resulting in chromatin looping

and transcriptional activation (Wilkinson-White et al., 2011; Love et al., 2014). Since we also observed an enrichment of the E-box motif among Ush bound regions (Fig. 1E), I speculate that GATA/E-box paired motifs might be potential Ush target sites. Overall, our results indicate that rather than controlling a small gene set, Ush seems to be a major regulator of transcription with wide ranging functions in hemocyte-specific gene expression, proliferation, and lipid metabolism.

2.3.2. Ush isoforms and the FOG repression motif

We have, for the first time, detected the expression of multiple Ush isoforms in *Drosophila* S2 cells (Fig. 1A-1B, Fig. S3) and identified a FOG repression motif at the N-terminus of Ush-B (Fig. 4B). This conserved amino acid sequence appears in a number of vertebrate zinc finger transcription factors (Lin et al., 2004), notably also in the mammalian Ush homologs FOG1 and FOG2 (Hong et al., 2005; Roche et al., 2008). The motif confers interaction with the NuRD complex by directly contacting MTA and RbAp proteins (Roche et al., 2008). The FOG1-interacting residues of RbAp48 are conserved in the *Drosophila* homolog dp55 (Lejon et al., 2011). Moreover, the region of mouse MTA-1 that contacts FOG2 is conserved in dMTA1-like (Roche et al., 2008). We hypothesize that Ush associates with dNuRD by binding to dp55 and dMTA1-like. The interaction can be efficiently dissociated by competitive peptides harboring the FOG repression motif sequence (Fig. 4G-4I). This suggests that the N-terminus of Ush-B is crucial for dNuRD binding and I consider it unlikely that additional domains in the Ush protein contribute significantly to this interaction. This is supported by the fact that other Ush isoforms, which only deviate from Ush-B in their N-termini, do not co-immunoprecipitate with dMi-2 (Fig. 4D).

It has to be noted that peptides derived from the mouse FOG1 N-terminus show a higher potential in competing with the Ush/dNuRD interaction than peptides derived from Ush-B N-termini (Fig 4H). This observation opens up the possibility that amino acids outside of the classical FOG repression motif (H_2N-MS**RRKQ**xx**P**; Lin et al., 2004) are able to modulate the affinity towards NuRD. In fact, a patient-derived mutation neighbouring the FOG repression motif of mouse Zeb2 (ZEB2R22G) abrogates its interaction with the NuRD complex (Wu et al. 2016). Additionally, post translational modifications of residues within the motif, specifically phosphorylation of Serin 2 in the BCL11B N-terminus, can impact its association with NuRD (Dubuissez et al., 2016).

A GST-fusion containing the FOG repression motif was able to purify NuRD complexes from extracts of rat cardiocytes and mouse erythroleukemia cells in one-step pulldown experiments (Roche et al., 2008; Hong et al., 2005). This suggests that the motif has evolved solely to interact with NuRD and that it does not associate significantly with other nuclear proteins. The generation of proteins containing this sequence may present a way of specifically involving NuRD in biological functions conferred by the respective factor. In interacting with NuRD, its catalytic capacities and its impact

on gene expression could be utilized on genomic targets of a FOG repression motif containing protein. To what extent a classical recruitment model can be applied here, will be subject to discussion in a separate section below.

We show that Ush cooperates with dNuRD in ensuring hemocyte-related gene expression, while impinging on cell cycle and lipid metabolism without employing dNuRD. This diversification is achieved by adding a FOG repression motif to the N-terminus of one Ush isoform (Ush-B) via alternative splicing and/or alternative promoter usage. Interestingly, in mouse erythroid cells different FOG1 proteins are produced by translation from alternative start codons. The longer FOG1 isoform contains the FOG repression motif whereas the shorter protein lacks this NuRD interaction domain (Snow et al., 2009). Likewise, the murine FOG2 gene can give rise to an isoform that lacks the FOG repression motif (Dale et al, 2007). Thus, diversification of FOG-like proteins to enable or disable NuRD interaction appears to be an evolutionary conserved principle.

Besides U-shaped, we have identified only one other protein encoded in the *Drosophila* genome that contains a N-terminal FOG repression motif: OAZ, a homolog of Olf/EBF-associated zinc finger factors. This protein is involved in the formation of posterior spiracles, which are part of the larval tracheal system (Krattinger et al., 2007). OAZ is not expressed in S2 cells but, due to its FOG repression motif, I speculate that it might cooperate with dNuRD during *Drosophila* development. In mammals, the EBF-interacting proteins Zfp423 and Zfp521 also contact NuRD via their N-terminal FOG repression motif, thereby contributing to transcriptional regulation (Liao, 2009). This raises the possibility for a conserved role of the dNuRD complex in EBF (*Drosophila* collier)-regulated transcription that relies on FOG repression motif containing proteins.

2.3.3. NuRD recruitment by FOG repression motif containing proteins

Ush binds to over 7000 genomic regions which are highly enriched for GATA motifs. More than half of these Ush binding sites are also occupied by dMi-2 and both proteins are implicated in the regulation of hemocyte-related gene expression. Moreover, we find an interaction of the Ush-B isoform with the dMi-2-containing dNuRD complex, which requires a short conserved motif in the Ush-B N-terminus. Taken together, these observations strongly evoke a hierarchical recruitment model in which GATA factors associate with DNA and tether Ush proteins to their target sites. This process requires the interaction of their Zinc finger domains (Chlon & Crispino, 2012). Ush-B N-termini then bind to dNuRD thereby recruiting it to the respective regions. A similar scenario has been proposed for the mammalian Ush-homologs FOG1 (Hong et al., 2005; Gao et al., 2010) and FOG2 (Roche et al., 2008) as well as for other proteins containing a FOG repression motif. Examples are ZFP296 (Kloet et al., 2018), Zeb2 (Verstappen et al., 2008; Wu et al., 2016), or ZFP827 (Conomos et al., 2014; Yang et al., 2018). A short FOG1 N-terminal peptide fused to dCas9 has even been used to

artificially tether NuRD to gene promoters resulting in the establishment of a repressive chromatin environment (O'Geen et al., 2017). Our work suggests that this mechanism of NuRD recruitment might already have existed in a common ancestor of vertebrates and *Drosophila*.

Despite the plethora of studies that invoke the above mentioned recruitment model, this concept has recently been challenged: In mouse embryonic stem cells, Sall4 is found to be associated with the majority of NuRD complexes due to its N-terminal FOG repression motif. Surprisingly, knock-out of Sall4 did not lead to dissociation of NuRD from most regions that were co-occupied by Sall4 and NuRD in wild type cells (Miller et al., 2016). I, too, conducted ChIP-qPCR experiments in *Drosophila* S2 cells addressing the Ush-dependent occupancy of dMi-2 and dMTA1-like at Ush/dNuRD target genes. Upon depletion of Ush-B I did not detect decreased dNuRD signal at the examined regions (data not shown). These observations suggest that the association of NuRD with FOG repression motifs is not alone sufficient to define its chromatin localization. I agree with the notion that FOG repression motif containing proteins can contribute to tethering NuRD to genomic sites; the motif fused to dCas9 is even sufficient to *de novo* recruit NuRD (O'Geen et al., 2017). However, the efficiency of this artificial recruitment was highly variable across cell types and target sites, suggesting that the FOG repression motif is presumably not the sole determinant of NuRD occupancy. Another example highlights this non-essential but merely contributive function of FOG1 in NuRD recruitment: In mouse erythroid cells NuRD is present at several GATA1 target genes (e.g. *Kit* and *Gata2)* even in absence of GATA1/FOG1 and its association with these loci only slightly increases upon induced GATA1/FOG1 occupancy (Miccio et al., 2010). At intricately structured regulatory regions, the NuRD complex likely engages in a multitude of associations with transcription factors, nucleosomes and other chromatin-bound proteins. Interfering with one of these interactions (e.g. by depleting a FOG repression motif containing protein) might not suffice to fully evict NuRD. The number and affinity of additional interactions at a respective locus might determine, how much NuRD residence depends on the presence of a FOG repression motif containing protein.

It is tempting to assume that the sole function of transcription factor/NuRD associations is to facilitate recruitment. While that is certainly one task, interactions with or within the NuRD complex can also confer regulation of its activity. For instance the *Drosophila* Ecdysone receptor is able to recruit dMi-2 to its response elements while simultaneously activating dMi-2 remodeling activity (Kreher et al., 2017). Moreover, the association of the MTA-1 ELM2 domain with histone deacetylases is implicated in the regulation of HDAC activity (Millard et al., 2013). A potential influence of FOG repression motif containing proteins on NuRD enzymatic activities would be an interesting subject to investigate.

2.3.4. Ush and hemocyte proliferation

Our study uncovers the Ush-regulated transcriptome in S2 cells. To our surprise we found a substantial number of genes involved in cell cycle regulation misexpressed upon Ush depletion. The majority of these genes require Ush for their expression (Fig. 2C-2D). Among the Ush-dependent cell cycle regulators we find crucial pro-proliferative factors like the mitotic kinases Aurora B, CDK1 and polo as well as Cyclin B (Fig. 2E). The expression changes upon Ush depletion are concomitant with a significant decrease in proliferative capacity and an accumulation of cells in G2/M-phase (Fig. 3). We conclude that Ush is required for cell cycle progression in S2 cells and attribute this role partly to the transcriptional regulation of pivotal pro-mitotic genes.

In the *Drosophila* embryo, mutations in the *ush* gene can influence the number of cardial and pericardial cells as well as hemocytes. Embryos with reduced Ush activity display an increased number of cardiocytes whereas overexpression of Ush in the mesoderm leads to a reduction in cardial cell number (Fossett et al., 2000). During embryonic hematopoiesis Ush represses the production of crystal cells (Fossett et al., 2001a). Both examples point out that Ush negatively regulates the number of differentiated cells. However, in using the term “production”, the authors leave open whether they assign this effect to proliferation or differentiation processes (Fossett et al., 2001a).

Another indication that Ush acts in hemocyte proliferation has been reported in larval lymph glands. Larvae with two non-functional Ush alleles (ush^{vx22}/ush^{r24}) display hypertrophy of lymph gland hemocytes in the third instar (Sorrentino et al., 2007). Also here, Ush inhibits overproduction of cells. In the L2 stage this effect was not observed (Sorrentino et al., 2007). An independent investigation of the same allele combination showed abnormal production of lamellocytes in lymph glands and the authors attribute this to Ush’s function in the suppression of lamellocyte differentiation (Tokusumi et al., 2010). Gao and colleagues detected an increased number of proliferating (phospho-H3 positive) prohemocytes in lymph glands from early L3 larvae carrying *ush* loss of function alleles (ush^{vx22}/ush^{r24}). Targeted depletion of Ush from prohemocytes by cell type-specific RNAi, however, did not lead to increased proliferation (Gao et al., 2016). Using RNAi-mediated depletion of Ush or inactivation by a different allele combination (ush^{r24}/ush^{r24}), we were unable to recapitulate the drastic hyperproliferation phenotype described by Sorrentino and colleagues (Fig. S8). On the contrary, we observed substantial hypoproliferation of cultured S2 cells (Fig. 3). This cell culture system enables us to investigate cell autonomous effects in a homogeneous embryonic hemocyte precursors line. Thus, the proliferation defects upon Ush depletion are more likely the consequence of an intrinsic disturbance of cascades rather than the effect of signals emitted by regulatory cell types. It is important to keep in mind, however, that S2 cells in culture may not completely recapitulate the behavior of prohemocytes in the embryo.

The discrepancies discussed above suggest that the function of Ush in cell cycle progression is highly context dependent. It appears that Ush affects proliferation differently in embryonic vs. larval hematopoiesis, L2 vs. L3 lymph glands, cultured cells vs. complex hematopoietic organs. To decipher the role that Ush plays in hemocyte proliferation, it would be helpful to study the aberrant signaling and the transcriptomic changes that arise from Ush loss of function in the organism on a single cell level. This might shed light on the complex intercellular communication networks and their changes upon Ush inactivation during embryonic and larval hematopoiesis.

Hypotheses aiming to interpret the proliferation phenotypes observed upon Ush loss of function often involve the gene regulatory capacity of Ush and its associated GATA factors. Studies on mammalian Ush homologs FOG1 and FOG2 highlight their non-transcriptional roles: Murine GATA-1 interacts with the pRb/E2F2 complex which leads to its sequestration and ultimately inhibits proliferation. In presence of FOG1, GATA-1 is competed off the complex, enabling phosphorylation of pRb and subsequent cell cycle progression (Kadri et al., 2009; Kadri et al., 2015). This function of FOG1 may not immediately rely on changes in FOG1/GATA-1 target gene expression and characterizes FOG1 as a pro-proliferative factor. Mammalian FOG2 contains a putative pRb-interacting motif (LXCXD), thereby possibly impinging on cell cycle progression by directly contacting pRb (Goupille et al., 2017). The *Drosophila* GATA factor Srp contains a LX(C/S)XE motif that is theoretically capable of interacting with retinoblastoma proteins (Kadri et al., 2009). Although it is not known whether functions of FOG proteins that involve pRb and E2F homologs are conserved, this transcription-independent influence on cell division may provide an additional layer at which Ush could be subject to context-dependent manipulation.

The dependency of S2 cell proliferation on Ush poses the question whether the protein itself is a cell cycle regulator. It would be interesting to investigate whether Ush expression levels change or whether the protein is post-translationally modified in a cell cycle-dependent manner. Moreover, since this function of Ush seems to be independent of the dNuRD complex (Fig. 3D-3E, Fig. 6C), it is still unclear if there are other cofactors required to ensure cell cycle progression.

The presented data demonstrate how products from a single gene, *U-shaped*, can tackle diverse functions (hematopoiesis, proliferation, lipid metabolism) by delegating these tasks to different isoforms. It furthermore shows how Ush commissions a ubiquitous epigenetic regulator, dNuRD, to participate in a subset of its functions by using a conserved, isoform-specific interaction motif.

2.4. Contribution statement

Most of the molecular and cell biological experiments were performed by me. Bioinformatic analyses were conducted by Dr. Robert Liefke, if not stated otherwise. Together with Prof. Dr. Alexander Brehm I conceptualized the study and designed most of the experiments. In particular, I have made the following contributions to this project:

- Establishment of an endogenous tagging protocol in *Drosophila* S2 cells, characterization of cell lines expressing endogenously tagged U-shaped and dMi-2 by Western blot and genomic DNA PCR (Fig. 1A, Fig. S1). Here, I collaborated with Julianne Funk and Prof. Dr. Klaus Förstemann.
- Execution of ChIP experiments that were analyzed by next generation sequencing (Fig. 1, Fig. 5, Fig. S2, Fig. S4). Illumina sequencing was operated by Dr. Andrea Nist and Prof. Dr. Thorsten Stiewe.
- Analysis of U-shaped occupancy at transcriptional start sites (Fig. 1D).
- Execution of RNAi experiments in S2 cells for RNA-sequencing, RT-qPCR and experiments addressing Ush function in cell cycle (Fig. 2, Fig. 3, Fig. 6, Fig. S3). Here, I was supported by Samuel Shoup.
- Gene Ontology term analysis of deregulated genes (Fig. 2C-D, Fig. 6B, Fig. S5-S6).
- Verification of gene deregulation upon depletion by RT-qPCR (Fig. 2E, Fig. 6C)
- Propidium iodide staining of S2 cells following RNAi and cell cycle analysis (Fig. 3C-D, Fig. S7). Here, Dr. Hartmann Raifer provided technical assistance.
- Observation of mitotic cyclin levels upon protein depletion using Western blot (Fig. 3E)
- Expression of GST-fusion proteins and GST pulldown assays, immunoprecipitation of FLAG-tagged U-shaped. Both interaction assays were combined with a competition approach using synthetic peptides (Fig. 4). Here, I collaborated with Julianne Funk (Fig. 4C-4D, 4H), Dr. Lea Albert and Prof. Dr. Olalla Vázquez (peptide synthesis).

All Figures and tables included in this publication were compiled by me with contributions of Dr. Robert Liefke (Fig. 1C, Fig. 5B-E, Fig. S2, Fig. S4), Dr. Tsuyoshi Tokusumi (Fig. 7A-C, Fig. S8) and Prof. Dr. Nancy Fossett (Fig. 7D-G, Table S3). Furthermore, I contributed to writing the manuscript together with Prof. Dr. Alexander Brehm.

3.

Distinct CoREST complexes act in a cell-type-specific manner

Igor Mačinković, Ina Theofel, Tim Hundertmark, Kristina Kovač, Stephan Awe, Jonathan Lenz, Ignasi Forné, Boris Lamp, Andrea Nist, Axel Imhof, Thorsten Stiewe, Renate Renkawitz-Pohl, Christina Rathke and Alexander Brehm

Nucleic Acids Research, 2019, Vol. 47, No. 22 11649-11666, doi: 10.1093/nar/gkz1050

3.1. Introduction

Initially identified in human cell lines (Andrés et al., 1999), homologs of the transcriptional co-repressor CoREST (co-repressor of RE1 silencing transcription factor) have since been discovered in many organisms, including *Xenopus leavis*, *Drosophila melanogaster*, and *Caenorhabditis elegans*. CoREST homologs exhibit a remarkably conserved function: They inhibit the expression of genes specific for neuronal tissues in cell types or developmental stages that do not require these factors (Lakowski et al., 2006, Maksour et al., 2020). In part, this repression is achieved together with sequence-specific transcription factors which interact with CoREST. The current model states that these proteins recruit CoREST to gene regulatory elements, thereby exerting transcriptional inhibition. Interestingly, CoREST is expressed in neural as well as non-neural tissues, suggesting that it allows the expression of neuronal genes in the brain, whereas it represses these genes in other tissues (Andrés et al., 1999; Dallman et al., 2004; Sáez et al., 2015; Maksour et al., 2020).

CoREST proteins are characterized by their common domain structure: They contain an N-terminal ELM2 (Egl-27 and MTA1 homology 2) domain as well as two SANT (SWI3, ADA2, N-Cor and TFIIIB) domains, although there are isoforms reported that lack the second SANT domain (Lakowski et al., 2006; Dallman et al., 2004; Sáez et al., 2015). Combinations of these domains occur in a number of chromatin regulators and are thought to establish contacts with histone tails, DNA and other proteins (Boyer et al., 2004).

Mammalian genomes encodes three paralogous *CoREST* genes (*rcor1, rcor2 & rcor3*) that give rise to multiple polypeptides. These protein products share an overall domain architecture and transcriptionally repressive potential. However, the mode and extent of repression differs between paralogs, probably due to altered interactions with co-repressor proteins. Moreover, mammalian CoREST paralogs and isoforms

show differential expression patterns across tissues, further contributing to their specialization (Barrios et al., 2014; Sáez et al., 2015; Maksour et al., 2020).

Several studies have identified CoREST-containing protein assemblies in mammals, the LSD1/CoREST complex probably being the best-studied one. Its core is composed of CoREST as well as the histone modifying enzymes LSD1 (H3K4 demethylase), and HDAC1/2 (histone deacetylases), which are able to create a transcriptionally repressive chromatin environment. This assembly exerts the classical CoREST task: It represses neuronal genes in non-neuronal cells. Furthermore, BHC80, BRAF35, ZNF217, and CtBP1 are described as stable complex subunits (You et al., 2001; Humphrey et al., 2001; Hakimi et al., 2002; Shi et al., 2005; Lee et al., 2005). Additional co-repressors, such as MeCP2 (Lunyak et al., 2002) and components of the SWI/SNF chromatin remodeling complexes (Battaglioli et al., 2002), can interact with CoREST and participate in LSD1/CoREST-mediated repression. An altered version of the LSD1/CoREST complex, which contains the histone deacetylase SIRT1 and the histone methyltransferase G9a, contributes to the repression of genes that respond to Notch signaling (Mulligan et al., 2011). These examples highlight the broad diversity of mammalian LSD1/CoREST assemblies, which are all based on a common CoREST-LSD1-HDAC core. This core acquires a variety of co-repressors, thereby engaging in specific repressive functions. CoREST and LSD1 have been shown to form another distinct assembly that does not harbor any HDACs, but contains the MBT domain protein SFMBT1. This so-called SLC complex (SFMBT, LSD1, and CoREST) regulates the cell cycle-dependent expression of histone genes (Zhang et al., 2013). It is worth noting that the majority of studies that identified CoREST-containing protein assemblies either focused on CoREST1 or did not distinguish between CoREST paralogs or isoforms. Thus, there might be a variety of CoREST complexes yet to be discovered.

In contrast to mammalian genomes, *Drosophila melanogaster* harbors a single *dCoREST* gene. Its transcripts undergo alternative splicing, giving rise to at least three different polypeptides. Based on the length of their amino acid sequences, these protein isoforms are referred to as dCoREST-L (Long), dCoREST-M (Medium) and dCoREST-S (Short). dCoREST is expressed ubiquitously in the *Drosophila* embryo with the small isoform being found predominantly in the central nervous system (Dallman et al., 2004).

dCoREST was identified as a subunit of the LINT (dL(3)mbt interacting) complex, which encompasses the MBT domain protein dL(3)mbt as well as dLint-1, a protein that contains a PHD finger-like domain (Meier et al., 2012). LINT is thought to bind to promoters of germ-line specific genes and inhibit their expression in larval brain tissue, cultured embryonic cells and somatic cells of the *Drosophila* ovary (Janic et al., 2010; Richter et al., 2011; Meier et al., 2012; Coux et al., 2018).

Little is known about other dCoREST-containing complexes in the fruit fly. Co-immunoprecipitation experiments in a *Drosophila* cell line and adult ovaries are indicative of an assembly containing dCoREST, dLSD1, and the histone deacetylase dRPD3, which might be reminiscent of the mammalian LSD1/CoREST complex (Dallman et al., 2004; Lee & Spradling, 2014). However, the subunit composition of the *Drosophila* version of this complex and its potential for transcriptional regulation has not been investigated comprehensively.

Here, we systematically study the composition and function of dCoREST-containing complexes using an embryonic *Drosophila melanogaster* cell line as well as *in vivo* models.

3.2. Synopsis of results

We characterized dCoREST-containing protein complexes in *Drosophila melanogaster*, using cultured S2 cells as a model. These cells express the medium and long isoform of dCoREST, while dCoREST-S is not detectable (Dallman et al., 2004). Size exclusion chromatography of nuclear extracts revealed that dCoREST is not only part of the LINT complex, but also exists in other protein assemblies, some of which might only contain one of the two dCoREST isoforms, dCoREST-M or dCoREST-L (Fig. 1B). Novel dCoREST-interacting proteins were characterized using immunoaffinity purification followed by mass spectrometry. We identified the previously described interaction partners dL(3)mbt, dLint-1, dRPD3, and dLSD1 (Meier et al., 2012; Dallman et al., 2004) as well as novel factors such as dG9a (Fig. 1C-1D & Table S1). To further assign these proteins to distinct dCoREST-assemblies, we conducted a multitude of biochemical experiments. In particular, FLAG-tagged proteins (FLAG-dLSD1, FLAG-dCoREST-M, or FLAG-dCoREST-L) were overexpressed in S2 cells and immunopurified. Immunoprecipitates were analyzed by Western blot and mass spectrometry. This revealed the existence of a dLSD1 complex that contains dRPD3 and seems to specifically interact with the larger dCoREST-L isoform (Fig. 2, Fig. S1 & Table S2-S3).

Since dCoREST-L contains a 234 amino acid insertion between its two SANT-domains, which is not present in dCoREST-M (Fig. 1A), we suspected that this sequence might be responsible for the isoform-specificity observed in the dLSD1-containing complex. To address this, I used a recombinant system to study the interaction of dCoREST isoforms with dLSD1. I generated baculoviruses containing dCoREST-M, dCoREST-L, or dLSD1 coding sequences and infected Sf9 insect cells with combinations of these viral expression vectors. Western blot analysis of anti-dCoREST immunoprecipitates showed that dLSD1 associates with dCoREST-L while only a small amount of dLSD1 co-precipitates with dCoREST-M (Fig. S2). This supports the notion that the dCoREST-L-specific insert is mainly responsible for its occurrence in the

dLSD1-containing complex. Moreover, the detection of interactions in this recombinant system suggests that these might indeed occur directly between dCoREST-L and dLSD1 proteins.

The methyltransferase dG9a coprecipitated with both dCoREST isoforms (Fig. 2B), which led us to hypothesize that this protein might be distinct from the dLSD1/dCoREST complex. To identify components of a putative dG9a-containing dCoREST complex, a GFP epitope sequence was inserted at the 3' end of endogenous dG9a alleles using a CRISPR/Cas9 approach (Böttcher et al., 2014). Co-immunoprecipitation and size exclusion chromatography experiments revealed that the dG9a complex is distinct from LINT and also separates from dLSD1-containing assemblies (Fig. 3 & Fig. S4). Rather dG9a seems to form a complex with dCoREST-M and dRPD3.

Our biochemical data suggests the existence of at least three dCoREST-containing complexes that share a common dCoREST/dRPD3 deacetylation module, but differ in accessory subunits (Fig. 8):
(1) dLSD1/dCoREST complex (containing dCoREST-L, dRPD3, and dLSD1),
(2) LINT complex (containing both dCoREST isoforms, dRPD3, dLint-1, and dL(3)mbt),
(3) dG9a/dCoREST complex (containing both dCoREST isoforms, dRPD3, and dG9a).

These assemblies might, of course, contain additional proteins that were not identified in our study.

Since the three dCoREST complexes harbor various proteins with chromatin-regulatory functions (Rudolph et al., 2007; Richter et al., 2011; Meier et al., 2012; Stabell et al., 2006), we asked whether they indeed bind to chromatin and, if so, whether their genomic binding sites overlapped according to the complex compositions. Using CRISPR/Cas9-mediated GFP-tagging of endogenous proteins (Fig. S3) and anti-GFP ChIP sequencing we determined the chromatin occupancy of dCoREST and signature subunits of each complex (dLSD1, dL(3)mbt, and dG9a) in *Drosophila* S2 cells. dCoREST was found predominantly on promoters, supporting its role in transcriptional regulation (Fig. 4A). We detected a large number of dL(3)mbt binding sites (4777), 73.4% of which were also occupied by dCoREST. Fewer dLSD1 and dG9a peaks were observed (1080 and 1601, respectively). Since most of dCoREST occupied regions were also bound by dL(3)mbt (73.6%), but less were shared with dLSD1 (17.6%) or dG9a (18.6%), we hypothesized that LINT is the predominant chromatin-bound dCoREST complex in S2 cells (Fig. 4B). Only few genomic sites were shared between dL(3)mbt and dLSD1 or dL(3)mbt and dG9a, suggesting that the three dCoREST-containing complexes bind to distinct chromatin regions (Fig. 4C-D).

All dCoREST assemblies that we identified contain chromatin modifying enzymes. This suggests that they take part in the regulation of gene transcription. To address this, we compared the transcriptomes of S2 cells upon depletion of dCoREST complex subunits. Simultaneous interference with the expression of both dCoREST isoforms lead to the deregulation of 696 genes most of which seemed to be repressed by

dCoREST (668 genes, 96%). The depletion of proteins residing in the dLSD1/dCoREST and the dG9a/dCoREST assemblies had only mild effects on gene expression in hemocyte-derived S2 cells (dCoREST-L RNAi: 8 genes deregulated; dLSD1 RNAi: 18 genes deregulated; dG9a RNAi: 10 genes deregulated). However, we observed misexpression of many genes upon depletion of LINT complex components (dLint-1 RNAi: 407 genes deregulated; dL(3)mbt RNAi: 640 genes deregulated). Again, most of these genes were derepressed upon depletion of dLint-1 (373 genes, 91.6%) and dL(3)mbt (584 genes, 91.3%) and substantially overlapped with dCoREST-repressed genes (Fig. 5A-5C & Fig. S5). Functionally LINT seems to inhibit lineage-inappropriate gene expression, especially the transcription of germ line-specific genes (Fig. 5D, Fig. S6-S7; Meier et al., 2012). Taken together we show that, in S2 cells, dCoREST acts predominantly in the context of the LINT complex. This is reflected in both, its widespread chromatin occupancy as well as its function as a transcriptional regulator.

So far, our functional characterization of dCoREST was informed by studying *Drosophila* S2 cells, which are derived from embryonic hemocyte precursors. In a next step, we aimed to describe the developmental function of dCoREST complexes *in vivo* using two different examples of differentiation processes: Firstly, the differentiation of wing veins and, secondly, *Drosophila* spermatogenesis. This was approached by observing phenotypic changes in the respective organs upon RNAi-mediated depletion of dCoREST and its associated factors. We observed that loss of dCoREST leads to defects in wing vein development. However this phenotype was not recapitulated upon depletion of dLSD1, dL(3)mbt, or dG9a, suggesting that this particular function of dCoREST is not mediated by one of the complexes we identified (Fig. S8-S9).

During spermatogenesis, chromatin undergoes major structural changes. As a consequence, the *Drosophila* male reproductive system is prone to the disturbance of many chromatin regulators (Rathke et al., 2014). Depletion of dCoREST in germ cells led to male infertility. Male flies with reduced levels of dL(3)mbt, dLint-1, or dG9a were still able to generate offspring. In contrast, flies containing dLSD1-depletion constructs also exhibited an infertility phenotype (Fig. 6A & Fig. S10-S11). We concluded that dCoREST is required for male fertility and that this function can be attributed specifically to the dLSD1/dCoREST complex. LINT or dG9a/dCoREST complexes do not seem to be essential in this context. We further observed a severe reduction of mature sperm in testes of dCoREST- and dLSD1-depleted males (Fig. 6B-6C). To determine whether this developmental defect is due to altered gene expression, we analyzed the transcriptome of dCoREST- and dLSD1-depleted testes using RNA-seq. We found a large number of genes derepressed in these testes compared to controls (dCoREST RNAi: 1721; dLSD1 RNAi: 1300). On the contrary, only few genes seemed to depend on dCoREST or dLSD1 for their appropriate expression (dCoREST RNAi: 61; dLSD1 RNAi: 125).

We determined 1091 genes that were co-repressed by both, dCoREST and dLSD1, thus, defining a gene set repressed by the dLSD1/dCoREST complex in *Drosophila* testes (Fig. 7). Interestingly these genes were enriched in Gene Ontology (GO) terms associated with neuronal differentiation and function (Fig. S12).

We hypothesize that the dLSD1/dCoREST complex restricts the expression of neuronal genes in the germ line and is required for proper spermatogenesis.

3.3. Discussion

3.3.1. Cell type specificity of dCoREST-containing complexes

We have uncovered the existence of three dCoREST-containing complexes in *Drosophila melanogaster*: LINT, dLSD1/dCoREST, and dG9a/dCoREST. These assemblies all share a common deacetylase core, consisting of dRPD3 and one dCoREST isoform. The three complexes vary in accessory subunits (dL(3)mbt, dLSD1, dG9a) that convey chromatin-binding or histone-modifying activities and are believed to support the inhibition of gene expression. We found that the repression of lineage-inappropriate genes in certain cell types or tissues largely depends on one specific dCoREST-complex while being barely affected by the depletion of components from other dCoREST-complexes: S2 cells seem to be particularly sensitive to ablation of LINT complexes, while the function of male germ cells was diminished only upon depletion of dLSD1/dCoREST complex subunits. The expression levels of dLSD1 (dLSD1/dCoREST complex subunit) and dL(3)mbt (LINT complex subunit) in testis vs. S2 cells do not correlate with this selective dependency. In fact, less dLSD1 expression is detected in testes compared to S2 cells, whereas dL(3)mbt mRNA levels are higher in testes than in S2 cells (FlyAtlas, 03/2021). Moreover, we show that, at least in S2 cells, all three complexes are present, can be biochemically separated, and exist as distinct entities on chromatin. In larval brain tissue, the signature subunits of the dLSD1/dCoREST assembly are expressed (Meier et al., 2012), yet it is unclear whether they form a complex. Thus, the surprising selective requirement of certain complexes in certain cell types can not be sufficiently explained by the expression level of characteristic subunits or even by the presence of the complex as a whole. This poses the question at which level the lineage-specific function of the three assemblies is regulated.

We postulate that dCoREST-containing complexes predominantly act on chromatin. One level of lineage-specific regulation could comprise transcription factors that facilitate recruitment of defined dCoREST-complexes. These recruiters would need to act in a cell type-specific manner and be dedicated to tethering the relevant dCoREST-containing complex to its targets. Ttk88, a dCoREST-interacting transcription factor, has been suggested to be one such protein in non-neuronal tissues (Dallman et al., 2004). It remains to be determined whether Ttk88 exhibits complex-specific interactions with dCoREST and if the interaction shows lineage specificity. Our list of dCoR-

EST interactors in S2 cells (Table S1) holds additional putative transcription factors, like the CENPB-type DNA-binding protein earthbound (ebd1) which facilitates transduction of Wingless-signaling in *Drosophila* flight muscles (Benchabane et al., 2011). Determining whether ebd1 interacts with a particular dCoREST complex could shed light on a possible role of dCoREST complexes in this tissue.

Since different dCoREST complexes contain different dCoREST isoforms, regulation on the level of alternative splicing is conceivable. Only dCoREST-L is present in the dLSD1/dCoREST complex while dCoREST-M is the predominant isoform in dG9a/dCoREST and LINT (Fig. 2 & Fig. 3; Meier et al., 2012). The inclusion of exons that encode the inter-SANT linker in dCoREST-L could shift the balance of complexes towards dLSD1/dCoREST. Likewise, skipping of these exons produces comparatively more dCoREST-M protein, possibly resulting in increased formation of LINT and dG9a/dCoREST complexes. This scenario, of course, relies on the premise that the amount of the other dCoREST-complex subunits is not limiting. It is worth noting that disturbing the ratio of dCoREST-L to dCoREST-M can also lead to unusual complex compositions: For instance, high exogenous overexpression of dCoREST-L in S2 cells led to its inclusion in the LINT complex. In this example, even dLSD1 was detected in LINT-specific fractions after two-step ion exchange chromatography (Mačinković, unpublished observation). It is unclear whether the expression levels achieved in this experimental setup reflect observable splicing equilibria in any fly tissue. However, it highlights that there might be a certain fluidity regarding the composition of dCoREST-containing complexes that may be influenced by the relative levels of dCoREST isoforms (Meier & Brehm, 2014).

Protein-protein interactions can be modulated by covalent modifications of crucial amino acid residues. For instance, human LSD1 is dimethylated at Lysin 114 (K114me2) which triggers its interaction with CHD1 (Metzger et al., 2016). This modification does not influence the association with CoREST1 and, moreover, Lysin 114 is not conserved in the *Drosophila* LSD1 homolog. However, this example highlights the paradigm of interactions that depend on post-translational modifications. I used the iProteinDB database (Hu et al., 2019) to predict residues in dCoREST-M and dCoREST-L that might potentially be covalently modified. Multiple putative phosphorylation sites were identified and most of them are located within the first 80 amino acids of the dCoREST N-terminus which is common to all dCoREST isoforms (data not shown). Characterizing different modification patterns of dCoREST and its associated factors in testis and S2 cells would be an interesting starting point to address the relevance of post-translational modifications in dCoREST complex assembly.

3.3.2. Significance of dCoREST as subunit of chromatin-modifying complexes

There seems to be a remarkable dichotomy of dCoREST-containing complexes in gene regulation: LINT represses germ line-specific genes in larval brain tissue (Janic et al., 2010; Meier et al., 2012), whereas dLSD1/dCoREST inhibits expression of neuronal genes in testis (Fig. 6, Fig. 7 & Fig. S12). Although dCoREST is present in both cell types, it permits the transcription of lineage-appropriate genes in one case while repressing these gene sets when they are deemed lineage-inappropriate. Despite the need for tissue specific regulation, which has been discussed above, this juxtaposition accentuates that the observed dCoREST function is largely dependent on its interacting factors. This evokes the idea that dCoREST might acts as a scaffold onto which enzyme complexes can assemble.

Besides merely providing interaction surfaces, two regions of dCoREST have the potential to enhance the activity of its associated enzymes. Mammalian ELM2-SANT1 tandem domains interact with class I HDACs and are required to stimulate the deacetylation reaction (Millard et al., 2013). Since we find the *Drosophila* HDAC1/2 homolog dRPD3 in all three dCoREST complexes, it is conceivable that one task of dCoREST is to keep dRPD3 in an active state. It would be interesting to assess whether genes that require dCoREST for their repression also depend on dRPD3 activity. A region of human CoREST1 that includes the second SANT domain and the inter-SANT linker contacts LSD1 and directs its demethylation activity towards nucleosomes (Yang et al., 2006). While free LSD1 is active on histone octamers, it is only able to demethylate nucleosomes in complex with CoREST (Shi et al., 2005). The domain that binds to human LSD1 is conserved in dCoREST-L but not in dCoREST-M which might explain why we do not find dLSD1 in complexes that contain only minor amounts of the longer dCoREST isoform (Fig. 2, Fig. S2 & Fig. S13; Meier et al., 2012).

Related to its stimulatory impact on enzyme activity, CoREST may also serve as a bridging factor that stabilizes catalytic protein complexes on their substrates. Recent structural studies have addressed the positioning of the LSD1/CoREST complex on the nucleosome with surprising discrepancies: One structure reveals the catalytic domain of LSD1 close to the nucleosome core with the CoREST SANT2 domain and HDAC1 in a rather distant position (Song et al., 2020). The second study finds the LSD1 amine oxidase domain mostly engaged with extranucleosomal DNA while observing the LSD1 tower and CoREST SANT2 domains in direct contact with histones and nucleosomal DNA (Kim et al., 2020). The latter observation especially highlights the importance of CoREST in mediating the interaction with the nucleosome. Although mammalian CoREST1 is particularly reminiscent of dCoREST-L (Fig. S13), the SANT2 domain is also found in dCoREST-M. It is therefore possible that this isoform might contribute to positioning LINT and dG9a/dCoREST complexes on nucleosomal substrates.

3.4. Contribution statement

I have made the following contributions to this project:

- Generation of baculoviruses harboring dCoREST-M, dCoREST-L and dLSD1 cDNA (Fig. S2)
- Recombinant expression of proteins in Sf9 cells using baculoviral infection (Fig. S2)
- Execution of immunoprecipitation and Western blot experiments (Fig. S2)
- Establishment of an endogenous tagging protocol in *Drosophila* S2 cells using CRISPR/Cas9
- Establishment of a ChIP-seq protocol using anti-GFP Nano-Trap resin

4. SUMMARY

In this thesis I am addressing the function of two transcriptional cofactors (U-shaped and dCoREST) and their interplay with epigenetic modifiers to regulate lineage-specific gene expression.

Firstly, I shed light on the molecular functions of the hemocyte regulator U-shaped. I provide genome wide data supporting that Ush binds to regulatory elements and that it regulates the expression of a large number of genes including factors implicated in hemocyte function, cell cycle, and lipid metabolism. Ush maintains the proliferative capacity of embryonic hemocyte precursors. I show that different isoforms of Ush are expressed in *Drosophila* S2 cells and that one of them interacts with the dMi-2/dNuRD complex using a conserved N-terminal peptide. Indeed, Ush and dMi-2 cooccupy many genomic sites. While being dispensable for the regulation of genes implicated in cell cycle and lipid metabolism, dMi-2 is required specifically for the repression of hemocyte-related genes. Moreover, Ush and dNuRD coregulate enhancer activity in larval lymph glands and cooperate in repressing hemocyte differentiation *in vivo*.

Secondly, I and my coworkers identify protein complexes containing the transcriptional corepressor dCoREST. We show that dCoREST exists in at least three complexes: LINT, dLSD1/dCoREST, and dG9a/dCoREST. Each of these assemblies is composed of a shared histone deacetylase core that contains dRPD3 and one or more dCoREST isoforms alongside complex-specific regulatory subunits. Genome wide transcriptomics led us to conclude that different complexes exert lineage-specific functions: While LINT is required for the repression of germ line-specific genes in a hemocyte progenitor cell line, the dLSD1/dCoREST complex inhibits the transcription of neuronal genes in the *Drosophila* germ line.

Taken together, this study adds to the notion that the regulatory capacity of ubiquitous chromatin modifiers can be narrowed down to specific lineages by engaging with lineage-specific transcriptional cofactors, their isoforms, and distinct complexes.

5. ZUSAMMENFASSUNG

In der vorliegenden Arbeit befasse ich mich mit der Rolle zweier transkriptioneller Kofaktoren (U-shaped und dCoREST) und wie deren Zusammenspiel mit epigenetischen Regulatoren gewebespezifische Genexpression beeinflusst.

Zunächst beleuchte ich die molekulare Funktionsweise des Hämozyten-spezifischen Proteins U-shaped. Meine genomweiten Daten lassen darauf schließen, dass Ush an regulatorische Elemente bindet und die Expression einer Vielzahl von Genen reguliert. Darunter befinden sich insbesondere Faktoren, die bei der Funktion von Hämozyten, während des Zellzyklus oder im Fettstoffwechsel eine wichtige Rolle spielen. Tatsächlich erhält Ush das proliferative Potential von embryonalen Blut-Vorläuferzellen aufrecht. Ich weise die Expression mehrerer U-shaped-Isoformen in *Drosophila* S2 Zellen nach und zeige, dass eine bestimmte Isoform mit dem dMi-2/dNuRD-Komplex mittels eines konservierten, N-terminalen Peptids interagiert. In der Tat kolokalisieren Ush und dMi-2 an vielen Stellen im Genom. Während dMi-2 nicht an der Regulation von Zellzyklus- und Fettstoffwechsel-Genen beteiligt ist, wird es insbesondere für die Repression von Hämozyten-spezifischen Genen benötigt. Darüberhinaus koregulieren Ush und dNuRD die Aktivität eines Enhancers in Lymphdrüsen von *Drosophila* Larven und inhibieren gemeinsam die Differenzierung von Hämozyten.

Des Weiteren identifizieren wir Proteinkomplexe, die den transkriptionellen Korepressor dCoREST enthalten. Wir weisen die Existenz dreier dCoREST-enthaltender Komplexe nach: LINT, dLSD1/dCoREST und dG9a/dCoREST. Diese bestehen aus einem gemeinsamen Histondeacetylase Kernmodul, welches dRPD3 und eine oder mehrere dCoREST-Isoformen enthält. Jeder Komplex beinhaltet außerdem spezifische regulatorische Untereinheiten. Unsere genomweiten Transkriptomanalysen lassen auf gewebespezifische Funktionen der verschiedenen Komplexe schließen: Während LINT die Repression von Keimbahn-spezifischen Genen in einer Hämozyten-Vorläuferzellinie veranlasst, hemmt der dLSD1/dCoREST-Komplex die Transkription neuronaler Gene in der *Drosophila* Keimbahn.

Zusammenfassend unterstützt diese Arbeit die Auffassung, dass die regulative Kapazität ubiquitärer Chromatin-Regulatoren in verschiedenen Zelltypen durch zwei verschiedene Mechanismen gesteuert werden kann: Erstens, durch die Ausbildung von Proteinkomplexen mit unterschiedlicher Zusammensetzung und Funktion sowie, zweitens, durch die Interaktion mit gewebespezifischen transkriptionellen Kofaktoren und deren Isoformen.

6. REFERENCES

Ahmad, S. M., Tansey, T. R., Busser, B. W., Nolte, M. T., Jeffries, N., Gisselbrecht, S. S., Rusan, N. M., & Michelson, A. M. (**2012**). Two Forkhead Transcription Factors Regulate the Division of Cardiac Progenitor Cells by a Polo-Dependent Pathway. *Developmental Cell*, 23(1), 97–111. https://doi.org/10.1016/j.devcel.2012.05.011

Andrés, M. E., Burger, C., Peral-Rubio, M. J., Battaglioli, E., Anderson, M. E., Grimes, J., Dallman, J., Ballas, N., & Mandel, G. (**1999**). CoREST: A functional corepressor required for regulation of neural- specific gene expression. *Proceedings of the National Academy of Sciences of the United States of America*, 96(17), 9873–9878. https://doi.org/10.1073/pnas.96.17.9873

Baldeosingh, R., Gao, H., Wu, X., & Fossett, N. (**2018**). Hedgehog signaling from the Posterior Signaling Center maintains U-shaped expression and a prohemocyte population in Drosophila. *Developmental Biology*, 441(1), 132–145. https://doi.org/10.1016/j.ydbio.2018.06.020

Bannister, A. J., & Kouzarides, T. (**2011**). Regulation of chromatin by histone modifications. *Cell Research*, 21(3), 381–395. https://doi.org/10.1038/cr.2011.22

Barrios, A. P., Gómez, A. V., Sáez, J. E., Ciossani, G., Toffolo, E., Battaglioli, E., Mattevi, A., & Andrés, M. E. (**2014**). Differential Properties of Transcriptional Complexes Formed by the CoREST Family. *Molecular and Cellular Biology*, 34(14), 2760–2770. https://doi.org/10.1128/mcb.00083-14

Basta, J., & Rauchman, M. (**2015**). The nucleosome remodeling and deacetylase complex in development and disease. *Translational Research*, 165(1), 36–47. https://doi.org/10.1016/j.trsl.2014.05.003

Battaglioli, E., Andrés, M. E., Rose, D. W., Chenoweth, J. G., Rosenfeld, M. G., Anderson, M. E., & Mandel, G. (**2002**). Rest repression of neuronal genes requires components of the hSWI·SNF complex. *Journal of Biological Chemistry*, 277(43), 41038–41045. https://doi.org/10.1074/jbc.M205691200

Benchabane, H., Xin, N., Tian, A., Hafler, B. P., Nguyen, K., Ahmed, A., & Ahmed, Y. (**2011**). Jerky/Earthbound facilitates cell-specific Wnt/Wingless signalling by modulating β-catenin-TCF activity. *EMBO Journal*, 30(8), 1444–1458. https://doi.org/10.1038/emboj.2011.67

Böttcher, R., Hollmann, M., Merk, K., Nitschko, V., Obermaier, C., Philippou-Massier, J., Wieland, I., Gaul, U., & Förstemann, K. (**2014**). Efficient chromosomal gene modification with CRISPR/cas9 and PCR-based homologous recombination donors in cultured Drosophila cells. *Nucleic Acids Research*, 42(11). https://doi.org/10.1093/nar/gku289

Boyer, L. A., Latek, R. R., & Peterson, C. L. (**2004**). The SANT domain: A unique histone-tail-binding module? *Nature Reviews Molecular Cell Biology*, 5(2), 158–163. https://doi.org/10.1038/nrm1314

Burgold, T., Barber, M., Kloet, S., Cramard, J., Gharbi, S., Floyd, R., Kinoshita, M., Ralser, M., Vermeulen, M., Reynolds, N., Dietmann, S., & Hendrich, B. (**2019**). The Nucleosome Remodelling and Deacetylation complex suppresses transcriptional noise during lineage commitment. *The EMBO Journal*, 38(12), 1–18. https://doi.org/10.15252/embj.2018100788

Cattenoz, P. B., Sakr, R., Pavlidaki, A., Delaporte, C., Riba, A., Molina, N., Hariharan, N., Mukherjee, T., & Giangrande, A. (**2020**). Temporal specificity and heterogeneity of Drosophila immune cells . *The EMBO Journal*, 39(12), 1–25. https://doi.org/10.15252/embj.2020104486

Chlon, T. M., & Crispino, J. D. (**2012**). Combinatorial regulation of tissue specification by GATA and FOG factors. *Development (Cambridge)*, 139(21), 3905–3916. https://doi.org/10.1242/dev.080440

Cho, B., Yoon, S. H., Lee, D., Koranteng, F., Tattikota, S. G., Cha, N., Shin, M., Do, H., Hu, Y., Oh, S. Y., Lee, D., Vipin Menon, A., Moon, S. J., Perrimon, N., Nam, J. W., & Shim, J. (**2020**). Single-cell transcriptome maps of myeloid blood cell lineages in Drosophila. *Nature Communications*, 11(1). https://doi.org/10.1038/s41467-020-18135-y

Clapier, C. R., Iwasa, J., Cairns, B. R., & Peterson, C. L. (**2017**). Mechanisms of action and regulation of ATP-dependent chromatin-remodelling complexes. *Nature Reviews Molecular Cell Biology*, 18(7), 407–422. https://doi.org/10.1038/nrm.2017.26

Conomos, D., Reddel, R. R., & Pickett, H. A. (**2014**). NuRD-ZNF827 recruitment to telomeres creates a molecular scaffold for homologous recombination. *Nature Structural and Molecular Biology*, 21(9), 760–770. https://doi.org/10.1038/nsmb.2877

Coux, R. X., Teixeira, F. K., & Lehmann, R. (**2018**). L(3)mbt and the LINT complex safeguard cellular identity in the Drosophila ovary. *Development (Cambridge)*, 145(7). https://doi.org/10.1242/dev.160721

Cubadda, Y., Heitzler, P., Ray, R. P., Bourouis, M., Ramain, P., Gelbart, W., Simpson, P., & Haenlin, M. (**1997**). u-shaped encodes a zinc finger protein that regulates the proneural genes achaete and scute during the formation of bristles in Drosophila. *Genes and Development*, 11(22), 3083–3095. https://doi.org/10.1101/gad.11.22.3083

Dale, R. M., Remo, B. F., & Svensson, E. C. (**2007**). An alternative transcript of the FOG-2 gene encodes a FOG-2 isoform lacking the FOG repression motif. *Biochemical and Biophysical Research Communications*, 357(3), 683–687. https://doi.org/10.1016/j.bbrc.2007.04.008

Dallman, J. E., Allopenna, J., Bassett, A., Travers, A., & Mandell, G. (**2004**). A conserved role but different partners for the transcriptional corepressor CoREST in fly and mammalian nervous system formation. *Journal of Neuroscience*, 24(32), 7186–7193. https://doi.org/10.1523/JNEUROSCI.0238-04.2004

De Dieuleveult, M., Yen, K., Hmitou, I., Depaux, A., Boussouar, F., Dargham, D. B., Jounier, S., Humbertclaude, H., Ribierre, F., Baulard, C., Farrell, N. P., Park, B., Keime, C., Carrière, L., Berlivet, S., Gut, M., Gut, I., Werner, M., Deleuze, J. F., … Gérard, M. (**2016**). Genome-wide nucleosome specificity and function of chromatin remodellers in ES cells. *Nature*, 530(7588), 113–116. https://doi.org/10.1038/nature16505

Denslow, S. A., & Wade, P. A. (**2007**). The human Mi-2/NuRD complex and gene regulation. *Oncogene*, 26(37), 5433–5438. https://doi.org/10.1038/sj.onc.1210611

Dubuissez, M., Loison, I., Paget, S., Vorng, H., Ait-Yahia, S., Rohr, O., Tsicopoulos, A., & Leprince, D. (**2016**). Protein Kinase C-Mediated Phosphorylation of BCL11B at Serine 2 Negatively Regulates Its Interaction with NuRD Complexes during CD4 + T-Cell Activation. *Molecular and Cellular Biology*, 36(13), 1881–1898. https://doi.org/10.1128/mcb.00062-16

Fossett, N., Zhang, Q., Gajewski, K., Choi, C. Y., Kim, Y., & Schulz, R. A. (**2000**). The multitype zinc-finger protein U-shaped functions in heart cell specification in the Drosophila embryo. *Proceedings of the National Academy of Sciences of the United States of America*, 97(13), 7348–7353. https://doi.org/10.1073/pnas.97.13.7348

Fossett, N., Tevosian, S. G., Gajewski, K., Zhang, Q., Orkin, S. H., & Schulz, R. A. (**2001a**). The friend of GATA proteins U-shaped, FOG-1, and FOG-2 function as negative regulators of blood, heart, and eye development in Drosophila. *Proceedings of the National Academy of Sciences of the United States of America*, 98(13), 7342–7347. https://doi.org/10.1073/pnas.131215798

Fossett, N., & Schulz, R. A. (**2001b**). Conserved cardiogenic functions of the multitype zinc-finger proteins: U-shaped and FOG-2. *Trends in Cardiovascular Medicine*, 11(5), 185–190. https://doi.org/10.1016/S1050-1738(01)00092-5

Fossett, N. (**2013**). Signal transduction pathways, intrinsic regulators, and the control of cell fate choice. *Biochimica et Biophysica Acta - General Subjects*, 1830(2), 2375–2384. https://doi.org/10.1016/j.bbagen.2012.06.005

Fu, Y., Huang, X., Zhang, P., van de Leemput, J., & Han, Z. (**2020**). Single-cell RNA sequencing identifies novel cell types in Drosophila blood. *Journal of Genetics and Genomics*, 47(4), 175–186. https://doi.org/10.1016/j.jgg.2020.02.004

Gao, H., Wu, X., & Fossett, N. (**2009**). Upregulation of the Drosophila Friend of GATA Gene u-shaped by JAK/STAT Signaling Maintains Lymph Gland Prohemocyte Potency. *Molecular and Cellular Biology*, 29(22), 6086–6096. https://doi.org/10.1128/mcb.00244-09

Gao, Z., Huang, Z., Olivey, H. E., Gurbuxani, S., Crispino, J. D., & Svensson, E. C. (**2010**). FOG-1-mediated recruitment of NuRD is required for cell lineage re-enforcement during haematopoiesis. *EMBO Journal*, 29(2), 457–468. https://doi.org/10.1038/emboj.2009.368

Gao, H., Wu, X., & Fossett, N. (**2013**). Drosophila E-Cadherin Functions in Hematopoietic Progenitors to Maintain Multipotency and Block Differentiation. *PLoS ONE*, 8(9). https://doi.org/10.1371/journal.pone.0074684

Gao, H., Baldeosingh, R., Wu, X., & Fossett, N. (**2016**). The friend of GATA transcriptional co-regulator, U-shaped, is a downstream antagonist of dorsal-driven prohemocyte differentiation in Drosophila. *PLoS ONE*, 11(5), 1–24. https://doi.org/10.1371/journal.pone.0155372

Gold, K. S., & Brückner, K. (**2014**). Drosophila as a model for the two myeloid blood cell systems in vertebrates. *Experimental Hematology*, 42(8), 717–727. https://doi.org/10.1016/j.exphem.2014.06.002

Goupille, O., Penglong, T., Kadri, Z., Granger-Locatelli, M., Denis, R., Luquet, S., Badoual, C., Fucharoen, S., Maouche-Chrétien, L., Leboulch, P., & Chrétien, S. (**2017**). The LXCXE Retinoblastoma Protein-Binding Motif of FOG-2 Regulates Adipogenesis. *Cell Reports*, 21(12), 3524–3535. https://doi.org/10.1016/j.celrep.2017.11.098

Greenberg, M. V. C., & Bourc'his, D. (**2019**). The diverse roles of DNA methylation in mammalian development and disease. *Nature Reviews Molecular Cell Biology*, 20(10), 590–607. https://doi.org/10.1038/s41580-019-0159-6

Grigorian, M., Mandal, L., & Hartenstein, V. (**2011**). Hematopoiesis at the onset of metamorphosis: Terminal differentiation and dissociation of the Drosophila lymph gland. *Development Genes and Evolution*, 221(3), 121–131. https://doi.org/10.1007/s00427-011-0364-6

Guruharsha, K. G., Rual, J. F., Zhai, B., Mintseris, J., Vaidya, P., Vaidya, N., Beekman, C., Wong, C., Rhee, D. Y., Cenaj, O., McKillip, E., Shah, S., Stapleton, M., Wan, K. H., Yu, C., Parsa, B., Carlson, J. W., Chen, X., Kapadia, B., … Artavanis-Tsakonas, S. (**2011**). A protein complex network of Drosophila melanogaster. *Cell*, 147(3), 690–703. https://doi.org/10.1016/j.cell.2011.08.047

Haenlin, M., Cubadda, Y., Blondeau, F., Heitzler, P., Lutz, Y., Simpson, P., & Ramain, P. (**1997**). Transcriptional activity of Pannier is regulated negatively by heterodimerization of the GATA DNA-binding domain with a cofactor encoded by the u-shaped gene of Drosophila. *Genes and Development*, 11(22), 3096–3108. https://doi.org/10.1101/gad.11.22.3096

Hakimi, M. A., Bochar, D. A., Chenoweth, J., Lane, W. S., Mandel, G., & Shiekhattar, R. (**2002**). A core-BRAF35 complex containing histone deacetylase mediates repression of neuronal-specific genes. *Proceedings of the National Academy of Sciences of the United States of America*, 99(11), 7420–7425. https://doi.org/10.1073/pnas.112008599

Henikoff, S., & Smith, M. M. (**2015**). Histone variants and epigenetics. *Cold Spring Harbor Perspectives in Biology*, 7(1). https://doi.org/10.1101/cshperspect.a019364

Hong, W., Nakazawa, M., Chen, Y. Y., Kori, R., Vakoc, C. R., Rakowski, C., & Blobel, G. A. (**2005**). FOG-1 recruits the NuRD repressor complex to mediate transcriptional repression by GATA-1. *EMBO Journal*, 24(13), 2367–2378. https://doi.org/10.1038/sj.emboj.7600703

Hota, S. K., & Bruneau, B. G. (**2016**). ATP-dependent chromatin remodeling during mammalian development. *Development (Cambridge)*, 143(16), 2882–2897. https://doi.org/10.1242/dev.128892

Hu, Y., Sopko, R., Chung, V., Foos, M., Studer, R. A., Landry, S. D., Liu, D., Rabinow, L., Gnad, F., Beltrao, P., & Perrimon, N. (**2019**). IProteinDB: An integrative database of drosophila post-translational modifications. *G3: Genes, Genomes, Genetics*, 9(1), 1–11. https://doi.org/10.1534/g3.118.200637

Humphrey, G. W., Wang, Y., Russanova, V. R., Hirai, T., Qin, J., Nakatani, Y., & Howard, B. H. (**2001**). Stable Histone Deacetylase Complexes Distinguished by the Presence of SANT Domain Proteins CoREST/kiaa0071 and Mta-L1. J*ournal of Biological Chemistry*, 276(9), 6817–6824. https://doi.org/10.1074/jbc.M007372200

Huot, G., Vernier, M., Bourdeau, V., Doucet, L., Saint-Germain, E., Gaumont-Leclerc, M. F., Moro, A., & Ferbeyre, G. (**2014**). CHES1/FOXN3 regulates cell proliferation by repressing PIM2 and protein biosynthesis. *Molecular Biology of the Cell*, 25(5), 554–565. https://doi.org/10.1091/mbc.E13-02-0110

Janic, A., Mendizabal, L., Llamazares, S., Rossell, D., & Gonzalez, C. (**2010**). Ectopic expression of germline genes drives malignant brain tumor growth in Drosophila. *Science*, 330(6012), 1824–1827. https://doi.org/10.1126/science.1195481

Jung, S. H., Evans, C. J., Uemura, C., & Banerjee, U. (**2005**). The Drosophila lymph gland as a developmental model of hematopoiesis. *Development*, 132(11), 2521–2533. https://doi.org/10.1242/dev.01837

Kadri, Z., Shimizu, R., Ohneda, O., Maouche-Chretien, L., Gisselbrecht, S., Yamamoto, M., Romeo, P. H., Leboulch, P., & Chretien, S. (**2009**). Direct binding of pRb/E2F-2 to GATA-1 regulates maturation and terminal cell division during erythropoiesis. *PLoS Biology*, 7(6). https://doi.org/10.1371/journal.pbio.1000123

Kadri, Z., Lefevre, C., Goupille, O., Penglong, T., Granger-Locatelli, M., Fucharoen, S., Maouche-Chretien, L., Leboulch, P., & Chretien, S. (**2015**). Erythropoietin and IGF-1 signaling synchronize cell proliferation and maturation during erythropoiesis. *Genes and Development*, 29(24), 2603–2616. https://doi.org/10.1101/gad.267633.115

Kashiwagi, M., Morgan, B. A., & Georgopoulos, K. (**2007**). The chromatin remodeler Mi-2β is required for establishment of the basal epidermis and normal differentiation of its progeny. *Development*, 134(8), 1571–1582. https://doi.org/10.1242/dev.001750

Kato, H., & Igarashi, K. (**2019**). To be red or white: Lineage commitment and maintenance of the hematopoietic system by the “inner myeloid.” *Haematologica*, 104(10), 1919–1927. https://doi.org/10.3324/haematol.2019.216861

Kim, J., Lu, C., Srinivasan, S., Awe, S., Brehm, A., & Fuller, M. T. (**2017**). Cell fate: Blocking promiscuous activation at cryptic promoters directs cell type-specific gene expression. *Science*, 356(6339), 717–721. https://doi.org/10.1126/science.aal3096

Kim, S. A., Zhu, J., Yennawar, N., Eek, P., & Tan, S. (**2020**). Crystal Structure of the LSD1/CoREST Histone Demethylase Bound to Its Nucleosome Substrate. *Molecular Cell*, 78(5), 903-914.e4. https://doi.org/10.1016/j.molcel.2020.04.019

Kim-Jo, C., Gatti, J. L., & Poirié, M. (**2019**). Drosophila cellular immunity against parasitoid wasps: A complex and time-dependent process. *Frontiers in Physiology*, 10(MAY). https://doi.org/10.3389/fphys.2019.00603

Kloet, S. L., Karemaker, I. D., van Voorthuijsen, L., Lindeboom, R. G. H., Baltissen, M. P., Edupuganti, R. R., Poramba-Liyanage, D. W., Jansen, P. W. T. C., & Vermeulen, M. (**2018**). NuRD-interacting protein ZFP296 regulates genome-wide NuRD localization and differentiation of mouse embryonic stem cells. *Nature Communications*, 9(1), 1–11. https://doi.org/10.1038/s41467-018-07063-7

Krattinger, A., Gendre, N., Ramaekers, A., Grillenzoni, N., & Stocker, R. F. (**2007**). DmOAZ, the unique Drosophila melanogaster OAZ homologue is involved in posterior spiracle development. Development Genes and Evolution, 217(3), 197–208. https://doi.org/10.1007/s00427-007-0134-7

Kreher, J., Kovač, K., Bouazoune, K., MačInković, I., Ernst, A. L., Engelen, E., Pahl, R., Finkernagel, F., Murawska, M., Ullah, I., & Brehm, A. (**2017**). EcR recruits dMi-2 and increases efficiency of dMi-2-mediated remodelling to constrain transcription of hormone-regulated genes. *Nature Communications*, 8(May 2016). https://doi.org/10.1038/ncomms14806

Lai, A. Y., & Wade, P. A. (**2011**). Cancer biology and NuRD: A multifaceted chromatin remodelling complex. *Nature Reviews Cancer*, 11(8), 588–596. https://doi.org/10.1038/nrc3091

Lakowski, B., Roelens, I., & Jacob, S. (**2006**). CoREST-like complexes regulate chromatin modification and neuronal gene expression. *Journal of Molecular Neuroscience*, 29(3), 227–239. https://doi.org/10.1385/JMN:29:3:227

Lawrence, M., Daujat, S., & Schneider, R. (**2016**). Lateral Thinking: How Histone Modifications Regulate Gene Expression. *Trends in Genetics*, 32(1), 42–56. https://doi.org/10.1016/j.tig.2015.10.007

Lebestky, T., Chang, T., Hartenstein, V., & Banerjee, U. (**2000**). Specification of Drosophila hematopoietic lineage by conserved transcription factors. *Science*, 288(5463), 146–149. https://doi.org/10.1126/science.288.5463.146

Lee, M. G., Wynder, C., Cooch, N., & Shiekhattar, R. (**2005**). An essential role for CoREST in nucleosomal histone 3 lysine 4 demethylation. *Nature*, 437(7057), 432–435. https://doi.org/10.1038/nature04021

Lee, M. C., & Spradling, A. C. (**2014**). The progenitor state is maintained by lysine-specific demethylase 1-mediated epigenetic plasticity during drosophila follicle cell development. *Genes and Development*, 28(24), 2739–2749. https://doi.org/10.1101/gad.252692.114

Lejon, S., Thong, S. Y., Murthy, A., AlQarni, S., Murzina, N. V., Blobel, G. A., Laue, E. D., & Mackay, J. P. (**2011**). Insights into association of the NuRD complex with FOG-1 from the crystal structure of an RbAp48·FOG-1 complex. *Journal of Biological Chemistry*, 286(2), 1196–1203. https://doi.org/10.1074/jbc.M110.195842

Letourneau, M., Lapraz, F., Sharma, A., Vanzo, N., Waltzer, L., & Crozatier, M. (**2016**). Drosophila hematopoiesis under normal conditions and in response to immune stress. *FEBS Letters*, 590(22), 4034–4051. https://doi.org/10.1002/1873-3468.12327

Li, G., & Reinberg, D. (**2011**). Chromatin higher-order structures and gene regulation. *Current Opinion in Genetics and Development*, 21(2), 175–186. https://doi.org/10.1016/j.gde.2011.01.022

Liao, D. (**2009**). Emerging roles of the EBF family of transcription factors in tumor suppression. *Molecular Cancer Research*, 7(12), 1893–1901. https://doi.org/10.1158/1541-7786.MCR-09-0229

Lin, A. C., Roche, A. E., Wilk, J., & Svensson, E. C. (**2004**). The N termini of Friend of GATA (FOG) proteins define a novel transcriptional repression motif and a superfamily of transcriptional repressors. *Journal of Biological Chemistry*, 279(53), 55017–55023. https://doi.org/10.1074/jbc.M411240200

Loughran, S. J., Comoglio, F., Hamey, F. K., Giustacchini, A., Errami, Y., Earp, E., Göttgens, B., Jacobsen, S. E. W., Mead, A. J., Hendrich, B., & Green, A. R. (**2017**). Mbd3/NuRD controls lymphoid cell fate and inhibits tumorigenesis by repressing a B cell transcriptional program. *Journal of Experimental Medicine*, 214(10), 3085–3104. https://doi.org/10.1084/jem.20161827

Love, P. E., Warzecha, C., & Li, L. Q. (**2014**). Ldb1 complexes: The new master regulators of erythroid gene transcription. *Trends in Genetics*, 30(1), 1–9. https://doi.org/10.1016/j.tig.2013.10.001

Lu, D. (**2013**). Epigenetic modification enzymes: catalytic mechanisms and inhibitors. *Acta Pharmaceutica Sinica B*, 3(3), 141–149. https://doi.org/10.1016/j.apsb.2013.04.007

Luger, K., Mäder, A. W., Richmond, R. K., Sargent, D. F., & Richmond, T. J. (**1997**). Crystal structure of the nucleosome core particle at 2.8 Å resolution. *Nature*, 389(6648), 251–260. https://doi.org/10.1038/38444

Lunyak, V. V., Burgess, R., Prefontaine, G. G., Nelson, C., Sze, S. H., Chenoweth, J., Schwartz, P., Pevzner, P. A., Glass, C., Mandel, G., & Rosenfeld, M. G. (**2002**). Corepressor-dependent silencing of chromosomal regions encoding neuronal genes. *Science*, 298(5599), 1747–1752. https://doi.org/10.1126/science.1076469

Maksour, S., Ooi, L., & Dottori, M. (**2020**). More than a corepressor: The role of corest proteins in neurodevelopment. *ENeuro*, 7(2). https://doi.org/10.1523/ENEURO.0337-19.2020

Mandal, L., Martinez-Agosto, J. A., Evans, C. J., Hartenstein, V., & Banerjee, U. (**2007**). A Hedgehog- and Antennapedia-dependent niche maintains Drosophila haematopoietic precursors. *Nature*, 446(7133), 320–324. https://doi.org/10.1038/nature05585

Marmorstein, R., & Trievel, R. C. (**2009**). Histone modifying enzymes: Structures, mechanisms, and specificities. *Biochimica et Biophysica Acta - Gene Regulatory Mechanisms*, 1789(1), 58–68. https://doi.org/10.1016/j.bbagrm.2008.07.009

Meier, K., Mathieu, E. L., Finkernagel, F., Reuter, L. M., Scharfe, M., Doehlemann, G., Jarek, M., & Brehm, A. (**2012**). LINT, a novel dL(3)mbt-containing complex, represses malignant brain tumour signature genes. *PLoS Genetics*, 8(5). https://doi.org/10.1371/journal.pgen.1002676

Meier, K., & Brehm, A. (**2014**). Chromatin regulation: How complex does it get? *Epigenetics*, 9(11), 1485–1495. https://doi.org/10.4161/15592294.2014.971580

Metzger, E., Willmann, D., McMillan, J., Forne, I., Metzger, P., Gerhardt, S., Petroll, K., Von Maessenhausen, A., Urban, S., Schott, A. K., Espejo, A., Eberlin, A., Wohlwend, D., Schüle, K. M., Schleicher, M., Perner, S., Bedford, M. T., Jung, M., Dengjel, J., … Schüle, R. (**2016**). Assembly of methylated KDM1A and CHD1 drives androgen receptor-dependent transcription and translocation. *Nature Structural and Molecular Biology*, 23(2), 132–139. https://doi.org/10.1038/nsmb.3153

Miccio, A., Wang, Y., Hong, W., Gregory, G. D., Wang, H., Yu, X., Choi, J. K., Shelat, S., Tong, W., Poncz, M., & Blobel, G. A. (**2010**). NuRD mediates activating and repressive functions of GATA-1 and FOG-1 during blood development. *EMBO Journal*, 29(2), 442–456. https://doi.org/10.1038/emboj.2009.336

Michael, A. K., & Thomä, N. H. (**2021**). Reading the chromatinized genome. *Cell*, 1–13. https://doi.org/10.1016/j.cell.2021.05.029

Millard, C. J., Watson, P. J., Celardo, I., Gordiyenko, Y., Cowley, S. M., Robinson, C. V., Fairall, L., & Schwabe, J. W. R. (**2013**). Class I HDACs share a common mechanism of regulation by inositol phosphates. *Molecular Cell*, 51(1), 57–67. https://doi.org/10.1016/j.molcel.2013.05.020

Miller, A., Ralser, M., Kloet, S. L., Loos, R., Nishinakamura, R., Bertone, P., Vermeulen, M., & Hendrich, B. (**2016**). Sall4 controls differentiation of pluripotent cells independently of the nucleosome remodelling and deacetylation (NuRD) complex. *Development (Cambridge)*, 143(17), 3074–3084. https://doi.org/10.1242/dev.139113

Morgan, M. A. J., & Shilatifard, A. (**2020**). Reevaluating the roles of histone-modifying enzymes and their associated chromatin modifications in transcriptional regulation. *Nature Genetics*, 52(12), 1271–1281. https://doi.org/10.1038/s41588-020-00736-4

Mulligan, P., Yang, F., Di Stefano, L., Ji, J. Y., Ouyang, J., Nishikawa, J. L., Toiber, D., Kulkarni, M., Wang, Q., Najafi-Shoushtari, S. H., Mostoslavsky, R., Gygi, S. P., Gill, G., Dyson, N. J., & Näär, A. M. (**2011**). A SIRT1-LSD1 Corepressor Complex Regulates Notch Target Gene Expression and Development. *Molecular Cell*, 42(5), 689–699. https://doi.org/10.1016/j.molcel.2011.04.020

Muratoglu, S., Garratt, B., Hyman, K., Gajewski, K., Schulz, R. A., & Fossett, N. (**2006**). Regulation of Drosophila Friend of GATA gene, u-shaped, during hematopoiesis: A direct role for Serpent and Lozenge. *Developmental Biology*, 296(2), 561–579. https://doi.org/10.1016/j.ydbio.2006.04.455

Muratoglu, S., Hough, B., Mon, S. T., & Fossett, N. (**2007**). The GATA factor Serpent cross-regulates lozenge and u-shaped expression during Drosophila blood cell development. *Developmental Biology*, 311(2), 636–649. https://doi.org/10.1016/j.ydbio.2007.08.015

Nishioka, K., Chuikov, S., Sarma, K., Erdjument-Bromage, H., Allis, C. D., Tempst, P., & Reinberg, D. (**2002**). Set9, a novel histone H3 methyltransferase that facilitates transcription by precluding histone tail modifications required for heterochromatin formation. *Genes and Development*, 16(4), 479–489. https://doi.org/10.1101/gad.967202

Nowick, K., & Stubbs, L. (**2010**). Lineage-specific transcription factors and the evolution of gene regulatory networks. *Briefings in Functional Genomics and Proteomics*, 9(1), 65–78. https://doi.org/10.1093/bfgp/elp056

Nüsslein-Volhard, C., & Wieschaus, E. (**1980**). Mutations affecting segment number and polarity in drosophila. *Nature*, 287(5785), 795–801. https://doi.org/10.1038/287795a0

O'Geen, H., Ren, C., Nicolet, C. M., Perez, A. A., Halmai, J., Le, V. M., MacKay, J. P., Farnham, P. J., & Segal, D. J. (**2017**). dCas9-based epigenome editing suggests acquisition of histone methylation is not sufficient for target gene repression. *Nucleic Acids Research*, 45(17), 9901–9916. https://doi.org/10.1093/nar/gkx578

Peterson, S. C., Samuelson, K. B., & Hanlon, S. L. (**2021**). Multi-scale organization of the drosophila melanogaster genome. *Genes*, 12(6). https://doi.org/10.3390/genes12060817

Radman-Livaja, M., & Rando, O. J. (**2010**). Nucleosome positioning: How is it established, and why does it matter? *Developmental Biology*, 339(2), 258–266. https://doi.org/10.1016/j.ydbio.2009.06.012

Rämet, M., Manfruelli, P., Pearson, A., Mathey-Prevot, B., & Ezekowitz, R. A. B. (**2002**). Functional genomic analysis of phagocytosis and identification of a Drosophila receptor for E. coli. *Nature*, 416(6881), 644–648. https://doi.org/10.1038/nature735

Rathke, C., Baarends, W. M., Awe, S., & Renkawitz-Pohl, R. (**2014**). Chromatin dynamics during spermiogenesis. *Biochimica et Biophysica Acta - Gene Regulatory Mechanisms*, 1839(3), 155–168. https://doi.org/10.1016/j.bbagrm.2013.08.004

Reynolds, N., O'Shaughnessy, A., & Hendrich, B. (**2013**). Transcriptional repressors: Multifaceted regulators of gene expression. *Development (Cambridge)*, 140(3), 505–512. https://doi.org/10.1242/dev.083105

Richter, C., Oktaba, K., Steinmann, J., Müller, J., & Knoblich, J. A. (**2011**). The tumour suppressor L(3)mbt inhibits neuroepithelial proliferation and acts on insulator elements. *Nature Cell Biology*, 13(9), 1029–1041. https://doi.org/10.1038/ncb2306

Roche, A. E., Bassett, B. J., Samant, S. A., Hong, W., Blobel, G. A., & Svensson, E. C. (**2008**). The zinc finger and C-terminal domains of MTA proteins are required for FOG-2-mediated transcriptional repression via the NuRD complex. *Journal of Molecular and Cellular Cardiology*, 44(2), 352–360. https://doi.org/10.1016/j.yjmcc.2007.10.023

Rodrigues, C. P., Shvedunova, M., & Akhtar, A. (**2021**). Epigenetic Regulators as the Gatekeepers of Hematopoiesis. *Trends in Genetics*, 37(2), 125–142. https://doi.org/10.1016/j.tig.2020.09.015

Rudolph, T., Yonezawa, M., Lein, S., Heidrich, K., Kubicek, S., Schäfer, C., Phalke, S., Walther, M., Schmidt, A., Jenuwein, T., & Reuter, G. (**2007**). Heterochromatin Formation in Drosophila Is Initiated through Active Removal of H3K4 Methylation by the LSD1 Homolog SU(VAR)3-3. *Molecular Cell*, 26(1), 103–115. https://doi.org/10.1016/j.molcel.2007.02.025

Sáez, J. E., Gómez, A. V., Barrios, Á. P., Parada, G. E., Galdames, L., González, M., & Andrés, M. E. (**2015**). Decreased expression of CoREST1 and CoREST2 together with LSD1 and HDAC1/2 during neuronal differentiation. *PLoS ONE*, 10(6), 1–16. https://doi.org/10.1371/journal.pone.0131760

Schneider, I. (**1972**). Cell lines derived from late embryonic stages of Drosophila melanogaster. *Development*, 27(2), 353–365. https://doi.org/10.1242/dev.27.2.353

Shi, Y. J., Matson, C., Lan, F., Iwase, S., Baba, T., & Shi, Y. (**2005**). Regulation of LSD1 histone demethylase activity by its associated factors. *Molecular Cell*, 19(6), 857–864. https://doi.org/10.1016/j.molcel.2005.08.027

Signolet, J., & Hendrich, B. (**2015**). The function of chromatin modifiers in lineage commitment and cell fate specification. *FEBS Journal*, 282(9), 1692–1702. https://doi.org/10.1111/febs.13132

Sinenko, S. A., Shim, J., & Banerjee, U. (**2012**). Oxidative stress in the haematopoietic niche regulates the cellular immune response in Drosophila. *EMBO Reports*, 13(1), 83–89. https://doi.org/10.1038/embor.2011.223

Snow, J. W., & Orkin, S. H. (**2009**). Translational isoforms of FOG1 regulate GATA1-interacting complexes. *Journal of Biological Chemistry*, 284(43), 29310–29319. https://doi.org/10.1074/jbc.M109.043497

Song, Y., Dagil, L., Fairall, L., Robertson, N., Wu, M., Ragan, T. J., Savva, C. G., Saleh, A., Morone, N., Kunze, M. B. A., Jamieson, A. G., Cole, P. A., Hansen, D. F., & Schwabe, J. W. R. (**2020**). Mechanism of Crosstalk between the LSD1 Demethylase and HDAC1 Deacetylase in the CoREST Complex. *Cell Reports*, 30(8), 2699-2711.e8. https://doi.org/10.1016/j.celrep.2020.01.091

Sorrentino, R. P., Tokusumi, T., & Schulz, R. A. (**2007**). The Friend of GATA protein U-shaped functions as a hematopoietic tumor suppressor in Drosophila. *Developmental Biology*, 311(2), 311–323. https://doi.org/10.1016/j.ydbio.2007.08.011

Stabell, M., Eskeland, R., Bjørkmo, M., Larsson, J., Aalen, R. B., Imhof, A., & Lambertsson, A. (**2006**). The Drosophila G9a gene encodes a multi-catalytic histone methyltransferase required for normal development. *Nucleic Acids Research*, 34(16), 4609–4621. https://doi.org/10.1093/nar/gkl640

Svensson, E. C., Huggins, G. S., Dardik, F. B., Polk, C. E., & Leiden, J. M. (**2000**). A functionally conserved N-terminal domain of the friend of GATA-2 (FOG- 2) protein represses GATA4-dependent transcription. *Journal of Biological Chemistry*, 275(27), 20762–20769. https://doi.org/10.1074/jbc.M001522200

Tokusumi, T., Russell, M., Gajewski, K., Fossett, N., & Schulz, R. A. (**2007**). U-shaped protein domains required for repression of cardiac gene expression in Drosophila. *Differentiation*, 75(2), 166–174. https://doi.org/10.1111/j.1432-0436.2006.00120.x

Tokusumi, T., Sorrentino, R. P., Russell, M., Ferrarese, R., Govind, S., & Schulz, R. A. (**2009**). Characterization of a lamellocyte transcriptional enhancer located within the misshapen gene of Drosophila melanogaster. *PLoS ONE*, 4(7), 0–9. https://doi.org/10.1371/journal.pone.0006429

Tokusumi, Y., Tokusumi, T., Stoller-Conrad, J., & Schulz, R. A. (**2010**). Serpent, suppressor of hairless and U-shaped are crucial regulators of hedgehog niche expression and pro hemocyte maintenance during Drosophila larval hematopoiesis. *Development*, 137(21), 3561–3568. https://doi.org/10.1242/dev.053728

Tokusumi, Y., Tokusumi, T., & Schulz, R. A. (**2018**). Mechanical stress to Drosophila larvae stimulates a cellular immune response through the JAK/STAT signaling pathway. *Biochemical and Biophysical Research Communications*, 502(3), 415–421. https://doi.org/10.1016/j.bbrc.2018.05.192

Verstappen, G., Van Grunsven, L. A., Michiels, C., Van de Putte, T., Souopgui, J., Van Damme, J., Bellefroid, E., Vandekerckhove, J., & Huylebroeck, D. (**2008**). Atypical Mowat-Wilson patient confirms the importance of the novel association between ZFHX1B/SIP1 and NuRD corepressor complex. *Human Molecular Genetics*, 17(8), 1175–1183. https://doi.org/10.1093/hmg/ddn007

Vlisidou, I., & Wood, W. (**2015**). Drosophila blood cells and their role in immune responses. *FEBS Journal*, 282(8), 1368–1382. https://doi.org/10.1111/febs.13235

Waltzer, L., Bataillé, L., Peyrefitte, S., & Haenlin, M. (**2002**). Two isoforms of serpent containing either one or two GATA zinc fingers have different roles in Drosophila haematopoiesis. *EMBO Journal*, 21(20), 5477–5486. https://doi.org/10.1093/emboj/cdf545

Wilkinson-White, L., Gamsjaeger, R., Dastmalchi, S., Wienert, B., Stokes, P. H., Crossley, M., Mackay, J. P., & Matthews, J. M. (**2011**). Structural basis of simultaneous recruitment of the transcriptional regulators LMO2 and FOG1/ZFPM1 by the transcription factor GATA1. *Proceedings of the National Academy of Sciences of the United States of America*, 108(35), 14443–14448. https://doi.org/10.1073/pnas.1105898108

Woodcock, C. L., & Ghosh, R. P. (**2010**). Chromatin higher-order structure and dynamics. *Cold Spring Harbor Perspectives in Biology*, 2(5), a000596–a000596. https://doi.org/10.1101/cshperspect.a000596

Wu, L. M. N., Wang, J., Conidi, A., Zhao, C., Wang, H., Ford, Z., Zhang, L., Zweier, C., Ayee, B. G., Maurel, P., Zwijsen, A., Chan, J. R., Jankowski, M. P., Huylebroeck, D., & Lu, Q. R. (**2016**). Zeb2 recruits HDAC-NuRD to inhibit Notch and controls Schwann cell differentiation and remyelination. *Nature Neuroscience*, 19(8), 1060–1072. https://doi.org/10.1038/nn.4322

Yang, M., Gocke, C. B., Luo, X., Borek, D., Tomchick, D. R., Machius, M., Otwinowski, Z., & Yu, H. (**2006**). Structural Basis for CoREST-Dependent Demethylation of Nucleosomes by the Human LSD1 Histone Demethylase. *Molecular Cell*, 23(3), 377–387. https://doi.org/10.1016/j.molcel.2006.07.012

Yang, S. F., Sun, A. A., Shi, Y., Li, F., & Pickett, H. A. (**2018**). Structural and functional characterization of the RBBP4–ZNF827 interaction and its role in NuRD recruitment to telomeres. *Biochemical Journal*, 475(16), 2667–2679. https://doi.org/10.1042/BCJ20180310

Ye, Z., & Sarkar, C. A. (**2018**). Towards a Quantitative Understanding of Cell Identity. *Trends in Cell Biology*, 28(12), 1030–1048. https://doi.org/10.1016/j.tcb.2018.09.002

You, A., Tong, J. K., Grozinger, C. M., & Schreiber, S. L. (**2001**). CoREST is an integral component of the CoREST-human histone deacetylase complex. *Proceedings of the National Academy of Sciences of the United States of America*, 98(4), 1454–1458. https://doi.org/10.1073/pnas.98.4.1454

Zhang, J., Bonasio, R., Strino, F., Kluger, Y., Holloway, J. K., Modzelewski, A. J., Cohen, P. E., & Reinberg, D. (**2013**). SFMBT1 functions with LSD1 to regulate expression of canonical histone genes and chromatin-related factors. *Genes and Development*, 27(7), 749–766. https://doi.org/10.1101/gad.210963.112

Zhao, Y., & Garcia, B. A. (**2015**). Comprehensive catalog of currently documented histone modifications. *Cold Spring Harbor Perspectives in Biology*, 7(9). https://doi.org/10.1101/cshperspect.a025064

Online resources:

FlyBase, http://flybase.org/reports/FBgn0003963
(date of access: June 2021; gene entry “Ush”)

FlyAtlas, http://flyatlas.org/atlas.cgi
(date of access: March 2021; search term for dLSD1: “CG17149”; search term for dL(3)mbt: “CG5954”)

iProteinDB, https://www.flyrnai.org/tools/iproteindb/web/protein/FBpp0292003/
(date of access: March 2021)

APPENDIX

I. Publications

“Ush regulates hemocyte-specific gene expression, fatty acid metabolism and cell cycle progression and cooperates with dNuRD to orchestrate hematopoiesis”

“Distinct CoREST complexes act in a cell-type-specific manner”

II. List of academic teachers

III. Acknowledgements

I. Publications

The following publications, which are discussed in this thesis, are attached:

Lenz, J., Liefke, R., Funk, J., Shoup, S., Nist, A., Stiewe, T., Schulz, R., Tokusumi, Y., Albert, L., Raifer, H., Förstemann, K., Vázquez, O., Tokusumi, T., Fossett, N., & Brehm, A. (**2021**). Ush regulates hemocyte-specific gene expression, fatty acid metabolism and cell cycle progression and cooperates with dNuRD to orchestrate hematopoiesis. *PLoS Genetics* (Vol. 17, Issue 2). https://doi.org/10.1371/JOURNAL.PGEN.1009318

MačInković, I., Theofel, I., Hundertmark, T., Kovač, K., Awe, S., Lenz, J., Forné, I., Lamp, B., Nist, A., Imhof, A., Stiewe, T., Renkawitz-Pohl, R., Rathke, C., & Brehm, A. (**2019**). Distinct CoREST complexes act in a cell-type-specific manner. *Nucleic Acids Research*, 47(22), 11649–11666. https://doi.org/10.1093/nar/gkz1050

PLOS GENETICS

RESEARCH ARTICLE

Ush regulates hemocyte-specific gene expression, fatty acid metabolism and cell cycle progression and cooperates with dNuRD to orchestrate hematopoiesis

Jonathan Lenz[1], Robert Liefke[1,2], Julianne Funk[3], Samuel Shoup[1], Andrea Nist[4], Thorsten Stiewe[4], Robert Schulz[5†], Yumiko Tokusumi[5], Lea Albert[6], Hartmann Raifer[7], Klaus Förstemann[8], Olalla Vázquez[6], Tsuyoshi Tokusumi[5], Nancy Fossett[9], Alexander Brehm[1]*

1 Institute of Molecular Biology and Tumor Research, Biomedical Research Center, Philipps-University, Marburg, Germany, **2** Department of Hematology, Oncology and Immunology, University Hospital Giessen and Marburg, Marburg, Germany, **3** Institute of Molecular Oncology, Philipps-University, Marburg, Germany, **4** Genomics Core Facility, Institute of Molecular Oncology, Member of the German Center for Lung Research (DZL), Philipps-University, Marburg, Germany, **5** Department of Biological Sciences, University of Notre Dame, Notre Dame, Indiana, United States of America, **6** Faculty of Chemistry, Philipps-University, Marburg, Germany, **7** Flow Cytometry Core Facility, Institute for Medical Microbiology and Hospital Hygiene, Biomedical Research Center, Philipps-University, Marburg, Germany, **8** Gene Center and Dept. of Biochemistry, Ludwig-Maximilians-Universität, München, Germany, **9** Center for Vascular and Inflammatory Diseases and the Department of Pathology, University of Maryland School of Medicine, Baltimore, Maryland, United States of America

† Deceased.
* brehm@imt.uni-marburg.de

Citation: Lenz J, Liefke R, Funk J, Shoup S, Nist A, Stiewe T, et al. (2021) Ush regulates hemocyte-specific gene expression, fatty acid metabolism and cell cycle progression and cooperates with dNuRD to orchestrate hematopoiesis. PLoS Genet 17(2): e1009318. https://doi.org/10.1371/journal.pgen.1009318

Editor: Brian Hendrich, University of Cambridge, UNITED KINGDOM

Received: August 12, 2020

Accepted: December 20, 2020

Published: February 18, 2021

Peer Review History: PLOS recognizes the benefits of transparency in the peer review process; therefore, we enable the publication of all of the content of peer review and author responses alongside final, published articles. The editorial history of this article is available here: https://doi.org/10.1371/journal.pgen.1009318

Data Availability Statement: Raw and analysed data can be accessed at the GEO database: accession no. GSE146382. In particular this

Abstract

The generation of lineage-specific gene expression programmes that alter proliferation capacity, metabolic profile and cell type-specific functions during differentiation from multipotent stem cells to specialised cell types is crucial for development. During differentiation gene expression programmes are dynamically modulated by a complex interplay between sequence-specific transcription factors, associated cofactors and epigenetic regulators. Here, we study U-shaped (Ush), a multi-zinc finger protein that maintains the multipotency of stem cell-like hemocyte progenitors during *Drosophila* hematopoiesis. Using genome-wide approaches we reveal that Ush binds to promoters and enhancers and that it controls the expression of three gene classes that encode proteins relevant to stem cell-like functions and differentiation: cell cycle regulators, key metabolic enzymes and proteins conferring specific functions of differentiated hemocytes. We employ complementary biochemical approaches to characterise the molecular mechanisms of Ush-mediated gene regulation. We uncover distinct Ush isoforms one of which binds the Nucleosome Remodeling and Deacetylation (NuRD) complex using an evolutionary conserved peptide motif. Remarkably, the Ush/NuRD complex specifically contributes to the repression of lineage-specific genes but does not impact the expression of cell cycle regulators or metabolic genes. This reveals a mechanism that enables specific and concerted modulation of functionally related portions of a wider gene expression programme. Finally, we use genetic assays to demonstrate that

includes raw reads from RNA-seq experiments (3 replicates each: dsEGFP, dsUsh, dsMi-2; 4 replicates each: dsEGFP, dsUsh-B) and ChIP-seq experiments (1 replicate each: Ush-GFP input, Ush-GFP ChIP, dMi-2-GFP input, dMi-2-GFP ChIP). For RNA-seq the following analysed data are provided: Normalised counts (dsEGFP, dsUsh & dsMi-2 replicates), differentially expressed genes (dsEGFP vs. dsUsh; dsEGFP vs. dsMi-2), Normalised counts (dsEGFP & dsUsh-B replicates), differentially expressed genes (dsEGFP vs. dsUsh-B). Coverage tracks of Ush and dMi-2 ChIP-seq experiments as well as corresponding inputs are available for two different *Drosophila* genome versions (bigWig files for dm3 and dm6).

Funding: JL, RL, LA, OV and AB were funded by the Deutsche Forschungsgemeinschaft (DFG, German Research Foundation) - TRR 81/3 - 109546710. The funders had no role in study design, data collection and analysis, decision to publish, or preparation of the manuscript.

Competing interests: The authors have declared that no competing interests exist. Author Robert Schulz was unable to confirm their authorship contributions. On their behalf, the corresponding author has reported their contributions to the best of their knowledge.

Ush and NuRD regulate enhancer activity during hemocyte differentiation *in vivo* and that both cooperate to suppress the differentiation of lamellocytes, a highly specialised blood cell type. Our findings reveal that Ush coordinates proliferation, metabolism and cell type-specific activities by isoform-specific cooperation with an epigenetic regulator.

Author summary

In multicellular organisms common progenitors differentiate into various kinds of specialised cells. During differentiation metabolic profiles and proliferation potentials are progressively adjusted and cell type-specific traits are established by the coordinated activation and inactivation of genes. Here we study U-shaped (Ush), a conserved gene regulator that acts during macrophage differentiation in *Drosophila melanogaster*. We uncover that Ush coordinates the activation and inactivation of three differentiation-related gene groups, thereby modulating lipid metabolism, promoting cell division and maintaining a progenitor state. These functions are conferred by different Ush protein isoforms and their associated co-factors. One such co-factor, the nucleosome remodeling and deacetylation complex dNuRD, contributes to progenitor state maintenance but is not required for other Ush-regulated processes. This exemplifies how a single gene regulator can simultaneously influence different aspects of cellular differentiation by employing protein isoforms and isoform-specific co-regulator interactions.

Introduction

Establishment of gene expression programmes during differentiation involves a close cooperation between lineage-specific transcription factors and ubiquitously expressed epigenetic regulators. Transcription factors often possess sequence-specific DNA binding activities to target specific genes. There, they interact with epigenetic regulators, such as histone modifying enzymes or nucleosome remodelers, which alter chromatin structure. This facilitates the establishment and maintenance of appropriate levels of transcription. The molecular details of this interplay are complex and incompletely understood.

During hematopoiesis multipotent stem cells differentiate into diverse lineages to produce the many different blood cell types. Lineage-specific expression of RUNX1, PU.1 and GATA transcription factors play a prominent role in guiding these cell fate decisions [1]. These sequence-specific transcription factors cooperate with a host of cofactors and epigenetic regulators to establish lineage-appropriate gene expression programmes [2]. Many of the key regulators of hematopoiesis are conserved between vertebrates and invertebrates. *Drosophila* possesses a simple hematopoietic system that is composed of only three differentiated cell types [3]. The macrophage-like plasmatocytes make up the bulk of *Drosophila* hemocytes. The rarer crystal cells perform special roles in melanisation. Finally, the ultra-rare lamellocytes are only produced in significant numbers under extreme stress conditions. All three cell types can be derived from a common hemocyte precursor. Given its simplicity, *Drosophila* has proven to be an excellent, genetically tractable model to uncover fundamental principles of hematopoiesis.

Like its mammalian homolog FOG1, U-shaped (Ush) is a transcriptional cofactor that cooperates with GATA transcription factors to regulate key decisions during *Drosophila* hematopoiesis [4–8]. Ush and FOG1 do not bind DNA and are recruited to their sites of action by sequence-specific GATA transcription factors. Genetic studies support the view that Ush acts with the GATA transcription factor Serpent to maintain pluripotency of hemocyte progenitors

and suppress their differentiation [9–13]. Changes in Ush levels govern cell fate choice: The stem cell-like pro-hemocytes express high levels of Ush. Ush expression is downregulated to lower levels as pro-hemocytes differentiate into plasmatocytes and crystal cells and completely shut off during lamellocyte differentiation [10]. Previous analyses have identified a small number of Ush-regulated genes critical for the repression of hemocyte differentiation [14]. It is not known if Ush is dedicated to the regulation of these genes or if it controls more extensive transcriptional programmes. Moreover, the potential interplay between Ush and epigenetic regulators has not been studied.

Here, we use ChIP-seq and RNA-seq to determine genomewide Ush-occupied chromatin regions and Ush-regulated genes in the hemocyte-derived S2 cell line. Ush associates predominantly with promoters and enhancers at thousands of loci that are enriched for GATA binding sites. It regulates the expression of more than 1,800 genes which designates Ush as a major transcriptome regulator. Bioinformatic analyses uncover both activating as well as repressive functions of Ush. Ush uses these opposing activities to coordinately regulate distinct sets of genes: genes with hemocyte-related functions, genes that encodes key enzymes of fatty acid metabolism and genes coding for critical cell cycle regulators. These findings suggest that Ush does not only control the expression of hemocyte-specific genes, as implied by prior genetic studies, but that it also shapes the metabolic profile and maintains the proliferative potential of hemocytes. Indeed, prolonged depletion of Ush abrogates cell division and results in a pronounced G2/M block as detected by flowcytometric analysis.

Biochemically, we identify two major Ush isoforms. We use a variety of protein interaction assays to demonstrate that only the Ush-B isoform interacts with subunits of the Nucleosome Remodeling and Deacetylation (NuRD) complex *in vitro* and *in vivo*. Their interaction depends on a short N-terminal sequence specific for Ush-B. This sequence is related to the FOG repression motif with which FOG1 interacts with mammalian NuRD [15]. Thus, we have identified an evolutionary conserved, peptide based interaction mode between FOG1/Ush and NuRD. ChIP-seq highlights extensive colocalisation of Ush and the NuRD ATPase subunit dMi-2 on chromatin suggesting that the Ush/NuRD complex occupies thousands of regulatory sequences. RNA-seq analysis of the transcriptomes of dMi-2 and Ush-B-depleted cells identifies a common set of Ush-B/dMi-2 repressed genes with hemocyte-specific functions. By contrast, genes encoding enzymes involved in fatty acid metabolism and cell cycle regulation are not significantly affected by Ush-B/dMi-2. Accordingly, dMi-2 and Ush-B-depletion does not significantly affect the cell cycle profile of S2 cells. Thus, a specific Ush isoform and its specific interaction with an epigenetic regulator make a dedicated contribution to the regulation of only one of the three gene classes controlled by Ush.

Finally, we have used genetic loss-of-function approaches to define the roles of Ush and NuRD during hematopoiesis *in vivo*. We show that Ush as well as NuRD subunits are required for the restriction of enhancer activity in the lymph gland and that Ush and NuRD cooperate in the suppression of stress-induced lamellocytes.

Transcriptional factors make use of selective coregulators to establish and maintain cell lineage specific transcription programmes during mammalian hematopoiesis [2]. Our data substantially elaborates this paradigm by revealing alternative splicing and isoform-specific interactions as mechanisms to guide selective coregulator usage.

Results

Ush associates with promoters and enhancers

We used hemocyte-derived S2 cells as a model to define the molecular functions of Ush. Western blot analysis of whole cell extracts verified expression of Ush in S2 cells (**Fig 1A**, left panel).

An established Ush antibody reacted with several polypeptides (lane 1; [6]). The antibody signals for polypeptides with apparent molecular masses of 180 kDa and 220 kDa, respectively, were abrogated upon treatment of S2 cells with double stranded RNA directed against the 3' portion of the Ush mRNA (lane 2). This suggests that S2 cells express at least two different isoforms of Ush or that the protein is post-translationally modified. We employed a CRISPR approach to insert GFP- or FLAG-tag coding sequences at the 3' end of the Ush gene (**S1A and S1B Fig**). Western blot analysis of nuclear extracts from these cell lines using GFP or FLAG antibody likewise detected two major polypeptides (**Fig 1A**, right panel).

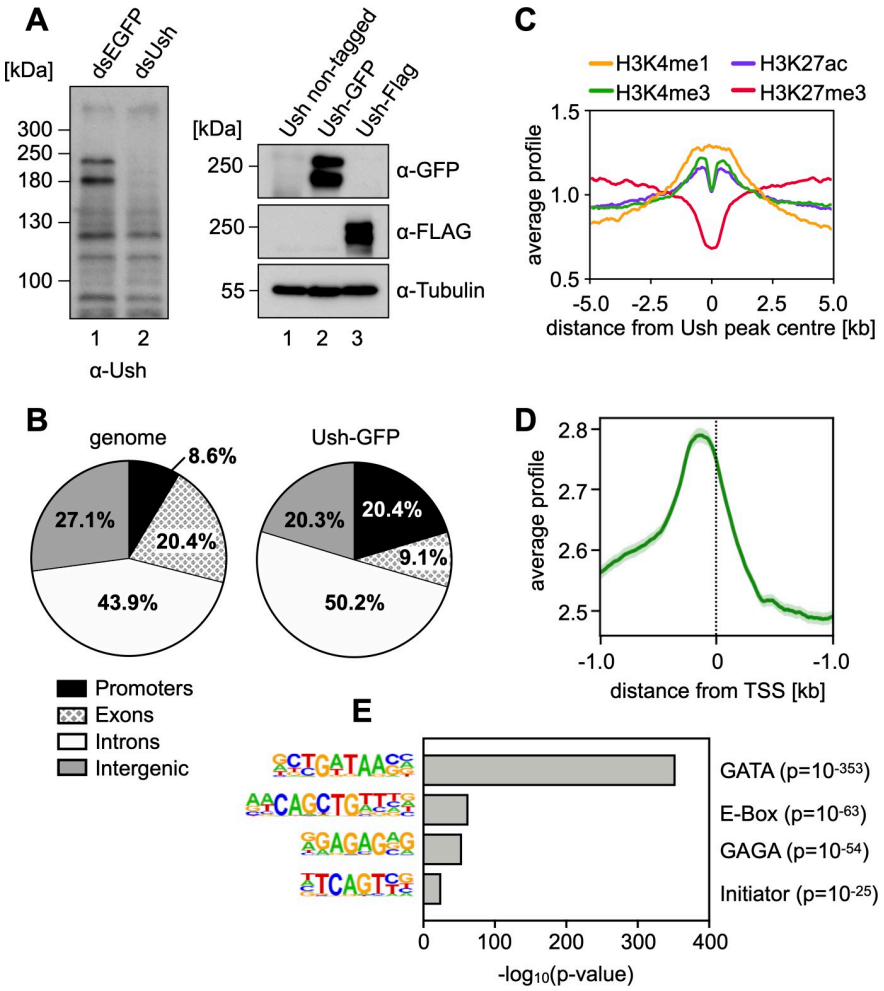

Fig 1. Ush is expressed in S2 cells and binds to regulatory elements. A Left panel: S2 cells were transfected with control dsRNA (dsEGFP) or dsRNA against Ush (dsUsh) and harvested after four days. Whole cell lysates were probed on Western blot using an antibody against Ush. Right panel: A GFP- or FLAG-tag sequence was inserted at the 3' end of the Ush gene in S2 cells using CRISPR/Cas9-mediated genome editing. Nuclear extracts of control cells and cells expressing Ush-GFP or Ush-FLAG was probed on Western blot using a GFP or FLAG antibody. Tubulin signal serves as loading control. **B** Genomic distribution of Ush-GFP binding sites identified by anti-GFP ChIP-seq. Fraction of Ush peaks found in each genomic location are shown in the right chart. Fractions of genomic locations in the *Drosophila* genome serve as reference (left chart). **C** Distribution of histone modifications surrounding Ush-bound regions. Signals of H3K4me1 (yellow), H3K4me3 (green), H3K27ac (blue) and H3K27me3 (red) are displayed within a region of 10 kb surrounding Ush peaks. **D** Distribution of Ush occupancy at transcription start sites (TSS). Average Ush binding (green) was evaluated in a 2 kb region surrounding all genomic TSS. Standard error is depicted in light green. **E** Analysis of DNA sequence motifs enriched at Ush binding sites. The enriched motif is depicted on the left and the corresponding transcription factor on the right. The -$\log_{10}$(p-value) for the enrichment of each motif is plotted and p-values are indicated on the right.

https://doi.org/10.1371/journal.pgen.1009318.g001

We next determined the genomewide chromatin binding pattern of Ush by anti-GFP chromatin immunopecipitation followed by high throughput sequencing (ChIP-seq). This identified 7012 genomic regions bound by Ush-GFP. Ush occupied sites were strongly enriched in promoters and moderately enriched in introns, which in the *Drosophila* genome often harbour enhancers (**Fig 1B**). Ush-bound regions were positively correlated with higher levels of H3K4 monomethylation (H3K4me1), H3K4 trimethylation (H3K4me3) and H3K27 acetylation (H3K27ac) - three histone modifications that are characteristic for active promoters (H3K4me3 and H3K27ac) and enhancers (H3K4me1 and H3K27ac) (**Fig 1C**). By contrast, Ush-occupied sites were on average depleted of H3K27 trimethylated (H3K27me3) nucleosomes, which are predominantly associated with genes that are stably silenced by Polycomb complexes PRC1 and PRC2. Concordant with histone modification patterns, elevated Ush levels were found directly upstream of transcriptional start sites (TSS), suggesting that Ush occupies gene promoter sequences (**Fig 1D**). A motif analysis revealed that Ush bound regions are in fact enriched for transcription factor binding sites, including GATA-, E-box-, GAGA- and Initiator motifs (**Fig 1E**). Of these the GATA motif was by far the most strongly enriched motif consistent with the established genetic and physical interactions between Ush and GATA transcription factors [4–8].

Collectively, these results suggest that Ush preferentially occupies gene regulatory sequences such as promoters and enhancers and that it is predominantly associated with transcription factors such as GATA factors. However, our findings also hint towards a possible complex formation with bHLH transcription factors, GAGA factor and general transcription factors binding to the initiator element. Given the high number of Ush bound genes we hypothesised that Ush plays a significant role in regulating the S2 transcriptome.

Ush is a major regulator of transcription

We depleted Ush from S2 cells by RNAi using a double stranded RNA that targets all Ush isoforms (**Fig 1A**). We then performed RNA-seq to analyse the resulting transcriptome changes. The levels of 1828 transcripts were significantly changed in Ush-depleted cells (adj. $p < 0.01$) supporting the hypothesis that Ush is a major transcriptional regulator. The majority of these transcripts (1268) was upregulated following Ush depletion suggesting that Ush predominantly represses transcription (**Fig 2A**). Nevertheless, a significant number (560) of differentially expressed genes were downregulated in Ush depleted cells indicating that Ush can also activate or maintain higher levels of transcription.

Comparison of the RNA-seq and ChIP-seq datasets revealed that approximately half of Ush-repressed genes (651 of 1268, 51%) and one third of Ush-activated genes (175 of 560, 31%) contain a Ush ChIP-seq peak in the promoter or gene body (**Fig 2B**). These 826 genes are, therefore, likely to be direct transcriptional targets of Ush.

Ush regulates genes with hemocyte, metabolic and cell cycle functions

A gene ontology analysis of Ush regulated genes revealed strong enrichment of three main classes of genes: (1) genes involved in hemocyte functions (139 genes), (2) genes involved in lipid and fatty acid metabolism (199 genes) and (3) genes involved in the cell cycle (176 genes) (**Fig 2C** and **2D**).

Our finding that Ush regulates genes involved in hemocyte functions agrees well with previous genetic work: Ush has long been established as a dosage-dependent repressor of hemocyte differentiation in *Drosophila* [10]. In the embryo Ush antagonises the expression of the transcription factor Lozenge (Lz) which is essential for crystal cell differentiation [5,6,16]. Crystal cell differentiation is accompanied by reduced Ush expression and consequent derepression of

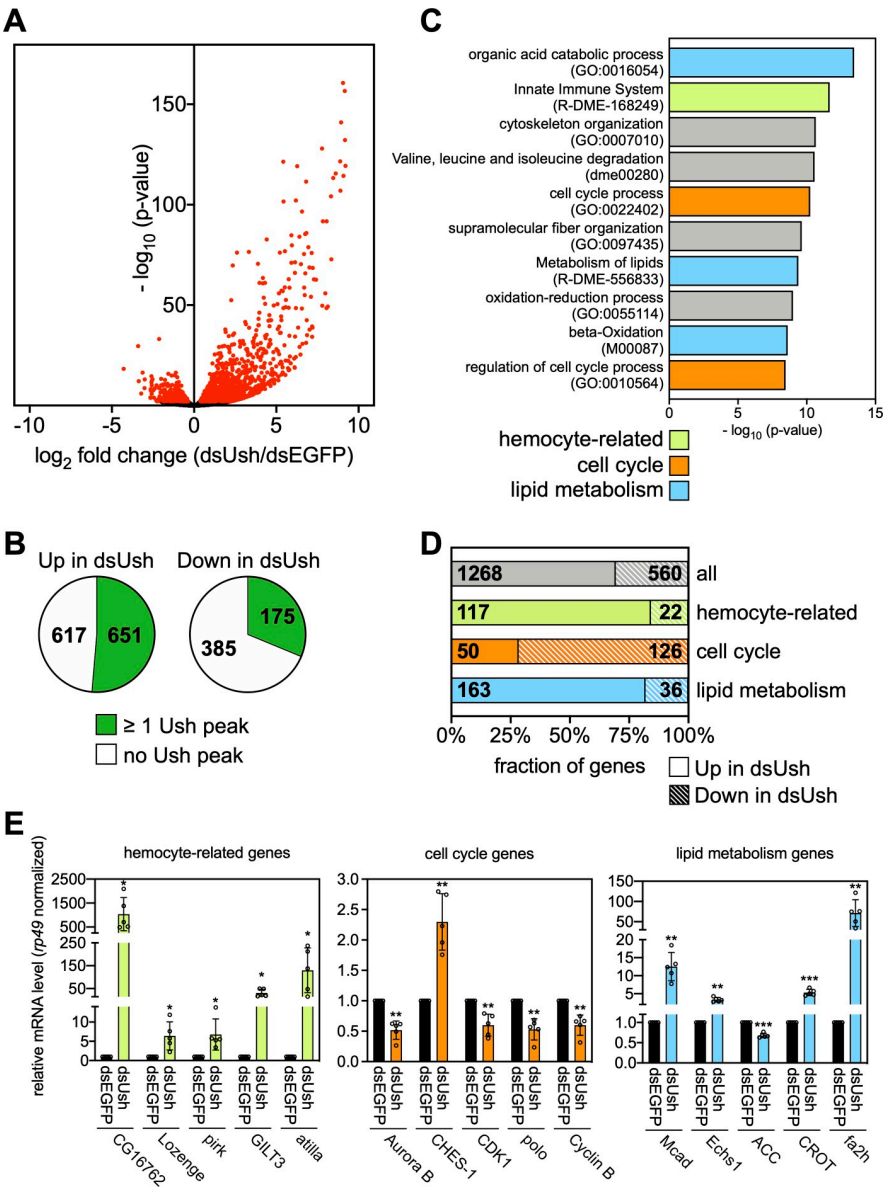

Fig 2. Ush regulates the S2 cell transcriptome. A Volcano plot of deregulated genes upon depletion of Ush in S2 cells. The -$\log_{10}$(p-value) is plotted against the $\log_2$ fold change of counts per gene in Ush-depleted (dsUsh) vs. control cells (dsEGFP). Red dots represent significantly deregulated genes (adj. $p < 0.01$) obtained from biological triplicates (n = 3). **B** Enrichment of Ush at Ush-regulated genes. Fraction of genes repressed (left chart) or activated by Ush (right chart) that contain at least one Ush peak is indicated in green. **C** Gene ontology analysis of Ush-regulated genes. GO terms associated with lipid metabolism (blue), hemocyte-specific functions (green) and cell cycle (orange) are highlighted respectively. **D** Genes contributing to the three GO term classes were divided into a Ush-activated (shaded) and a Ush-repressed (solid) fraction. The entirety of all Ush-regulated genes serves as reference (grey). Gene numbers in each fraction are indicated. **E** Representative genes from all three gene classes were analysed upon depletion of Ush (dsUsh) by RT-qPCR. Gene names are indicated below. Expression was calculated relative to control treated cells (dsEGFP) and normalised using the mRNA levels of *rp49*. Error bars represent the standard deviation from biological replicates (n = 5) (T-test: *** $p < 0.001$, ** $p < 0.01$, * $p < 0.05$). Individual values of each replicate are displayed as circles.

https://doi.org/10.1371/journal.pgen.1009318.g002

lz. Indeed, we find that the *lz* gene is bound by Ush and derepressed following Ush depletion suggesting that it is a direct target of Ush (**Figs 2E and S2**). This demonstrates that genetic relationships identified in fly embryos are recapitulated in S2 cells.

Unexpectedly, Ush also regulates a large number of genes which are involved in lipid metabolism and cell cycle control. Notably, cell cycle genes were mostly dependent on Ush for their robust expression while hemocyte- and metabolism-related genes were mostly repressed by Ush (Fig 2D). This suggests that the repressing and activating activities of Ush are predominantly used to control distinct transcription programmes that are modulating different cellular outcomes including hemocyte-specific functions, metabolic profile and cell cycle progression.

We selected representative genes from each class to confirm their regulation by Ush by RT-qPCR following Ush depletion (Fig 2E). Some of these genes had Ush ChIP-seq peaks within gene body and/or promoter and are, therefore, putative direct targets (CG16267, pirk, GILT3, Lozenge, CHES-1, Cyclin B, Mcad, Echs1, ACC, fa2h). Others were not bound by Ush and represent genes that might be indirectly regulated by Ush (Attila, AurB, CDK1, polo, CROT) (S1 Table). The levels of all five mRNAs encoding genes with hemocyte-related functions were increased by factors between five fold and about one thousand fold. Four cell cycle genes were downregulated upon Ush knockdown. These include important positive regulators of mitosis such as CDK1, polo, Cyclin B and Aurora B. By contrast, the forkhead transcription factor CHES-1, which in mammals has anti-proliferative activity, showed increased RNA expression [17]. Mcad (an acyl CoA dehydrogenase), Echs1 (Enoyl coenzyme A hydrolase), fa2h (fatty acid 2-hydroxylase) and CROT (a carnitin acyl transferase) collaborate in the degradation of fatty acids and the production of NADH, FADH2 and acetyl CoA. The levels of RNAs encoding these enzymes all increase upon Ush depletion. By contrast, levels of the RNA encoding acetyl CoA carboxylase (ACC), a key enzyme of fatty acid synthesis, decrease.

Thus, Ush appears to regulate different cellular processes in a coordinated fashion. It increases the expression of genes required for progression through mitosis and decreases the expression of an anti-proliferative gene. Likewise, it favours the expression of enzymes essential for fatty acid degradation while simultaneously lowering the expression of an enzyme that catalyses a key step in fatty acid synthesis.

Ush is essential for cell cycle progression

A prediction from these observations is that proliferation should be adversely affected in Ush depleted cells. We simultaneously depleted all Ush isoforms by RNAi using two alternative double stranded RNAs. Compared to control cells that were treated with double stranded RNA targeting luciferase, Ush depletion dramatically decreased proliferation (Fig 3A). These cells were still viable which suggests that the observed reduction in cell number was not due to cell death (Fig 3B). We subjected S2 cells to flow cytometry after PI staining of DNA to determine the cell cycle profiles of control cells and Ush-depleted cells. Compared to control cells, Ush-depleted cells showed a pronounced reduction of cells with a 2n DNA complement and an accumulation of cells with a 4n complement. This suggests that Ush-depleted cells can replicate their genome but fail to enter or proceed through mitosis (Fig 3C and 3D). We then asked if this apparent G2/M block was accompanied by changes in the levels of mitotic cyclins which are required for progression into M phase. Again, we used two independent double stranded RNAs to deplete all Ush isoforms and determined Cyclin A and Cyclin B protein levels by Western blot (Fig 3E). Protein concentrations of both cyclins were reduced in Ush-depleted cells (compare controls in lanes 1 and 2 with lanes 3 and 4). Given that Ush depletion also results in a decrease of Cyclin B mRNA levels (Fig 2E) these data indicate that Ush promotes progression through the cell cycle, at least in part, by supporting the transcription of mitotic cyclins.

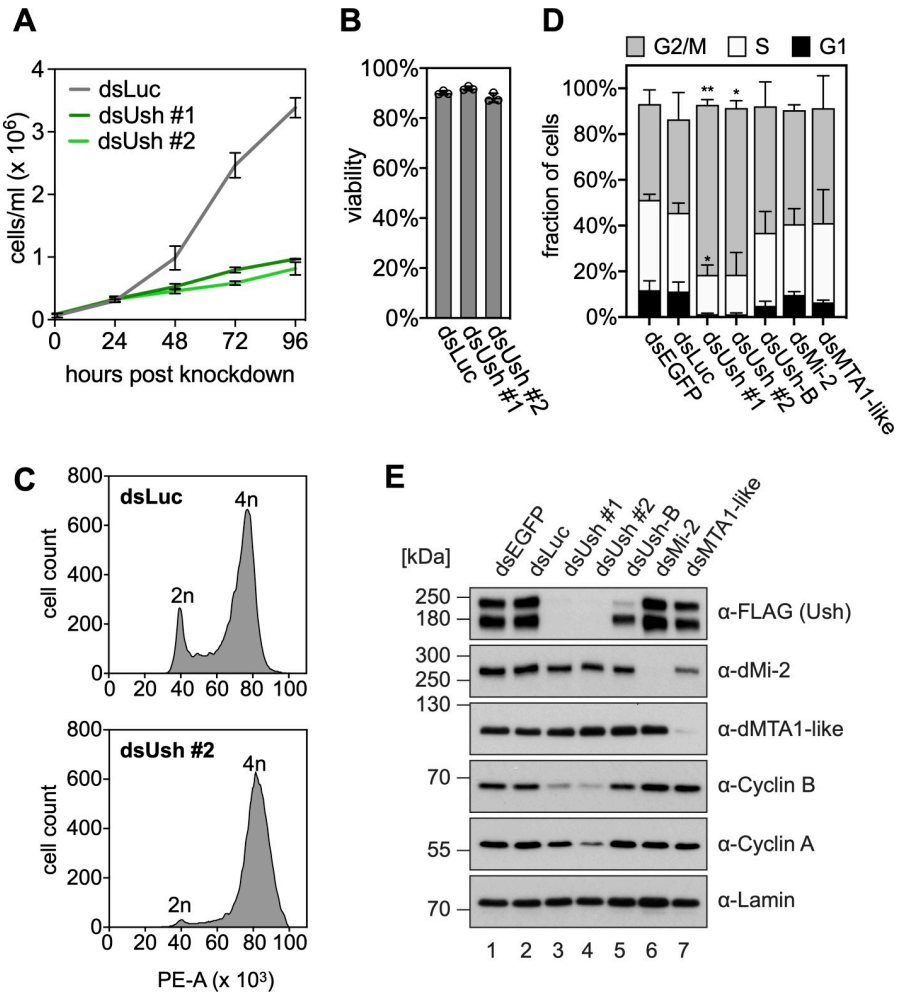

Fig 3. Ush is necessary for cell cycle progression. A Proliferation assay of S2 cells upon depletion of Ush. Cells were transfected with control dsRNA (dsLuc, grey) or with two different dsRNA constructs directed against Ush (dsUsh #1 in dark green, dsUsh #2 in light green). Cell numbers were determined every 24 hours. Error bars represent the standard deviation from biological triplicates (n = 3). **B** Viability assay of S2 cells upon depletion of Ush. Viability of cells transfected with control dsRNA (dsLuc) or dsRNA constructs targeting Ush (dsUsh #1 and dsUsh #2) was measured 96 hours post transfection. Error bars represent the standard deviation from biological triplicates (n = 3) and individual values are indicated with circles. **C** Flow cytometry following PI-staining of Ush-depleted (dsUsh #2) and control S2 cells (dsLuc). dsRNA-transfected cells were fixed, stained with PI and subjected to flow cytometry. Histograms show the number of cells plotted against the PI signal (Area of PE channel). The diploid cell population (2n) and cells that have undergone replication (4n) are indicated. **D** Quantification of cell populations obtained from flow cytometry of PI-stained cells upon depletion of indicated proteins (G1 phase: black, S phase: white, G2/M phase: grey). Error bars represent the standard deviation from biological triplicates (n = 3) (T-test: ** $p < 0.01$, * $p < 0.05$). **E** Western blot of whole cell extracts from S2 cells expressing endogenously FLAG-tagged Ush upon depletion of the proteins indicated above. Antibodies used for detection are indicated on the right. Lamin signal serves as loading control.

https://doi.org/10.1371/journal.pgen.1009318.g003

Ush isoforms

How can Ush support the transcription of cell cycle genes and at the same time repress the transcription of many lipid metabolism- and hemocyte-related genes? We considered the possibilities that the activating and repressing functions of Ush are mediated by different Ush isoforms and/or association with different cofactors.

Indeed, the Ush gene structure predicts the expression of at least five different mRNAs generated by usage of alternative promoters and by alternative splicing (**Figs** 4A and S3). These mRNAs encode three Ush proteins that share a 1175 amino acids region at their C-termini which encompasses nine zinc fingers (Fig 4B). The three Ush isoforms differ in their unique short N-termini. Isoform Ush-D gives rise to a 1175 amino acid protein. Isoforms Ush-A and Ush-C produce two identical proteins which possess an additional 16 amino acid N-terminal extension (from hereon referred to as Ush-A) that is not present in Ush-D. Ush-B and Ush-E generate two identical proteins with a 23 amino acid N-terminal extension (from hereon referred to as Ush-B). As illustrated in Fig 4B, the first 7 and 14 amino acids of Ush-A and Ush-B, respectively, are unique to these isoforms. Our transcriptome data demonstrates expression of exons encoding both of these unique N-termini providing support for the expression of at least two different Ush protein isoforms in S2 cells (S3 Fig). If Ush isoforms do indeed possess isoform-specific functions they are likely to be mediated by these short N-terminal sequences.

An unbiased, large scale proteomic screen has previously identified several candidate interactors of Ush in S2 cells [18]. These include 6 subunits of the dNuRD complex. We immunoprecipitated nuclear extracts from S2 cells expressing FLAG-tagged Ush to verify these interactions (**Figs** 1A **and** 4C). Western blot analysis of the immunoprecipitate demonstrated that several subunits of the dNuRD complex coprecipitate with Ush. Importantly, dMEP-1, the signature subunit of the dMi-2-containing dMec complex, was not recovered [19]. This suggests that Ush specifically associates with the dNuRD complex but not with the dMec complex.

We also asked if immunoprecipitation of dMi-2 would coprecipitate Ush. Again, we used a CRISPR approach to add a FLAG-tag to the C-terminus of endogenous dMi-2 (S1C–S1E Fig). Western blot analysis of anti-FLAG immunoprecipitates from nuclear extract of these cells revealed that only the slower migrating of the two major Ush polypeptides coprecipitated with dMi-2 (Fig 4D, compare lanes 2 and 5). We used Ush isoform-specific RNA interference to identify Ush isoforms. The slower migrating isoform was efficiently depleted when cells were treated with double stranded RNA targeting an RNA region specific for Ush-B (lane 3). Immunoprecipitation of dMi-2-FLAG from nuclear extracts of Ush-B depleted cells failed to coprecipitate Ush protein (lane 6). We conclude that dMi-2 specifically forms a complex with the Ush-B isoform.

Inspection of the unique N-terminal sequence of Ush-B revealed that the first 9 amino acids are identical to the FOG repression motif (Fig 4E). This motif mediates interaction between several zinc finger transcription factors, including FOG1, and NuRD in mammalian cells [15,20–24]. We hypothesised that this motif does also mediate the interaction between Ush-B and dNuRD and that such a peptide-based NuRD binding mechanism is conserved between mammals and *Drosophila*. To test this hypothesis we incubated a GST fusion containing the N-terminus of mouse FOG1 (amino acids 1-45) with nuclear extracts of *Drosophila* S2 cells and *Drosophila* embryos (Fig 4F). All five dNuRD subunits we assayed interacted with GST-FOG1 but not with the GST control. We did not detect binding of the dMec subunit dMEP-1, the dMi-2 paralogue dCHD3 which does not assemble into a dNuRD complex and several components of other repressive chromatin regulating complexes (dPc, dE(z), dLSD1).

In order to compare the affinity of dNuRD for binding the FOG1 and Ush N-termini we designed 15 amino acid peptides derived from the FOG1 and the Ush-B N-termini (FOG1-wt, Ush-wt; Fig 4G). In addition, we generated mutant versions of these peptides where three amino acids important for binding of mammalian NuRD to FOG1 where changed (FOG1--mut, Ush-mut) [15]. As an additional control we used FOG1 and Ush-B peptides with scrambled sequences. We then competed binding of dNuRD to the GST-FOG1 fusion with these

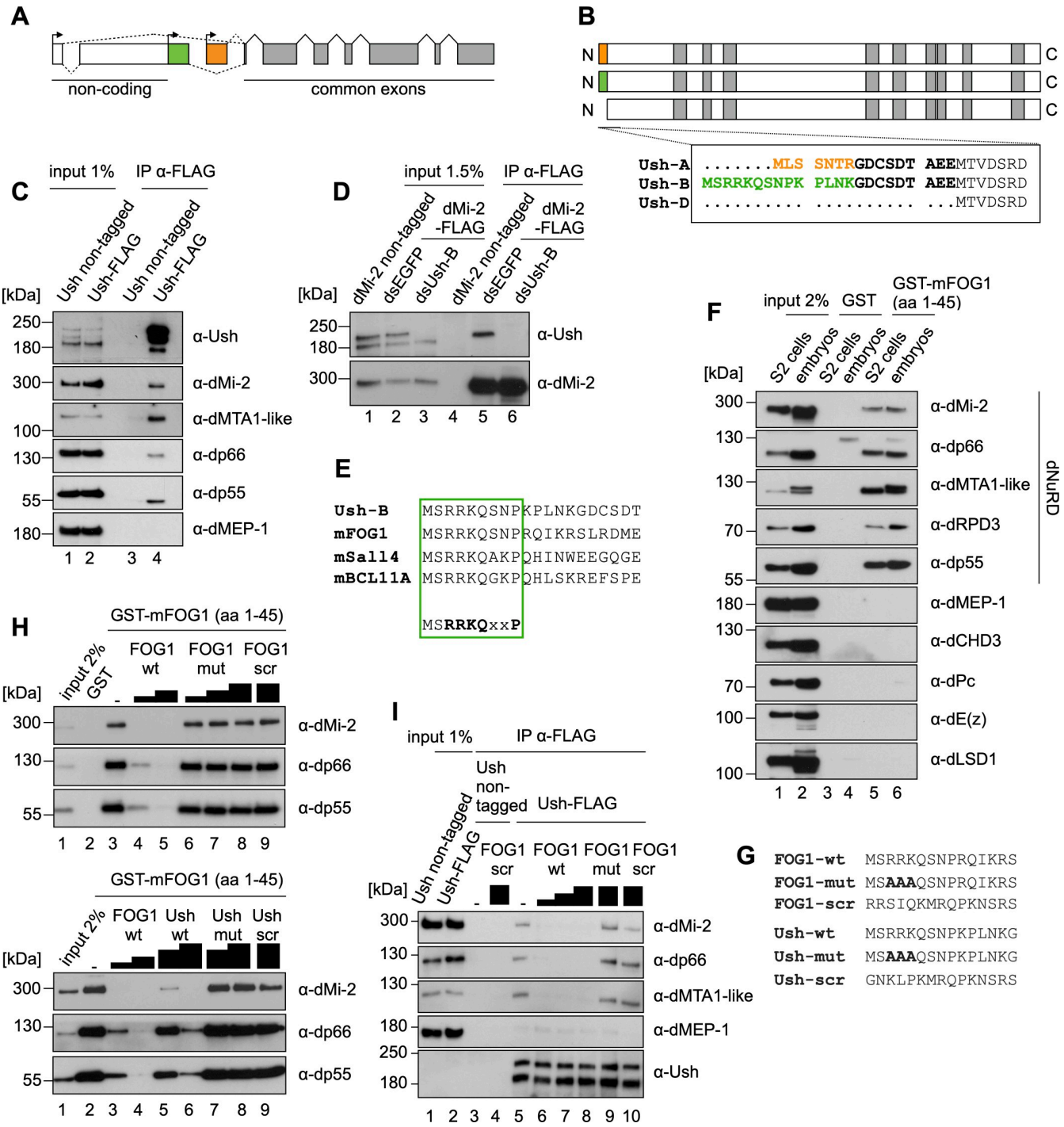

Fig 4. The Ush isoform Ush-B interacts with NuRD via a conserved N-terminal motif. A Schematic structure of the Ush gene locus. Boxes represent exons and the connecting lines indicate splicing events (dashed lines: alternative splicing). Exons marked in grey are common to all Ush isoforms. (Sections of) exons marked in white are untranslated. Possible transcriptional start sites are indicated by arrows. **B** Scheme of polypeptides generated from the Ush gene. Zinc finger domains are marked in grey. Sequences in the box indicate the N-termini of Ush proteins emanating from five possible Ush mRNAs. Isoform specific N-termini are marked in orange and green. **C** Anti-FLAG immunoprecipitation of nuclear extract from control and Ush-FLAG expressing cells. Antibodies used for examination of co-precipitation by Western blot are indicated on the right. **D** Anti-FLAG immunoprecipitation of nuclear extract from control and dMi-2-FLAG expressing cells following Ush-B depletion (dsUsh-B) or cells transfected with control dsRNA (dsEGFP). Co-precipitation of Ush was determined by Western blot. **E** Sequence alignment of the Ush-B N-terminus with N-terminal sequences from murine proteins containing the FOG repression motif (in bolt letters below). **F** GST pulldown from nuclear extracts of S2 cells or *Drosophila* embryos using the first 45 amino acids of murine FOG1 fused to GST (GST-mFOG1 (aa 1-45)) or control bait (GST). Interacting proteins were analysed by Western blot against NuRD complex components

(specified on the right) and additional chromatin-regulating proteins. Antibodies used for immuno-detection are indicated on the right. **G** Sequences of peptides derived from FOG1 and Ush-B N-termini that were used in competition experiments. **H** GST pulldown assays from S2 cell nuclear extracts using the GST-mFOG1(1-45) fusion protein. Pulldown reactions were performed in presence of different concentrations of the indicated peptides (FOG1 derived peptides: top panel; Ush-B derived peptides: bottom panel). Interaction of NuRD with the GST-fusion was detected by Western blot using antibodies indicated on the right. **I** Anti-FLAG immunoprecipitation of nuclear extract from control and Ush-FLAG expressing cells in presence of FOG1 derived peptides. The identity of peptides and the amount used is indicated above. Antibodies used for examination of co-precipitation by Western blot are indicated on the right.

https://doi.org/10.1371/journal.pgen.1009318.g004

peptides (Fig 4H). Both the FOG1-wt and Ush-wt peptides efficiently abrogated binding of the dNuRD subunits dMi-2, dp66 and dp55 to GST-FOG1. A higher excess of Ush-wt peptide was required for complete inhibition of binding suggesting that the affinity of the FOG1-wt peptide for binding to dNuRD is higher than the affinity of the Ush-wt peptide under our experimental conditions. Importantly, the mutant versions of both peptides as well as the scrambled controls did not compete for binding.

We next sought to test if FOG repression motif containing peptides are able to disrupt dNuRD/Ush complexes that have formed *in vivo*. We carried out FLAG-immunoprecipitation from nuclear extracts of S2 cells expressing FLAG-tagged Ush in the absence or presence of FOG1-wt, FOG1-mut or scrambled peptides and then analysed the immunoprecipitates by Western blot (Fig 4I). The FOG1-wt but not the FOG1-mut or the scrambled peptides disrupted the dNuRD/Ush complex.

These results suggest that the FOG repression motif present in the N-terminus of Ush is critical for binding dNuRD. Moreover, residues within the FOG repression motif that are essential for binding mammalian NuRD complexes are also critical for contacting the *Drosophila* NuRD complex. Taken together our analysis has revealed a highly conserved, peptide-based mechanism that mediates an isoform-specific interaction between Ush and dNuRD.

dMi-2 and Ush co-occupy many sites on chromatin

We asked if Ush and dNuRD do not only interact in solution but are also associated on chromatin. We determined the genomewide chromatin binding of dMi-2-GFP by ChIP-seq. This identified 8459 peaks. Comparison of this dataset with two dMi-2 ChIP-seq profiles generated previously using two different dMi-2 antibodies demonstrated a highly similar binding pattern between the datasets (S4 Fig).

Comparison of our Ush-GFP and dMi-2-GFP ChIP-seq datasets uncovered a remarkable degree of co-localisation of the two proteins. About two thirds (64.9%) of Ush peaks overlapped with dMi-2 peaks (Fig 5A). Moreover, regions with strong Ush binding generally also displayed elevated dMi-2 binding (Fig 5B). Visual inspection of Ush and dMi-2 ChIP-seq profiles confirmed co-occupancy at many promoters, introns and intergenic regions (Fig 5C) while also revealing regions that are exclusively occupied by only one of the two factors (**Fig 5C, first panel**). We then assigned Ush/dMi-2 co-occupied regions as well as "Ush-only" and "dMi-2-only" ChIP-seq peaks to genomic regions (Fig 5D). Ush-only peaks show a strong preference of introns. dMi-2-only peaks on the other hand are most strongly enriched at promoters. Co-occupied regions show preferential association with both promoters and introns. In agreement with these findings analysis of histone marks at Ush-only peaks revealed a strong enrichment of H3K4me1, a histone modification that is characteristic for enhancers (Fig 5E). dMi-2-only peaks contained high levels of H3K4me3, a hallmark of active promoters. Co-occupied regions displayed elevated levels of both H3K4me1 and H3K4me3.

Collectively, these results supports the hypothesis that Ush/NuRD complexes act at regulatory regions such as promoters and enhancers.

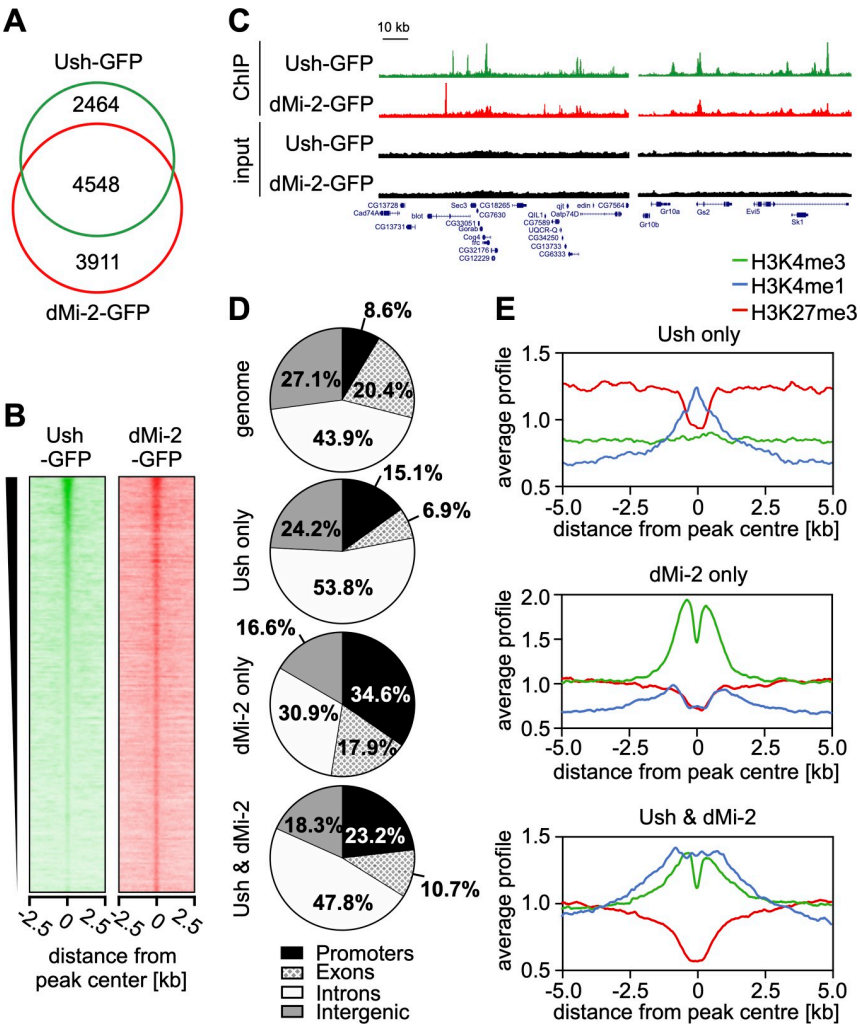

Fig 5. Ush and dMi-2 co-localise on chromatin. A Venn diagram of loci bound by Ush-GFP (green) and dMi-2-GFP (red) determined by anti-GFP ChIP-seq. Numbers of peaks are indicated in each section. **B** Heatmap of Ush-GFP and dMi-2-GFP signals centred at Ush-bound regions and sorted by Ush signal intensity. A region of 5 kb surrounding the Ush peak is displayed. **C** Genome browser snapshots of exemplary regions displaying Ush (green) and dMi-2 (red) occupancy. Input signals are shown in black. Location of genes is displayed below with boxes indicating exons. Scale bar represents a distance of 10 kb. **D** Genomic distribution of regions identified by anti-GFP ChIP-seq that were bound by Ush only, dMi-2 only or by both Ush and dMi-2 (indicated on the left). Fraction of peaks found in each genomic location are displayed. Fractions of genomic locations in the *Drosophila* genome serve as reference (top chart). **E** Distribution of histone modifications surrounding regions bound by Ush only (top), dMi-2 only (middle) or both Ush and dMi-2 (bottom). Signals of H3K4me3 (green), H3K4me1 (blue) and H3K27me3 (red) are displayed within a region of 10 kb surrounding peak centres.

https://doi.org/10.1371/journal.pgen.1009318.g005

Taken together these results suggest that Ush and dNuRD are indeed associated on chromatin. The Ush/dNuRD complex binds regulatory sequences indicating that Ush-B and dNuRD might cooperate in the regulation of transcription.

Ush-B and dMi-2 regulate hemocyte-related genes

We have identified three classes of genes that display significant expression changes when all Ush isoforms are depleted simultaneously: genes related to hemocyte functions, genes encoding enzymes of the lipid metabolism and genes involved in cell cycle progression. We sought

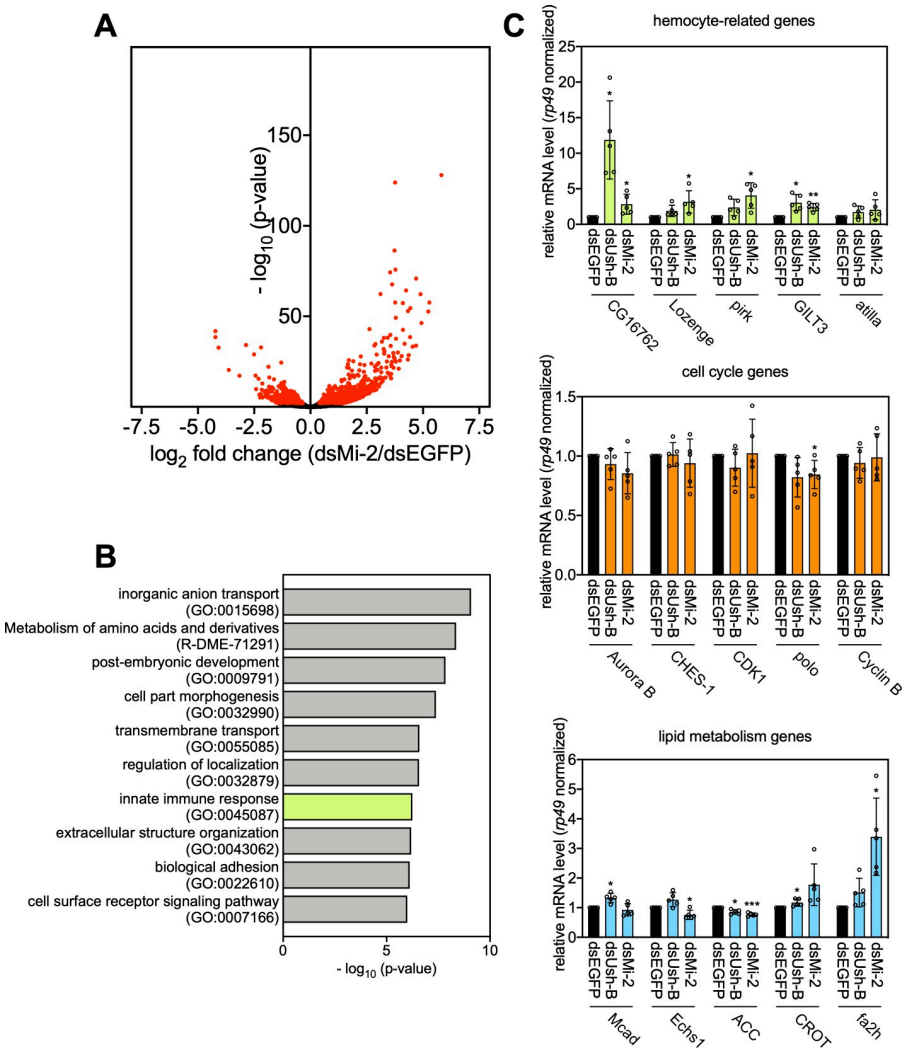

Fig 6. dMi-2 and Ush-B regulate genes associated with hemocyte functions. A Volcano plot of deregulated genes upon depletion of dMi-2 in S2 cells. The -$\log_{10}$(p-value) is plotted against the $\log_2$ fold change of counts per gene in dMi-2-depleted (dsMi-2) vs. control cells (dsEGFP). Red dots represent significantly deregulated genes (adj. $p < 0.01$) obtained from biological triplicates (n = 3). **B** Gene ontology analysis of dMi-2-regulated genes. GO terms associated with hemocyte functions are highlighted in green. **C** Representative genes from all three gene classes regulated by Ush were analysed upon depletion of dMi-2 (dsMi-2) and Ush-B (dsUsh-B) by RT-qPCR. Gene names are indicated below. Expression was calculated relative to control treated cells (dsEGFP) and normalised using the mRNA levels of rp49. Error bars represent the standard deviation from biological replicates (n = 5) (T-test: *** $p < 0.001$, ** $p < 0.01$, * $p < 0.05$). Individual values of each replicate are displayed as circles.

https://doi.org/10.1371/journal.pgen.1009318.g006

to determine the contribution of Ush-B/dNuRD to these three transcription programmes. We depleted dMi-2 by RNAi and used a double stranded RNA specifically targeting the Ush-B isoform to deplete Ush-B (Fig 3D). We then measured changes to the transcriptome by RNA-seq. dMi-2 depletion led to significant changes in the levels of 945 transcripts (adj. $p < 0.01$; Fig 6A). A gene ontology analysis identified a number of GO terms associated with a wide range of biological processes (Fig 6B). These included "post-embryonic development" and "cell part morphogenesis" in agreement with the established role of dMi-2 in several differentiation processes [25–27]. GO terms related to the cell cycle or lipid metabolism were not strongly enriched. However, the GO term "innate immune response" was among the top 10 most strongly enriched GO terms.

Depletion of Ush-B had a comparatively mild impact on the transcriptome. 85 transcripts showed significant expression changes (adj. $p < 0.05$; **S5 and S6 Figs** and **S2 Table**). A significant fraction of these (18 genes, 21%) were either associated with GO terms related to immune response or macrophage function, have established roles in hemocyte biology or show specific expression in hemocytes. By contrast, only very few of the Ush-B regulated genes appeared to be involved in cell cycle regulation and/or could be related to metabolic pathways (**S5 and S6 Figs** and **S2 Table**).

We used RNAi and direct RT-qPCR to verify these results on representative hemocyte-related, metabolism and cell cycle genes (**Fig 6C**). Both depletion of Ush-B and dMi-2 resulted in increased expression of most hemocyte-related genes tested. By contrast, none of the genes encoding cell cycle regulators displayed drastic changes in expression after Ush-B or dMi-2 knockdown. Also, with the exception of fa2h which was upregulated upon dMi-2 depletion, and ACC which showed marginal expression changes in Ush-B or dMi-2 depleted cells, none of the lipid metabolism related genes responded to lowering the concentrations of Ush-B or dMi-2.

Taken together these results suggest that the Ush-B/dNuRD complex makes a contribution to the transcriptional programme that governs hemocyte functions but does not impinge on the transcriptional programmes regulating cell cycle and lipid metabolism. In a broader sense, these findings highlight how transcription cofactors make use of isoforms and isoform specific interactions with chromatin regulators to differentially regulate distinct gene expression programmes.

Ush-B/dNuRD complex does not regulate the cell cycle

Unlike the simultaneous depletion of all Ush isoforms, the specific depletion of Ush-B or dMi-2 did not result in significant changes in the levels of cell cycle related transcripts. We, therefore, hypothesised that the Ush-B/dNuRD complex is not essential for cell proliferation. Indeed, neither isoform specific depletion of Ush-B, nor depletion of dMi-2 or the dNuRD subunit dMTA1-like produced the pronounced G2/M block observed following simultaneous depletion of all Ush isoforms (**Figs 3D** and **S7**). Although the percentage of cells in G2/M appeared to be somewhat increased and that of cells in G1 decreased these changes were not significant. Also, unlike simultaneous depletion of all Ush isoforms, depletion of Ush-B, dMi-2 or dMTA1-like did not alter protein expression levels of Cyclin A or Cyclin B (**Fig 3E**). We conclude that progression through the cell cycle does not rely on the Ush-B/dNuRD assembly. It is likely guided by other Ush isoforms or depends on redundant functions of several isoforms.

Ush/dNuRD regulate hemocyte differentiation *in vivo*

While neither Ush-B nor dMi-2 depletion resulted in significant changes to genes encoding enzymes of the lipid metabolism and cell cycle genes, their depletion did lead to changes in the expression of several genes related to immune functions in the hemocyte-derived S2 cell line. This suggests that Ush-B/dNuRD contributes to the establishment and/or maintenance of specific functions of hemocytes. We, therefore, hypothesised that Ush-B/dNuRD might play a role in the regulation of hemocyte differentiation *in vivo*.

We have previously demonstrated that Ush restricts the activity of a *Hedgehog* enhancer in lymph glands, an important organ that limits hemocyte differentiation in L3 larvae [14,28,29]. Lymph glands are divided into a posterior signaling center (PSC), a medullary zone (MZ) containing hemocyte progenitors and a cortical zone (CZ) composed of differentiating and differentiated hemocytes. Cells in the PSC are secreting Hedgehog (Hh) which keeps the hemocyte

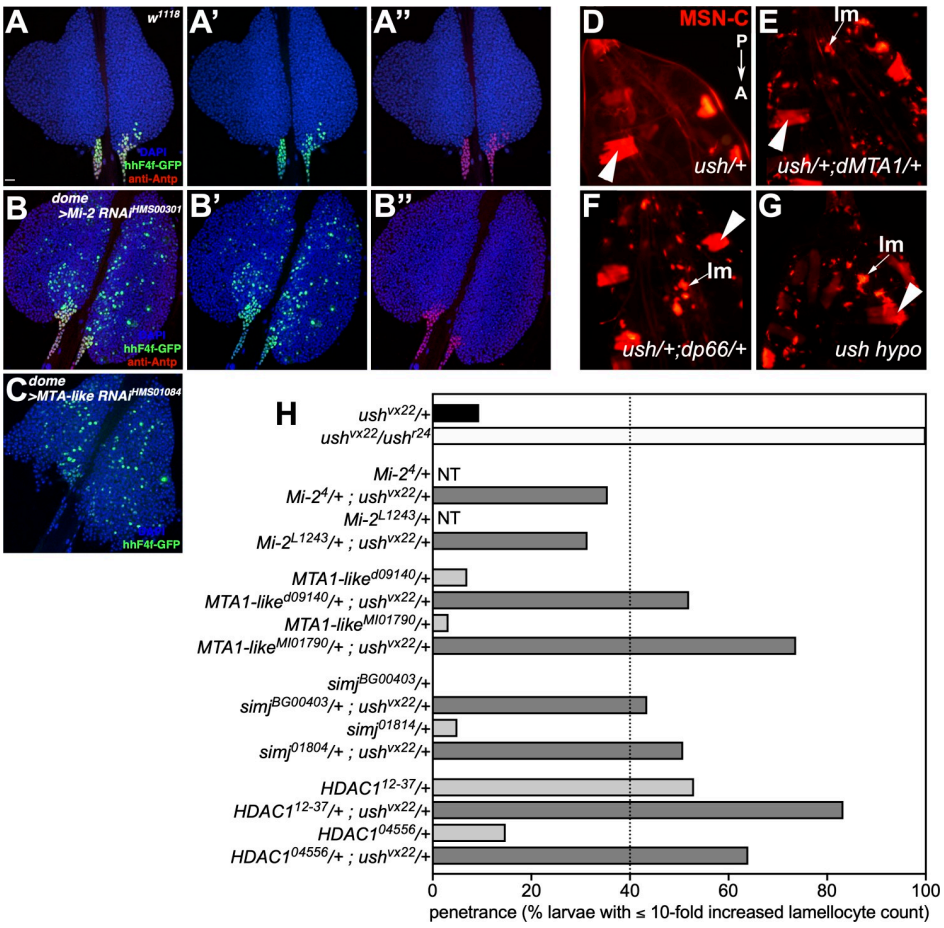

Fig 7. Ush and NuRD regulate a hemocyte-specific enhancer and lamellocyte differentiation in *Drosophila* larvae. **A-C** Lymph glands isolated from wild type larvae (**A**), larvae that express a dsRNA against dMi-2 (**B**), or dMTA1-like (**C**) under control of the domeless promoter (dome) active in the medullary zone. All larvae carry a construct, reporting the activity of a minimal *Hedgehog* enhancer by GFP expression (hhF4f-GFP; green). PSC is marked using immunostaining of Antennapedia (Antp; red). **D-H** Panels showing the dorsal view of the posterior region of late 3rd instar larvae. The orientation is from top to bottom: posterior (P) to anterior (A). Lamellocyte (lm) differentiation is blocked in ush heterozygotes (**D**). In contrast, ush/+;dMTA1-like/+ (**E**) and ush/+;dp66/+ (**F**) double heterozygotes show lamellocyte differentiation. Likewise, $ush^{vx22/r24}$ (ush hypo; **G**) shows lamellocyte differentiation. Lamellocytes express the MSN-cherry fluorescent transgene (MSN-C) and are marked with arrows. Larval muscles also express MSN-C and are marked with large arrowheads. Penetrance of the lamellocyte differentiation phenotype was quantified in **H**. Only larvae with a more than ten fold increased lamellocyte count were considered. Genotypes of respective crosses are indicated below. For each NuRD allele two different mutant strains were tested as single heterozygotes (light grey) or double heterozygous along with ush^{vx22} (dark grey). Dashed line indicates the arbitrary cut-off for identification of genetic interactors. NT: not tested.

https://doi.org/10.1371/journal.pgen.1009318.g007

progenitors in the MZ in a quiescent state and prevents their premature differentiation. *Hh* expression in PSC cells is driven by an enhancer located in the first intron of the *Hh* gene [14]. Ush, which is expressed in the MZ but not in the PSC, is required for shutting off this enhancer in the MZ and CZ, thereby limiting expression to the PSC. Accordingly, Ush loss of function results in spurious *Hh* enhancer activity in the MZ and the CZ [14] (**S8 Fig**). We asked if dNuRD, like Ush, was also involved in *Hh* enhancer repression. We used a fly strain carrying a GFP reporter under control of an *Hh* enhancer fragment to address this question. In lymph glands GFP activity is restricted to cells of the PSC as demonstrated by expression of the PSC marker Antennapedia (Antp) (**Fig 7A**). We used the UAS/GAL4 system to deplete dMi-2 by

RNAi in the MZ (dome>dMi-2 RNAi). This resulted in the detection of GFP positive cells throughout the MZ and CZ (**Fig 7B**). Importantly, Antp expression remained restricted to the PSC demonstrating that PSC cells had not migrated into the MZ and CZ. We obtained the same result upon downregulation of the dNuRD subunit dMTA1-like (**Fig 7C**). These results establish that dNuRD is required to repress *Hh* enhancer activity in cells of the MZ and CZ and suggest that a Ush/dNuRD complex limits *Hh* expression to the PSC.

Next, we sought to determine if dNuRD cooperates with Ush to affect cell lineage decisions during hematopoiesis. In L3 larvae, Ush functions to suppress lamellocyte differentiation in absence of an appropriate trigger such as the injection of parasitic wasp eggs into the larva.

Whereas Ush hypomorphic ($ush^{vx22/r24}$) larvae exhibit aberrant differentiation of progenitors into lamellocytes, a single wild type copy of Ush (*ush* heterozygotes) is sufficient to block lamellocyte differentiation [11,13]. In the past, we have exploited this situation to perform second-site non-complementation (SSNC) screens to identify factors that genetically cooperate with Ush in blocking lamellocyte differentiation [30,31]. In SSNC singular heterozygotes display a wild-type phenotype, whereas animals doubly heterozygous for two different genes exhibit a mutant phenotype.

We have constructed a fly stock that enables us to rapidly assay for SSNC with *ush* [28]. This stock carries a *ush* null allele (ush^{vx22}) and the *misshapen-mCherry* (*MSN-C*) fluorescent reporter gene on the same chromosome. *MSN-C* is a marker for lamellocytes [32] and allowed us to rapidly identify larvae with increased numbers of lamellocytes using fluorescence microscopy. *MSN-C* is also constitutively active in larval muscle and serves as a marker for larvae that carry the ush^{vx22}, *MSN-C* chromosome (**Fig 7D–7G**). In a screen setting, we routinely use an arbitrary level of at least 40% penetrance of the lamellocyte phenotype in double heterozygotes to identify robust genetic interactors. While this is less than penetrance levels typically observed for ush hypomorphs (70% to 100%), it is significantly greater than penetrance levels observed in negative controls (9.4%; **Fig 7H and S3 Table**). Here, we performed SSNC assays by combining ush^{vx22} with mutant alleles of four dNuRD subunits: dMTA1-like, dp66 (simj), dRPD3 (HDAC1) and dMi-2 (**Fig 7H** and **S3 Table**). For each dNuRD subunit we carried out the assay with two independent mutant alleles. In all combinations we identified larvae with dramatically increased numbers of circulating *MSN-C*-positive lamellocytes (**Fig 7F and 7G**). Three of the four dNuRD complex subunits tested (dMTA1-like, dp66/simj and dRPD3/HDAC1), exhibited a greater than 40% penetrance when carried as double heterozygous with *ush* (**Fig 7H** and **S3 Table**). The two dMi-2 alleles exhibited 35% and 27% penetrance, respectively. While this was significantly greater than the control, it was less than the 40% penetrance we routinely use as a cut off.

We then tested if heterozygous alleles of the three dNuRD complex subunits that showed a robust genetic interaction with *ush* could produce lamellocytes when carried as singular heterozygotes in a *ush* wild-type background. Both alleles of dMTA1-like and dp66/simj exhibited minimal lamellocyte differentiation with a penetrance less than that of the control (**Fig 7H** and **S3 Table**). This strongly suggests that dMTA1-like and dp66 cooperate with Ush to block lamellocyte differentiation. In contrast, one of the two dRPD3/HDAC1 alleles tested exhibited a greater than 50% penetrance when carried as a singular heterozygote (**Fig 7H** and **S3 Table**). Currently, we do not understand the basis for this effect. Taken together with the fact that dRPD3 is not only a dNuRD subunit but exists in several other histone deacetylase complexes we cannot derive a clear conclusion as to the involvement of dRPD3 in lamellocyte differentiation. Nevertheless, the SSNC analysis identifies a robust genetic cooperation between *ush* and at least two dNuRD subunits, dMTA1-like and dp66, in blocking lamellocyte differentiation.

Taken together, our results demonstrate a function of Ush and dNuRD in regulating enhancer activity during hematopoiesis. Furthermore, we reveal that at Ush and dNuRD genetically cooperate in cell lineage commitment.

Discussion

Ush regulated transcription programmes

Ush genetically and physically interacts with GATA transcription factors to govern hemocyte differentiation during *Drosophila* hematopoiesis [6,7,13,14]. Ush has been demonstrated to modulate the expression of reporter genes and a small number of genes encoding hematopoietic regulators. However, the transcription programme controlled by Ush has not been defined on a genomewide level. We have determined genomewide binding sites of Ush and identified the genes regulated by Ush in the hemocyte-derived S2 cell line.

Ush binds more than 7,000 genomic locations and modulates the transcription of more than 1,800 genes. This demonstrates that, rather than being dedicated to the control of a small number of hematopoietic master regulators, Ush is a major regulator of the S2 transcriptome. We find that Ush bound regions are dramatically enriched for GATA sites on a genomewide level. This expands genetic and biochemical data that suggest that Ush cooperates with GATA transcription factors [6–8,13,14]. However, the binding sites for several other transcription factors are also strongly enriched in Ush bound regions. Interestingly, these include the E-box, a binding site for helix-loop-helix transcription factors. In mammals, composite GATA/E-box sites where the two elements are separated by 10 or less base pairs play a prominent role in determining lineage-specific gene expression during hematopoiesis [2]. These composite sites are bound by multisubunit transcription factor complexes containing GATA1, the Ush homolog FOG1, the basic helix-loop-helix transcription factors TAL1 and E47 and/or other hematopoietic regulators including LMO2 and LDB1. Our data suggest that similar composite GATA/E-box sites function in the *Drosophila* genome. In addition to GATA motifs and E-boxes, the GAGA and initiator sequences are present with high frequency in Ush-occupied regions. However, it remains to be demonstrated that Ush indeed forms complexes with these transcription factors and that together they regulate gene expression.

Our analysis of Ush regulated genes revealed that Ush modulates the expression of genes with hemocyte-related functions. S2 cells were derived from a primary culture of late embryos. They are believed to represent pro-hemocytes that are in the process of differentiating into macrophage-like plasmatocytes. Embryonic pro-hemocytes have the potential to either differentiate into plasmatocytes or into crystal cells [3]. Ush is expressed at high levels in pro-hemocytes but Ush expression is downregulated as pro-hemocytes differentiate into plasmatocytes and crystal cells. Differentiation into crystal cells relies on the expression of the Runx family transcription factor Lozenge (Lz). Our analysis reveals that reduction of Ush expression by RNAi in S2 cells derepresses *lz*. This suggests that the genetic suppression of crystal cell differentiation by Ush is based, at least in part, on its transcriptional repression of the crystal cell master regulator Lz [12].

Unexpectedly, we have also identified a large number of genes involved in lipid metabolism and cell cycle regulation that likewise require Ush to maintain their appropriate expression levels. Ush appears to be able to both positively and negatively affect gene regulation and it uses these opposing activities to coordinately regulate cellular functions at the transcriptional level.

Ush regulates fatty acid metabolism

An illustrative example is provided by Ush's coordinated regulation of fatty acid metabolism. Several genes encoding enzymes of the beta-oxidation pathway that degrades fatty acids are

repressed by Ush. By contrast, the acetyl CoA carboxylase gene which encodes the key enzyme driving fatty acid synthesis requires Ush for its full expression. Accordingly, Ush appears to limit fatty acid degradation while it simultaneously promotes fatty acid synthesis. Interestingly, polarisation of mammalian macrophages is accompanied by the coordinated activation of fatty acid degradation in certain contexts [33]. This suggests that the transcriptional regulation of fatty acid metabolism by Ush might contribute to a metabolic profile that counteracts differentiation.

Ush regulates the cell cycle

Ush also regulates cell cycle genes in a coordinated fashion. The RNA levels of several genes encoding proteins essential for the entry into and progression through mitosis are maintained at appropriate levels by Ush. This transcriptional regulation has functional significance since Ush depleted cells have strongly decreased proliferative capacity and exhibit a pronounced G2/M block. Ush is expressed in proliferating pro-hemocytes but downregulated in terminally differentiated plasmatocytes, crystal cells and lamellocytes [6]. We speculate that Ush supports the expansion of pro-hemocytes. Conversely, downregulation of Ush during lineage determination might allow these cells to exit the cell cycle for terminal differentiation. The human Ush homolog FOG1 has also been proposed to play a pro-proliferative role when overexpressed in NIH 3T3 cells [34,35]. However, this does not appear to involve the transcriptional regulation of cell cycle genes.

Ush isoforms

Eukaryotes expand the diversity of their proteome by expressing multiple mRNA isoforms from the same protein coding gene. These can be generated by alternative splicing or the use of alternative transcriptional start sites. Indeed, more than 90% of human protein coding transcripts are estimated to be alternatively spliced. Functionally distinct isoforms of transcriptional regulators increase the capacity for fine-tuning transcriptional control. However, the molecular mechanisms by which different isoforms of transcriptional regulators contribute to gene expression are only beginning to be unravelled. Here, we have revealed that Ush is expressed in distinct isoforms that differ in their N-termini in S2 cells. We show that an N-terminal sequence unique to the Ush-B isoform mediates interaction with the dNuRD chromatin remodeling complex.

This dNuRD binding peptide is closely related to the FOG repression motif originally identified as a NuRD binding site in the mouse hematopoietic regulator FOG1 [15]. Related motifs are found in several other NuRD binding zinc finger proteins including FOG2, Sall4 and BCL11A. Importantly, dNuRD binds to both the N-terminus of Ush as well as to the N-terminus of FOG1. This demonstrates that this peptide based NuRD binding mechanism has been highly conserved in evolution.

Ush is the first *Drosophila* protein found to possess a dNuRD binding FOG repression motif. We have identified a second protein with an N-terminal FOG repression motif in the *Drosophila* proteome by sequence analysis, the O/E-associated zinc finger protein (OAZ). OAZ is not expressed in S2 cells and its relationship with dNuRD is unknown. Nevertheless, this finding hints that also in *Drosophila* the FOG repression motif is utilised in several proteins to mediate NuRD interaction.

In mammals FOG repression motif peptides have been shown to contact two NuRD subunits, RbAp46/RbAp48 and MTA1/2/3 but not the CHD4 ATPase [15,36]. Likewise, the *Drosophila* Mi-2 ATPase does not appear to directly bind the FOG repression motif given that the dMi-2-containing dMec complex does not bind to Ush or FOG repression motif peptides. We

propose that the FOG repression motif directly contacts dp55 (the homolog of RbAp46/RbAp48) and/or dMTA1-like. This hypothesis is supported by the observation that FOG repression motif mutations that disrupt binding to RbAp48 and MTA1/2/3 likewise abrogate binding to dNuRD [15,23].

It is interesting that the FOG1 peptide used in our study binds with higher affinity to dNuRD than the Ush peptide even though the FOG repression motif contained within both peptides is identical. This suggests that amino acids outside of the FOG repression motif contribute to dNuRD binding. It is also possible that interaction between dNuRD and Ush is modulated by post-translational modification within or in the vicinity of the FOG repression motif *in vivo*. Indeed, phosphorylation of serine residue 2 within the FOG repression motif has previously been shown to lower NuRD binding [37].

Impact of Ush-B/dNuRD on transcription in S2 cells

Specific depletion of Ush-B by RNAi had a mild effect on the S2 transcriptome compared to the simultaneous depletion of all Ush isoforms. In principle, it is possible that Ush-B occupies a smaller set of genomic loci compared to other isoforms. We consider this to be unlikely. A large number of Ush bound regions contains binding sites for GATA transcription factors that have been implicated in recruiting Ush to chromatin. GATA transcription factors interact with zinc fingers that are shared in all Ush isoforms which should, therefore, be recruited equally well to all GATA transcription factor occupied sites. We consider it more likely that Ush-B and other Ush isoforms both contribute to gene regulation. In this scenario, Ush-B depletion does only change the transcript levels of genes that require high concentrations of Ush for their repression or that are particularly dependent on Ush-B and the Ush-B/dNuRD complex. Many of these Ush-B depletion-sensitive genes have hemocyte-related functions. Indeed, progressive downregulation of Ush drives gene expression changes that are required for the differentiation of specialised hemocytes such as plasmatocytes, crystal cells and lamellocytes *in vivo*. Unlike cell cycle and metabolism genes, these genes appear to be uniquely sensitive to modest reduction of overall Ush expression levels obtained by selective depletion of Ush-B. Moreover, these genes are also repressed by dMi-2 suggesting that they are, indeed, targets of the Ush-B/dNuRD complex. This suggests that the Ush-B/dNuRD complex is particularly important for regulating the transcription of genes characteristic for macrophage function.

Ush and dNuRD cooperate in hemocyte differentiation *in vivo*

Hematopoiesis in *Drosophila* occurs at various developmental stages including embryogenesis and larval development. Our results have revealed that Ush and dNuRD mould the metabolism, proliferation and hemocyte-related functions of S2 cells by maintaining an extensive gene expression programme. S2 cells are derived from embryonic hemocytes indicating gene regulatory roles for Ush and dNuRD during embryonic hematopoiesis. Our genetic loss-of-function analyses show that Ush and dNuRD also regulate hematopoiesis at later developmental stages. In particular, we have shown that Ush and dNuRD subunits are required to restrict *Hedgehog* enhancer activity to cells of the posterior signaling center in lymph glands of L3 larvae. This result suggests that Ush and dNuRD actively modulate gene expression programmes also at the larval stage. Moreover, Ush and dNuRD suppress lamellocyte differentiation in unstressed larvae. We do not yet know to which extent the different Ush isoforms are required for lamellocyte suppression. However, the finding that mutations in dNuRD subunits result in excessive lamellocyte differentiation only in a genetic background with reduced Ush activity demonstrates genetic cooperativity between Ush and dNuRD. This is consistent with the hypothesis that a Ush-B/dNuRD complex is active during larval hematopoiesis.

The function of dNuRD in hematopoiesis identified by our work solidifies the important role of this complex as a regulator of differentiation in *Drosophila*. We have previously shown that dMi-2 cooperates with transcription factors such as Tramtrack 69 or Kumgang to determine cell lineages in different developmental settings ranging from neurogenesis to spermatogenesis [25–27,38]. In each of these scenarios a different lineage-specific transcriptional regulator (Tramtrack 69, Kumgang, Ush) utilises the ubiquitously expressed dMi-2 complex to establish lineage- and stage-appropriate gene expression programmes.

Although the process of hematopoiesis in *Drosophila* is far less complex than in mammals, Ush and FOG1 play remarkably similar roles in suppressing certain hematopoietic lineages. FOG1 facilitates erythroid and megakaryocyte differentiation while suppressing mast cell differentiation. While high Ush levels in hemocyte progenitors counteracts differentiation into all three *Drosophila* hemocyte cell types, intermediate Ush levels are sufficient to suppress crystal cell and lamellocyte differentiation but compatible with differentiation of plasmatocytes [10]. Both FOG1 and Ush cooperate with NuRD using a highly conserved short peptide motif. Thus, our study identifies the FOG1/Ush-NuRD complex as an ancient component of the machinery regulating hematopoiesis.

Cell lineage differentiation relies on a finely orchestrated series of events that change cell morphology and function at multiple levels. These include division of stem cells, the proliferation of progenitors, their withdrawal from the cell cycle for terminal differentiation, the timely expression of lineage-specific genes and the generation of changing metabolic profiles that are appropriate for each stage of differentiation. By coordinately regulating the transcription of cell cycle genes, genes encoding metabolic enzymes and genes performing macrophage-specific functions Ush simultaneously controls several cellular activities that are relevant to the differentiation process. A classical 'master regulator' of differentiation sits on top of a hierarchy and directs the expression of downstream transcription factors that in turn generate gene expression profiles committing cells to a certain lineage. By contrast, Ush appears to be more "hands-on" and directly regulates the expression of different types of genes that are key for diverse processes impinging on differentiation.

Materials and methods

Cell culture

Drosophila melanogaster S2 and S2[Cas9] cells (S2 cells expressing the Cas9 nuclease from Streptococcus pyogenes; generous gift from Klaus Förstemann, Munich) were cultured in Schneider's *Drosophila* Medium (2172001, Gibco) supplemented with 10% (v/v) fetal bovine serum (FBS; F7524, Sigma) and 1% (v/v) Penicillin-Streptomycin (15140122, Gibco). Cell lines were grown under standard conditions at 26˚C.

Endogenous tagging using CRISPR/Cas9

CRISPR/Cas9-based insertion of epitope-tag sequences into the genome of *Drosophila* S2 cells was performed as previously described (Bottcher et al., 2014). DNA sequences coding for GFP- or FLAG-tags were inserted at the 3' end of the coding region of the U-shaped or dMi-2 gene locus, leading to expression of C-terminally tagged proteins.

In brief, S2 cells stably expressing the Cas9 nuclease (S2[Cas9] cells) were transfected with double stranded linear DNA constructs (1) encoding for sgRNA and (2) providing a template for homologous recombination (HR). Both of these constructs were generated by PCR using gene specific primers (S4 Table). The sgRNA sequences were designed to target Cas9 as close to the respective STOP codon as possible with respect to the nearest available protospacer adjacent motif (PAM) (targeting sequences: CATTTGAGAAAGCCAGCTG (Ush) and

TCGAATAATTCCGGCGTCT (dMi-2)). Homologous recombination templates were amplified from plasmids containing GFP- or FLAG-tag sequences including a STOP codon as well as a resistance marker under control of a copia promoter. This insert was amplified using primers containing 60 bp sequences homologous to regions directly up- and downstream of the original STOP codon. In particular, HR templates for C-terminal tagging of U-shaped were amplified using the following plasmids: pSK23 (GFP-tag & Puromycin resistance marker; Addgene #72851) and pSK25 (2xFLAG-tag & Puromycin resistance marker; Addgene #72853). HR templates for C-terminal tagging of dMi-2 were amplified using the following plasmids: pMH3 (GFP-tag & Blasticidin resistance marker; Addgene #52528) and pMH4 (2xFLAG-tag & Blasticidin resistance marker; Addgene #52529).

To favour double strand break repair by HR, the protein amount of key enzymes involved in non-homologues end joining (NHEJ) and microhomology-mediated end joining (MMEJ) was lowered by transfecting S2[Cas9] cells with 1 μg/ml dsRNA targeting lig4 (NHEJ) and mus308 (MMEJ) transcripts. After three days, cells were transfected with HR and sgRNA templates using FuGENE HD transfection reagent (E2311, Promega). Four days post transfection cells were transferred to medium containing 2 μg/ml Puromycin (540411, Merck) or 10 μg/ml Blasticidin (A11139, Gibco) respectively. Cells were kept under selection for at least 14 days or until non-resistant control cells declined.

To retrieve monoclones, cells were serially diluted in 96 well plates. Monoclones were expanded and screened by PCR on genomic DNA using primers flanking the insertion site.

RNA interference in *Drosophila* S2 cells, proliferation and viability assay

Double-stranded RNA (dsRNA) was synthesised using the MEGAscript T7 kit (AMB1334, Invitrogen) according to manufacturer's instructions. In brief, dsRNA was generated using T7 Polymerase *in vitro* transcription from PCR amplicons obtained with T7 minimal promotor containing primers using a cDNA template from S2[Cas9] cells. 10-15 μg of dsRNA was added to $0.3x10^6$ S2[Cas9] cells in a total of 3 ml Schneider's *Drosophila* Medium. For different cell numbers, the amount of dsRNA and medium was scaled accordingly. Cells were harvested for RNA isolation four days post transfection and for cell cycle analysis and protein extraction three days post transfection.

To monitor proliferation, cells were re-seeded immediately after transfection. The cell density was determined from three independent dsRNA transfections every 24 hours using a hemocytometer. Cell viability was determined four days post transfection by measuring cell dilutions on a CASY Cell Analyser (OMNI Life Science).

Cell cycle analysis by flow cytometry

Cell cycle distribution of *Drosophila* cell lines was analysed as described in [39] with minor changes. In brief, cells were harvested, washed and resuspended in 500 μl PBS. While vortexing cells were fixed by the addition of 5 ml ice cold 95% (v/v) ethanol. One day prior to analysis cells were rehydrated in PBS for 5 min on ice, washed and finally resuspended in 1 ml PBS. 25 μl of RNAse A digestion mix (10 mM PIPES/NaOH pH 6.8, 100 mM NaCl, 2 mM $MgCl_2$, 0.25 mM EDTA, 0.2% (w/v) Triton X-100, 100 μg/μl RNAse A) and 50 μl propidium iodide solution (0.5 mg/ml propidium iodide in 38 mM sodium citrate) were added and DNA was stained overnight at 4˚C with rotation.

Flow cytometry was performed on an ARIA III cytometer (BD) with DIVA 8.0.2 software. After gating the cells of interest in an FSC-A/SSC-A plot debris and doublets were excluded with an PE-Area vs. PE-Width Plot. Measurements were taken from three independent dsRNA transfections where 10,000 cells were counted per replicate. For visualisation and

record of the PI-signal a histogram for the PE-channel (excitation 561 nm) was used with a 582/15 bandpass filter. For analysis of the recorded signals the exported fcs (3.0) files were loaded in FlowJo (10.6.1). The Watson Pragmatic algorithm was used for computation of G1, S and G2/M fractions [40].

Preparation of protein extracts

For whole cell extracts cells were washed in PBS and lysed in RIPA buffer (50 mM Tris/HCl pH 8.0, 150 mM NaCl, 1 mM EDTA, 1 mM EGTA, 1% (w/v) NP-40, 0,5% (w/v) sodium deoxycholate, 0,1% (w/v) SDS, 10% (v/v) glycerol, 1 mM DTT) for 20 min with rotation at 4˚C followed by freeze/thaw lysis in liquid nitrogen. Lysates were cleared by centrifugation at 21,100 g and 4˚C for 20 min. The protein content was determined using DC Protein Assay (5000112, Biorad) according to manufacturer's instructions.

Nuclear extracts were obtained by washing cells in PBS followed by hypotonic lysis in buffer B (10 mM Hepes/KOH pH 7.6, 10 mM KCl, 1.5 mM $MgCl_2$, 1 mM DTT) for 15-20 min with rotation at 4˚C. Nuclei were pelleted by centrifugation at 4,500 g and 4˚C for 15 min. Nuclear proteins were extracted in buffer C (20 mM Hepes/KOH pH 7.6, 420 mM NaCl, 1.5 mM $MgCl_2$, 0.2 mM EDTA, 25% (v/v) glycerol, 1 mM DTT) for 30 min with rotation at 4˚C. Extracts were cleared by centrifugation at 21,100 g and 4˚C for 45 min. The protein content was determined via Bradford method using Protein Assay (5000006, Biorad) according to manufacturer's instructions.

Nuclear extract from *Drosophila* embryos (TRAX) was obtained as previously described [41].

RT-qPCR and RNA-seq

Total RNA was isolated using the peqGOLD Total RNA Kit (12-6834-02, Peqlab) together with the peqGOLD DNase I Digestion Kit (732-2982, Peqlab) and the integrity of RNA was evaluated on a 1.2% Agarose/TAE gel. For RT-qPCR cDNA was prepared from 1 μg of total RNA using the SensiFAST cDNA Synthesis Kit (BIO-65054, Bioline) and analysed by qPCR using the SensiFast SYBR Lo-ROX Kit (BIO-94050, Bioline) according to manufacturer's instructions together with gene-specific primers (S4 Table). Amplification reactions were measured in triplicates on a Stratagene Mx3000P thermocycler (Agilent Technologies) and the mean values were calculated according to the ΔΔCt method using the mRNA levels of Rp49 as a normalisation reference. mRNA expression was calculated relative to samples treated with a non-targeting dsRNA against GFP. Error bars represent the standard deviation from five biological replicates.

For RNA sequencing the total RNA from three independent dsRNA transfections was isolated. The integrity of RNA was assessed on an Experion StdSens RNA Chip (Bio-Rad). RNA-seq libraries were prepared using a TruSeq Stranded mRNA Library Prep kit (Illumina). Libraries were quantified on a Bioanalyzer (Agilent Technologies) and sequenced on an Illumina HiSeq 1500 platform, rapid-run mode, single-read 50 bp (HiSeq SR Rapid Cluster Kit v2, HiSeq Rapid SBS Kit v2, 50 cycles) according to the manufacturer's instructions.

SDS-PAGE and Western blot

Proteins were electrophoretically separated on a SDS-polyacrylamid gel (SDS-PAGE) and then transferred onto activated polyvinylidene difluride (PVDF) membranes (T830.1, Roth) by Western Blotting in Pierce Western Blot Transfer Buffer (35040, Thermo Fisher Scientific). Membranes were saturated in Blocking buffer (PBS, 0.1% (w/v) Tween-20, 5% (w/v) non-fat dry milk) for 1 h at room temperature and subsequently incubated with the respective

antibody dilution in Blocking buffer overnight at 4˚C. After washing the membranes four times for 5 min at room temperature in Washing buffer (PBS, 0.1% (w/v) Tween-20) appropriate HRP-coupled secondary antibodies (anti-mouse IgG (NA931, GE Healthcare), anti-rabbit IgG (NA934, GE Healthcare), anti-rat IgG (31470, Thermo Fisher Scientific), anti-guinea pig IgG (706-035-148, Jackson ImmunoResearch)) were applied in Blocking buffer for 2 h at room temperature. After four washing cycles for 5 min in Washing buffer Western blot signals were detected by chemiluminescence using the Immobilon Western Blot Chemiluminescence HRP substrate (WBKLS0500, Millipore).

Antibodies and antisera were used in the following dilutions: Ush (1:5,000; (Fossett et al., 2001)), GFP (1:5,000; clone [3H9] from Chromotek), FLAG (1:8,000; clone M2 from Sigma), Tubulin beta (1:8,000; clone KMX-1 from Merck Millipore), dMi-2 (1:8,000; [42]), dMTA1--like (1:10,000; [38]), Cyclin B (1:5,000; clone F2F4 from DHSB), Cyclin A (1:1,000; clone A12 from DHSB), Lamin Dm0 (1:5,000; clone ADL67.10 from DHSB), dp66 (1:10,000; [43]), dp55 (1:20,000; [44]), dMEP-1 (1:10,000; [38]), dRPD3 (1:10,000; [42]), dCHD3 (1:10,000; [45]), dPc (1:50,000; [46]), dE(z) (1:1,000; [47]), dLSD1 (1:5,000; [48]).

Peptide Synthesis and usage in competition assays

Peptides were synthesised in a 10 μmol scale (0.25 mmol/g) following the standard solid phase peptide synthesis (SPPS) methodology, using Fmoc-amino acids and Oxyma/DIC as coupling agents. Final deprotection and cleavage from the solid support was performed with 1.5 ml of cleavage cocktail: 94 TFA/1 TIS/ 2.5 DODT/2.5 H_2O for 3 h. Obtained peptides were purified at 25˚C by preparative reverse phase (RP)-HPLC performed on a PLC 2020 personal purification system (Gilson) with a preparative Nucleodur C18 HTec-column (5 μm, 250 × 16 mm; Macherey Nagel) and a flow rate of 10 ml/min. Detection of the signals was achieved with a UV detector at 220 nm wavelength. The eluents were MilliQ H_2O and MeCN with addition of 0.1% TFA applied at a gradient of 5-40% MeCN.

Peptides were diluted and concentrations were determined according to [49]. The following concentrations were used in interaction assays: 3.5 μM, 7.0 μM, 14.0 μM (FOG1 peptides) and 17.5 μM, 35 μM (Ush peptides) in GST pulldown assays; 1.0 μM, 2.0 μM, 3.0 μM FOG1 peptides in immunoprecipitation assays.

Co-Immunoprecipitation of epitope-tagged proteins

1 mg of nuclear extract was diluted 1:4.2 with buffer C-0 (20 mM Hepes/KOH pH 7.6, 1.5 mM $MgCl_2$, 0.2 mM EDTA, 25% (v/v) glycerol, 0.131% (w/v) NP-40, 1 mM DTT) and adjusted to 1 ml final volume with buffer C-100 (20 mM Hepes/KOH pH 7.6, 100 mM NaCl, 1.5 mM $MgCl_2$, 0.2 mM EDTA, 25% (v/v) glycerol, 0.1% (w/v) NP-40, 1 mM DTT). 5 U/ml of Benzonase was added (70664, Millipore), samples were incubated for 1 h at 4˚C with rotation and diluted extracts were cleared of contingent precipitates by centrifugation (15 min, 21,100 g, 4˚C). 25 μl of GFP-Trap Agarose (gta, ChromoTek) or ANTI-FLAG M2 Affinity Gel (A2220, Sigma) was blocked in buffer C-100 containing 1 mg/ml BSA and 1% (w/v) fish skin gelatin for 1 h at 4˚C with rotation and then added to the diluted extracts. Immunoprecipitation was carried out overnight at 4˚C with rotation. The resin was washed four times with 1 ml IP150 buffer (25 mM Hepes/KOH pH 7.6, 150 mM NaCl, 12.5 mM $MgCl_2$, 0.1 mM EDTA, 10% (v/v) glycerol 0.1% (w/v) NP-40, 1 mM DTT) and finally resuspended in SDS-PAGE loading buffer (50 mM Tris/HCl pH 6.8, 2% (w/v) SDS, 10% (v/v) glycerol, 0.1% (w/v) bromophenol blue, 100 mM DTT). Immunoprecipitates were analysed by SDS-PAGE and Western blot.

Chromatin Immunoprecipitation followed by next-generation sequencing (ChIP-seq)

10^8 S2[Cas9] cells expressing endogenously tagged proteins were cross-linked with 1% Formaldehyde for 10 min at RT with agitation. Fixation was quenched by addition of Glycin to a final concentration of 240 mM and incubation for 10 min at RT with agitation. After two times washing in PBS cells were lysed in 1 ml of ChIP Lysis buffer (50 mM Tris/HCl pH 8.0, 10 mM EDTA, 1% (w/v) SDS, 1 mM DTT) for 10 min on ice. Chromatin was sheared by sonication in the Bioruptor UCD-200TM-EX (Diagenode) supplied with ice water in three cycles over 30 min. Each cycle lasted for 10 min with 10x 30 s intervals of sonication at high power followed by 30 s without sonication to ensure proper cooling. Cell debris were pelleted by centrifugation (20 min, 21,100 g, 4˚C) and the supernatant containing fragmented chromatin was stored at -80˚C. The fragment size was monitored by decrosslinking 50 μl of chromatin-containing lysate in presence of RNase A (400 ng/μl; A3832, Applichem) and Proteinase K (400 ng/μl; 7528.1, Roth) for 3 h at 55˚C followed by 65˚C overnight. DNA was purified using the QIAquick PCR Purification Kit (28106, Qiagen) and fragment sizes were evaluated on a 1.2% Agarose/TAE gel.

For one ChIP reaction 140 μl of chromatin lysate was pre-cleared by diluting it 1:10 in ChIP IP buffer (16.7 mM Tris/HCl pH 8.0, 1.2 mM EDTA, 167 mM NaCl, 1.1% (w/v) Triton X-100, 0.01% (w/v) SDS, 1 mM DTT) and addition of 40 μl Protein A Sepharose resin (nProtein A Sepharose 4 Fast Flow, 17-5280, GE Healthcare) that had been blocked for 1 h in ChIP Blocking buffer (ChIP Low salt buffer containing 2 mg/ml BSA and 2% (w/v) fish skin gelatin). After incubation at 4˚C for 1 h with rotation, beads were collected (centrifugation for 10 min at 21,100 g and 4˚C) and the supernatant was added to 25 μl of blocked GFP-Trap Agarose (gta, ChromoTek).

Immunoprecipitation (IP) took place overnight at 4˚C with rotation followed by extensive washing: Three times with 1 ml of ChIP Low salt buffer (20 mM Tris/HCl pH 8.0, 2 mM EDTA, 150 mM NaCl, 1% (w/v) Triton X-100, 0.1% (w/v) SDS, 1 mM DTT), three times with 1 ml of ChIP High salt buffer (20 mM Tris/HCl pH 8.0, 2 mM EDTA, 500 mM NaCl, 1% (w/v) Triton X-100, 0.1% (w/v) SDS, 1 mM DTT), once with 1 ml of ChIP LiCl buffer (10 mM Tris/HCl pH 8.0, 1 mM EDTA, 250 mM LiCl, 0.1% (w/v) NP-40, 1 mM DTT) and finally twice with TE buffer (10 mM Tris/HCl pH 8.0, 1 mM EDTA). Each washing step was carried out at 4˚C for 5 min with rotation and the resin was pelleted in between by centrifugation (4 min, 400 g, 4˚C).

Cross-linked protein-DNA complexes were eluted twice from the resin in 250 μl ChIP elution buffer (100 mM $NaHCO_3$, 1% (w/v) SDS) for 20 min at RT with rotation. The resin was pelleted by centrifugation (3 min, 1,200 g, RT) and the eluate was removed. After the second elution cycle the resin-buffer suspension was incubated at 95˚C for 10 min, the resin was pelleted and both eluates were pooled. 14 μl of pre-cleared chromatin was added to 500 μl of ChIP elution buffer as "input" sample. 40 μM of NaCl was added to IP and input samples and protein-DNA complexes were decrosslinked overnight at 65˚C with agitation. 40 mM Tris/HCl pH 6.8, 1 mM EDTA and 40 ng/μl Proteinase K (7528.1, Roth) was added to each sample and proteins were digested at 45˚C for one hour with agitation. The DNA was purified using QIAquick PCR purification kit (28106, Qiagen).

Purified DNA from up to six ChIP reactions was pooled, concentrated (Concentrator 5301, Eppendorf) and quantified using the Qubit dsDNA High-Sensitivity Assay Kit (Q32851, ThermoFisher scientific). Libraries were generated from 1 ng of DNA using the MicroPlex Library Preparation Kit v2 (C05010012, Diagenode) according to manufacturer's instructions. The amplified libraries were purified using AMPure XP beads (A63880, Beckman Coulter) and eluted in TE buffer.

The quality of sequencing libraries was controlled on a Bioanalyzer 2100 using the Agilent High Sensitivity DNA Kit (Agilent). Pooled sequencing libraries were quantified with digital polymerase chain reaction (PCR) (QuantStudio 3D, Thermo Fisher) and sequenced on an Illumina HiSeq 1500 platform, rapid-run mode, single-read 50 bp (HiSeq SR Rapid Cluster Kit v2, HiSeq Rapid SBS Kit v2, 50 cycles) according to the manufacturer's instructions.

GST pulldown assay

pGEX2T-mFOG1(1-45) [15] or pGEX4T1 expression constructs were transformed into an E. coli BL21DE3 strain (C2527H, NEB). The culture was expanded and expression was induced at an OD_{600} of 0.7 with 0.4 mM IPTG. After 24 h at 18˚C bacteria were harvested, washed with PBS and resuspended in PBS/Triton (PBS containing 1% (w/v) Triton X-100). For lysis, cells were sonicated 12 times for 12 s on an ultrasonic homogenizer (HD2200, Bendelin electronics) at 25% output while keeping the suspension on ice in between. The suspension was frozen in liquid nitrogen and thawed on ice three times before cell debris were pelleted by centrifugation at 4˚C and 27,000 g for 30 min. GST-fusion proteins were coupled to Glutathione Sepharose 4 Fast Flow (17-5132-01, GE Healthcare) for 2 h at 4˚C with rotation. Unbound proteins were removed by washing three times with PBS/Triton and twice with PBS for 5 min at 4˚C with rotation. The amount of GST-fusion protein bound to the Sepharose resin was evaluated by comparison to a BSA standard on a Coomassie stained SDS-PA gel.

GST pulldown interaction assays were performed using 10-20 μg of GST fusion proteins and 1 mg of S2 cell nuclear extract or TRAX per pulldown reaction. The resin was blocked for 1 h at 4˚C with rotation in GST Pulldown Buffer containing 1 mg/ml BSA and 1% (w/v) fish skin gelatin. Binding took place overnight at 4˚C with rotation in 1 ml GST Pulldown buffer (25 mM Hepes/KOH pH 7.6, 150 mM KCl, 12.5 mM $MgCl_2$, 0.1 mM EDTA, 20% (v/v) glycerol 0.1% (w/v) NP-40, 1 mM DTT). The resin was washed four times with 1 ml GST Pulldown buffer for 5 min at 4˚C with rotation followed by centrifugation (4 min, 1,500 g, 4˚C). Interacting proteins were analyzed by SDS-PAGE and Western blot.

Fly stocks

The w^{1118} served as the wild-type control. The following stocks were obtained from the Bloomington stock center: w^{1118};MTA1-like^{d09140}/TM6B,Tb^1, y^1 w*;MTA1-like^{MI01790}, w^{1118}; simj^{BG00403}/TM6B, Tb^1, simj^{01814} ry^{506}, y^1 w*;HDAC1$^{12\text{-}37}$/TM6B,Tb^1, HDAC1^{04556} ry^{506}/TM3,ry^{RK} Sb^1 Ser^1, Mi-2^4 red^1 e^4/TM6B, Sb^1 Tb^1 ca^1, y^1 w^{1118}; Mi-2^{L1243}/TM3, Ser^1. The dome-GAL4 line was a gift from U. Banerjee (UCLA). y w^{67c23}; ush^{vx22}/CyO y$^+$ and y w^{67c23}; ush^{R24}/CyO y$^+$, the misshapen-mCherry (MSN-C) and the hhF4f-GFP fluorescent reporter transgene stocks have been described previously [11,14,32]. The y w;ush^{VX22}, MSN-C/CyO y$^+$ was created using standard recombination procedures. Larvae were cultured at 23˚C and late 3rd instar wandering larvae were assayed for lamellocyte differentiation. Fluorescent microscopy was conducted using a Zeiss Axioplan microscope.

Second site non complementation assays

Larvae were cultured at 23˚C and late 3rd instar wandering larvae were assayed for lamellocyte differentiation. Larvae were placed on a slide with a drop of PBS and observed under fluorescent microscopy using a Zeiss Axioplan microscope. Only larvae with *MSN-C* fluorescent reporter transgene expression were scored.

Hh enhancer reporter assay in larval lymph glands

The dome-Gal4 line was crossed with appropriate hhF4f-GFP;UAS-RNAi lines, mid-third instar larvae were collected and lymph glands were dissected lymph glands. Immunostaining was performed as described previously [14]. The following antibodies were used to identify PSC cells: mouse anti-Antp (primary antibody; 1:100; 4C3, Developmental Studies Hybridoma Bank); Alexa 555-conjugated mouse IgG antibody (secondary antibody; A28180, Thermo Fisher Scientific). Cell nuclei were stained with DAPI (Invitrogen). Immunostained samples were analysed with a Nikon A1R laser-scanning confocal microscope.

Bioinformatical analysis

ChIP-Seq data were aligned to *Drosophila* Genome dm3, using bowtie2 [50]. Bigwig files were obtained using Galaxy/deepTools [51] normalised to genome Coverage. Data were visualised in the UCSC genome browser [52]. Data analysis was performed using Galaxy [53], Cistrome [54] and Bioconductor/R [55]. Peaks were identified using MACS2 [56] with the following settings: Set lower mfold bound = 5; Set upper mfold bound = 50; Band width for picking regions to compute fragment size = 300; Peak detection based on = q-value; Minimum FDR = 0.05. Overlap between peaks was obtained using the Venn Diagram tool within Galaxy/Cistrome platform. Peaks were considered overlapping at ≥ 1 common nucleotide. Enriched motifs were identified using HOMER [57]. Heatmaps were obtained using Galaxy/deepTools. Overlap with genomic features was determined using "CEAS: Enrichment on chromosome and annotation" [58] within the Galaxy/Cistrome platform. Profiles of the histone marks were obtained using Galaxy/deepTools. Following public datasets were used: H3K4me1 (GSM2259983, GSM2259984), H3K4me3 (GSM2259985, GSM2259986), H3K27ac (GSM2259987, GSM2259988) [59], H3K27me3 (GSM2776903) [60], Mi-2 modeENCODE (GSM1147259, GSM1147260), Mi-2 (ERR1331728, ERR1331729) [26]. Transcription start site (TSS) annotation was obtained from the UCSC table browser and coverage profiles were calculated using Galaxy/deepTools.

RNA-Seq data were aligned to *Drosophila* transcriptome using RNA Star (2.7.2b) [61]. Counts per gene were determined using FeatureCounts (1.6.4) [62]. Differentially expressed genes and normalised reads were determined using DeSeq2 (2.11.40.6) [63]. Gene ontology analysis on significantly deregulated genes (adj. $p < 0.01$) was performed using the Metascape tool (version 3.5, 2019-08-14, [64]) on "Express Analysis" settings. Additional GO terms and transcript expression patterns were obtained from FlyBase (version FB2019_06) and the Berkley *Drosophila* Genome Project (release 3, 2019-06-04) respectively.

Supporting information

S1 Fig. Insertion of GFP- or FLAG-tag sequences at *Ush* and *dMi-2* 3' ends using CRISPR/Cas9. A Schematic representation of the *Ush* gene locus before (top) and after insertion of GFP (middle) and FLAG (bottom) tagging constructs. Black boxes represent exons, black (broken) lines represent introns. The inserted tag sequences (GFP: green, FLAG, red) and selection marker (promoter: ochre, Puromycin resistance: orange) are highlighted. The positions of primers used for genotyping of Ush alleles are indicated with purple arrowheads. **B** PCR from genomic DNA of control cells and cells modified to express GFP- or FLAG-tagged Ush, respectively. Insertion of the tag sequence followed by a Puromycin selection marker is monitored using primers surrounding the 3' end of the coding region within the Ush gene. Non-tagged alleles give rise to a 216 bp amplicon, GFP- and FLAG-tagged alleles result in 1991 bp and 1311 bp fragments respectively. **C** Schematic representation of the *dMi-2* gene locus before (top) and after insertion of GFP (middle) and FLAG (bottom) tagging constructs. Black boxes

represent exons, black (broken) lines represent introns. The inserted tag sequences (GFP: green, FLAG, red) and selection marker (promoter: light blue, Blasticidin resistance: dark blue) are highlighted. The positions of primers used for genotyping of Ush alleles are indicated with purple arrowheads. **D** PCR from genomic DNA of control cells and cells modified to express GFP- or FLAG-tagged dMi-2, respectively. Insertion of the tag sequence followed by a Blasticidin selection marker is monitored using primers surrounding the 3' end of the coding region within the Ush gene. Non-tagged alleles give rise to a 200 bp amplicon, GFP- and FLAG-tagged alleles result in 1737 bp and 1077 bp fragments respectively. **E** Nuclear extracts of control cells and cells expressing endogenously tagged dMi-2-GFP or dMi-2-FLAG was probed on Western blot using antibodies against dMi-2, GFP or FLAG. Tubulin signal serves as loading control.
(TIF)

S2 Fig. Ush occupancy at the *lozenge* and the *atilla* gene locus. A Genome browser snapshots of the *lozenge* (*lz*) (top) and the *atilla* (bottom) gene locus displaying Ush occupancy (green) determined by Ush-GFP ChIP-seq. Input signals are shown in black. Location of genes is displayed below with boxes indicating exons.
(TIF)

S3 Fig. Expression of Ush isoforms in S2 cells. A Genome browser snapshots of the Ush gene locus displaying RNA-seq coverage in S2 cells from biological triplicates. Exons encoding unique N-termini are highlighted in green (Ush-B specific) and orange (Ush-A specific).
(TIF)

S4 Fig. Comparison of dMi-2 ChIP-seq datasets. A dMi-2 ChIP-seq peaks obtained in this study were ranked and signals were compared to two other datasets (Kreher et al., 2017 and modENCODE ID 5070) in a region of 5 kb surrounding the respective peak. **B** Genome browser snapshots of an exemplary region displaying dMi-2 occupancy (red: this study; ochre: Kreher et al., 2017; blue: modENCODE ID 5070). Input signals of this study are shown in black. Location of genes is displayed below with boxes indicating exons.
(TIF)

S5 Fig. Ush-B repressed genes. Tables of genes that are significantly upregulated (adj. $p < 0.05$) upon depletion of of Ush-B. Gene symbols are indicated along with the respective fold change relative to cells transfected with control dsRNA (dsEGFP). Respective -log10(p-values) are indicated in the last row. Coloured boxes mark genes associated with hemocyte functions or are specifically expressed in *Drosophila* hemocytes (green), genes associated with cell cycle (orange), and genes involved in lipid metabolism (blue).
(TIF)

S6 Fig. Ush-B activated genes. Tables of genes that are significantly downregulated (adj. $p < 0.05$) upon depletion of of Ush-B. Gene symbols are indicated along with the respective fold change relative to cells transfected with control dsRNA (dsEGFP). Respective -log10(p-values) are indicated in the last row. Coloured boxes mark genes associated with hemocyte functions or are specifically expressed in *Drosophila* hemocytes (green), genes associated with cell cycle (orange), and genes involved in lipid metabolism (blue).
(TIF)

S7 Fig. Cell cycle profiles upon depletion of Ush or NuRD complex components. A Flow cytometry following PI-staining of S2 cells upon dsRNA-mediated depletion of indicated proteins. dsRNA-transfected cells were fixed, stained with PI and subjected to flow cytometry. Histograms show the number of cells plotted against the PI signal (Area of PE channel). The

diploid cell population (2n) and cells that have undergone replication (4n) are indicated. Transfection of dsEGFP and dsLuc severd as control. Two different dsRNA constructs against Ush (all isoforms) were used (dsUsh #1 & dsUsh #2). **B** Viability assay of S2 cells upon depletion of indicated proteins. Viability of cells transfected with control dsRNA (dsEGFP and dsLuc) or dsRNA constructs targeting Ush (dsUsh #1 and dsUsh #2), Ush-B, dMi-2 and dMTA1-like was measured 96 hours post transfection. Error bars represent the standard deviation from biological triplicates (n = 3) and individual values are indicated with circles.
(TIF)

S8 Fig. *Hedgehog* enhancer activity upon loss of Ush expression. Lymph glands isolated from larvae that express a dsRNA against Ush in the medullary zone (**A**), or from larvae that carry homozygous Ush mutant alleles (**B**). All larvae carry a construct, reporting the activity of a minimal *Hedgehog* enhancer by GFP expression (hhF4f-GFP; green).
(TIF)

S1 Table. Occupancy of Ush and dMi-2 at Ush-regulated genes. Representative Ush-regulated genes of each gene class (investigated in Figs 2E and 6C) are listed. Columns 3 and 4 indicate binding of Ush and dMi-2 to the respective gene loci detected by anti-GFP ChIP sequencing (see Figs 1 and 5).
(PDF)

S2 Table. Genes deregulated upon Ush-B RNAi. List of genes that show significant changes (adj. $p < 0.05$) upon depletion of Ush-B. Gene identifiers, fold changes and p-values of each gene are listed. Genes were sorted into the groups "hemocyte-related" (green), "cell cycle" (orange) or "lipid metabolism" (blue) according to the references given in columns 10 and 11.
(PDF)

S3 Table. Ush and dNuRD regulate lamellocyte differentiation in *Drosophila* larvae. Total numbers of examined larvae and penetrance levels of increased lamellocyte counts associated with Fig 7H. Genotypes and the affected dNuRD complex subunit are listed in columns 1-2.
(PDF)

S4 Table. Oligonucleotides used in this study. List of all oligonucleotides and primers used in this study. Sequences and applications are given. References are indicated in column 5.
(PDF)

Acknowledgments

We thank U.Banerjee, J.Müller, P. Verrijzer, R. Nusse, G. Reuter, C. Wu and J. Mackay for the generous gift of fly lines, antibodies and plasmids, T. Zimmermann for bioinformatical support and Uta-Maria Bauer for critically reading the manuscript.

Author Contributions

Conceptualization: Jonathan Lenz, Olalla Vázquez, Tsuyoshi Tokusumi, Nancy Fossett, Alexander Brehm.

Data curation: Andrea Nist, Thorsten Stiewe, Hartmann Raifer.

Formal analysis: Jonathan Lenz, Robert Liefke.

Funding acquisition: Robert Liefke, Olalla Vázquez, Alexander Brehm.

Investigation: Jonathan Lenz, Julianne Funk, Samuel Shoup, Yumiko Tokusumi, Lea Albert, Tsuyoshi Tokusumi.

Methodology: Hartmann Raifer, Klaus Förstemann.

Project administration: Alexander Brehm.

Resources: Robert Schulz, Lea Albert, Klaus Förstemann, Nancy Fossett.

Supervision: Alexander Brehm.

Visualization: Jonathan Lenz, Robert Liefke, Tsuyoshi Tokusumi, Nancy Fossett.

Writing – original draft: Jonathan Lenz, Nancy Fossett, Alexander Brehm.

Writing – review & editing: Jonathan Lenz, Nancy Fossett, Alexander Brehm.

References

1. Kato H, Igarashi K. To be red or white: lineage commitment and maintenance of the hematopoietic system by the "inner myeloid". Haematologica. 2019; 104(10):1919–27. Epub 2019/09/14. https://doi.org/10.3324/haematol.2019.216861 PMID: 31515352.
2. DeVilbiss AW, Tanimura N, McIver SC, Katsumura KR, Johnson KD, Bresnick EH. Navigating Transcriptional Coregulator Ensembles to Establish Genetic Networks: A GATA Factor Perspective. Curr Top Dev Biol. 2016; 118:205–44. Epub 2016/05/04. https://doi.org/10.1016/bs.ctdb.2016.01.003 PMID: 27137658.
3. Banerjee U, Girard JR, Goins LM, Spratford CM. Drosophila as a Genetic Model for Hematopoiesis. Genetics. 2019; 211(2):367–417. https://doi.org/10.1534/genetics.118.300223 PMID: 30733377; PubMed Central PMCID: PMC6366919.
4. Cubadda Y, Heitzler P, Ray RP, Bourouis M, Ramain P, Gelbart W, et al. u-shaped encodes a zinc finger protein that regulates the proneural genes achaete and scute during the formation of bristles in Drosophila. Genes Dev. 1997; 11(22):3083–95. https://doi.org/10.1101/gad.11.22.3083 PMID: 9367989; PubMed Central PMCID: PMC316693.
5. Fossett N, Schulz RA. Functional conservation of hematopoietic factors in Drosophila and vertebrates. Differentiation. 2001; 69(2-3):83–90. https://doi.org/10.1046/j.1432-0436.2001.690202.x PMID: 11798069.
6. Fossett N, Tevosian SG, Gajewski K, Zhang Q, Orkin SH, Schulz RA. The Friend of GATA proteins U-shaped, FOG-1, and FOG-2 function as negative regulators of blood, heart, and eye development in Drosophila. Proc Natl Acad Sci U S A. 2001; 98(13):7342–7. https://doi.org/10.1073/pnas.131215798 PMID: 11404479; PubMed Central PMCID: PMC34670.
7. Haenlin M, Cubadda Y, Blondeau F, Heitzler P, Lutz Y, Simpson P, et al. Transcriptional activity of pannier is regulated negatively by heterodimerization of the GATA DNA-binding domain with a cofactor encoded by the u-shaped gene of Drosophila. Genes Dev. 1997; 11(22):3096–108. https://doi.org/10.1101/gad.11.22.3096 PMID: 9367990; PubMed Central PMCID: PMC316702.
8. Waltzer L, Bataille L, Peyrefitte S, Haenlin M. Two isoforms of Serpent containing either one or two GATA zinc fingers have different roles in Drosophila haematopoiesis. EMBO J. 2002; 21(20):5477–86. https://doi.org/10.1093/emboj/cdf545 PMID: 12374748; PubMed Central PMCID: PMC129077.
9. Dragojlovic-Munther M, Martinez-Agosto JA. Extracellular matrix-modulated Heartless signaling in Drosophila blood progenitors regulates their differentiation via a Ras/ETS/FOG pathway and target of rapamycin function. Dev Biol. 2013; 384(2):313–30. Epub 2013/04/23. https://doi.org/10.1016/j.ydbio.2013.04.004 PMID: 23603494; PubMed Central PMCID: PMC4256155.
10. Fossett N. Signal transduction pathways, intrinsic regulators, and the control of cell fate choice. Biochim Biophys Acta. 2013; 1830(2):2375–84. Epub 2012/06/19. https://doi.org/10.1016/j.bbagen.2012.06.005 PMID: 22705942; PubMed Central PMCID: PMC3477240.
11. Gao H, Wu X, Fossett N. Upregulation of the Drosophila Friend of GATA gene U-shaped by JAK/STAT signaling maintains lymph gland prohemocyte potency. Mol Cell Biol. 2009; 29(22):6086–96. https://doi.org/10.1128/MCB.00244-09 PMID: 19737914; PubMed Central PMCID: PMC2772570.
12. Muratoglu S, Hough B, Mon ST, Fossett N. The GATA factor Serpent cross-regulates lozenge and u-shaped expression during Drosophila blood cell development. Dev Biol. 2007; 311(2):636–49. Epub 2007/09/18. https://doi.org/10.1016/j.ydbio.2007.08.015 PMID: 17869239; PubMed Central PMCID: PMC2132443.

13. Sorrentino RP, Tokusumi T, Schulz RA. The Friend of GATA protein U-shaped functions as a hematopoietic tumor suppressor in Drosophila. Dev Biol. 2007; 311(2):311–23. https://doi.org/10.1016/j.ydbio.2007.08.011 PMID: 17936744.

14. Tokusumi Y, Tokusumi T, Stoller-Conrad J, Schulz RA. Serpent, suppressor of hairless and U-shaped are crucial regulators of hedgehog niche expression and prohemocyte maintenance during Drosophila larval hematopoiesis. Development. 2010; 137(21):3561–8. https://doi.org/10.1242/dev.053728 PMID: 20876645; PubMed Central PMCID: PMC2964091.

15. Hong W, Nakazawa M, Chen YY, Kori R, Vakoc CR, Rakowski C, et al. FOG-1 recruits the NuRD repressor complex to mediate transcriptional repression by GATA-1. EMBO J. 2005; 24(13):2367–78. https://doi.org/10.1038/sj.emboj.7600703 PMID: 15920470; PubMed Central PMCID: PMC1173144.

16. Fossett N, Hyman K, Gajewski K, Orkin SH, Schulz RA. Combinatorial interactions of serpent, lozenge, and U-shaped regulate crystal cell lineage commitment during Drosophila hematopoiesis. Proc Natl Acad Sci U S A. 2003; 100(20):11451–6. https://doi.org/10.1073/pnas.1635050100 PMID: 14504400; PubMed Central PMCID: PMC208778.

17. Huot G, Vernier M, Bourdeau V, Doucet L, Saint-Germain E, Gaumont-Leclerc MF, et al. CHES1/FOXN3 regulates cell proliferation by repressing PIM2 and protein biosynthesis. Mol Biol Cell. 2014; 25(5):554–65. Epub 2014/01/10. https://doi.org/10.1091/mbc.E13-02-0110 PMID: 24403608; PubMed Central PMCID: PMC3937083.

18. Guruharsha KG, Obar RA, Mintseris J, Aishwarya K, Krishnan RT, Vijayraghavan K, et al. Drosophila protein interaction map (DPiM): a paradigm for metazoan protein complex interactions. Fly (Austin). 2012; 6(4):246–53. Epub 2012/12/12. https://doi.org/10.4161/fly.22108 PMID: 23222005; PubMed Central PMCID: PMC3519659.

19. Kunert N, Wagner E, Murawska M, Klinker H, Kremmer E, Brehm A. dMec: a novel Mi-2 chromatin remodelling complex involved in transcriptional repression. EMBO J. 2009; 28(5):533–44. https://doi.org/10.1038/emboj.2009.3 PMID: 19165147; PubMed Central PMCID: PMC2657585.

20. Cismasiu VB, Adamo K, Gecewicz J, Duque J, Lin Q, Avram D. BCL11B functionally associates with the NuRD complex in T lymphocytes to repress targeted promoter. Oncogene. 2005; 24(45):6753–64. https://doi.org/10.1038/sj.onc.1208904 PMID: 16091750.

21. Kloet SL, Baymaz HI, Makowski M, Groenewold V, Jansen PW, Berendsen M, et al. Towards elucidating the stability, dynamics and architecture of the nucleosome remodeling and deacetylase complex by using quantitative interaction proteomics. FEBS J. 2015; 282(9):1774–85. https://doi.org/10.1111/febs.12972 PMID: 25123934.

22. Lauberth SM, Rauchman M. A conserved 12-amino acid motif in Sall1 recruits the nucleosome remodeling and deacetylase corepressor complex. J Biol Chem. 2006; 281(33):23922–31. https://doi.org/10.1074/jbc.M513461200 PMID: 16707490.

23. Roche AE, Bassett BJ, Samant SA, Hong W, Blobel GA, Svensson EC. The zinc finger and C-terminal domains of MTA proteins are required for FOG-2-mediated transcriptional repression via the NuRD complex. J Mol Cell Cardiol. 2008; 44(2):352–60. https://doi.org/10.1016/j.yjmcc.2007.10.023 PMID: 18067919; PubMed Central PMCID: PMC2277079.

24. Verstappen G, van Grunsven LA, Michiels C, Van de Putte T, Souopgui J, Van Damme J, et al. Atypical Mowat-Wilson patient confirms the importance of the novel association between ZFHX1B/SIP1 and NuRD corepressor complex. Hum Mol Genet. 2008; 17(8):1175–83. https://doi.org/10.1093/hmg/ddn007 PMID: 18182442.

25. Kim J, Lu C, Srinivasan S, Awe S, Brehm A, Fuller MT. Blocking promiscuous activation at cryptic promoters directs cell type-specific gene expression. Science. 2017; 356(6339):717–21. https://doi.org/10.1126/science.aal3096 PMID: 28522526.

26. Kreher J, Kovac K, Bouazoune K, Macinkovic I, Ernst AL, Engelen E, et al. EcR recruits dMi-2 and increases efficiency of dMi-2-mediated remodelling to constrain transcription of hormone-regulated genes. Nat Commun. 2017; 8:14806. https://doi.org/10.1038/ncomms14806 PMID: 28378812; PubMed Central PMCID: PMC5382322.

27. Murawsky CM, Brehm A, Badenhorst P, Lowe N, Becker PB, Travers AA. Tramtrack69 interacts with the dMi-2 subunit of the Drosophila NuRD chromatin remodelling complex. EMBO Rep. 2001; 2(12):1089–94. https://doi.org/10.1093/embo-reports/kve252 PMID: 11743021; PubMed Central PMCID: PMC1084170.

28. Baldeosingh R, Gao H, Wu X, Fossett N. Hedgehog signaling from the Posterior Signaling Center maintains U-shaped expression and a prohemocyte population in Drosophila. Dev Biol. 2018; 441(1):132–45. https://doi.org/10.1016/j.ydbio.2018.06.020 PMID: 29966604; PubMed Central PMCID: PMC6064674.

29. Mandal L, Martinez-Agosto JA, Evans CJ, Hartenstein V, Banerjee U. A Hedgehog- and Antennapedia-dependent niche maintains Drosophila haematopoietic precursors. Nature. 2007; 446(7133):320–4.

Epub 2007/03/16. https://doi.org/10.1038/nature05585 PMID: 17361183; PubMed Central PMCID: PMC2807630.

30. Gao C, Dimitrov T, Yong KJ, Tatetsu H, Jeong HW, Luo HR, et al. Targeting transcription factor SALL4 in acute myeloid leukemia by interrupting its interaction with an epigenetic complex. Blood. 2013; 121 (8):1413–21. https://doi.org/10.1182/blood-2012-04-424275 PMID: 23287862; PubMed Central PMCID: PMC3578956.

31. Gao H, Baldeosingh R, Wu X, Fossett N. The Friend of GATA Transcriptional Co-Regulator, U-Shaped, Is a Downstream Antagonist of Dorsal-Driven Prohemocyte Differentiation in Drosophila. PLoS One. 2016; 11(5):e0155372. Epub 2016/05/11. https://doi.org/10.1371/journal.pone.0155372 PMID: 27163255; PubMed Central PMCID: PMC4862636.

32. Tokusumi T, Sorrentino RP, Russell M, Ferrarese R, Govind S, Schulz RA. Characterization of a lamellocyte transcriptional enhancer located within the misshapen gene of Drosophila melanogaster. PLoS One. 2009; 4(7):e6429. Epub 2009/07/31. https://doi.org/10.1371/journal.pone.0006429 PMID: 19641625; PubMed Central PMCID: PMC2713827.

33. Mehla K, Singh PK. Metabolic Regulation of Macrophage Polarization in Cancer. Trends Cancer. 2019; 5(12):822–34. Epub 2019/12/10. https://doi.org/10.1016/j.trecan.2019.10.007 PMID: 31813459.

34. Kadri Z, Lefevre C, Goupille O, Penglong T, Granger-Locatelli M, Fucharoen S, et al. Erythropoietin and IGF-1 signaling synchronize cell proliferation and maturation during erythropoiesis. Genes Dev. 2015; 29(24):2603–16. Epub 2015/12/19. https://doi.org/10.1101/gad.267633.115 PMID: 26680303; PubMed Central PMCID: PMC4699388.

35. Kadri Z, Shimizu R, Ohneda O, Maouche-Chretien L, Gisselbrecht S, Yamamoto M, et al. Direct binding of pRb/E2F-2 to GATA-1 regulates maturation and terminal cell division during erythropoiesis. PLoS Biol. 2009; 7(6):e1000123. Epub 2009/06/11. https://doi.org/10.1371/journal.pbio.1000123 PMID: 19513100; PubMed Central PMCID: PMC2684697.

36. Lejon S, Thong SY, Murthy A, AlQarni S, Murzina NV, Blobel GA, et al. Insights into association of the NuRD complex with FOG-1 from the crystal structure of an RbAp48.FOG-1 complex. J Biol Chem. 2011; 286(2):1196–203. https://doi.org/10.1074/jbc.M110.195842 PMID: 21047798; PubMed Central PMCID: PMC3020727.

37. Dubuissez M, Loison I, Paget S, Vorng H, Ait-Yahia S, Rohr O, et al. Protein Kinase C-Mediated Phosphorylation of BCL11B at Serine 2 Negatively Regulates Its Interaction with NuRD Complexes during CD4+ T-Cell Activation. Mol Cell Biol. 2016; 36(13):1881–98. Epub 2016/05/11. https://doi.org/10.1128/MCB.00062-16 PMID: 27161321; PubMed Central PMCID: PMC4911745.

38. Reddy BA, Bajpe PK, Bassett A, Moshkin YM, Kozhevnikova E, Bezstarosti K, et al. Drosophila transcription factor Tramtrack69 binds MEP1 to recruit the chromatin remodeler NuRD. Mol Cell Biol. 2010; 30(21):5234–44. https://doi.org/10.1128/MCB.00266-10 PMID: 20733004; PubMed Central PMCID: PMC2953047.

39. de la Cruz AF, Edgar BA. Flow cytometric analysis of Drosophila cells. Methods Mol Biol. 2008; 420:373–89. Epub 2008/07/22. https://doi.org/10.1007/978-1-59745-583-1_24 PMID: 18641961.

40. Watson JV, Chambers SH, Smith PJ. A pragmatic approach to the analysis of DNA histograms with a definable G1 peak. Cytometry. 1987; 8(1):1–8. Epub 1987/01/01. https://doi.org/10.1002/cyto.990080101 PMID: 3803091.

41. Kunert N, Brehm A. Mass production of Drosophila embryos and chromatographic purification of native protein complexes. Methods Mol Biol. 2008; 420:359–71. https://doi.org/10.1007/978-1-59745-583-1_23 PMID: 18641960.

42. Brehm A, Langst G, Kehle J, Clapier CR, Imhof A, Eberharter A, et al. dMi-2 and ISWI chromatin remodelling factors have distinct nucleosome binding and mobilization properties. EMBO J. 2000; 19 (16):4332–41. https://doi.org/10.1093/emboj/19.16.4332 PMID: 10944116; PubMed Central PMCID: PMC302042.

43. Kon C, Cadigan KM, da Silva SL, Nusse R. Developmental roles of the Mi-2/NURD-associated protein p66 in Drosophila. Genetics. 2005; 169(4):2087–100. Epub 2005/02/08. https://doi.org/10.1534/genetics.104.034595 PMID: 15695365; PubMed Central PMCID: PMC1449583.

44. Martinez-Balbas MA, Tsukiyama T, Gdula D, Wu C. Drosophila NURF-55, a WD repeat protein involved in histone metabolism. Proc Natl Acad Sci U S A. 1998; 95(1):132–7. Epub 1998/02/21. https://doi.org/10.1073/pnas.95.1.132 PMID: 9419341; PubMed Central PMCID: PMC18150.

45. Murawska M, Kunert N, van Vugt J, Langst G, Kremmer E, Logie C, et al. dCHD3, a novel ATP-dependent chromatin remodeler associated with sites of active transcription. Mol Cell Biol. 2008; 28(8):2745–57. https://doi.org/10.1128/MCB.01839-07 PMID: 18250149; PubMed Central PMCID: PMC2293103.

46. Papp B, Muller J. Histone trimethylation and the maintenance of transcriptional ON and OFF states by trxG and PcG proteins. Genes Dev. 2006; 20(15):2041–54. Epub 2006/08/03. https://doi.org/10.1101/gad.388706 PMID: 16882982; PubMed Central PMCID: PMC1536056.

47. Gambetta MC, Oktaba K, Muller J. Essential role of the glycosyltransferase sxc/Ogt in polycomb repression. Science. 2009; 325(5936):93–6. Epub 2009/05/30. https://doi.org/10.1126/science.1169727 PMID: 19478141.

48. Rudolph T, Yonezawa M, Lein S, Heidrich K, Kubicek S, Schafer C, et al. Heterochromatin formation in Drosophila is initiated through active removal of H3K4 methylation by the LSD1 homolog SU(VAR)3-3. Mol Cell. 2007; 26(1):103–15. https://doi.org/10.1016/j.molcel.2007.02.025 PMID: 17434130.

49. Kuipers BJ, Gruppen H. Prediction of molar extinction coefficients of proteins and peptides using UV absorption of the constituent amino acids at 214 nm to enable quantitative reverse phase high-performance liquid chromatography-mass spectrometry analysis. J Agric Food Chem. 2007; 55(14):5445–51. Epub 2007/06/02. https://doi.org/10.1021/jf070337l PMID: 17539659.

50. Langmead B, Salzberg SL. Fast gapped-read alignment with Bowtie 2. Nat Methods. 2012; 9(4):357–9. Epub 2012/03/06. https://doi.org/10.1038/nmeth.1923 PMID: 22388286; PubMed Central PMCID: PMC3322381.

51. Ramirez F, Dundar F, Diehl S, Gruning BA, Manke T. deepTools: a flexible platform for exploring deep-sequencing data. Nucleic Acids Res. 2014; 42(Web Server issue):W187–91. Epub 2014/05/07. https://doi.org/10.1093/nar/gku365 PMID: 24799436; PubMed Central PMCID: PMC4086134.

52. Kent WJ, Sugnet CW, Furey TS, Roskin KM, Pringle TH, Zahler AM, et al. The human genome browser at UCSC. Genome Res. 2002; 12(6):996–1006. Epub 2002/06/05. https://doi.org/10.1101/gr.229102 PMID: 12045153; PubMed Central PMCID: PMC186604.

53. Afgan E, Baker D, Batut B, van den Beek M, Bouvier D, Cech M, et al. The Galaxy platform for accessible, reproducible and collaborative biomedical analyses: 2018 update. Nucleic Acids Res. 2018; 46 (W1):W537–W44. Epub 2018/05/24. https://doi.org/10.1093/nar/gky379 PMID: 29790989; PubMed Central PMCID: PMC6030816.

54. Liu T, Ortiz JA, Taing L, Meyer CA, Lee B, Zhang Y, et al. Cistrome: an integrative platform for transcriptional regulation studies. Genome Biol. 2011; 12(8):R83. Epub 2011/08/24. https://doi.org/10.1186/gb-2011-12-8-r83 PMID: 21859476; PubMed Central PMCID: PMC3245621.

55. Huber W, Carey VJ, Gentleman R, Anders S, Carlson M, Carvalho BS, et al. Orchestrating high-throughput genomic analysis with Bioconductor. Nat Methods. 2015; 12(2):115–21. Epub 2015/01/31. https://doi.org/10.1038/nmeth.3252 PMID: 25633503; PubMed Central PMCID: PMC4509590.

56. Zhang Y, Liu T, Meyer CA, Eeckhoute J, Johnson DS, Bernstein BE, et al. Model-based analysis of ChIP-Seq (MACS). Genome Biol. 2008; 9(9):R137. https://doi.org/10.1186/gb-2008-9-9-r137 PMID: 18798982; PubMed Central PMCID: PMC2592715.

57. Heinz S, Benner C, Spann N, Bertolino E, Lin YC, Laslo P, et al. Simple combinations of lineage-determining transcription factors prime cis-regulatory elements required for macrophage and B cell identities. Mol Cell. 2010; 38(4):576–89. Epub 2010/06/02. https://doi.org/10.1016/j.molcel.2010.05.004 PMID: 20513432; PubMed Central PMCID: PMC2898526.

58. Shin H, Liu T, Manrai AK, Liu XS. CEAS: cis-regulatory element annotation system. Bioinformatics. 2009; 25(19):2605–6. Epub 2009/08/20. https://doi.org/10.1093/bioinformatics/btp479 PMID: 19689956.

59. Henriques T, Scruggs BS, Inouye MO, Muse GW, Williams LH, Burkholder AB, et al. Widespread transcriptional pausing and elongation control at enhancers. Genes Dev. 2018; 32(1):26–41. Epub 2018/01/31. https://doi.org/10.1101/gad.309351.117 PMID: 29378787; PubMed Central PMCID: PMC5828392.

60. Huang C, Yang F, Zhang Z, Zhang J, Cai G, Li L, et al. Mrg15 stimulates Ash1 H3K36 methyltransferase activity and facilitates Ash1 Trithorax group protein function in Drosophila. Nat Commun. 2017; 8 (1):1649. Epub 2017/11/22. https://doi.org/10.1038/s41467-017-01897-3 PubMed Central PMCID: PMC5696344. PMID: 29158494

61. Dobin A, Davis CA, Schlesinger F, Drenkow J, Zaleski C, Jha S, et al. STAR: ultrafast universal RNA-seq aligner. Bioinformatics. 2013; 29(1):15–21. https://doi.org/10.1093/bioinformatics/bts635 PMID: 23104886; PubMed Central PMCID: PMC3530905.

62. Liao Y, Smyth GK, Shi W. featureCounts: an efficient general purpose program for assigning sequence reads to genomic features. Bioinformatics. 2014; 30(7):923–30. Epub 2013/11/15. https://doi.org/10.1093/bioinformatics/btt656 PMID: 24227677.

63. Love MI, Huber W, Anders S. Moderated estimation of fold change and dispersion for RNA-seq data with DESeq2. Genome Biol. 2014; 15(12):550. https://doi.org/10.1186/s13059-014-0550-8 PMID: 25516281; PubMed Central PMCID: PMC4302049.

64. Zhou Y, Zhou B, Pache L, Chang M, Khodabakhshi AH, Tanaseichuk O, et al. Metascape provides a biologist-oriented resource for the analysis of systems-level datasets. Nat Commun. 2019; 10(1):1523. Epub 2019/04/05. https://doi.org/10.1038/s41467-019-09234-6 PMID: 30944313; PubMed Central PMCID: PMC6447622.

Supplementary Figure 1

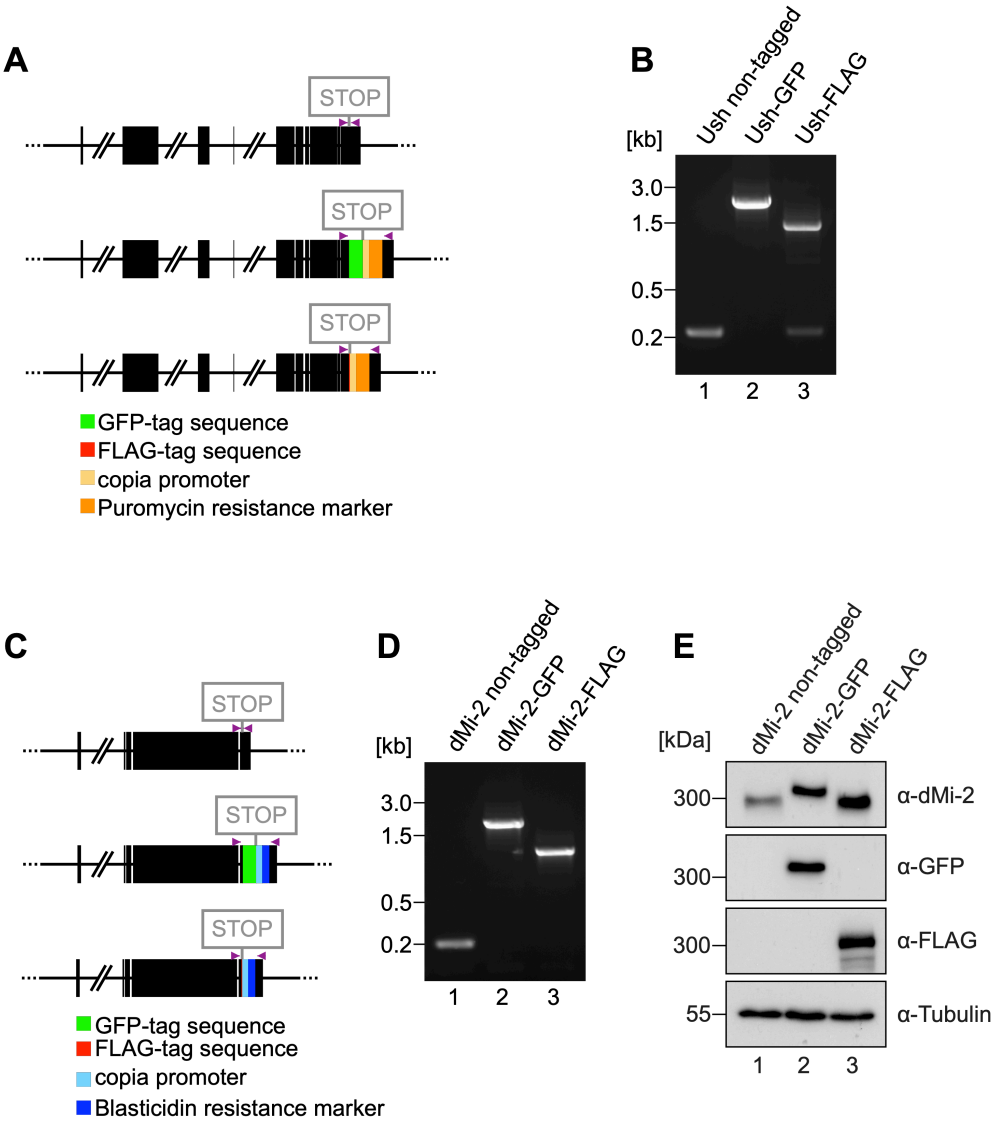

Supplementary Figure 2

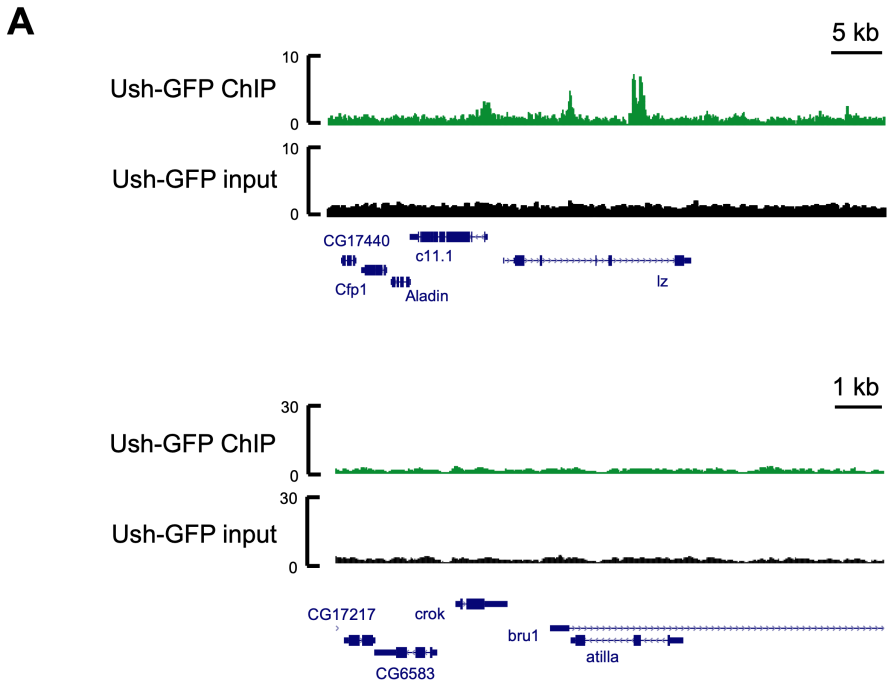

Supplementary Figure 3

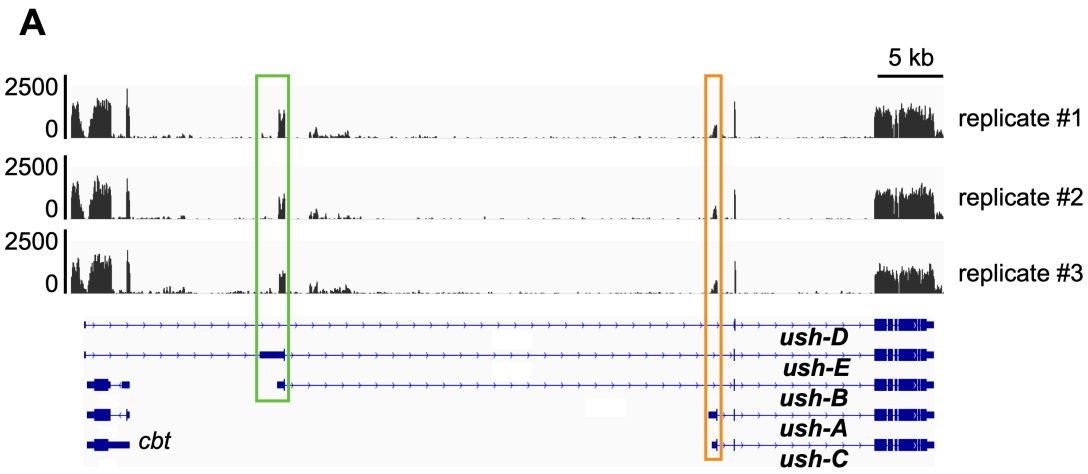

Supplementary Figure 4

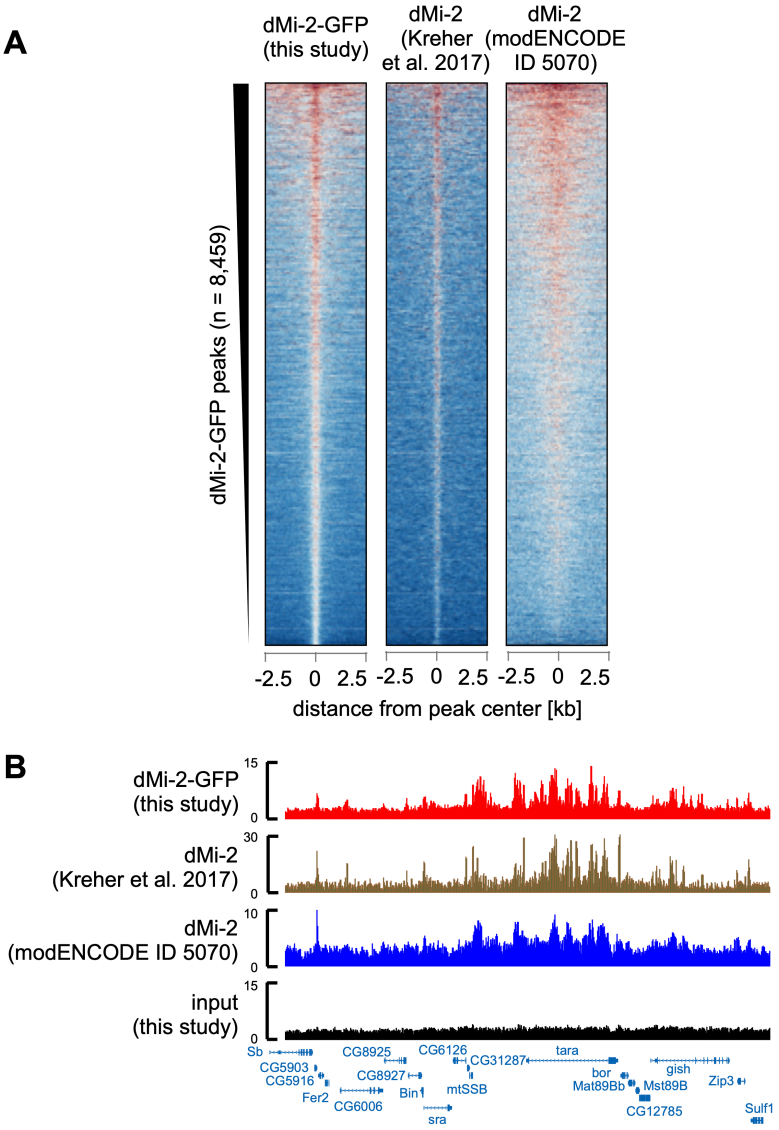

Supplementary Figure 5

A

gene symbol	FC dsUsh-B/ dsEGFP	-log10 (p-value)
comm2	3.58	17.62
CG3246	1.98	3.37
axo	1.97	3.37
CG14879	1.88	2.72
CG12075	1.83	2.74
RpL18	1.82	3.46
pirk	1.80	2.29
Cyp310a1	1.74	2.74
CG8312	1.74	2.13
GILT3	1.73	1.77
Cyt-b5-r	1.71	1.75
CG4611	1.71	3.37
CG1077	1.68	1.63
Ugt36Bc	1.67	1.56
CG42324	1.67	1.58
path	1.66	1.58
CG3655	1.66	1.55
lncRNA:CR44	1.66	1.53
nkd	1.66	1.53
AdamTS-A	1.62	1.37
CG4872	1.61	2.26
p38c	1.61	1.33
CG42458	1.60	1.36
CG8563	1.59	1.75
Phk-3	1.53	1.56
ATPsyndelta	1.53	1.48
CG10737	1.53	2.37
CG30069	1.52	2.14
CG32280	1.51	1.64
IP3K1	1.45	3.29
Pmp70	1.45	3.57
CG3408	1.43	1.36
Rac1	1.43	1.79
CD98hc	1.40	1.55
AsnS	1.40	1.35
ThrRS	1.40	1.36
14-3-3epsilon	1.37	1.79
SCaMC	1.35	1.61
bbc	1.31	1.64
TyrRS	1.31	1.75
CG17746	1.30	1.56
eIF3d1	1.29	1.40
CysRS	1.29	1.72
kay	1.26	1.35
CG1354	1.23	2.51
TBCB	1.22	1.55
muc	1.16	1.64

hemocyte-related
cell cycle
lipid metabolism

Supplementary Figure 6

B

gene symbol	FC dsUsh-B/ dsEGFP	-log$_{10}$ (p-value)
Col4a1	0.41	6.57
vkg	0.46	4.19
CG5397	0.48	3.84
CG5849	0.51	3.33
Tsp42Ed	0.54	2.53
lncRNA:CR44	0.54	2.72
Spn28Dc	0.54	3.60
kek1	0.55	3.06
ATP8B	0.55	2.26
CG34034	0.57	3.37
CG8008	0.60	1.55
mahe	0.61	3.15
Pfdn5	0.61	1.59
Traf4	0.62	1.73
Arc2	0.63	1.75
Pdfr	0.63	1.59
N	0.64	1.65
CG8046	0.64	1.33
CG3448	0.64	1.53

gene symbol	FC dsUsh-B/ dsEGFP	-log$_{10}$ (p-value)
CG31777	0.64	1.59
CG18088	0.65	2.84
unc-13	0.67	2.14
Rab23	0.67	1.55
GstE2	0.67	1.64
Tsp96F	0.69	1.79
CG12868	0.69	3.06
ver	0.72	3.71
Bin1	0.72	3.60
Tsp42Ee	0.73	1.53
Marc	0.75	1.35
IscU	0.75	4.14
Lst8	0.76	1.58
mre11	0.78	1.77
DNAlig4	0.79	1.58
CG33169	0.79	1.35
CG11436	0.80	1.59
CG4239	0.80	1.79
CG6171	0.81	1.35

hemocyte-related
cell cycle
lipid metabolism

Supplementary Figure 7

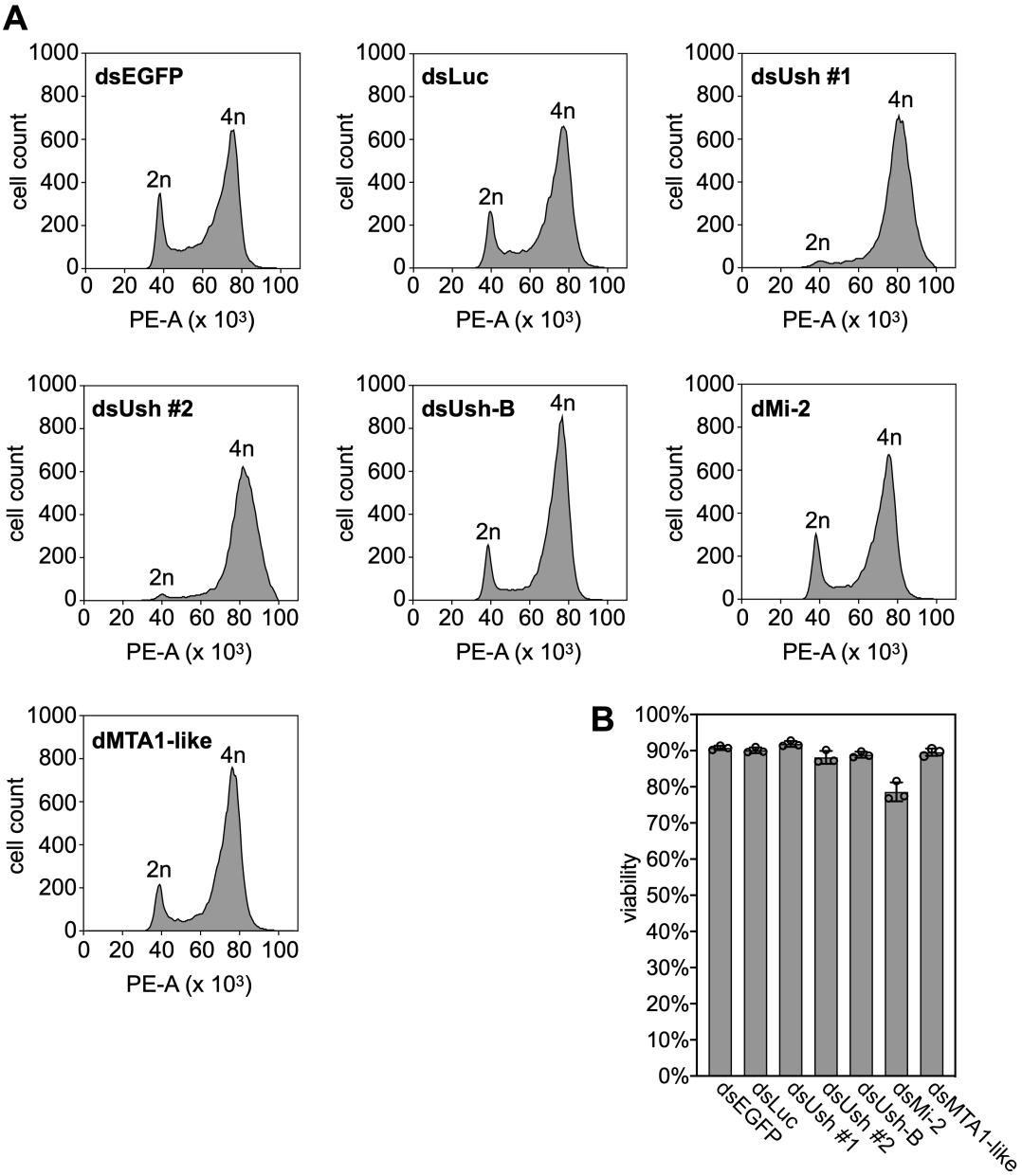

Supplementary Figure 8

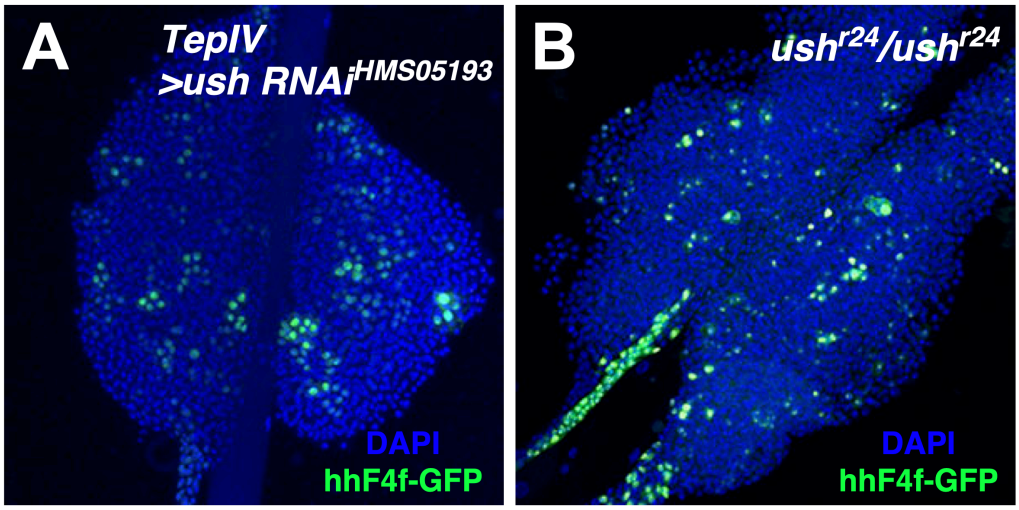

		annotated peak within promoter and/or gene body	
Genes validated by RTqPCR	**category**	**Ush-GFP**	**dMi-2-GFP**
CG16267	**hemocyte-related**	yes	yes
pirk	**hemocyte-related**	yes	yes
GILT3	**hemocyte-related**	yes	no
Lozenge	**hemocyte-related**	yes	no
atilla	**hemocyte-related**	no	no
AurB	**cell cycle**	no	no
CHES-1	**cell cycle**	yes	yes
CDK1	**cell cycle**	no	yes
polo	**cell cycle**	no	yes
Cyclin B	**cell cycle**	yes	yes
Mcad	**lipid metabolism**	yes	yes
Echs1	**lipid metabolism**	yes	yes
ACC	**lipid metabolism**	yes	yes
CROT	**lipid metabolism**	no	no
fa2h	**lipid metabolism**	yes	yes

hemocyte-related	cell cycle	lipid metabolism	gene symbol	FlyBase ID	log_2(FC dsUsh-B/ dsEGFP)	FC dsUsh-B/ dsEGFP	$-log_{10}$(p-value)	p-value	FlyBase GO_Biological Function / additional references	expression pattern (BDGP)
X	X		**N**	FBgn0004647	-0.652	0.64	1.65	2.26E-02	regulation of crystal cell differentiation (GO:0042689); lamellocyte differentiation (GO:0035171); negative regulation of lamellocyte differentiation (GO:0035204); crystal cell differentiation (GO:0042688); larval lymph gland hemopoiesis (GO:0035167); embryonic crystal cell differentiation (GO:0035165); regulation of mitotic cell cycle (GO:0007346); positive regulation of G1/S transition of mitotic cell cycle (GO:1900087); hemocyte proliferation (GO:0035172); embryonic hemopoiesis (GO:0035162); positive regulation of cell population proliferation (GO:0008284); positive regulation of crystal cell differentiation (GO:0042691)	
X	X		**kay**	FBgn0001297	0.331	1.26	1.35	4.50E-02	positive regulation of biosynthetic processes of antibacterial peptides active against Gram-negative bacteria (GO:0006964); positive regulation of peptidoglycan recognition protein signaling pathway (GO:0061059); regulation of cyclin-dependent protein serine/threonine kinase activity involved in G2/M transition of mitotic cell cycle (GO:0031660)	plasmatocytes A (stage 11-12)
X		X	**Cyt-b5-r**	FBgn0000406	0.775	1.71	1.75	1.79E-02	lipid metabolic process (GO:0006629)	procrystal cells (stage 11-12), crystal cells (stage 13-16)
X			**Col4a1 / Cg25c**	FBgn0000299	-1.289	0.41	6.57	2.71E-07		plasmatocytes A (stage 11-12), plasmatocytes (stage 13-16)
X			**vkg**	FBgn0016075	-1.114	0.46	4.19	6.52E-05		plasmatocytes A (stage 11-12), plasmatocytes (stage 13-16)
X			**CG5397**	FBgn0031327	-1.068	0.48	3.84	1.44E-04		plasmatocytes (stage 13-16)
X			**Spn28Dc**	FBgn0031973	-0.876	0.54	3.60	2.48E-04	negative regulation of melanization defense response (GO:0035009)	
X			**Traf4**	FBgn0026319	-0.681	0.62	1.73	1.86E-02	defense response to Gram-negative bacterium (GO:0050829)	
X			**CG8046**	FBgn0033388	-0.646	0.64	1.33	4.64E-02	positive regulation of peptidoglycan recognition protein signaling pathway (GO:0061059); positive regulation of antimicrobial humoral response (GO:0002760); peptidoglycan transport (GO:0015835)	
X			**Tsp96F**	FBgn0027865	-0.541	0.69	1.79	1.64E-02		procrystal cells (stage 11-12)
X			**CD98hc**	FBgn0037533	0.489	1.40	1.55	2.83E-02		procrystal cells, plasmatocytes A (stage 11-12)
X			**Rac1**	FBgn0010333	0.520	1.43	1.79	1.64E-02	hemocyte development (GO:0007516); immune response-regulating cell surface receptor signaling pathway involved in phagocytosis (GO:0002433); hemocyte migration (GO:0035099); melanotic encypsulation of foreign target (GO:0035011)	
X			**Phk-3**	FBgn0035089	0.616	1.53	1.56	2.74E-02	response to bacterium (GO:0009617)	
X			**p38c**	FBgn0267339	0.690	1.61	1.33	4.64E-02	response to bacterium (GO:0009617)	
X			**Ugt36Bc**	FBgn0040260	0.742	1.67	1.56	2.74E-02		crystal cell SA (stage 9-10), procrystal cells (stage 11-12), crystal cell (stage 13-16)
X			**GILT3**	FBgn0039098	0.790	1.73	1.77	1.70E-02	Involved in the immune response to bacterial infection (Kongton et al., 2014)	
X			**Cyp310a1**	FBgn0032693	0.801	1.74	2.74	1.83E-03		plasmatocytes A (stage 11-12), plasmatocytes (stage 13-16)
X			**pirk**	FBgn0034647	0.847	1.80	2.29	5.07E-03	negative regulation of peptidoglycan recognition protein signaling pathway (GO:0061060)	
	X		**mre11**	FBgn0020270	-0.365	0.78	1.77	1.70E-02	mitotic G2 DNA damage checkpoint (GO:0007059); intra-S DNA damage checkpoint (GO:0031573)	
	X		**14-3-3epsilon**	FBgn0020238	0.451	1.37	1.79	1.62E-02	mitotic cell cycle checkpoint (GO:0007093); regulation of mitotic nuclear division (GO:0007088)	
		X	**Pmp70**	FBgn0031069	0.539	1.45	3.57	2.72E-04	long-chain fatty acid import into peroxisome (GO:0015910)	
			CG5849	FBgn0038897	-0.975	0.51	3.33	4.65E-04		
			Tsp42Ed	FBgn0029507	-0.889	0.54	2.53	2.97E-03		
			lncRNA:CR44458	FBgn0265651	-0.879	0.54	2.72	1.90E-03		
			kek1	FBgn0015399	-0.855	0.55	3.06	8.76E-04		
			ATP8B	FBgn0037989	-0.854	0.55	2.26	5.55E-03		
			CG34034	FBgn0054034	-0.822	0.57	3.37	4.22E-04		
			CG8008	FBgn0033387	-0.729	0.60	1.55	2.83E-02		

hemocyte-related	cell cycle	lipid metabolism	gene symbol	FlyBase ID	log_2(FC dsUsh-B/ dsEGFP)	FC dsUsh-B/ dsEGFP	$-log_{10}$(p-value)	p-value	FlyBase GO_Biological Function / additional references	expression pattern (BDGP)
			mahe	FBgn0029979	-0.722	0.61	3.15	7.07E-04		
			Pfdn5 / CG7048	FBgn0038976	-0.714	0.61	1.59	2.58E-02		
			Arc2	FBgn0033928	-0.668	0.63	1.75	1.79E-02		
			Pdfr	FBgn0260753	-0.665	0.63	1.59	2.58E-02		
			CG3448	FBgn0035996	-0.640	0.64	1.53	2.94E-02		
			CG31777	FBgn0051777	-0.634	0.64	1.59	2.55E-02		
			CG18088	FBgn0032082	-0.627	0.65	2.84	1.44E-03		
			unc-13	FBgn0025726	-0.582	0.67	2.14	7.22E-03		
			Rab23	FBgn0037364	-0.574	0.67	1.55	2.84E-02		
			GstE2	FBgn0063498	-0.568	0.67	1.64	2.30E-02		
			CG12868	FBgn0033945	-0.534	0.69	3.06	8.76E-04		
			ver	FBgn0262524	-0.471	0.72	3.71	1.94E-04		
			Bin1	FBgn0024491	-0.469	0.72	3.60	2.48E-04		
			Tsp42Ee	FBgn0029506	-0.445	0.73	1.53	2.95E-02		
			Marc / CG1665	FBgn0033451	-0.415	0.75	1.35	4.46E-02		
			IscU	FBgn0037637	-0.407	0.75	4.14	7.28E-05		
			Lst8	FBgn0264691	-0.397	0.76	1.58	2.64E-02		
			DNAlig4 / Lig4	FBgn0030506	-0.344	0.79	1.58	2.64E-02		
			CG33169	FBgn0053169	-0.342	0.79	1.35	4.46E-02		
			CG11436	FBgn0029713	-0.319	0.80	1.59	2.55E-02		
			CG4239	FBgn0030745	-0.313	0.80	1.79	1.64E-02		
			CG6171	FBgn0026737	-0.300	0.81	1.35	4.47E-02		
			muc	FBgn0283658	0.218	1.16	1.64	2.30E-02		
			TBCB	FBgn0034451	0.282	1.22	1.55	2.83E-02		
			CG1354	FBgn0030151	0.293	1.23	2.51	3.09E-03		
			CysRS / Aats-cys	FBgn0027091	0.363	1.29	1.72	1.92E-02		
			eIF3d1 / eIF-3p66	FBgn0040227	0.371	1.29	1.40	4.02E-02		
			CG17746	FBgn0035425	0.376	1.30	1.56	2.74E-02		
			TyrRS /Aats-tyr	FBgn0027080	0.389	1.31	1.75	1.77E-02		
			bbc	FBgn0033844	0.390	1.31	1.64	2.30E-02		
			SCaMC	FBgn0052103	0.431	1.35	1.61	2.46E-02		
			ThrRS / Aats-thr	FBgn0027081	0.483	1.40	1.36	4.37E-02		
			AsnS	FBgn0270926	0.484	1.40	1.35	4.48E-02		
			CG3408	FBgn0036008	0.520	1.43	1.36	4.34E-02		
			IP3K1	FBgn0032147	0.541	1.45	3.29	5.11E-04		
			CG32280	FBgn0052280	0.595	1.51	1.64	2.30E-02		
			CG30069	FBgn0050069	0.605	1.52	2.14	7.22E-03		
			CG10737	FBgn0034420	0.612	1.53	2.37	4.23E-03		
			ATPsyndelta	FBgn0028342	0.614	1.53	1.48	3.35E-02		

hemocyte-related	cell cycle	lipid metabolism	gene symbol	FlyBase ID	log_2(FC dsUsh-B/ dsEGFP)	FC dsUsh-B/ dsEGFP	$-log_{10}$(p-value)	p-value	FlyBase GO_Biological Function / additional references	expression pattern (BDGP)
			CG8563	FBgn0035777	0.665	1.59	1.75	1.77E-02		
			CG42458	FBgn0259935	0.675	1.60	1.36	4.34E-02		
			CG4872	FBgn0030799	0.691	1.61	2.26	5.55E-03		
			AdamTS-A	FBgn0286071	0.700	1.62	1.37	4.29E-02		
			nkd	FBgn0002945	0.727	1.66	1.53	2.96E-02		
			lncRNA:CR44138	FBgn0264987	0.728	1.66	1.53	2.94E-02		
			CG3655	FBgn0040397	0.729	1.66	1.55	2.83E-02		
			path	FBgn0036007	0.731	1.66	1.58	2.62E-02		
			CG42324	FBgn0259224	0.738	1.67	1.58	2.64E-02		
			CG1077	FBgn0037405	0.748	1.68	1.63	2.37E-02		
			CG4611	FBgn0035591	0.774	1.71	3.37	4.22E-04		
			CG8312	FBgn0037720	0.796	1.74	2.13	7.33E-03		
			RpL18	FBgn0035753	0.860	1.82	3.46	3.44E-04		
			CG12075	FBgn0030065	0.869	1.83	2.74	1.84E-03		
			CG14879	FBgn0038419	0.908	1.88	2.72	1.92E-03		
			axo	FBgn0262870	0.978	1.97	3.37	4.22E-04		
			CG3246	FBgn0031538	0.983	1.98	3.37	4.22E-04		
			comm2	FBgn0041160	1.841	3.58	17.62	2.42E-18		

NuRD complex subunit	Genotype crossed to *y w;ush^{VX22}, MSN-C/CyO y+ or y w; MSN-C*	genetic background (selected based on *MSN-C*, *y* and/or *Tb* phenotypic markers)	number of *MSN* larvae tested	number of *MSN* larvae with ≥10x lm*	% larvae w/ ≥10x lm*	Estimated penetrance
	w^{1118}	*y w;ush^{VX22}, MSN-C/+*	32	3	9.4	9.4
	y; ush^{r24}/CyO y+ #	*y w;ush^{VX22}, MSN-C/ush^{r24}*	14	14	100.0	100.0
dMTA-1like	*w^{1118}; MTA1-like^{d09140}/TM6B, Tb^{1}* +	*w^{1118}/yw; MSN-C/+; MTA1-like^{d09140}/+*	28	2	7.1	7.1
		w^{1118}/yw; ush^{VX22}, MSN-C/+; MTA1-like^{d09140}/+	48	25	52.1	52.1
	y^{1} w*; MTA1-like^{MI01790} **	*y w; MSN-C/+; MTA1-like^{MI01790}/+*	31	1	3.2	3.2
		y w;ush^{VX22}, MSN-C/+; MTA1-like^{MI01790}/+	38	28	73.7	73.7
dp66	*w^{1118}; simj^{BG00403}/TM6B, Tb^{1}* +	*w^{1118}/yw; MSN-C/+; simj^{BG00403}/+*	26	0	0.0	0.0
		w^{1118}/y w;ush^{VX22}, MSN-C/+; simj^{BG00403}/+	39	17	43.6	43.6
	simj^{01814} ry^{506} **	*y w/+; MSN-C/+; simj^{01814} ry^{506}/+*	40	2	5.0	5.0
		y w/+;ush^{VX22}, MSN-C/+; simj^{01814} ry^{506}/+	61	31	50.8	50.8
dRpd3	*y^{1} w*; HDAC1$^{12-37}$/TM6B, Tb^{1}* *	*y w; MSN-C/+; HDAC1$^{12-37}$ /+*	30	15	50.0	50.0
		y w;ush^{VX22}, MSN-C/+; HDAC1$^{12-37}$ /+	42	35	83.3	83.3
	HDAC1^{04556} ry^{506}/TM3, ry^{RK} Sb^{1} Ser^{1} ++	*y w/+; MSN-C/+; HDAC1^{04556} ry^{506} /+ AND y w/+; MSN-C/+; TM3, ry^{RK} Sb^{1} Ser^{1} /+*	27	2	7.4	14.8
		y w/+;ush^{VX22}, MSN-C/+; HDAC1^{04556} ry^{506} /+ AND y w/+;ush^{VX22}, MSN-C/+; TM3, ry^{RK} Sb^{1} Ser^{1} /+	53	17	32.1	64.2
dMi-2	*Mi-2^{4} red^{1} e^{4}/TM6B, Sb^{1} Tb^{1} ca^{1}* +	*y w/+; MSN-C/+; Mi-2^{4} red^{1} e^{4}/+*	NT	NT	NT	NT
		y w/+;ush^{VX22}, MSN-C/+; Mi-2^{4} red^{1} e^{4}/+	45	16	35.6	35.6
	y^{1} w^{1118}; Mi-2^{L1243}/TM3, Ser^{1} ++	*y w; MSN-C/+; Mi-2^{L1243}/+ AND y w; MSN-C/+; TM3, Ser^{1}/+*	NT	NT	NT	NT
		y w;ush^{VX22}, MSN-C/+; Mi-2^{L1243}/+ AND y w;ush^{VX22}, MSN-C/+; TM3, Ser^{1}/+	51	8	15.7	31.4

*Estimated number of lamellocytes (lm)
#To identify animals with the *ush^{r24}/ ush^{vx22}, MSN* genotype, larvae with yellow mouth hooks were selected.
+The Tb balancer chromosome is easily distinguished from the MTA-1 like chromosome.
**Homozygous viable
++Heterozygous, which assumes only 50% of the animals that carry the *ush; MSN-mCherry* chromosome are double heterozygotes and thus, the estimated penetrance may be twice the value of the % larvae with increased lamellocyte differentiation.
NT: not tested

name	sequence	application	method
sgRNA_scaffold	GTTTAAGAGCTATGCTGGAAACAGCATAGCAAGTTTAAATAAGGCTAGTCCGTTATCAACTTGAAAAAGTGGCACCGAGTCGGTGC	general sgRNA template synthesis	endogenous tagging
U6-promotor_s	GCTCACCTGTGATTGCTCCTAC	general sgRNA template synthesis	endogenous tagging
sgRNA_as	gcttattctcAAAAAAGCACCGACTCGGTGCCACT	general sgRNA template synthesis	endogenous tagging
lig4_RNAi_s	taatacgactcactatagggCCCAATGATCCAAAGTGTTTTTGCA	generation of dsRNA against lig4	endogenous tagging
lig4_RNAi_as	taatacgactcactatagGGAAGTAGGATGCCTTCGCGA	generation of dsRNA against lig4	endogenous tagging
mus308_RNAi_s	taatacgactcactataggGCTGGGACTCCACCGGAAAG	generation of dsRNA against mus308	endogenous tagging
mus308_RNAi_as	taatacgactcactatagggTACCGTCGCCGTCCAGTAATG	generation of dsRNA against mus308	endogenous tagging
CRISPR_Mi2_Ct	cctattttcaatttaacgtcgTCGAATAATTCCGGCGTCTgtttaagagctatgctg	sgRNA synthesis dMi-2 C-term	endogenous tagging of dMi-2
Mi2_Ctag_s	TTTGCCAACTTTCGGCCACAGTTCTCGGTGCCCGGCCAGCTATCGAATAATTCCGGCGTCggatcttccggatggctcgag	generation of homology donors for dMi-2	endogenous tagging of dMi-2
Mi2_Ctag_as	TTGAGTAAAGTATATTTGCATGGAATACGAATGCTCTTAACATAGATATTGAGGAGATGCgaagttcctattctctagaaagtataggaacttccatatg	generation of homology donors for dMi-2	endogenous tagging of dMi-2
Mi2_PCR_C_us_s	tgccagcattcacgagcggaccg	genotyping of cell lines containing tagged dMi-2 alleles	endogenous tagging of dMi-2
Mi2_PCR_C_ds_as	gtgggtgtgcaggtgtgttaccgtg	genotyping of cell lines containing tagged dMi-2 alleles	endogenous tagging of dMi-2
CRISPR_ush_Ct	cctattttcaatttaacgtcgCATTTGAGAAAGCCAGCTGgtttaagagctatgctg	sgRNA synthesis Ush C-term	endogenous tagging of Ush
ush_Ctag_s	GGCCTGGTCGGCGGACACGGCCAGCAGAAGAACAAGGAAAACCTGCAGGAGGCGGCCATTggatcttccggatggctcgag	generation of homology donors for Ush	endogenous tagging of Ush
ush_Ctag_as	GAAGCACGTGTAATACCACTCAAGCTGCTTGCGCTGCGCCTCCCACCGCAGCTGGCTTTCgaagttcctattctctagaaagtataggaacttccatatg	generation of homology donors for Ush	endogenous tagging of Ush
ush_PCR_us_s	AGTCCGAATCACCTGGGCGGAGG	genotyping of cell lines containing tagged Ush alleles	endogenous tagging of Ush
ush_PCR_ds_as	GAGGCTAGGATTCGATTAGTTTCGA	genotyping of cell lines containing tagged Ush alleles	endogenous tagging of Ush
EGFP-T7-RNAi-fw	gaattaatacgactcactatagggaGAGCTGGACGGCGACGTAA	generation of dsRNA against EGFP	RNAi
EGFP-T7-RNAi-rv	gaattaatacgactcactatagggagACTTGTACAGCTCGTCCATG	generation of dsRNA against EGFP	RNAi
Luc-T7-RNAi-fw	taatacgactcactatagggCTGGTTCCTGGAACAATTGC	generation of dsRNA against Luciferase	RNAi
Luc-T7-RNAi-rv	taatacgactcactatagggTGACGAACGTGTACATCGA	generation of dsRNA against Luciferase	RNAi
Ush-T7-RNAi-1-fw	taatacgactcactatagggCAGCCCAAGCACTCCG	generation of dsRNA against Ush (#1)	RNAi
Ush-T7-RNAi-1-rv	taatacgactcactatagggGCTGTAGGAGCACTGG	generation of dsRNA against Ush (#1)	RNAi
Ush-T7-RNAi-2-fw	taatacgactcactatagggACACTTCCCTGGACAACCTG	generation of dsRNA against Ush (#2)	RNAi
Ush-T7-RNAi-2-rv	taatacgactcactatagggAGTTGTGGTAGATGCCCCTG	generation of dsRNA against Ush (#2)	RNAi
Mi-2-T7-RNAi-fw	taatacgactcactatagggTTAACTCGCTGACCAAGGCT	generation of dsRNA against dMi-2	RNAi
Mi-2-T7-RNAi-rv	taatacgactcactatagggATATCGTTGTGGGGATTCCA	generation of dsRNA against dMi-2	RNAi
Ush-B-T7-RNAi-fw	taatacgactcactatagggGCTTCGAACGGACGTCTTTA	generation of dsRNA against Ush-B	RNAi
Ush-B-T7-RNAi-rv	taatacgactcactatagggGGGCAATCAATGCGATTACT	generation of dsRNA against Ush-B	RNAi
MTA-T7-RNAi-fw	taatacgactcactatagggCAGAACGCGAGACAACAAAA	generation of dsRNA against dMTA1-like	RNAi
MTA-T7-RNAi-rv	taatacgactcactatagggTGGAACTTTAGAGCGCGATT	generation of dsRNA against dMTA1-like	RNAi

name	sequence	application	method
rp49-RT-fw	TGTCCTTCCAGCTTCAAGATGACCATC	amplification of rp49 cDNA fragment in qPCR	RT-qPCR
rp49-RT-rv	CTTGGGCTTGCGCCATTTGTG	amplification of rp49 cDNA fragment in qPCR	RT-qPCR
CG16762-RT-fw	GGTATCGATGCCGACTTCC	amplification of CG16762 cDNA fragment in qPCR	RT-qPCR
CG16762-RT-rv	TGGAGCCCACATTGGCA	amplification of CG16762 cDNA fragment in qPCR	RT-qPCR
lz-RT-fw	CGAATTGGTGCGCACGAG	amplification of Lozenge cDNA fragment in qPCR	RT-qPCR
lz-RT-rv	CCCGGATGGTGACATAGGTG	amplification of Lozenge cDNA fragment in qPCR	RT-qPCR
pirk-RT-fw	AGCGGCGATGCCAAGAAAAG	amplification of pirk cDNA fragment in qPCR	RT-qPCR
pirk-RT-rv	GCTCCGTGCCGTATCGTTAG	amplification of pirk cDNA fragment in qPCR	RT-qPCR
GILT3-RT-fw	CAAGGCGGGGTTCTACAACA	amplification of GILT3 cDNA fragment in qPCR	RT-qPCR
GILT3-RT-rv	TCCGAATGTCCAGGGTCTCAA	amplification of GILT3 cDNA fragment in qPCR	RT-qPCR
atilla-RT-fw	AAACAAGTGATTTTCGTGCTCCT	amplification of atilla cDNA fragment in qPCR	RT-qPCR
atilla-RT-rv	CGCGGATGTTAGAGGCAGA	amplification of atilla cDNA fragment in qPCR	RT-qPCR
AurB-RT-fw	TACGGACAGCCATACGATTGGAG	amplification of Aurora B cDNA fragment in qPCR	RT-qPCR
AurB-RT-rv	ACCAGATAGTGCGAGTGGCG	amplification of Aurora B cDNA fragment in qPCR	RT-qPCR
CHES-1-RT-fw	CAGTGAGGAGAATCACAACATCAC	amplification of CHES-1 cDNA fragment in qPCR	RT-qPCR
CHES-1-RT-rv	CTGAGCCGCACTCCACAATC	amplification of CHES-1 cDNA fragment in qPCR	RT-qPCR
Cdk1-RT-fw	CCGCGATCAGAGAAATTTCGTTG	amplification of Cdk1 cDNA fragment in qPCR	RT-qPCR
Cdk1-RT-rv	GAGGTCCATCGATAGGAATTCAAAG	amplification of Cdk1 cDNA fragment in qPCR	RT-qPCR
polo-RT-fw	TCTGCACGACGCCATTACCG	amplification of polo cDNA fragment in qPCR	RT-qPCR
polo-RT-rv	AGAATTCGCGGCTTTCCGTT	amplification of polo cDNA fragment in qPCR	RT-qPCR
CycB-RT-fw	CCCACTAAAGTTACAGTCAAGTCC	amplification of Cyclin B cDNA fragment in qPCR	RT-qPCR
CycB-RT-rv	CTGAAACTCCCATCACGGGT	amplification of Cyclin B cDNA fragment in qPCR	RT-qPCR
Mcad-RT-fw	GTTTGGATCATTTCGCTGGCA	amplification of Mcad cDNA fragment in qPCR	RT-qPCR
Mcad-RT-rv	CAGCAAGCTTGTTGAGGAAC	amplification of Mcad cDNA fragment in qPCR	RT-qPCR
Echs1-RT-fw	ATCGGCACCCACTCCAATCT	amplification of Echs1 cDNA fragment in qPCR	RT-qPCR
Echs1-RT-rv	CTTGCGATCGGCCGTGGAG	amplification of Echs1 cDNA fragment in qPCR	RT-qPCR
ACC-RT-fw	ACAAGATTGGCTTCCCCGTAATG	amplification of ACC cDNA fragment in qPCR	RT-qPCR
ACC-RT-rv	GCTTGAACCTGGCGGAACAG	amplification of ACC cDNA fragment in qPCR	RT-qPCR
CROT-RT-fw	TGCATAAAGAAATTGCTCCCAC	amplification of CROT cDNA fragment in qPCR	RT-qPCR
CROT-RT-rv	TTGTTGGATGACGCCCTCAG	amplification of CROT cDNA fragment in qPCR	RT-qPCR
fa2h-RT-fw	GATAGTATGGAGCACCTAGTGGAC	amplification of fa2h cDNA fragment in qPCR	RT-qPCR
fa2h-RT-rv	CCAAGGGTCAAAGAGACGCA	amplification of fa2h cDNA fragment in qPCR	RT-qPCR

Published online 8 November 2019 *Nucleic Acids Research, 2019, Vol. 47, No. 22* **11649–11666**
doi: 10.1093/nar/gkz1050

Distinct CoREST complexes act in a cell-type-specific manner

Igor Mačinković[1], Ina Theofel[2], Tim Hundertmark[2], Kristina Kovač[1], Stephan Awe[1], Jonathan Lenz[1], Ignasi Forné[3], Boris Lamp[4], Andrea Nist[4], Axel Imhof[3], Thorsten Stiewe[4], Renate Renkawitz-Pohl[2], Christina Rathke[2] and Alexander Brehm[1,*]

[1]Institute of Molecular Biology and Tumor Research, Biomedical Research Center, Philipps-University, Hans-Meerwein-Strasse 2, 35043, Marburg, Germany, [2]Department of Biology, Philipps-University, Karl-von-Frisch-Strasse 8, 35043, Marburg, Germany, [3]Protein Analysis Unit, BioMedical Center, Faculty of Medicine, Ludwig-Maximilians-University Munich, Großhadernerstrasse 9, 82152 Martinsried, Germany and [4]Genomics Core Facility, Institute of Molecular Oncology, Philipps-University, Hans-Meerwein-Strasse 3, 35043 Marburg, Germany

Received October 31, 2018; Revised October 16, 2019; Editorial Decision October 18, 2019; Accepted October 23, 2019

ABSTRACT

CoREST has been identified as a subunit of several protein complexes that generate transcriptionally repressive chromatin structures during development. However, a comprehensive analysis of the CoREST interactome has not been carried out. We use proteomic approaches to define the interactomes of two dCoREST isoforms, dCoREST-L and dCoREST-M, in *Drosophila*. We identify three distinct histone deacetylase complexes built around a common dCoREST/dRPD3 core: A dLSD1/dCoREST complex, the LINT complex and a dG9a/dCoREST complex. The latter two complexes can incorporate both dCoREST isoforms. By contrast, the dLSD1/dCoREST complex exclusively assembles with the dCoREST-L isoform. Genome-wide studies show that the three dCoREST complexes associate with chromatin predominantly at promoters. Transcriptome analyses in S2 cells and testes reveal that different cell lineages utilize distinct dCoREST complexes to maintain cell-type-specific gene expression programmes: In macrophage-like S2 cells, LINT represses germ line-related genes whereas other dCoREST complexes are largely dispensable. By contrast, in testes, the dLSD1/dCoREST complex prevents transcription of germ line-inappropriate genes and is essential for spermatogenesis and fertility, whereas depletion of other dCoREST complexes has no effect. Our study uncovers three distinct dCoREST complexes that function in a lineage-restricted fashion to repress specific sets of genes thereby maintaining cell-type-specific gene expression programmes.

INTRODUCTION

Multisubunit protein complexes that regulate chromatin activity often form families of related complexes that share a set of core subunits (1). This common core can associate with different accessory subunits to yield alternative complexes with new functionality.

The *RE1 silencing transcription factor* (REST) cooperates with the *corepressor of REST* (CoREST) to silence neuron-specific genes in non-neuronal cell types (2). CoREST is an integral component of multi-subunit *lysine-specific demethylase 1 (LSD1)* complexes which modify nucleosomes by histone deacetylation and demethylation to repress transcription (3–7). The precise composition of LSD1/CoREST complexes differs depending on cell type and purification conditions. However, several core subunits have been identified in independent studies (5,6). These include CoREST, LSD1, histone deacetylases HDAC1 and HDAC2, CtBP1, ZNF217, BHC80 and BRAF35.

CoREST and LSD1 are also part of distinct molecular assemblies. Together with SFMBT1 they form the *SFMBT1-LSD1-CoREST* (SLC) complex which represses histone genes in a cell-cycle-dependent manner (8). In addi-

*To whom correspondence should be addressed. Tel: +49 6421 2866840; Fax: +49 6421 2866842; Email: brehm@imt.uni-marburg.de
Present addresses:
Ina Theofel, MRC London Institute of Medical Sciences (LMS), Institute of Clinical Sciences (ICS), Faculty of Medicine, Imperial College London, Du Cane Road, London W120NN, UK.
Kristina Kovač, Department of Biology, Stanford University, 371 Serra Mall, Stanford, CA 94305, USA.
Christina Rathke, Dekanat Fachbereich Medizin, Justus-Liebig-University, Klinikstr. 29, Gießen, Germany.

tion, LSD1 and CoREST coexist with SIRT1 in a complex that represses Notch target genes (9).

The co-existence of LSD1 and CoREST in all of the complexes described above suggests that these two proteins form a core that can associate with different accessory subunits. So far, LSD1 and CoREST have not been demonstrated to exist in separate complexes in mammals.

Both CoREST and LSD1 are conserved in *Drosophila*. Genetic studies imply that they cooperate in the differentiation of wing structures and ovarian follicle cells by regulating signalling pathways including Notch and DPP/TGFbeta (9–12). These observations suggest that *Drosophila* LSD1/CoREST complexes exist that are similar to their mammalian counterparts. In support of this notion, dLSD1 and dCoREST interact when overexpressed in S2 cells and both proteins are associated in ovary extracts (12,13). However, dLSD1/dCoREST complexes are poorly characterized. Indeed, several subunits of mammalian LSD1/CoREST complexes do not have apparent homologues in *Drosophila* (e.g. ZNF217, BHC80 and BRAF35) raising questions about the existence and subunit composition of putative dLSD1/dCoREST complexes.

The only *Drosophila* CoREST-containing complex biochemically characterized to date is the L(3)mbt-interacting (LINT) complex which functions to prevent the expression of lineage-inappropriate genes in both ovaries and in Kc cells (14,15). LINT consists of dL(3)mbt, the dL(3)mbt-interacting protein 1 (dLint-1), the histone deacetylase dRPD3 and dCoREST (15). Notably, dLSD1 is not a stoichiometric subunit of LINT and is not required to repress LINT target genes (15). The existence of additional dCoREST complexes has not been systematically analysed.

The *dCoREST* gene expresses two major isoforms by alternative splicing, dCoREST-L and dCoREST-M (Figure 1A; (13)). Both isoforms contain an ELM2 domain and two SANT domains. dCoREST-L is characterized by a 234 amino acid insertion in the linker that is separating the two SANT domains that is absent in dCoREST-M. It is unknown, if these two isoforms reside in different complexes or are fully redundant.

In this study, we systematically define the interactome of dCoREST in *Drosophila* cells. We use gel filtration, immunoaffinity purification, mass spectrometry and reconstitution from recombinant subunits to identify three distinct dCoREST-containing complexes: the LINT complex described above, a stable dLSD1/dCoREST complex and a dG9a/dCoREST complex. Whereas LINT subunits and dG9a interact with both dCoREST-L and dCoREST-M, dLSD1 displays a striking isoform specificity and associates exclusively with dCoREST-L. We employ ChIP-seq and RNA interference combined with RNA-seq to systematically identify the genome-wide distribution of dCoREST complexes and their target genes. Strikingly, our results identify LINT as the major effector of dCoREST-mediated transcriptional repression in macrophage-like S2 cells, whereas spermatogenesis and maintenance of a germ line-specific gene expression programme rely exclusively on the dLSD1/dCoREST complex. Collectively, our data support the model that different cell lineages employ specific dCoREST complexes to generate and maintain their cell-type-specific transcriptional programmes.

MATERIALS AND METHODS

Cell culture

Spodoptera frugiperda Sf9, *Drosophila melanogaster* S2 and *D. melanogaster* S2[Cas9] (kind gift from Klaus Förstemann, Munich) cell lines were maintained in Sf-900 medium (Gibco) and Schneider's medium (Gibco), respectively, supplemented with 10% (v/v) Fetal calf serum (Sigma) and 1% (v/v) Penicillin-Streptomycin (Gibco) under standard conditions (26°C).

Nuclear extract preparation

S2 cells were harvested, washed in phosphate-buffered saline (PBS) and resuspended in three volumes of low salt buffer (10 mM Hepes pH 7.6, 1.5 mM $MgCl_2$, 10 mM KCl, 1.0 mM dithiothreitol (DTT)). After incubation on ice for 10 min, cells were collected by centrifugation at 21 100 × *g* for 1 min at 4°C. The supernatant was discarded, and nuclei were resuspended in 1.5 volumes of high salt buffer (20 mM Hepes pH 7.6, 1.5 mM $MgCl_2$, 420 mM NaCl, 0.2 mM ethylenediaminetetraacetic acid (EDTA), 20% (v/v) glycerol, 1.0 mM DTT). The suspension was incubated for 20 min on ice and subsequently centrifuged at 21 100 × *g* for 30 min at 4°C. The supernatant (nuclear extract) was aliquoted, frozen in liquid nitrogen and stored at −80°C.

Preparation of nuclear extract from *Drosophila* embryos was done as described previously (16).

The protein concentration of nuclear extracts was determined using Protein Assay Dye Reagent (Bio-Rad) according to the manufacturer's instructions using BSA (Roth) as a standard.

Gel filtration

A total of 1 mg of S2 nuclear extract or embryo (0–12 h after egg deposition) nuclear extract were applied to a Superose 6 HR 10/30 gel filtration column (GE Healthcare) using a 200-µl sample loading loop on an Äkta purifier system (GE Healthcare). Samples were resolved in 10 mM Hepes pH 7.6, 1.5 mM MgCl2, 300 mM KCl, 0.5 mM EGTA and 10% (v/v) glycerol and 0.5 ml fractions were collected with a F9-R fraction collector following the manufacturer's instructions. Fractions were precipitated using 5 µl StrataClean resin (Agilent) or immunoprecipitated using GFP-Trap® (Chromotek) and subjected to western blot analysis. Elution volumes of proteins with known molecular weights were determined using the Gel Filtration Calibration Kit (GE Healthcare) according to the manufacturer's instructions.

Co-immunoprecipitations

Anti-GFP (Chromotek) co-immunoprecipitation of fractions (0.5 ml) collected after gel filtration was performed according to the manufacturer's instructions. The fractions were diluted 1:1 with 10 mM Hepes pH 7.6, to lower the salt concentration of KCl to 150 mM and incubated with 25 µl of equilibrated GFP-Trap® overnight at 4°C. Unbound proteins were removed by washing four times with IP-150 buffer (25 mM Hepes pH 7.6, 12.5 mM $MgCl_2$, 150

mM NaCl, 0.1 mM EDTA, 10% (v/v) glycerol, 0.1% (v/v) NP-40) for 5 min, and the bound proteins were eluted by incubating the beads with 30 μl of 1× NuPAGE® LDS Sample Buffer (Invitrogen). A total of 20 μl of the eluate was analysed by western blot.

For co-immunoprecipitation of endogenous dCoREST, anti-CoREST rabbit polyclonal antibody was cross-linked to Protein G Sepharose (GE Healthcare) and co-immunoprecipitation was performed as previously described (17). In brief, four independent cross-linking reactions were prepared using 30 μg of anti-CoREST rabbit polyclonal antibody or 30 μg of IgG (Normal Rabbit IgG, Cell Signalling) and 70 μl of Protein G Sepharose (GE Healthcare). Additionally, the beads were blocked for 1 h with 1% Gelatin from cold water fish skin (Sigma) and 0.2 mg/ml Albumin from chicken egg white (Sigma). Cross-linked beads were incubated overnight with 6 mg of S2 nuclear extract. Unbound proteins were removed by washing three times with high salt buffer supplemented with 0.05% NP-40 (Fluka) for 5 min, followed by washing with high salt buffer and finally two washes with 50 mM $(NH_4)HCO_3$ (Roth). About 10% of the affinity-purified material was electrophoresed and analysed by silver staining (SilverQuest™ Staining Kit, Invitrogen) and the rest was subjected to LC-MS/MS analysis.

Anti-FLAG (Sigma) co-immunoprecipitation was performed according to the manufacturer's instructions in high salt buffer. A total of 200 μl of anti-FLAG® M2 Affinity Gel was equilibrated and blocked for 1 h with 1% Gelatin from cold water fish skin (Sigma) and 0.2 mg/ml Albumin from chicken egg white (Sigma) in high salt buffer. A total of 10 mg of S2 nuclear extract was incubated overnight with 200 μl of beads. Unbound proteins were removed by washing three times with high salt buffer supplemented with 0.05% NP-40 (Fluka) for 5 min, followed by washing with high salt buffer and finally two washes with 50 mM $(NH_4)HCO_3$ (Roth). 10% of the affinity-purified material was electrophoresed and analysed by silver staining (SilverQuest™ Staining Kit, Invitrogen), 10% of the affinity-purified material was electrophoresed and analysed by western blot. The rest (80%) was subjected to LC-MS/MS analysis.

LC-MS/MS analysis

LC-MS/MS sample preparation and analysis was carried out according to methods described in (18). Briefly, after immunoaffinity purification, beads were washed with 50 mM $(NH_4)HCO_3$ and incubated with 10 ng/μl Trypsin in 1 M urea, 50 mM $(NH_4)HCO_3$ for 30 min, washed with 50 mM $(NH_4)HCO_3$ and the supernatant was digested overnight in the presence of 1 mM DTT. Digested peptides were alkylated and desalted prior to LC-MS/MS analysis.

For LC-MS/MS purposes, desalted peptides were injected in an Ultimate 3000 RSLCnano system (Thermo), separated in a 15-cm analytical column (75 μm ID home-packed with ReproSil-Pur C18-AQ 2.4 μm from Dr Maisch) with a 50-min gradient from 5 to 60% acetonitrile in 0.1% formic acid. The effluent from the HPLC was directly electrosprayed into a Qexactive HF (Thermo) operated in data dependent mode to automatically switch between full scan MS and MS/MS acquisition. Survey full scan MS spectra (from m/z 375–1600) were acquired with resolution $R = 60\,000$ at m/z 400 (AGC target of 3×10^6). The 10 most intense peptide ions with charge states between 2 and 5 were sequentially isolated to a target value of 1×10^5, and fragmented at 27% normalized collision energy. Typical mass spectrometric conditions were: spray voltage, 1.5 kV; no sheath and auxiliary gas flow; heated capillary temperature, 250°C; ion selection threshold, 33.000 counts. MaxQuant 1.5.2.8 was used to identify proteins and quantify by iBAQ with the following parameters: Database, Uniprot_0803_Dmelanogaster_20180723; MS tol, 10ppm; MS/MS tol, 20ppm; Peptide FDR, 0.1; Protein FDR, 0.01 Min. peptide Length, 5; Variable modifications, Oxidation (M); Fixed modifications, Carbamidomethyl (C); Peptides for protein quantitation, razor and unique; Min. peptides, 1; Min. ratio count, 2. Identified proteins were analysed in Perseus with a *t*-test adjusted for multiple comparisons.

Antibodies

dCoREST (G. Mandel), dLSD1 (dSu(var)3–3; G. Reuter) and dG9a (M. Yamaguchi) antibodies were generous gifts. Rabbit polyclonal anti-dL(3)mbt, anti-dLint-1, anti-dMi-2 (anti-dMi2-Nterm), anti-dRpd3 and anti-MstF77 antibodies have been previously described (15,19). Anti-beta-Tubulin (clone KMX-1), anti-FLAG rabbit polyclonal antibody and anti-FLAG M2 agarose were purchased from Millipore and Sigma Aldrich, respectively. Anti-GFP was purchased from Chromotek.

HRP linked anti-Mouse IgG (Amersham, NA931), anti-rabbit IgG (Amersham, NA934) or anti-rat IgG (Invitrogen, 31470) secondary antibodies were used to visualize western blot signals by chemiluminescence using the Immobilon Western Chemiluminescence HRP substrate (Millipore, WBKLS0500).

Chromatin Immunoprecipitation

Exponentially growing S2[Cas9] cells (1×10^8) expressing GFP-tagged proteins were cross-linked with 1% Formaldehyde (Roth) for 10 min at room temperature. Cross-linking was stopped by adding Glycine to a final concentration of 240 mM and incubating samples for 10 min at room temperature. Cells were then washed twice in PBS and lysed in 1 ml of ChIP Lysis buffer (50 mM Tris/HCl pH 8.0, 10 mM EDTA, 1% (w/v) SDS, 1 mM DTT) for 10 min on ice. Chromatin was sheared by sonication in a Bioruptor UCD-200TM-EX (Diagenode) supplied with ice water. Three sonication cycles were applied, each cycle lasting for 10 min with 30 s intervals of sonication at high power interrupted by 30 s of resting. Cell debris were pelleted by centrifugation (20 min, 21 100 × *g*, 4°C) and the supernatant containing fragmented chromatin was stored at −80°C. The fragment size was monitored by decrosslinking 50 μl of chromatin-containing lysate in the presence of RNase A (400 ng/μl, Applichem) and Proteinase K (400 ng/μl, Applichem) for 3 h at 55°C followed by 65°C over night. DNA was purified using the QIAquick PCR purification kit (Qiagen) and the fragment size was evaluated on a 1.2% Agarose/TAE gel.

For ChIP 1 ml of chromatin lysate was precleared by 1:10 dilution in ChIP IP buffer (16.7 mM Tris/HCl pH 8.0, 1.2

mM EDTA, 167 mM NaCl, 1 mM DTT) and addition of 285 μl Protein A Sepharose resin (GE Healthcare) that had been blocked for 1 h in ChIP Blocking buffer (ChIP Low salt buffer containing 2 mg/ml BSA and 2% (w/v) Gelatin from cold water fish skin). After incubation at 4°C for 1 h with rotation, beads were precipitated (centrifugation for 10 min, 21 100 × *g*, 4°C) and the supernatant was added to 200 μl of blocked GFP-Trap.

Immunoprecipitation took place over night at 4°C with rotation followed by washing: 3× with 15 ml of ChIP Low salt buffer (20 mM Tris/HCl pH 8.0, 2 mM EDTA, 150 mM NaCl, 1% (w/v) Triton X-100, 0.1% (w/v) SDS, 1 mM DTT), 3× with 15 ml of ChIP High salt buffer (20 mM Tris/HCl pH 8.0, 2 mM EDTA, 500 mM NaCl, 1% (w/v) Triton X-100, 0.1% (w/v) SDS, 1 mM DTT), 1× with 15 ml of ChIP LiCl buffer (10 mM Tris/HCl pH 8.0, 1 mM EDTA, 250 mM LiCl, 0.1% (w/v) NP-40, 1 mM DTT), 2× with TE buffer (10 mM Tris/HCl pH 8.0, 1 mM EDTA, 1 mM DTT). Each washing step was performed at 4°C for 5 min with rotation and the resin was precipitated in between by centrifugation (4 min, 400 × *g*, 4°C).

Crosslinked protein–DNA complexes were eluted twice from the resin in 500 μl ChIP Elution buffer (100 mM $NaHCO_3$, 2% (w/v) SDS) for 20 min at RT with rotation followed by 10 min incubation at 95°C. Pooled eluates were 1:1 diluted with 100 mM $NaHCO_3$. As 'input' sample, 14 μl of precleared chromatin was added to 250 μl of ChIP Elution buffer and diluted 1:1 with 100 mM $NaHCO_3$. 5 M NaCL was added to the samples to the final concentration of 40 μM. Protein–DNA complexes were decrosslinked over night at 65°C with agitation. 40 mM Tris/HCl pH 6.8, 1 mM EDTA and 40 ng/μl Proteinase K (Applichem) was added to each sample and proteins were digested at 45°C for 1 h with agitation. The DNA was purified using QIAquick PCR purification kit (Qiagen) and the concentration was determined using Quant-iT™ dsDNA High-Sensitivity Assay Kit according to the manufacturer's instruction.

ChIP-seq

Libraries for ChIP-seq analysis were prepared from 500 pg of DNA using MicroPlex Library Preparation Kit v2 (diagenode) following manufacturer's instructions including library size selection using AMPure XP beads (Beckman Coulter). The quality of sequencing libraries was controlled on a Bioanalyzer 2100 using the Agilent High Sensitivity DNA Kit (Agilent). Pooled sequencing libraries were quantified with digital polymerase chain reaction (PCR) (QuantStudio 3D, Thermo Fisher) and sequenced on the NextSeq 550 platform (Illumina) using a high output v2.5 flow cell and 50 base single reads.

Raw Illumina sequence reads were aligned to *D. melanogaster* genome (BDGP6_dm6, ucsc) with the Bowtie2 tool and peak calling was performed with the MACS2 callpeak tool using the Galaxy Server of University of Giessen (default settings). Peaks were filtered using fold change values ≥ 4 and pileup values ≥ 35. Genomic distribution of the peaks was analysed using CEAS: Enrichment on chromosome tool and diagrams were generated using the Venn Diagram tool of Cistrome Galaxy server.

RNAi treatment in cell culture

RNA interference experiments were performed as in (1,20). Briefly, double-stranded RNA was generated by T7 Polymerase *in vitro* transcription from PCR amplimers generated with T7 promoter-containing primers (Supplementary Table S4) using MEGAscript™ T7 Transcription Kit (ThermoFischer) according to the manufacturer's instruction. Double-stranded RNAs (15 μg) were transfected into S2 cells (1.2×10^6 cells) using Effectene (Qiagen), and the cells were harvested 3 to 4 days after transfection. The efficiency of knock-down was confirmed by qPCR and western blot analysis.

Fly lines and crosses

RNA interference experiments in flies were performed using stocks from the VDCR RNAi Library (http://stockcenter.vdrc.at/control/main) carrying RNAi transgenes under UAS control (VDRC RNAi #: dCoREST – 34179; – 34180 and –104900; dLSD1 – 106147; dL(3)mbt – 104563; dLint-1 – 105932; dG9a – 25473; dCHD3 – 102689; CG9973 – 102273; CG2083 - 110549). For knockdown experiments the GAL4-driver strains *engrailed*-GAL4 (wing) and *bam*-GAL4 (germ line) were used, respectively. All flies were collected as virgins before setting up the crosses. Flies were kept at 26°C in a fly incubator.

RNA-seq analysis

Total RNA from *Drosophila* S2 cells was isolated using the peqGOLD Total RNA Kit (S-Line, peqlab) according to manufacturer's instructions. Total RNA from dissected *Drosophila* testes was isolated using the TRIzol (Invitrogen) reagent according to the manufacturer's protocol. Following chloroform extraction, ethanol precipitation and DNase digestion, RNAs were purified using a RNeasy Mini Kit (Qiagen).

RNA integrity was assessed on an Experion StdSens RNA Chip (Bio-Rad). RNA-seq libraries were prepared using a TruSeq Stranded mRNA Library Prep kit (Illumina). Libraries were quantified on a Bioanalyzer (Agilent Technologies) and were sequenced on an Illumina HiSeq 1500 platform, rapid-run mode, single-read 50 bp (HiSeq SR Rapid Cluster Kit v2, HiSeq Rapid SBS Kit v2, 50 cycles) according to the manufacturer's instructions.

For transcriptome analysis, sequenced reads were aligned to the *D. melanogaster* genome (Ensembl revision 89) using STAR (version 2.4.1a) (21). Fragments per kilobase per million (FPKM) were calculated based on the total raw read count per gene and length of merged exons. For the study with cultured S2 cells, differential expression was assessed using DESeq2 (version 1.12.3) (22). To investigate differential gene expression of pooled *Drosophila* testes, logFC values were calculated between the log2 medians of each group after a constant of 1/60 to avoid undefined algorithms. For both analyses, genes that did not yield a minimum raw count of 50 and a minimum FPKM of 0.3 in at least two samples were discarded due to insufficient coverage. Of the remaining genes, genes were considered differentially expressed if the absolute of the log2 FC was at least 1

(twofold induction/repression) and in case of DESeq2 analysis if the corrected *P*-value was less or equal 0.05.

Phase contrast microscopy and immunofluorescence staining

Triple-bam-GAL4 female virgins (bam-GAL4/bam-GAL4;CyO/Sp;Sb/Bam-GAL4) were crossed with males of appropriate RNAi-lines (CoREST: VDRC-34179/GD and Su(var)3–3: VDRC-10647/KK). Offspring were raised in standard conditions (26°C).

For dissection and imaging up to 1-day old males were used. Only males that were non-Sb (i.e. carried 2xbam-GAL4) were selected. Used undriven RNAi lines as controls (up to 1-day old).

Dissected testes in PBS and mounted whole unfixated testes on lysin-coated slides in PBS were imaged at 10× and 20× magnification in phase contrast using a Leica DMR microscope equipped with Quantifire-X1 camera (Intas Science Imaging Instruments). For imaging spermatocytes testes were squashed by removing PBS from under the coverslip.

Images were processed and assembled in GIMP and Inkscape.

Immunofluorescence staining of squashed testis was carried out essentially as described before (19,23,24).

RESULTS

Different dCoREST-containing protein complexes

Alternative splicing produces two main isoforms of dCoREST in macrophage-like S2 cells: dCoREST-L and dCoREST-M (13). dCoREST-L contains a unique 234 amino acid insertion in the linker region separating the two SANT domains that is absent in dCoREST-M (Figure 1A). We have previously shown that both dCoREST isoforms associate with the malignant brain tumour (MBT) domain-containing protein dL(3)mbt, dLint-1 and the histone deacetylase dRPD3 to form the dL(3)mbt-interacting (LINT) complex (15). We hypothesized that additional dCoREST-containing complexes exist. We used gel filtration of nuclear extracts from S2 cells to test this hypothesis. Indeed, only a minor fraction of dCoREST coeluted with the LINT signature subunit dL(3)mbt (Figure 1B). The bulk of dCoREST-L and dCoREST-M eluted in fractions with high apparent molecular mass (>440 kDa) that contained little or no detectable dL(3)mbt. This suggests that dCoREST is a component of additional protein complexes other than LINT. In addition, we observed that dCoREST-L (main peak in fraction 25) and dCoREST-M (main peak in fraction 19) do not peak in the same fractions indicating that isoform-specific complexes might exist.

We used an antibody recognising both dCoREST isoforms to affinity purify dCoREST-interacting proteins from S2 nuclear extract (13). SDS-PAGE followed by silver staining revealed several proteins that specifically co-purified with dCoREST-L/M but were not detected in controls (Figure 1C; compare lane 3 with lanes 1 and 2). Mass spectrometry analysis (LC-MS/MS) identified 373 proteins as putative dCoREST interactors (Supplementary Table S1). All four components of the LINT complex (dL(3)mbt, dLint-1, dRPD3 and dCoREST) were strongly enriched in the immunoprecipitate (Figure 1D).

An isoform-specific dLSD1/dCoREST complex

In mammalian cells, CoREST is an integral part of the LSD1/CoREST complex (3–7).

In S2 cells, dCoREST-L and dLSD1 can interact when both proteins are overexpressed suggesting that this interaction is conserved between vertebrate and invertebrate species (13). Indeed, our purification of endogenous dCoREST enriched three potential subunits of a putative *Drosophila* LSD1/CoREST complex: dLSD1, dCoREST and the HDAC1/2 homologue dRPD3 (Figure 1D, Supplementary Table S1).

We generated an S2 cell line allowing the inducible expression of FLAG-tagged dLSD1 (Figure 2A). FLAG-affinity purification from nuclear extracts of induced cells revealed that dLSD1 co-purified dRPD3 and dCoREST-L. Whilst this result does not allow us to judge to what extent these interactions are stoichiometric it strongly supports the existence of a dLSD1/dCoREST complex. Strikingly, dCoREST-M was not detected in the dLSD1 immunoprecipitate suggesting that dLSD1 binds dCoREST in an isoform-specific manner.

We next established two S2 cell lines for inducible expression of FLAG-tagged dCoREST-L and FLAG-tagged dCoREST-M, respectively (Supplementary Figure S1). dLSD1 was not detected in the FLAG-dCoREST-M immunoprecipitate by western blot (Figure 2B). By contrast, dLSD1 efficiently co-purified with FLAG-tagged dCoREST-L. This isoform-specificity of the dLSD1 interaction was not observed for subunits of the LINT complex: dL(3)mbt, dLint-1 and dRPD3 all co-precipitated with both dCoREST isoforms. We also subjected FLAG-dCoREST-L and FLAG-dCoREST-M immunoprecipitates to LC-MS/MS analysis. In agreement with the western blot result, the LINT subunits dL(3)mbt and dRPD3, and to a lesser extent also dLint-1, were enriched in the FLAG-dCoREST-L immunoprecipitate (Figure 2C and Supplementary Table S2). Likewise, all three LINT subunits were also enriched in the dCoREST-M immunoprecipitate (Figure 2D and Supplementary Table S3). By contrast, dLSD1 was significantly enriched in the dCoREST-L interactome only.

Finally, we generated baculoviruses expressing recombinant dLSD1, dCoREST-L and dCoREST-M. Pairwise co-infection of Sf9 cells followed by co-immunoprecipitation confirmed that dLSD1 preferentially interacts with dCoREST-L (Supplementary Figure S2). Thus, the isoform-specific interaction of dLSD1 with dCoREST-L can be recapitulated with recombinant proteins.

In summary, our results support the hypothesis that dLSD1 and dCoREST-L, but not dLSD1 and dCoREST-M, form a stable complex.

A novel dG9a/dCoREST complex

In addition to LINT subunits and dLSD1, we identified the H3K9-specific methyltransferase dG9a as one of the most abundant interaction partners of endogenous dCoREST (Figure 1D and Supplementary Table S1). dG9a was

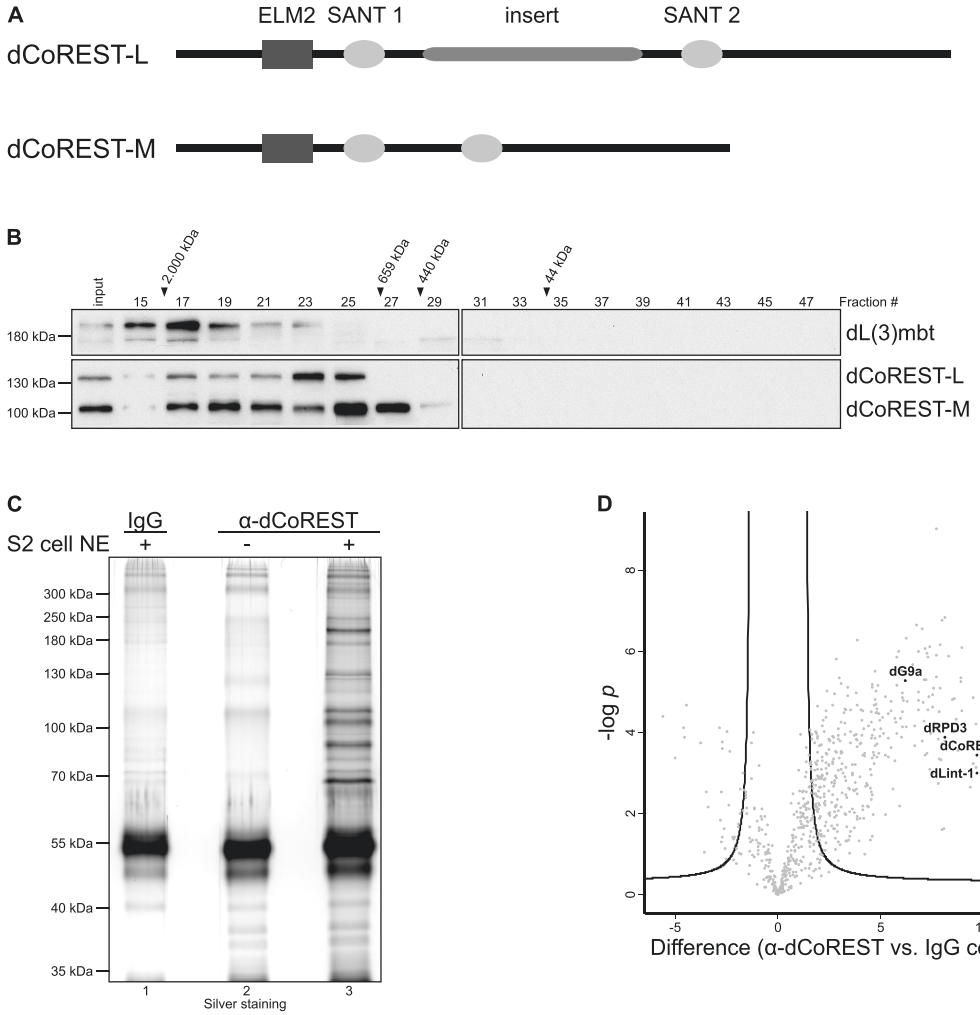

Figure 1. Purification of dCoREST interactors. (**A**) Schematic representation of the two major CoREST protein isoforms in *Drosophila*, dCoREST-L and dCoREST-M. Black rectangles depict ELM2 domains and grey ovals indicate SANT domains. The thick grey line represents a 234 amino acid insert unique to dCoREST-L. (**B**) Nuclear extract from S2 cells was fractionated over a Superose 6 column. Fractions were analysed by western blot using the antibodies indicated on the right. Fraction numbers and molecular mass standards are denoted on top. Input: 5% of extract loaded onto the column. (**C**) Nuclear extracts from S2 cells were subjected to IgG (lane 1) or anti-CoREST (lane 3) affinity purification and the bound material was analysed by sodium dodecyl sulphate-polyacrylamide gelelectrophoresis (SDS-PAGE) and silver staining. As an additional control anti-dCoREST antibody not incubated with nuclear extract was loaded (lane 2). (**D**) Volcano plot with -log10 *P*-values (*y*-axis) and log2 iBAQ fold-difference (*x*-axis) after comparison of anti-CoREST affinity purification versus IgG control. The point labeled 'dCoREST-M' was derived from peptides common to dCoREST-M and dCoREST-L. The point labeled 'dCoREST-L' was derived from peptides mapping the insert region that is exclusive to dCoREST-L. The complete list of the interacting proteins is presented in Supplementary Table S1 ($n = 4$, FDR = 0.01, s0 = 2).

also detected by western blot following the immunoprecipitation of both FLAG-tagged dCoREST isoforms (Figure 2B).

To confirm this interaction we used CRISPR/Cas to add a sequence encoding a GFP-tag to the 3′ end of the endogenous dG9a coding sequence (Supplementary Figure S3 and Table S5). Purification of the resulting dG9a-GFP fusion verified both dCoREST isoforms as well as dRPD3 as interactors of dG9a (Figure 3A). By contrast, neither dL(3)mbt nor dLSD1 were recovered to a significant extent. These results suggest that dG9a is not part of the LINT or dLSD1/dCoREST complexes but forms a separate assembly with dCoREST and dRPD3.

We next asked if dG9a forms a stoichiometric complex with dCoREST. We analysed dG9a-GFP purified from nuclear extracts by SDS-PAGE and silver staining (Figure 3B). This resulted in the co-purification of four polypeptides ranging in apparent molecular masses from 250 to 300 kDa. These masses correspond well to the mass expected for dG9a-GFP. We do not currently know if these polypeptides represent isoforms of dG9a, posttranslationally modified dG9a, degradation products or, indeed, interaction partners. It is clear, however, that this purification did not reveal polypeptides with apparent molecular masses similar to those of dCoREST-L, dCoREST-M or dRPD3 arguing that the bulk of dG9a is not associated with dCoREST and dRPD3. We considered the possibility that addition of the GFP moiety to the C-terminus of endogenous dG9a might disrupt interactions with dCoREST and dRPD3. Therefore, we used CRISPR/Cas to cre-

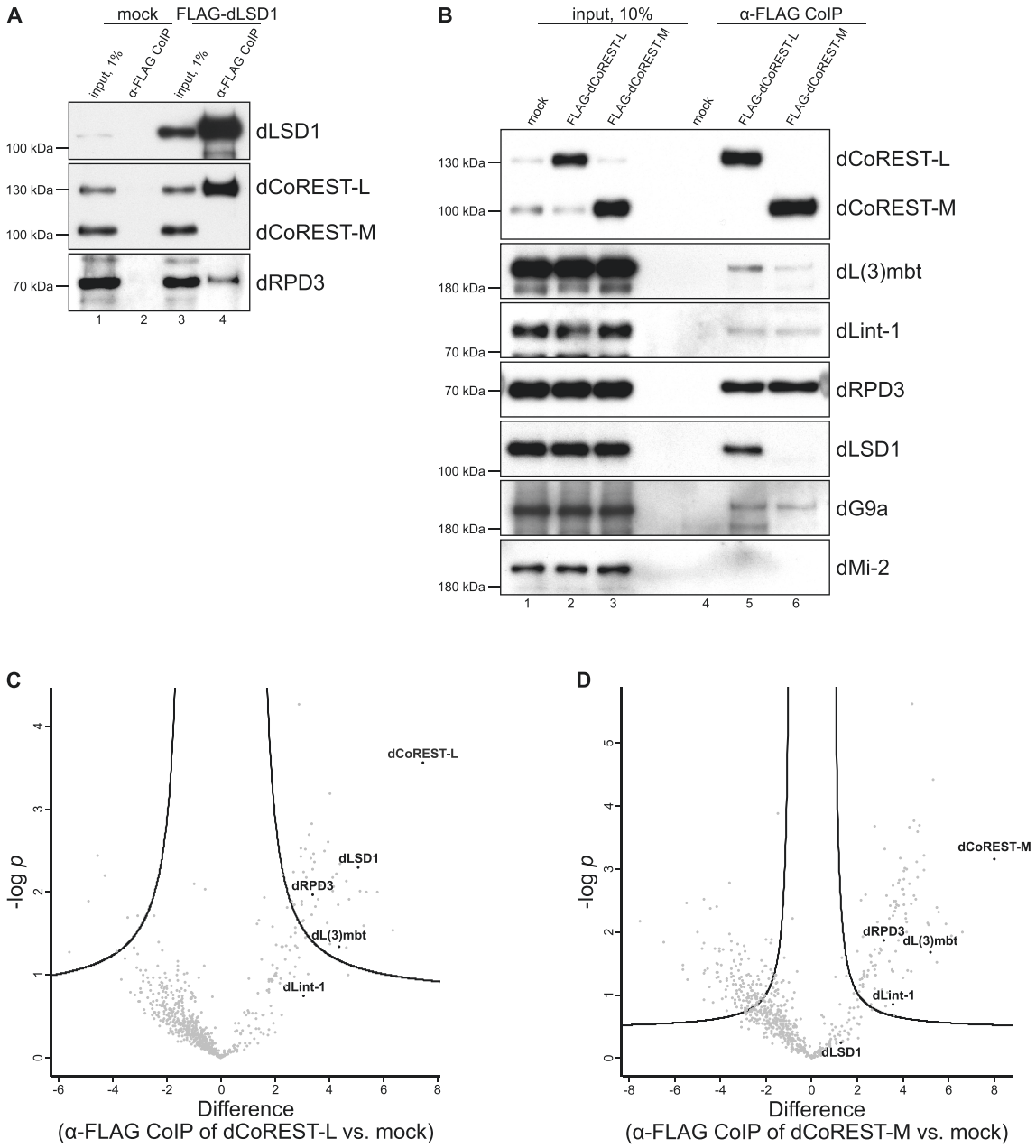

Figure 2. dLSD1 is an isoform-specific dCoREST-L interactor. (**A**) Nuclear extracts from control S2 cells (mock, lanes 1 and 2) and S2 cells stably expressing FLAG-dLSD1 (lanes 3 and 4) were precipitated with anti-FLAG antibody (lanes 2 and 4) and analysed by western blot using the antibodies indicated on the right (lanes 2 and 4). Lanes 1 and 3: 1% input. (**B**) Nuclear extracts from control S2 cells (mock, lanes 1 and 4), S2 cells stably expressing FLAG-dCoREST-L (lanes 2 and 5) or FLAG-dCoREST-M (lanes 3 and 6) were precipitated with anti-FLAG antibody (lanes 4 to 6) and analysed by western blot using antibodies indicated on the right (lanes 4–6). dMi-2 served as a negative control. Lanes 1–3: 10% input. (**C** and **D**) Volcano plot with -log10 *P*-values (*y*-axis) and log2 iBAQ fold-difference (*x*-axis) between the mock control and either the FLAG-CoREST-L affinity purification (C) or the FLAG-CoREST-M affinity purification (D). The complete list of the interacting proteins is presented in Supplementary Tables S2 and 3. ($n = 4$, FDR = 0.2, s0 = 1).

ate two additional cell lines expressing endogenous dG9 with a FLAG-tag at the N-terminus and C-terminus, respectively. Again, anti-FLAG affinity purification followed by SDS/PAGE and silver staining failed to detect interaction partners with apparent molecular masses similar to those of dCoREST or dRPD3 (data not shown). In conclusion, these results identify a dG9a/dCoREST complex but also make clear that the majority of dG9a molecules in nuclear extract are not associated with this complex.

Our proteomic analyses suggest that at least three distinct dCoREST histone deacetylase complexes exist in *Drosophila* which share a common dCoREST/dRPD3 core and are characterized by specific accessory subunits: the LINT complex, a dLSD1/dCoREST complex and a dG9a/dCoREST complex. To provide further support for

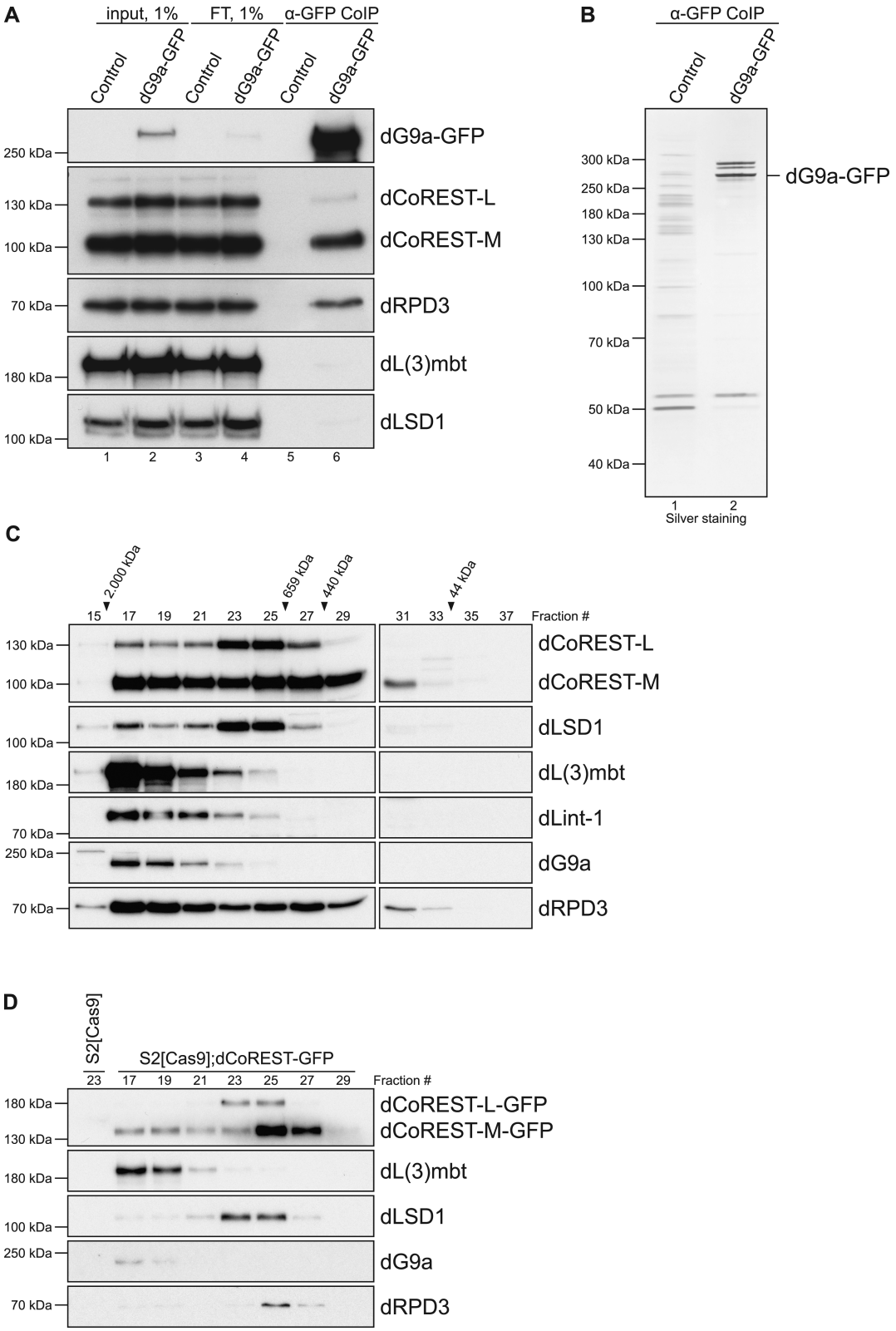

Figure 3. dG9a is a novel dCoREST-interacting protein. (**A**) Nuclear extracts from control S2[Cas9] cells (lanes 1, 3 and 5) and a dG9a-GFP tagged S2[Cas9] cell line (lanes 2, 4 and 6) were precipitated with anti-GFP antibody (lanes 5 and 6) and analysed by western blot using the antibodies indicated on the right. Lanes 1 and 2: 1% input. Lanes 3 and 4: 1% flow through. (**B**) SDS-PAGE and sliver staining of anti-GFP immunopurified nuclear extracts from control S2[Cas9] cells (lane 1) and a dG9a-GFP tagged S2[Cas9] cell line (lane 2). (**C**) A total of 1 mg of nuclear extract from S2 cells was fractionated over a Superose 6 column. Fractions were analysed by western blot using the antibodies indicated on the right. Fraction numbers and molecular mass standards are denoted on top. (**D**) A total of 1 mg of nuclear extract from S2[Cas9];dCoREST-GFP cells was fractionated over a Superose 6 column. Fractions were co-immunoprecipitated using GFP-Trap resin and analysed by western blot using the antibodies indicated on the right. Fraction numbers and molecular mass standards are denoted on top. Fraction #23 from non-tagged parental S2[Cas9] cells was used as a control.

this hypothesis we determined the gel filtration profile for dCoREST, dLSD1, dL(3)mbt, dLint-1, dG9a and dRPD3 using S2 nuclear extract (Figure 3C) and embryo nuclear extract (Supplementary Figure S4). In both cases, dCoREST-L, dCoREST-M and dRPD3 were detected in several fractions representing a broad range of apparent molecular masses (440 to 2000 kDa) in agreement with the notion that these proteins are components of several distinct complexes. dLSD1 and dCoREST-L co-eluted in the same peak fractions (fractions 25 and 19 (S2 nuclear extract); fractions 22 and 23 (embryo nuclear extract) further supporting the hypothesis that dLSD1 and dCoREST-L form a complex. By contrast, dL(3)mbt and dLint-1 peaked in fraction 26 (S2 nuclear extract) and fraction 27 (embryo nuclear extract). dG9a co-eluted with these LINT subunits in S2 nuclear extract (fraction 26) but not in embryo nuclear extract (peak fraction 20). Next, we separated nuclear extracts of S2 cells expressing GFP-tagged dCoREST by gel filtration, immunoprecipitated fractions with GFP antibody and analysed the immunoprecipitates by western blot (Figure 3D). This verified that the dCoREST interaction partners did not only co-elute with dCoREST but were indeed physically associated with dCoREST in their respective gel filtration fractions.

Taken together, three dCoREST-containing complexes can be separated by both immuno-precipitation and gel filtration. This strongly suggests that the dLSD1/dCoREST-L, the LINT and the dG9a/dCoREST complexes can exist as distinct entities. In addition, the similarity of gel filtration profiles derived from S2 nuclear extract and embryo nuclear extract indicates that these complexes are present in different cell types.

Chromatin binding by dCoREST complexes

Our biochemical studies suggest that three separate dCoREST complexes exist in nuclear extract of S2 cells. In order to assess if these assemblies are also associated with chromatin we performed ChIP-seq analyses. We employed CRISPR/Cas-mediated genome editing to generate S2 cell lines expressing GFP-tagged dCoREST, the LINT subunit dL(3)mbt, dLSD1 and dG9a, respectively (Supplementary Figure S3 and Table S5). This allowed us to determine the genome-wide binding profiles for these proteins by ChIP-seq using the same antibody (anti-GFP) in each case. We identified 4855 dCoREST bound sites in the *Drosophila* genome. dCoREST binding sites are greatly enriched in promoters implying a role in the regulation of transcription (Figure 4A). About 73.6% of dCoREST sites are also bound by dL(3)mbt (Figure 4B and D). By contrast, only 17.6 and 18.6% of dCoREST sites are co-occupied by dLSD1 and dG9a, respectively. This suggests that on chromatin the LINT complex is more abundant than either dLSD1/dCoREST or dG9a/dCoREST complexes. About 73.4% of all dL(3)mbt sites are also bound by dCoREST (Figure 4B and D). By contrast, only 10.2 and 7.3% of all dL(3)mbt sites are co-occupied by dLSD1 and dG9a, respectively (Figure 4C). This further supports the notion that the LINT complex is largely distinct from dLSD1/dCoREST and dG9a/dCoREST assemblies. dCoREST is associated with 79.0% of all dLSD1 binding sites (Figure 4B and D). This is in agreement with the notion that the majority of dLSD1 molecules bind chromatin as part of the dLSD1/dCoREST complex and demonstrates that the dLSD1/dCoREST complex associates with chromatin. About 59.0% of all dG9a binding sites are also bound by dCoREST (Figure 4B and D). Whilst this indicates that more than half of dG9a molecules bind chromatin as part of a dG9a/dCoREST assembly it is clear that a significant fraction of dG9a (41.0%) associates with chromatin independently of dCoREST. In conclusion, the comparison of chromatin binding profiles supports the notion that the three dCoREST complexes that we have defined by analysing soluble nuclear extract do indeed form on chromatin.

Gene regulation by CoREST-containing complexes in S2 cells

All three dCoREST complexes identified in our study contain histone modifying enzymes (dRPD3, dLSD1, dG9a) expected to generate closed chromatin structures and to repress gene transcription. Moreover, dCoREST complexes associate predominantly with promoter sequences. Therefore, we next asked what contributions the three dCoREST complexes would make to regulating the transcriptome of S2 cells. We used RNAi-mediated depletion followed by RNA-seq to address this question. S2 cells were treated with double stranded RNAs targeting EGFP (control) and two double stranded RNAs directed against dCoREST. One of these RNAs corresponded to a region shared by both L- and M-isoforms and efficiently depleted both dCoREST-L and dCoREST-M simultaneously (Figure 5A, lane 2). The other RNA hybridized to the insert unique to dCoREST-L and downregulated the dCoREST-L isoform specifically (Figure 5A, lane 3). We noted that depletion of dCoREST-L for four days resulted in slightly reduced western blot signals for most proteins tested suggesting an unspecific effect of dCoREST-L RNAi-treatment on the expression or stability of many proteins (Figure 5A, lane 3). We, therefore, shortened the RNAi treatment to three days (Figure 5A, lanes 8–10). Under these conditions the simultaneous depletion of both dCoREST isoforms as well as the depletion of dCoREST-L alone specifically decreased dLSD1 protein levels without affecting the levels of other proteins. This suggests that dCoREST-L binding to dLSD1 contributes to dLSD1 stability. As we have reported previously, depletion of dL(3)mbt had a similar destabilising effect on dLint-1 ((15); Figure 5A, lane 6).

Simultaneous depletion of both dCoREST-L and dCoREST-M upregulated 668 protein coding genes by a factor of 2.0 or more (log2FC $\geq$ 1) as determined by RNA-seq (Figure 5B). A much smaller number of genes (28) were downregulated. This supports the hypothesis that dCoREST complexes predominantly function to repress transcription. Importantly, 483 (68%) of the genes that change expression upon dCoREST knockdown are bound by dCoREST as determined by ChIP-seq analysis suggesting that these genes are direct targets of dCoREST repressor complexes.

To determine to what extent the three individual dCoREST complexes contribute to gene regulation we analysed

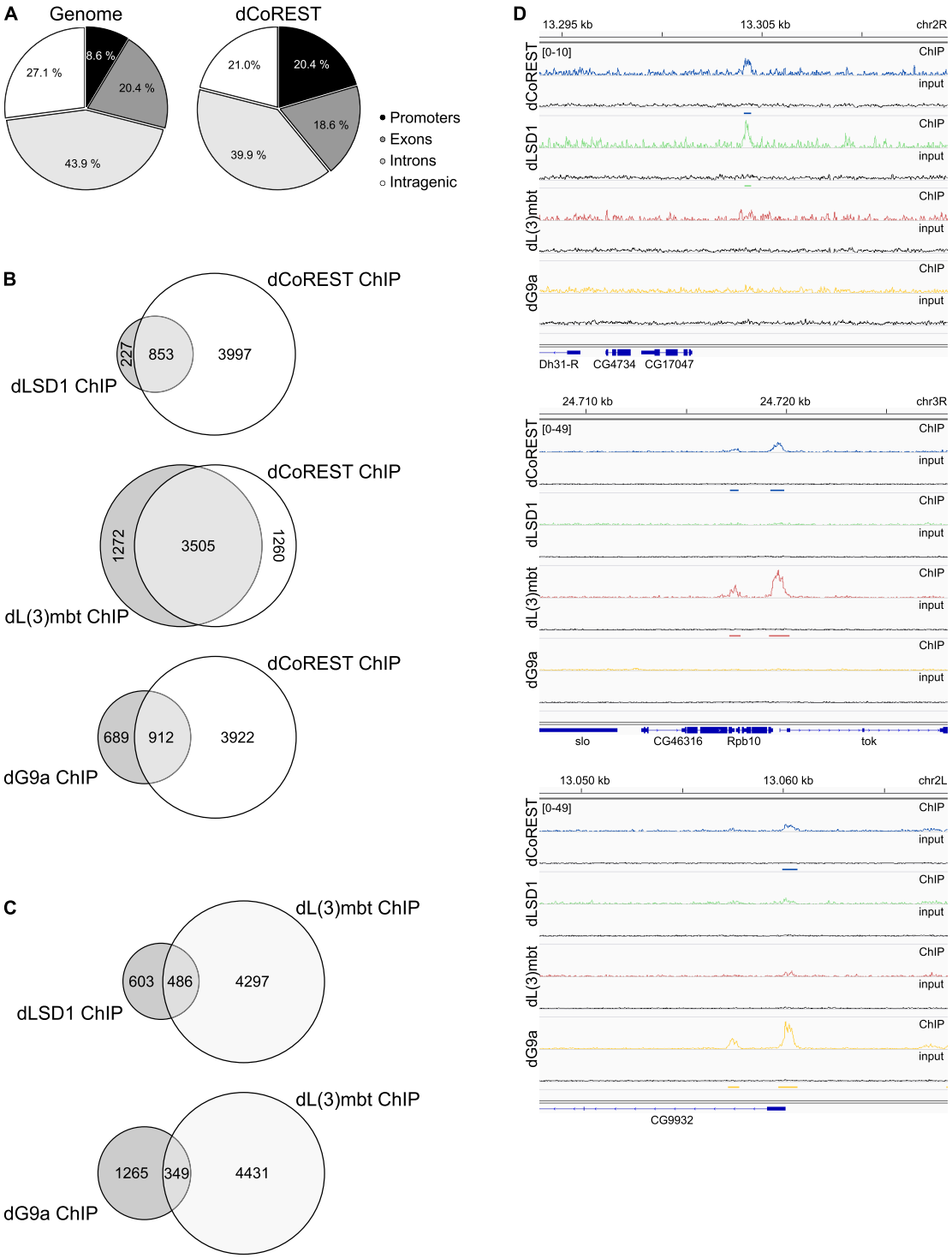

Figure 4. Genome-wide binding profiles of dCoREST, dLSD1, dL(3)mbt and dG9a by ChIP-seq analysis. (**A**) dCoREST binding sites are greatly enriched in promoters. (**B**) Venn diagrams depicting shared and unique ChIP-seq peaks for dCoREST and dLSD1 (top panel), dCoREST and dL(3)mbt (middle panel, and dCoREST and dG9a (bottom panel). (**C**) Venn diagrams depicting shared and unique ChIP-seq peaks for dL(3)mbt and dLSD1 (top panel) and dL(3)mbt and dG9a (bottom panel). Note that one peak of one data set can simultaneously overlap with two or more peaks of the data set it is compared to. As a consequence, the total number of peaks for any given protein is slightly different between Venn diagrams. The actual total numbers of peaks identified are as follows: dCoREST — 4855; dLSD1 — 1126; dL(3)mbt—4785; dG9a—1614). (**D**) Genome browser view of dCoREST and dLSD1 (top panel), dCoREST and dL(3)mbt (middle panel), and dCoREST and dG9a (bottom panel) chromatin associations. Data were visualized with the Integrative Genomics Viewer (Version 2.6.2) and snapshots were taken from representative regions.

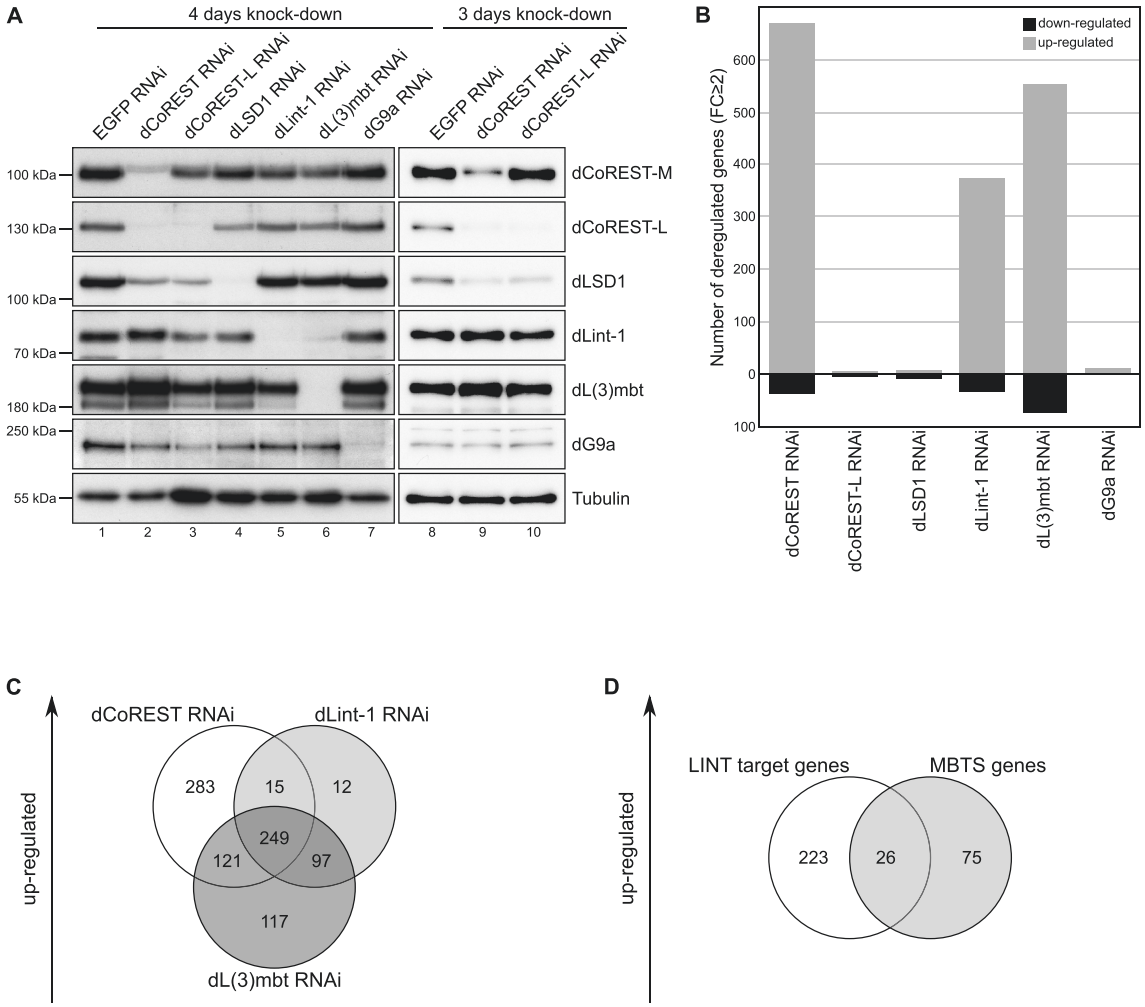

Figure 5. The LINT complex is a major repressor of transcription in S2 cells. S2 cells were treated with dsRNA directed against EGFP, dCoREST, dCoREST-L, dLSD1, dLint-1, dL(3)mbt and dG9a. (**A**) Nuclear extracts of RNAi treated S2 cells were subjected to western blot and analysed using antibodies indicated on the right. (**B**) RNA from these cells was analysed by RNA-seq. The diagram depicts the numbers of down- and upregulated genes (fold change $\geq$2) using transcript levels of EGFP RNAi treated cells as a reference ($n = 3$). (**C**) Venn diagram of genes upregulated upon dCoREST, dL(3)mbt and dLint-1 knockdown (fold change $\geq$2.0, adj. $P \leq 0.05$). (**D**) Venn diagram comparing LINT-repressed genes and malignant brain tumour signature (MBTS) genes.

transcriptomes after depletion of complex-specific subunits (Figure 5A).

Specific depletion of dLSD1 resulted in only few genes being misexpressed (Figure 5B; eight genes upregulated, ten genes downregulated). Likewise, very few genes were misregulated in S2 cells specifically depleted of dCoREST-L (four genes upregulated, four genes downregulated). These results are reminiscent of weak transcriptional effects of LSD1 depletion that have been reported previously: for example, RNAi-mediated depletion of LSD1 in mouse ES cells results in only a weak derepression of LSD1 target genes that does not exceed a factor of 2-fold (29). Therefore, we lowered the threshold of our analysis and considered genes misexpressed by a factor of 1.5 or more (log2FC$\geq$0.58). This, indeed, increased the number of dLSD1-repressed genes to 113 and the number of dCoREST-L-regulated genes to 41 (Supplementary Figure S5). Importantly, 78% of genes upregulated by dCoREST-L depletion were likewise upregulated by dLSD1 depletion suggesting that these genes are indeed repressed by a dLSD1/dCoREST-L complex. Nevertheless, it is clear that the dLSD1/dCoREST-L complex controls a comparatively small proportion of dCoREST-regulated genes in S2 cells even though 853 genomic sites are co-occupied by dCoREST and dLSD1.

Similar to what we observed after depletion of dLSD1, dG9a depletion upregulated only few genes by a factor of 2.0 or more (Figure 5B; 10 genes upregulated, 0 genes downregulated). In this case, including genes that were misregulated by a factor of 1.5-fold or more did not markedly increase the number of affected genes (18 genes upregulated, 16 genes downregulated). We conclude that dG9a does not play a major role in regulating gene transcription in S2 cells.

In stark contrast to the moderate to weak effects of depleting dLSD1/dCoREST complex and dG9a/dCoREST complex-specific subunits, depletion of LINT-specific subunits changed the expression levels of hundreds of genes by a factor of 2.0 or more (Figures 5B; dL(3)mbt: 584 genes upregulated, 56 genes downregulated; dLint-1: 373 genes upregulated, 34 genes downregulated). This suggests that the LINT complex is responsible for the regulation of a large fraction of dCoREST-dependent genes in S2 cells, in agreement with the LINT complex being the predominant chromatin-associated dCoREST complex as demonstrated by ChIP-seq analysis. In support of this hypothesis we find a high degree of overlap between genes that are derepressed by dCoREST, dL(3)mbt or dLint-1 depletion (Figure 5C). A total of 249 genes were upregulated when either dL(3)mbt, dLint-1 or dCoREST was targeted and we consider these to be high confidence LINT targets. Moreover, 385 genes were upregulated in at least two of the three knockdowns. Thus, approximately half of the dCoREST-regulated genes appear to be repressed by the LINT complex. We note that 283 genes are upregulated in dCoREST-depleted cells but neither in dL(3)mbt nor in dLint-1 depleted cells (Figure 5C). At present it is unclear if this is a consequence of a differential requirement for LINT complex subunits at subsets of LINT target genes or if these genes represent targets of as yet unidentified dCoREST complexes.

LINT represses germ line genes in S2 cells

dL(3)mbt and LINT have previously been implicated in the repression of *malignant brain tumour signature* (MBTS) genes. MBTS genes encode mostly germ line-specific proteins that are upregulated in brain tumours of *l(3)mbt* mutant larvae (14–15,30–31). In addition, dL(3)mbt regulates a group of genes targeted by the Salvador-Warts-Hippo (SWH) pathway (31). In agreement with our previous results obtained in Kc cells, LINT-repressed genes in S2 cells included a significant proportion of MBTS genes (26 out of 101) but none of the SWH targets (Figure 5D).

A gene ontology (GO)-term analysis of the 249 high confidence LINT-repressed genes revealed a number of terms that were significantly enriched (Supplementary Figure S6). These included genes linked with the GO-terms "germ line stem cell symmetric division" and "synapsis". Together with our finding that many of the germ line-specific MBTS transcripts are upregulated upon knockdown of LINT subunits, this indicates that LINT functions to repress genes involved in germ cell differentiation in S2 cells.

We had previously determined LINT target genes in Kc cells by microarray analysis (15). Based on the comparative analysis of their transcriptomes, both Kc cells and S2 cells are believed to be derived from embryonal macrophages and LINT might be expected to repress similar sets of genes in both cell lines (32). Indeed, comparison of the LINT regulated genes in Kc and S2 cells revealed a significant degree of overlap (Supplementary Figure S7).

In conclusion, our analyses suggest that LINT shapes the transcriptomes of macrophage-derived cell lines by preventing the inappropriate expression of genes characteristic of other cell types.

Depletion of dCoREST disrupts wing vein differentiation

In order to gain insight into the roles of different dCoREST complexes during fly development we performed RNA interference using the UAS/GAL4 system (33). We investigated two developmental systems, wing and testis, both of which have been shown to be sensitive to mutation or deregulation of several chromatin regulators (10,34–35). For example, RNAi-mediated depletion of dCoREST and dLSD1 throughout the wing imaginal disc has been demonstrated to result in ectopic vein phenotypes (10,36). We used the *engrailed*-GAL4 driver line to direct expression of UAS-shRNA constructs to the posterior half of the developing wing. Indeed, we observed vein phenotypes with high penetrance (100%) when dCoREST was targeted by RNAi (Supplementary Figure S8). Depletion of dLint-1 caused a strong deformation of wing shape that largely precluded an analysis of vein phenotypes. The molecular basis for the dLint-1 phenotype is currently unclear. Whilst depletion of dL(3)mbt, dLSD1 and dG9a did result in vein phenotypes with lower penetrance (<20% of wings analysed), such low penetrance phenotypes were also observed in the driver line (*en*-GAL4) and when RNAi was directed against transcripts unrelated to dCoREST complexes (dChd3, CG9973 and CG2083; Supplementary Figure S8). We therefore conclude that low penetrance vein phenotypes are unlikely to be a specific consequence of depletion of these dCoREST complex subunits. We considered the possibility that the lack of specific phenotypes caused by dL(3)mbt, dLSD1 and dG9a depletion was due to insufficient expression of RNAi constructs. We therefore repeated all crosses and phenotype analyses at an elevated temperature (30°C) known to enhance expression in the UAS-GAL4 system (37). This resulted in an enhancement of the severity of the dCoREST and dLint-1 RNAi phenotypes but still failed to produce specific wing alterations when dL(3)mbt, dLSD1 or dG9a were targeted (Supplementary Figure S9). However, measurement of dL(3)mbt, dLSD1 and dG9a RNA levels in wing discs by qPCR revealed no or only mild RNAi-mediated reductions of expression, precluding us from evaluating the role of these proteins in wing development (data not shown).

Taken together, these results suggest that in our experimental system dCoREST is critical for wing vein differentiation. However, they do not inform on which individual or which combination of the three dCoREST complexes is playing a role.

dLSD1/dCoREST is essential for spermatogenesis

Several of the dCoREST interactors identified in this study have been linked to the regulation of germ cell differentiation: Homozygous dLSD1 mutant females fail to produce oocytes and male flies are infertile (12,38–39). Similarly, mutations in dL(3)mbt, dLint1 and dG9a produce ovary defects and female sterility (14,40). We sought to systematically compare the importance of LINT, dLSD1/dCoREST and dG9a/dCoREST complex subunits for spermatogenesis and male fertility. Towards this end we used the *bag of marbles (bam)* GAL4 driver strain to direct expression of RNAi constructs to germ cells. We first compared

three different RNAi lines expressing shRNA constructs expected to simultaneously downregulate both dCoREST-L and dCoREST-M. Indeed, dCoREST-L and dCoREST-M mRNA expression in testes was reduced to levels ranging from 10 to 35% when these responder lines were crossed to *bam* driver lines (Supplementary Figure S10). Male progeny resulting from these crosses was infertile in agreement with our previous findings (34). This is consistent with the hypothesis that dCoREST-containing complexes are essential for fertility. We then set up a series of crosses to knock down dCoREST, dLSD1, dL(3)mbt, dLint-1 or dG9a in developing male germ cells. To verify efficiency of these knock downs we analysed RNA prepared from testes by qPCR (Supplementary Figure S11 and Table S6). mRNA expression of all RNAi targets was efficiently reduced. We then crossed virgin females with control males or RNAi-depleted males to assess male fertility. Out of 11 lines tested, only dCoREST and dLSD1-depleted males failed to generate offspring (Figure 6A). The fertility of males depleted of dL(3)mbt, dLint-1 or dG9a was indistinguishable from that of controls. This suggests a differential role of dCoREST complexes in male fertility: The dLSD1/dCoREST complex appeared to be essential for fertility whereas both LINT and dG9a/dCoREST complexes seemed dispensable.

Indeed, analysis of testes morphology by phase contrast microscopy revealed that seminal vesicles of control testes contained sperm, whereas seminal vesicles of dCoREST and dLSD1-depleted testes were empty (Figure 6B, panels 1, 2 and 3). Premeiotic spermatocytes did not show any obvious defects (panels 1′, 2′ and 3′). In addition, post meiotic spermatids identified by their flagella extending along a large part of the testis were present in both control and RNAi-depleted testes. This suggests that defects manifest at later stages such as spermatid nuclei elongation, histone-protamine exchange, individualization of sperm or release into the seminal vesicle.

We used immunofluorescence microscopy to identify possible alterations caused by dCoREST and dLSD1 depletion at postmeiotic stages (Figure 6C). During spermiogenesis round spermatid nuclei elongate (canoe stage), individualize and eventually form mature sperm. Histones are removed from DNA and degraded during the canoe stage. Concomitantly protamines and Mst77F are expressed to replace histones in mature sperm (23,28). dCoREST or dLSD1 knockdown did not affect this histone-to-protamine switch as judged by the timely expression and chromatin association of Mst77F. However, spermatid nuclei failed to elongate and no mature, elongated sperm were detected. As hardly any transcription takes place after meiotic divisions, these defects likely are a consequence of aberrant gene regulation during the spermatocyte phase (28). The striking similarity of the phenotypes produced after both dCoREST and dLSD1 knockdowns further strengthens the hypothesis that it is the dLSD1/dCoREST complex that is essential for the cellular processes that govern nuclei elongation.

The dLSD1/dCoREST complex did not appear to be a major regulator of gene transcription in macrophage-like S2 cells (Figure 5). Nevertheless, we hypothesized that it might regulate gene expression during germ cell development. We prepared RNA from bam>>dCoREST RNAi, bam>>dLSD1 RNAi and control testes and analysed their transcriptomes by RNA-seq. In both, dCoREST-depleted and dLSD1-depleted testes, a large number of genes was activated by a factor of 2.0 or more (log2FC≥1; dCoREST-depleted testes: 1721 genes up-regulated, 61 genes downregulated; dLSD1-depleted testes: 1300 genes upregulated, 125 genes downregulated) (Figure 7A). Importantly, 1091 genes were upregulated in both scenarios which corresponds to 63% of all dCoREST-repressed genes and 84% of all dLSD1-repressed genes (Figure 7B). We consider these genes to be high confidence targets of the dLSD1/dCoREST complex. GO-term analysis of these identified 20 GO-terms that were over-represented (Supplementary Figure S12). Eight of these were associated with genes involved in neuron development and function. These findings are consistent with the hypothesis that the dLSD1/dCoREST complex is required to prevent the inappropriate expression of neuron-specific genes in the male germ line.

Collectively, our results demonstrate that dCoREST functions to maintain cell-type-specific gene expression profiles in both macrophage-like S2 cells and in the male germ line. However, to do so different dCoREST complexes are used in a cell-type-specific manner.

DISCUSSION

Multisubunit protein complexes that regulate chromatin often exist as families of complexes with related subunit composition (1). Typically, a set of shared core subunits can associate with diverse complex-specific accessory subunits. Accessory subunits endow complexes with specific functionality by regulating the enzymatic activities of core subunits, adding new enzymatic, nucleosome or RNA binding activities and/or by influencing the targeting to specific genome regions.

Whereas extensive complex families have recently been described for PRC1, PRC2 and SWI/SNF, the number of complexes containing the CoREST repressor that have been identified is comparatively small: In mammalian cells, the bulk of CoREST appears to reside in complexes with LSD1 (6,8,12). Although several studies have found that CoREST can bind additional chromatin regulators it is not clear if these interactions reflect the existence of additional, stable CoREST complexes or are the products of transient binding events. In *Drosophila,* dCoREST and dLSD1 have been shown to interact in ovary extracts and when both proteins are overexpressed in S2 cells (12,13). We have previously identified dCoREST as a subunit of the dL(3)mbt interacting LINT complex (15). In the current study we have used proteomic approaches to systematically determine and characterize the interactome of dCoREST in S2 cells.

Using gel filtration, immunoaffinity purification, mass spectrometry and co-immunoprecipitation approaches we have identified three distinct dCoREST-containing complexes (Figure 8). All three of these complexes contain a heterodimeric core composed of dCoREST itself (either the -L or the -M isoform) and the histone deacetylase dRPD3. This core can associate with additional subunits and histone modifying activities to form either the LINT complex,

A

#	Fly line	Fertile
1	bam-GAL4 driver	+
2	dCoREST RNAi control	+
3	bam>>dCoREST RNAi	-
4	dLSD1 RNAi control	+
5	bam>>dLSD1 RNAi	-
6	dL(3)mbt RNAi control	+
7	bam>>dL(3)mbt RNAi	+
8	dLint-1 RNAi control	+
9	bam>>dLint-1 RNAi	+
10	dG9a RNAi control	+
11	bam>>dG9a RNAi	+

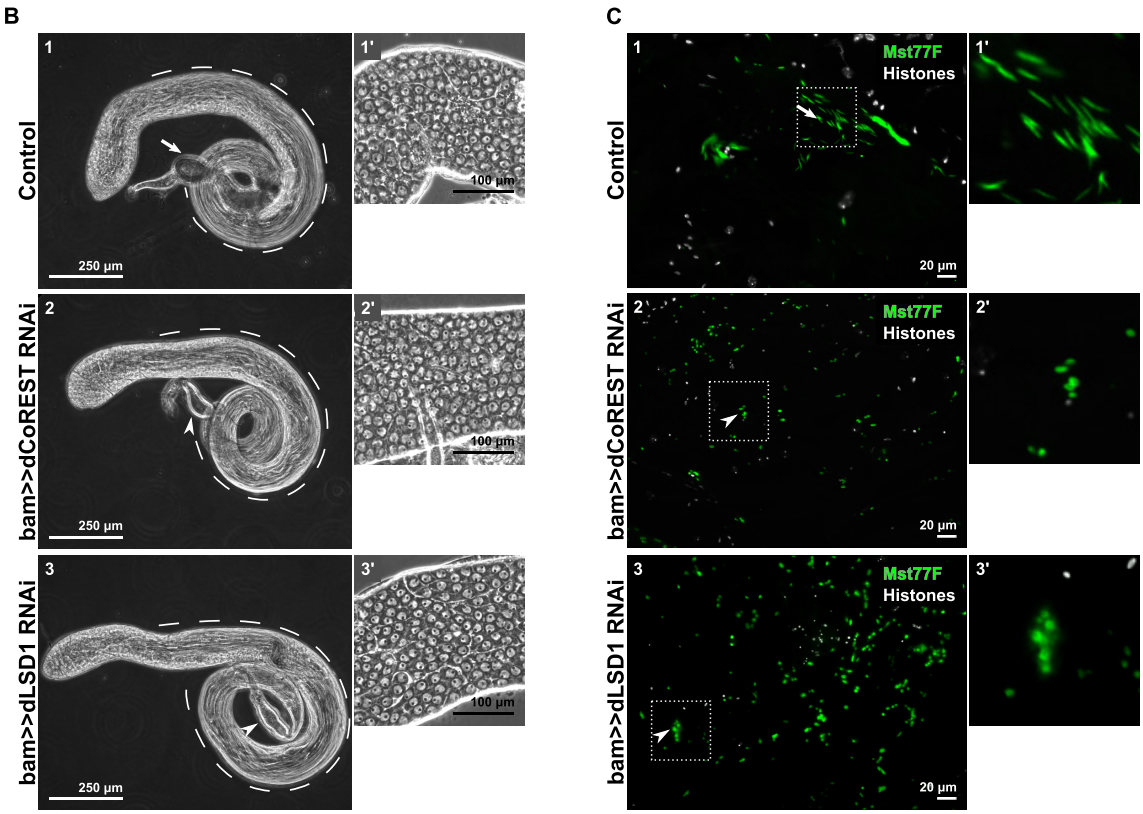

Figure 6. dLSD1/dCoREST complex is essential for spermatogenesis. (**A**) Male fertility tests of control flies and flies in which dCoREST or its interactors were depleted by RNAi ($n = 10$). Only bam>>dCoREST RNAi and bam>>dLSD1 RNAi flies produced no offspring (-). (**B**) Phase contrast images of 1 day old testes from control flies (1 and 1′), bam>>dCoREST RNAi flies (2 and 2′) and bam>>dLSD1 RNAi flies (3 and 3′). Post-meiotic spermatids identified by their flagella extending along a large part of the testis (marked by dashed line) were visible in all testes. Seminal vesicles of control testes (arrow in panel 1) contained sperm, seminal vesicles of RNAi depleted testes were empty (arrowheads in panels 2 and 3). Phase contrast microscopy of spermatocytes of indicated crosses (1′, 2′ and 3′) showed no visible defects. Scale bars: 250 µm (1, 2 and 3) and 100 µm (1′, 2′ and 3′). (**C**) Knockdown of dCoREST and dLSD1 leads to post-meiotic spermatid nuclei elongation defects. Histones (white) and the spermatid-specific protein Mst77F (green) were visualized by immunofluorescence in post-meiotic spermatid nuclei of control testes (1 and 1′) and upon RNAi in bam>>dCoREST RNAi (2 and 2′) and bam>>dLSD1 RNAi (3 and 3′) testes. Scale bars: 20 µm.

a dLSD1/dCoREST complex or a dG9a/dCoREST complex. LINT contains the signature subunits dL(3)mbt and dLint-1, the dLSD1/dCoREST complex is defined by the histone demethylase dLSD1 and the dG9a/dCoREST complex harbours the H3K9 histone methyltransferase dG9a. Thus, all three dCoREST complexes identified in our study have the potential to generate repressive chromatin structures by altering the histone methylation and acetylation status of nucleosomes.

Importantly, the three dCoREST complexes can be separated by immunoprecipitation and gel filtration under mild conditions suggesting that they indeed exist as distinct assemblies in the nucleus. Moreover, ChIP-seq analysis has demonstrated that the majority of dCoREST bound sites

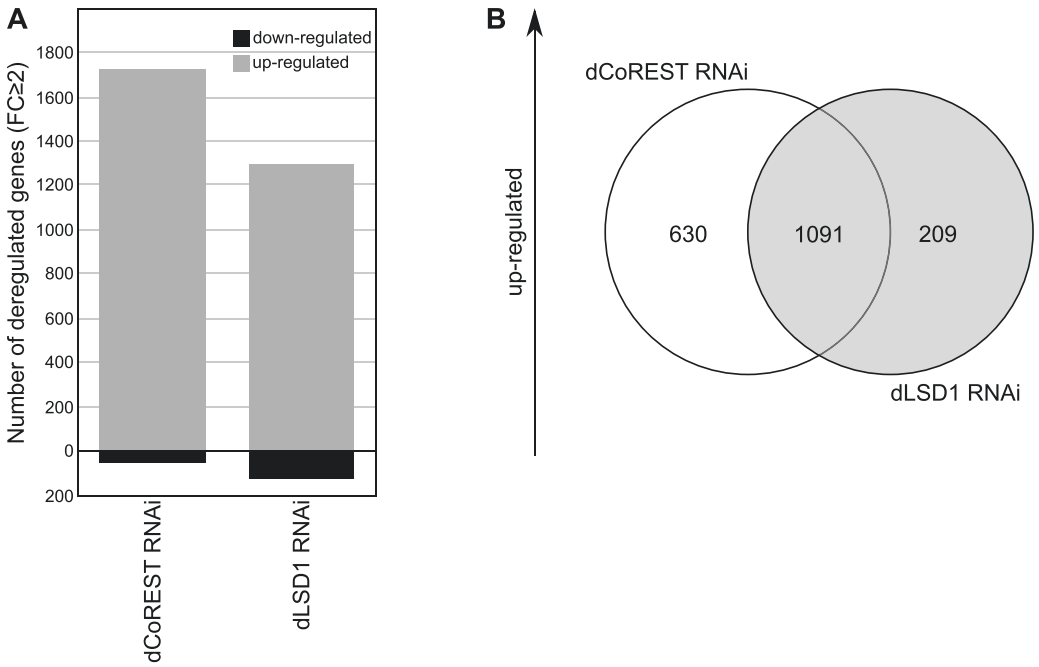

Figure 7. dLSD1/dCoREST complex is a major repressor of transcription during spermatogenesis. (**A**) Bar diagram showing the number of up- and downregulated protein coding genes of testes depleted for dCoREST or dLSD1 as determined by RNA-seq (total 850 testes from at least three biological replicates per condition). (**B**) Venn diagram showing comparison of dCoREST and dLSD1 up-regulated genes (fold change ≥2.0, adj. $P \leq 0.05$).

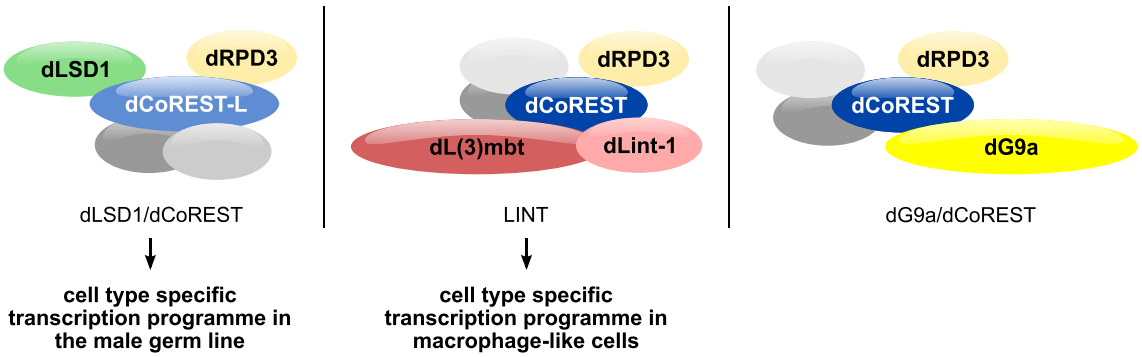

Figure 8. Schematic representation of different dCoREST complexes in Drosophila. Three distinct dCoREST containing complexes share a common dCoREST/dRPD3 core. The dLSD1/dCoREST complex is dCoREST isoform-specific and regulates transcription in the male germ line. The LINT complex is a major repressor of transcription in macrophage-like cells. The targets of the dG9a/dCoREST complex are unknown.

are co-occupied by dL(3)mbt but not by dLSD1 or dG9a further supporting the notion that the complexes associate as independent entities with chromatin. Our proteomic screens for dCoREST interactors have identified additional proteins with established roles in chromatin regulation that we have not yet characterized further. This leaves open the possibility that additional dCoREST-containing complexes might exist.

dCoREST-L and dCoREST-M differ in a 234 aa insertion between the SANT domains that is present in dCoREST-L but not in dCoREST-M (Figure 1A). Our results suggest that both isoforms can be integrated into the LINT and dG9a/dCoREST complexes. By contrast, reciprocal co-immunoprecipitation and reconstitution experiments demonstrate that only dCoREST-L but not dCoREST-M can form a complex with dLSD1. This agrees well with the prior observation that dLSD1 co-immunoprecipitates preferentially with dCoREST-L in ovary extracts. What determines the isoform specificity of this interaction? The structure of a complex formed by fragments of human CoREST and human LSD1 has been solved (41). This structure shows that the interaction surface of CoREST that contacts LSD1 is composed of a part of the region separating the two SANT domains and the second SANT domain itself. Sequence alignment of dCoREST-L with human CoREST reveals conservation across the entire LSD1 contact region (Supplementary Figure S13). The N-terminal part of this region is formed by the dCoREST-L-specific insertion that is missing in dCoREST-M. Thus, a potential explanation for why dCoREST-M cannot stably interact with dLSD1 is that an essential part of the interaction surface is missing in this isoform.

Although human CoREST is also expressed in different alternative splice forms, the strict isoform-specific dLSD1 interaction that we have identified in *Drosophila* does not appear to be conserved: all three major human CoREST isoforms interact with LSD1 (42).

Regulation of alternative splicing is an important mechanism for shaping cell-type-specific proteomes in higher metazoans. It is conceivable that the relative abundance of the three dCoREST complexes in different cell types could be modified by regulating alternative splicing of the dCoREST transcript: increased expression of dCoREST-M at the expense of dCoREST-L would be expected to result in a higher proportion of LINT and dG9a/dCoREST complexes (which can incorporate both isoforms) and a concomitant decrease in dLSD1/dCoREST complex levels. Indeed, the relative expression levels of dCoREST-L and dCoREST-M are significantly different in S2 cells and embryo extracts (compare e.g. Figures 1B, 3C and Supplementary Figure S4), suggesting that regulation of dCoREST expression at the level of alternative splicing might occur.

We have analysed the role of dCoREST complexes in wing development and spermatogenesis and in regulating transcription in the macrophage-like S2 cell line and in the male germ line. In all these settings lowering the expression of dCoREST complexes by RNAi depletion of their shared dCoREST subunits has profound effects on differentiation and changes the transcription of hundreds of genes. In both macrophage-like cells and male germ cells the number of upregulated genes exceeds the number of downregulated genes by a factor of 20-fold or higher. This suggests that dCoREST complexes are important regulators of differentiation in a variety of developmental settings and that they contribute to the maintenance of cell-type-specific transcription programmes predominantly by acting as repressors of transcription.

S2 cells and the male germ line respond with remarkable specificity to the inactivation of individual dCoREST complexes: In macrophage-like S2 cells, depletion of LINT complex signature subunits derepresses hundreds of genes whereas depletion of dLSD1, the dLSD1/dCoREST complex-specific dCoREST-L isoform or dG9a has only minor effects. It remains possible that dLSD1, dCoREST-L and dG9a depletion does lead to small expression changes of weakly expressed genes that our analysis has not been able to detect. In addition, it is possible that dCoREST-L depletion is compensated by dCoREST-M, e.g. by increased binding of dCoREST-M containing complexes to dLSD1/dCoREST-L bound regions. In any case, our study identifies LINT as an important repressor of genes that are inappropriate for macrophages such as the germ line-specific MBTS genes. Our results call into question whether dLSD1 and dG9a play important roles in regulating transcription in macrophage-like cells at all, at least under our experimental conditions, even though they are clearly associated with chromatin and occupy more than a thousand sites. An interesting parallel to our results is the finding that LSD1 knockdown does not result in major transcriptional effects in mouse ES cells (29). This is consistent with the hypothesis that also in mammals the ubiquitous LSD1/CoREST complex regulates transcription in a cell type-restricted manner.

In stark contrast to our results in S2 cells, depletion of dLSD1 (and depletion of dCoREST) results in the derepression of more than 1000 genes in the male germ line, the disruption of spermiogenesis and infertility. Amongst the genes repressed by dLSD1/dCoREST many appear to be specific for non-germ line lineages such as neurons. Depletion of LINT subunits or dG9a has no effect on spermatogenesis. Indeed, LSD1 plays also an important role in mammalian spermatogenesis: The SLC complex containing LSD1, CoREST and SFMB1 is highly expressed in mouse spermatocytes (8). Moreover, LSD1 and SFMBT1 colocalize at meiotic chromosomes. Conditional ablation of LSD1 expression in mouse testis results in misexpression of genes involved in stem cell and progenitor maintenance and differentiation, defective meiosis, complete loss of mature sperm and infertility (43,44). Although these studies did not directly address the role of CoREST these data are consistent with an important role of LSD1/CoREST complexes in spermatogenesis that is remarkably conserved between mouse and fly.

Unlike the LINT and dLSD1/dCoREST complexes for which we have identified important functions as transcriptional regulators in S2 cells and the male germ line, respectively, dG9a depletion did not produce significant effects in any of our experimental systems. These findings agree with earlier studies that have shown that although dG9a is abundantly expressed in the male germ line, dG9a mutants do not display a reduction of H3K9 methylation levels in germ cells (45,46). Moreover, dG9a is a non-essential gene and dG9a null mutants display mostly behavioural phenotypes (47–50). Defects of dG9a deficient flies have been reported under various conditions of stress (50–52). It is conceivable, that the dG9a/dCoREST complex is important in cell types that have not been analysed in our study or exerts its most prominent effects only under particular stress conditions.

A simple explanation for the cell-type- and lineage-specific differences in dCoREST complex function revealed in our study would be a potential differential expression of dCoREST complex signature subunits in S2 cells and testis. Indeed, on the RNA level G9a expression is only moderate in S2 cells and low in testis (Fly Atlas, *data not shown*), thus, providing a potential explanation for the weak effects on transcription when dG9a is depleted in these cells. However, on the protein level, dG9a has been demonstrated to be abundantly expressed in testis (45,46). dLSD1 expression is much higher in S2 cells, where the dLSD1/dCoREST complex represses only few genes, compared to testis, where the dLSD1/dCoREST complex is a major repressor of transcription and essential for spermatogenesis. In addition, dLint-1 expression is higher in testis compared to S2 cells even though depletion of LINT has no effect on spermatogenesis. Taken together, these observations suggest that differences in dCoREST complex repression activity cannot be easily attributed to differences in expression levels.

How is dCoREST complex activity confined to particular cell types and lineages? It is possible that cell-type-specific post-translational modifications of dCoREST complexes activate or inactivate their functions. Alternatively, gene repression by dCoREST complexes might be dependent on cell-type-specific transcription factors that recruit dCoREST complexes to chromatin. These cell-type-specific

transcription factors would specifically interact with one of the dCoREST complexes, potentially by contacting one of their signature subunits, and recruit this complex to sets of genes that need to be silenced in the given cell type. Indeed, we have recently identified such a mechanism involving the germ line-specific transcription factor Kumgang and the chromatin regulator dMi-2 that is responsible for the repression of hundreds of genes in the male germ line (34).

Our study has identified a set of distinct histone deacetylase complexes that are built around a dCoREST/dRPD3 core which have the potential to generate repressive chromatin structures by altering nucleosome acetylation and methylation. These complexes serve to repress lineage inappropriate genes, such as neuronal genes in the male germ line or germ line-specific genes in macrophage-like cells and often play critical roles in differentiation. We have revealed an unexpected division of labour amongst these complexes with individual dCoREST complexes being dedicated to preventing inappropriate gene expression in specific cell lineages and cell types.

In a broader sense, our study adds to the growing appreciation that chromatin regulating complexes are not all purpose machines that exert the same functions in all cell types but, instead, that they are tailored by the inclusion of specific accessory subunits to perform distinct cell type- and lineage-specific roles. Future analyses will aim to define the molecular mechanisms by which this specificity is achieved.

DATA AVAILABILITY

Data generated in this study are available as follows: IP/MS data at ProteomeXchange, identifier PXD014857 (MS identification of dCoREST interactors); raw ChIP-seq data have been deposited in the ArrayExpress database at EMBL-EBI (www.ebi.ac.uk/arrayexpress) under accession number E-MTAB-8341; raw RNA-seq data have been deposited in the ArrayExpress database at EMBL-EBI (www.ebi.ac.uk/arrayexpress) under accession number E-MTAB-7440 (S2 cells) and E-MTAB-7439 (*Drosophila* testes).

SUPPLEMENTARY DATA

Supplementary Data are available at NAR Online.

ACKNOWLEDGEMENTS

We are grateful to Gail Mandel, Gunther Reuter and Masamitsu Yamaguchi for the kind gifts of dCoREST, dLSD1 and dG9a antibodies, respectively, and to Ulla Kopiniak, Corinna Webert, Thomas Plagge and Jonathan Trautwein for experimental assistance. We thank Guntram Suske for critical reading of the manuscript and Peeyush Sahu, Marek Bartkuhn, Robert Liefke and Tobias Zimmermann for assistance with bioinformatic analyses.

FUNDING

Deutsche Forschungsgemeinschaft (DFG) [BR2102/6 to I.M., J.L., A.B.; TRR81/B13 to I.T., T.H., R.R.-P., C.R.; TRR81/A01 to K.K., A.B.]. Funding for open access charge: DFG [TRR81].

Conflict of interest statement. None declared.

REFERENCES

1. Meier,K. and Brehm,A. (2014) Chromatin regulation: how complex does it get? *Epigenetics*, **9**, 1485–1495.
2. Andres,M.E., Burger,C., Peral-Rubio,M.J., Battaglioli,E., Anderson,M.E., Grimes,J., Dallman,J., Ballas,N. and Mandel,G. (1999) CoREST: a functional corepressor required for regulation of neural-specific gene expression. *Proc. Natl. Acad. Sci. U.S.A.*, **96**, 9873–9878.
3. Hakimi,M.A., Bochar,D.A., Chenoweth,J., Lane,W.S., Mandel,G. and Shiekhattar,R. (2002) A core-BRAF35 complex containing histone deacetylase mediates repression of neuronal-specific genes. *Proc. Natl. Acad. Sci. U.S.A.*, **99**, 7420–7425.
4. Humphrey,G.W., Wang,Y., Russanova,V.R., Hirai,T., Qin,J., Nakatani,Y. and Howard,B.H. (2001) Stable histone deacetylase complexes distinguished by the presence of SANT domain proteins CoREST/kiaa0071 and Mta-L1. *J. Biol. Chem.*, **276**, 6817–6824.
5. Lee,M.G., Wynder,C., Cooch,N. and Shiekhattar,R. (2005) An essential role for CoREST in nucleosomal histone 3 lysine 4 demethylation. *Nature*, **437**, 432–435.
6. Shi,Y.J., Matson,C., Lan,F., Iwase,S., Baba,T. and Shi,Y. (2005) Regulation of LSD1 histone demethylase activity by its associated factors. *Mol. Cell*, **19**, 857–864.
7. You,A., Tong,J.K., Grozinger,C.M. and Schreiber,S.L. (2001) CoREST is an integral component of the CoREST- human histone deacetylase complex. *Proc. Natl. Acad. Sci. U.S.A.*, **98**, 1454–1458.
8. Zhang,J., Bonasio,R., Strino,F., Kluger,Y., Holloway,J.K., Modzelewski,A.J., Cohen,P.E. and Reinberg,D. (2013) SFMBT1 functions with LSD1 to regulate expression of canonical histone genes and chromatin-related factors. *Genes Dev.*, **27**, 749–766.
9. Mulligan,P., Yang,F., Di Stefano,L., Ji,J.Y., Ouyang,J., Nishikawa,J.L., Toiber,D., Kulkarni,M., Wang,Q., Najafi-Shoushtari,S.H. *et al.* (2011) A SIRT1-LSD1 corepressor complex regulates Notch target gene expression and development. *Mol. Cell*, **42**, 689–699.
10. Curtis,B.J., Zraly,C.B. and Dingwall,A.K. (2013) Drosophila LSD1-CoREST demethylase complex regulates DPP/TGFbeta signaling during wing development. *Genesis*, **51**, 16–31.
11. Domanitskaya,E. and Schupbach,T. (2012) CoREST acts as a positive regulator of Notch signaling in the follicle cells of Drosophila melanogaster. *J. Cell Sci.*, **125**, 399–410.
12. Lee,M.C. and Spradling,A.C. (2014) The progenitor state is maintained by lysine-specific demethylase 1-mediated epigenetic plasticity during Drosophila follicle cell development. *Genes Dev.*, **28**, 2739–2749.
13. Dallman,J.E., Allopenna,J., Bassett,A., Travers,A. and Mandel,G. (2004) A conserved role but different partners for the transcriptional corepressor CoREST in fly and mammalian nervous system formation. *J. Neurosci.*, **24**, 7186–7193.
14. Coux,R.X., Teixeira,F.K. and Lehmann,R. (2018) L(3)mbt and the LINT complex safeguard cellular identity in the Drosophila ovary. *Development*, **145**, dev160721.
15. Meier,K., Mathieu,E.L., Finkernagel,F., Reuter,L.M., Scharfe,M., Doehlemann,G., Jarek,M. and Brehm,A. (2012) LINT, a novel dL(3)mbt-containing complex, represses malignant brain tumour signature genes. *PLos Genet.*, **8**, e1002676.
16. Kunert,N. and Brehm,A. (2008) Mass production of Drosophila embryos and chromatographic purification of native protein complexes. *Methods Mol. Biol.*, **420**, 359–371.
17. van den Berg,D.L., Snoek,T., Mullin,N.P., Yates,A., Bezstarosti,K., Demmers,J., Chambers,I. and Poot,R.A. (2010) An Oct4-centered protein interaction network in embryonic stem cells. *Cell Stem Cell*, **6**, 369–381.
18. Schmidt,A., Forne,I. and Imhof,A. (2014) Bioinformatic analysis of proteomics data. *BMC Syst. Biol.*, **8**, S3.
19. Rathke,C., Barckmann,B., Burkhard,S., Jayaramaiah-Raja,S., Roote,J. and Renkawitz-Pohl,R. (2010) Distinct functions of Mst77F and protamines in nuclear shaping and chromatin condensation during Drosophila spermiogenesis. *Eur. J. Cell Biol.*, **89**, 326–338.
20. Murawska,M., Kunert,N., van Vugt,J., Langst,G., Kremmer,E., Logie,C. and Brehm,A. (2008) dCHD3, a novel ATP-dependent

chromatin remodeler associated with sites of active transcription. *Mol. Cell Biol.*, **28**, 2745–2757.
21. Dobin,A., Davis,C.A., Schlesinger,F., Drenkow,J., Zaleski,C., Jha,S., Batut,P., Chaisson,M. and Gingeras,T.R. (2013) STAR: ultrafast universal RNA-seq aligner. *Bioinformatics*, **29**, 15–21.
22. Love,M.I., Huber,W. and Anders,S. (2014) Moderated estimation of fold change and dispersion for RNA-seq data with DESeq2. *Genome Biol.*, **15**, 550.
23. Rathke,C., Baarends,W.M., Jayaramaiah-Raja,S., Bartkuhn,M., Renkawitz,R. and Renkawitz-Pohl,R. (2007) Transition from a nucleosome-based to a protamine-based chromatin configuration during spermiogenesis in Drosophila. *J. Cell Sci.*, **120**, 1689–1700.
24. Hundertmark,T., Theofel,I., Eren-Ghiani,Z., Miller,D. and Rathke,C. (2017) Analysis of chromatin dynamics during drosophila spermatogenesis. *Methods Mol. Biol.*, **1471**, 289–303.
25. Livak,K.J. and Schmittgen,T.D. (2001) Analysis of relative gene expression data using real-time quantitative PCR and the 2(-Delta Delta C(T)) Method. *Methods*, **25**, 402–408.
26. Bottcher,R., Hollmann,M., Merk,K., Nitschko,V., Obermaier,C., Philippou-Massier,J., Wieland,I., Gaul,U. and Forstemann,K. (2014) Efficient chromosomal gene modification with CRISPR/cas9 and PCR-based homologous recombination donors in cultured Drosophila cells. *Nucleic Acids Res.*, **42**, e89.
27. Scharf,A.N., Meier,K., Seitz,V., Kremmer,E., Brehm,A. and Imhof,A. (2009) Monomethylation of lysine 20 on histone H4 facilitates chromatin maturation. *Mol. Cell Biol.*, **29**, 57–67.
28. Rathke,C., Baarends,W.M., Awe,S. and Renkawitz-Pohl,R. (2014) Chromatin dynamics during spermiogenesis. *Biochim. Biophys. Acta*, **1839**, 155–168.
29. Nair,V.D., Ge,Y., Balasubramaniyan,N., Kim,J., Okawa,Y., Chikina,M., Troyanskaya,O. and Sealfon,S.C. (2012) Involvement of histone demethylase LSD1 in short-time-scale gene expression changes during cell cycle progression in embryonic stem cells. *Mol. Cell Biol.*, **32**, 4861–4876.
30. Janic,A., Mendizabal,L., Llamazares,S., Rossell,D. and Gonzalez,C. (2010) Ectopic expression of germline genes drives malignant brain tumor growth in Drosophila. *Science*, **330**, 1824–1827.
31. Richter,C., Oktaba,K., Steinmann,J., Muller,J. and Knoblich,J.A. (2011) The tumour suppressor L(3)mbt inhibits neuroepithelial proliferation and acts on insulator elements. *Nat. Cell Biol.*, **13**, 1029–1039.
32. Cherbas,L., Willingham,A., Zhang,D., Yang,L., Zou,Y., Eads,B.D., Carlson,J.W., Landolin,J.M., Kapranov,P., Dumais,J. *et al.* (2011) The transcriptional diversity of 25 Drosophila cell lines. *Genome Res.*, **21**, 301–314.
33. Brand,A.H. and Perrimon,N. (1993) Targeted gene expression as a means of altering cell fates and generating dominant phenotypes. *Development*, **118**, 401–415.
34. Kim,J., Lu,C., Srinivasan,S., Awe,S., Brehm,A. and Fuller,M.T. (2017) Blocking promiscuous activation at cryptic promoters directs cell type-specific gene expression. *Science*, **356**, 717–721.
35. Kovac,K., Sauer,A., Macinkovic,I., Awe,S., Finkernagel,F., Hoffmeister,H., Fuchs,A., Muller,R., Rathke,C., Langst,G. *et al.* (2018) Tumour-associated missense mutations in the dMi-2 ATPase alters nucleosome remodelling properties in a mutation-specific manner. *Nat. Commun.*, **9**, 2112.
36. Curtis,B.J., Zraly,C.B., Marenda,D.R. and Dingwall,A.K. (2011) Histone lysine demethylases function as co-repressors of SWI/SNF remodeling activities during Drosophila wing development. *Dev. Biol.*, **350**, 534–547.
37. Duffy,J.B. (2002) GAL4 system in drosophila: a fly geneticist's Swiss army knife. *Genesis*, **34**, 1–15.
38. Rudolph,T., Yonezawa,M., Lein,S., Heidrich,K., Kubicek,S., Schafer,C., Phalke,S., Walther,M., Schmidt,A., Jenuwein,T. *et al.* (2007) Heterochromatin formation in Drosophila is initiated through active removal of H3K4 methylation by the LSD1 homolog SU(VAR)3-3. *Mol. Cell*, **26**, 103–115.
39. Szabad,J., Reuter,G. and Schroder,M.B. (1988) The effects of two mutations connected with chromatin functions on female germ-line cells of Drosophila. *Mol. Gen. Genet.*, **211**, 56–62.
40. Lee,K.S., Yoon,J., Park,J.S. and Kang,Y.K. (2010) Drosophila G9a is implicated in germ cell development. *Insect Mol. Biol.*, **19**, 131–139.
41. Yang,M., Gocke,C.B., Luo,X., Borek,D., Tomchick,D.R., Machius,M., Otwinowski,Z. and Yu,H. (2006) Structural basis for CoREST-dependent demethylation of nucleosomes by the human LSD1 histone demethylase. *Mol. Cell*, **23**, 377–387.
42. Barrios,A.P., Gomez,A.V., Saez,J.E., Ciossani,G., Toffolo,E., Battaglioli,E., Mattevi,A. and Andres,M.E. (2014) Differential properties of transcriptional complexes formed by the CoREST family. *Mol. Cell Biol.*, **34**, 2760–2770.
43. Lambrot,R., Lafleur,C. and Kimmins,S. (2015) The histone demethylase KDM1A is essential for the maintenance and differentiation of spermatogonial stem cells and progenitors. *FASEB J.*, **29**, 4402–4416.
44. Myrick,D.A., Christopher,M.A., Scott,A.M., Simon,A.K., Donlin-Asp,P.G., Kelly,W.G. and Katz,D.J. (2017) KDM1A/LSD1 regulates the differentiation and maintenance of spermatogonia in mice. *PLoS One*, **12**, e0177473.
45. Stabell,M., Eskeland,R., Bjorkmo,M., Larsson,J., Aalen,R.B., Imhof,A. and Lambertsson,A. (2006) The Drosophila G9a gene encodes a multi-catalytic histone methyltransferase required for normal development. *Nucleic Acids Res.*, **34**, 4609–4621.
46. Ushijima,Y., Inoue,Y.H., Konishi,T., Kitazawa,D., Yoshida,H., Shimaji,K., Kimura,H. and Yamaguchi,M. (2012) Roles of histone H3K9 methyltransferases during Drosophila spermatogenesis. *Chromosome Res.*, **20**, 319–331.
47. Anreiter,I., Kramer,J.M. and Sokolowski,M.B. (2017) Epigenetic mechanisms modulate differences in Drosophila foraging behavior. *Proc. Natl. Acad. Sci. U.S.A.*, **114**, 12518–12523.
48. Kramer,J.M., Kochinke,K., Oortveld,M.A., Marks,H., Kramer,D., de Jong,E.K., Asztalos,Z., Westwood,J.T., Stunnenberg,H.G., Sokolowski,M.B. *et al.* (2011) Epigenetic regulation of learning and memory by Drosophila EHMT/G9a. *PLoS Biol.*, **9**, e1000569.
49. Seum,C., Bontron,S., Reo,E., Delattre,M. and Spierer,P. (2007) Drosophila G9a is a nonessential gene. *Genetics*, **177**, 1955–1957.
50. Shimaji,K., Konishi,T., Tanaka,S., Yoshida,H., Kato,Y., Ohkawa,Y., Sato,T., Suyama,M., Kimura,H. and Yamaguchi,M. (2015) Genomewide identification of target genes of histone methyltransferase dG9a during Drosophila embryogenesis. *Genes Cells*, **20**, 902–914.
51. An,P.N.T., Shimaji,K., Tanaka,R., Yoshida,H., Kimura,H., Fukusaki,E. and Yamaguchi,M. (2017) Epigenetic regulation of starvation-induced autophagy in Drosophila by histone methyltransferase G9a. *Sci. Rep.*, **7**, 7343.
52. Merkling,S.H., Bronkhorst,A.W., Kramer,J.M., Overheul,G.J., Schenck,A. and Van Rij,R.P. (2015) The epigenetic regulator G9a mediates tolerance to RNA virus infection in Drosophila. *PLoS Pathog.*, **11**, e1004692.

SUPPLEMENTARY MATERIAL AND METHODS

Cas9 gene editing and transfections

Endogenous dCoREST, dLSD1, dL(3)mbt, and dG9a were epitope-tagged using CRISPR/Cas9: Four days before transfection, S2[Cas9] cells were first transiently depleted of the essential NHEJ-factor Lig4 and the MMEJ-factor Mus308 via RNAi to favour homologous recombination. U6-sgRNA template and homologous recombination template (for the introduction of the GFP-tag at the C-terminus and the puromycin resistance cassette) for tagging were generated as described in (17) and transfected into cells. After four days, puromycin-resistant cells were selected in 2.5 µg/ml puromycin for two weeks. Monoclonal cell lines were prepared by serial dilution and clones were analysed by PCR and Western blot. Primers used to generate PCR products are listed in Supplementary Table S5.

For introduction of transgene by stable transfection, plasmids expressing full-length FLAG-tagged dCoREST-L, dCoREST-M or dLSD1 under control of a metallothionein promoter were co-transfected with pBS-Puro (which confers resistance to puromycin) into S2 cells as described previously (16). In brief, a total of $7.4x10^6$ S2 cells were seeded in 10 cm plates (Sarstedt). The next day cells were transfected with 30 µg of pRmHa-3 plasmid containing the coding sequence of full-length FLAG-tagged dCoREST-L, dCoREST-M or dLSD1 under control of the metallothionein promoter and 1.5 µg of the pBS-Puro by calcium-phosphate transfection. Medium was exchanged 24 hours after transfection. After three days cells were split and selected in 10 µg/ml puromycin for three weeks. Transgene expression was induced by adding $CuSO_4$ to a final concentration of 100 µm and nuclear extracts were prepared 24 hours later and analysed by Western blot.

Protein expression in Sf9 cells and co-immunoprecipitation

Baculoviruses expressing dCoREST-L, dCoREST-M and dLSD1 were generated with the Bac-to-Bac Baculovirus Expression System (Invitrogen) according to the manufacturer's instructions. Sf9 cells were harvested 72 hours after infection and lysed by three freeze/thaw cycles in Lysis buffer (20 mM Hepes pH 7.6, 200 mM KCl, 10% (v/v) glycerol, 0.1% (v/v) NP-40). Lysates were cleared by centrifugation (30 min, 17,000 x g, 4 °C).

200 µl of Sf9 extracts with comparable amounts of the target proteins were mixed with 1 ml of IP150-buffer (25 mM Hepes pH 7.9, 150 mM NaCl, 12.5 mM $MgCl_2$, 0.1 mM EDTA, 10% (v/v) glycerol, 0.1% (v/v) NP-40). 3 µl of antibody (anti-dCoREST, (13)) was added to each sample and the reaction was rotated for two hours at 4 °C. Protein G Sepharose 4 Fast Flow beads (GE Healthcare) were blocked for one hour with 0.5 mg/ml BSA and 1% (w/v) Gelatin from cold water fish skin. 20 µl of blocked beads were added to each IP reaction and rotated for one hour at 4 °C. Immune complexes were precipitated by centrifugation (4 min, 1,500 x g, 4 °C) and washed four times with 1 ml of IP150-buffer. Precipitates were eluted with SDS-loading buffer and analyzed by SDS-PAGE and Western Blot.

RNA isolation and qPCR

RNA isolation was performed using the peqGOLD Total RNA Kit (S-Line, peqlab) according to the manufacturer's instructions from three independent RNAi experiments in S2 cells or from a pool of 50 testes from 3 independent crosses. RNA was additionally treated with DNase I (peqGOLD DNase I Digest Kit, peqlab) according to the manufacturer's instruction. Upon quantification (NanoDrop; Thermo Scientific), cDNA synthesis was carried out in triplicate from 0.2 µg (testis) or 1.0 µg (S2 cells) of isolated RNA using the SensiFAST™ cDNA Synthesis Kit (Bioline) according to the manufacturer's protocol. cDNA was diluted ten times for further use in qPCR reactions. qPCR was performed using the SensiFAST™ SYBR® Lo-ROX Kit (Bioline) on a Mx3000P cycler (Agilent Technologies) according to the instruction manual. Calculations were done according to (23). Data presented in the graphs represent mean values of three biological (S2 cells) or three technical (testes) replicates with standard deviation. For determination of RNA expression in testes, testes from several independent crosses were pooled prior to RNA preparation. Primer sequences are listed in Supplementary Table S6.

SUPPLEMENTARY TABLES

Supplementary Table S1. List of proteins identified by LC-MS/MS analysis in the anti-CoREST co-immunoprecipitation experiment (n=4, FDR=0.01, s0=2).

Supplementary Table S2. List of proteins identified by LC-MS/MS analysis in the anti-FLAG co-immunoprecipitation experiment of FLAG-dCoREST-L (n=4, FDR=0.2, s0=1).

Supplementary Table S3. List of proteins identified by LC-MS/MS analysis in anti-FLAG co-immunoprecipitation experiment of FLAG-dCoREST-M (n=4, FDR=0.2, s0=1).

Supplementary Table S4. List of primers used for amplification of the templates for dsRNA synthesis by *in vitro* transcription.

No.	Name	Sequence
1	EFGP-RNAi-fw	gaattaatacgactcactatagggAGAGCTGGACGGCGACGTAA
2	EFGP-RNAi-rv	gaattaatacgactcactatagggAGACTTGTACAGCTCGTCCATG
3	dCoREST-RNAi-fw	taatacgactcactatagggCATTCGCTCAGTTTTCTGACG
4	dCoREST-RNAi-rv	taatacgactcactatagggCCACCGAAATGTACTCCTCC
5	dCoREST-L-RNAi-fw	taatacgactcactatagggAAGATTTGCAACGTGGTCTG
6	dCoREST-L-RNAi-rv	taatacgactcactatagggTTCCGCCAAATAGAGACTGG
7	dLSD1-RNAi-fw	taatacgactcactatagggAAAGAAACGTCAATCACCCG
8	dLSD1-RNAi-rv	taatacgactcactatagggCCTCTTCGTTGGGTGTCATT
9	dL(3)mbt-RNAi-fw	taatacgactcactatagggGTTGGTTTGGGTGCTGTCTT
10	dL(3)mbt-RNAi-rv	taatacgactcactatagggGCGTCTAAAGTTCAGCCAGG
11	dLint-1-RNAi-fw	taatacgactcactatagggATGAAAGGGTCGCTGGATT
12	dLint-1-RNAi-rv	taatacgactcactatagggGCTCGGCACTGGAATCAT
13	dG9a-RNAi-fw	taatacgactcactatagggAAACCAAGTGTTACTTTGAGAG
14	dG9a-RNAi-rv	taatacgactcactatagggTGTACAAAATATGCCACATCCT

Supplementary Table S5. List of primers used in CRISPR/Cas9 tagging experiments.

No.	Name	Sequence
1	Crispr dCoREST	CCTATTTTCAATTTAACGTCGCAGAGTTCCTGGCCAACTGGTTTAAGAGCTATGCTG
2	Sense dCoREST	GCGAAGAAAATCGCGCTCAGCACCGGAGGCGGAAGCAGCGTCGCAGAGTTCCTGGCCAACGGATCTTCCGGATGGCTCGAG
3	Antisense dCoREST	ATGTTATGTATCGGTATATATCTATGCGTGCATATATATCGCGAGTGAACACGTCGCTCCGAAGTTCCTATTCTCTAGAAAGTATAGGAACTTCCATATG
4	dCoREST-GFP-seq_fw	TCTCTTCTCCTCCTCCACAG
5	dCoREST-GFP-seq_rv	CGTCCCCCAAAACATCAATC
6	Crispr dLSD1	CCTATTTTCAATTTAACGTCGAACAATGTATTTAGCGTGAGTTTAAGAGCTATGCTG
7	Sense dLSD1	TCGTCAAAGAAGTCGGAGGAGAATTCAAACTCAAACACTGCCGACTCTACGGAGCTACAGGGATCTTCCGGATGGCTCGAG
8	Antisense dLSD1	CAAAACTAAACGCTCTAGGAGTAACTGCTGGGGACCAAATGCATCACGCTAAATACATTGGAAGTTCCTATTCTCTAGAAAGTATAGGAACTTCCATATG
9	dLSD1-GFP-seq_fw	CCCAATCTATCTGACTCCTC
10	dLSD1-GFP-seq_rv	TTACAGCGGCCTAGCTTCGT
11	Crispr dL(3)mbt	CCTATTTTCAATTTAACGTCGCCCTTGCGCACGTCCTCTTGTTTAAGAGCTATGCTG
12	Sense dL(3)mbt	TCCGACGGCGATGTGGCGATGGTGCCGATGGAAGTGCGCACGCCCTTGCGCACGTCCTCTGGATCTTCCGGATGGCTCGAG
13	Antisense dL(3)mbt	GGTGCAACAAAATAATCTTATAAATCAATCAACGGAAGCGGATGCCTGGTATCCGGAGTCGAAGTTCCTATTCTCTAGAAAGTATAGGAACTTCCATATG
14	dL(3)mbt-GFP-seq_fw	ATGGGGATGGCGATTGTGAA
15	dL(3)mbt-GFP-seq_rv	ATAATACCCGAATGGGCCGA
16	Crispr dG9a	CCTATTTTCAATTTAACGTCGGAGAAAATTGGACACGCGTGTTTAAGAGCTATGCTG
17	Sense dG9a	GCACCGGAAAATGAAACGGGAACGCTGTCGTCTACAAATACGGAGAAAATTGGACACGCGGGATCTTCCGGATGGCTCGAG
18	Antisense dG9a	TTTTATTTGTTGGATGAGACTGTGAAATCTGCAATCATCTCAGGTTTAGGTGGTTTTAGCGAAGTTCCTATTCTCTAGAAAGTATAGGAACTTCCATATG
19	dG9a-GFP-seq_fw	CACCGGAAAATGAAACGGGA
20	dG9a-GFP-seq_rv	ACCGGGCTTCGATAACGATT

Supplementary Table S6. List of primers used for qPCR gene expression analysis.

No.	Name	Sequence
1	Rp49-RT-fw	TGTCCTTCCAGCTTCAAGATGACCATC
2	Rp49-RT-rv	CTTGGGCTTGCGCCATTTGTG
3	dCoREST-RT-fw	TCAAGGATGGCTCCGAGAAC
4	dCoREST-L-RT-rv	TGTGCCATGCCCTTTCTTGT
5	dCoREST-RT-fw	TCAAGGATGGCTCCGAGAAC
6	dCoREST-M-RT-rv	CCTATTCTTCTGTATCTTGT
7	dLSD1-RT-fw	ACGGCGAGTAGAGGAGAAAT
8	dLSD1-RT-rv	GATTATGATGTCATCCGTCA
9	dL(3)mbt-RT-fw	TTTCTGGCACCACATTTCTG
10	dL(3)mbt-RT-rv	CTCTCCTTCTGCGTACTCTGC
11	dLint-1-RT1-fw	GCAGGAGCAGCAAAGACG
12	dLint-1-RT1-rv	CTCAAAGAGGCCGAGGAAC
13	dLint-1-RT2-fw	CCGTGAAGCTGAAGGAGAAC
14	dLint-1-RT2-rv	GGAAGTGCTTGCGAATAAGC
15	dG9a-RT-fw	AACGATGACTTGGAGCGTGTA
16	dG9a-RT-rv	GGGAGTCAGCACGTTGAAGT

SUPPLEMENTARY FIGURES

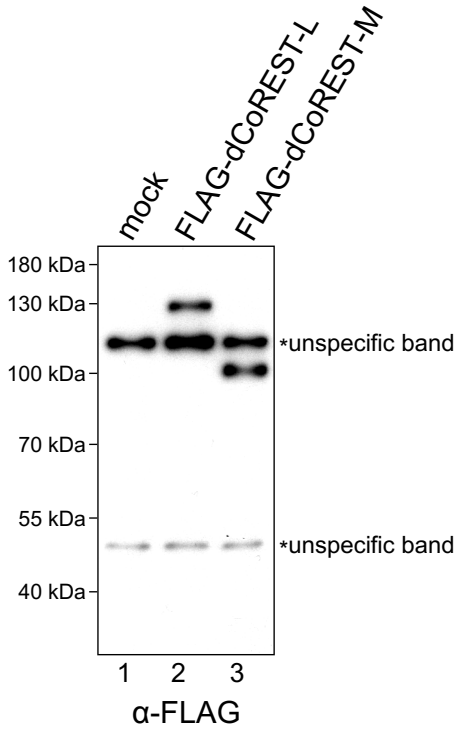

Supplementary Figure S1. Stable expression of FLAG-dCoREST-L and FLAG-dCoREST-M in S2 cells. Nuclear extracts from control cells (mock, lane 1) and cells stably expressing FLAG-dCoREST-L (lane 3) and FLAG-dCoREST-M (lane 4) were analysed by anti-FLAG Western blot.

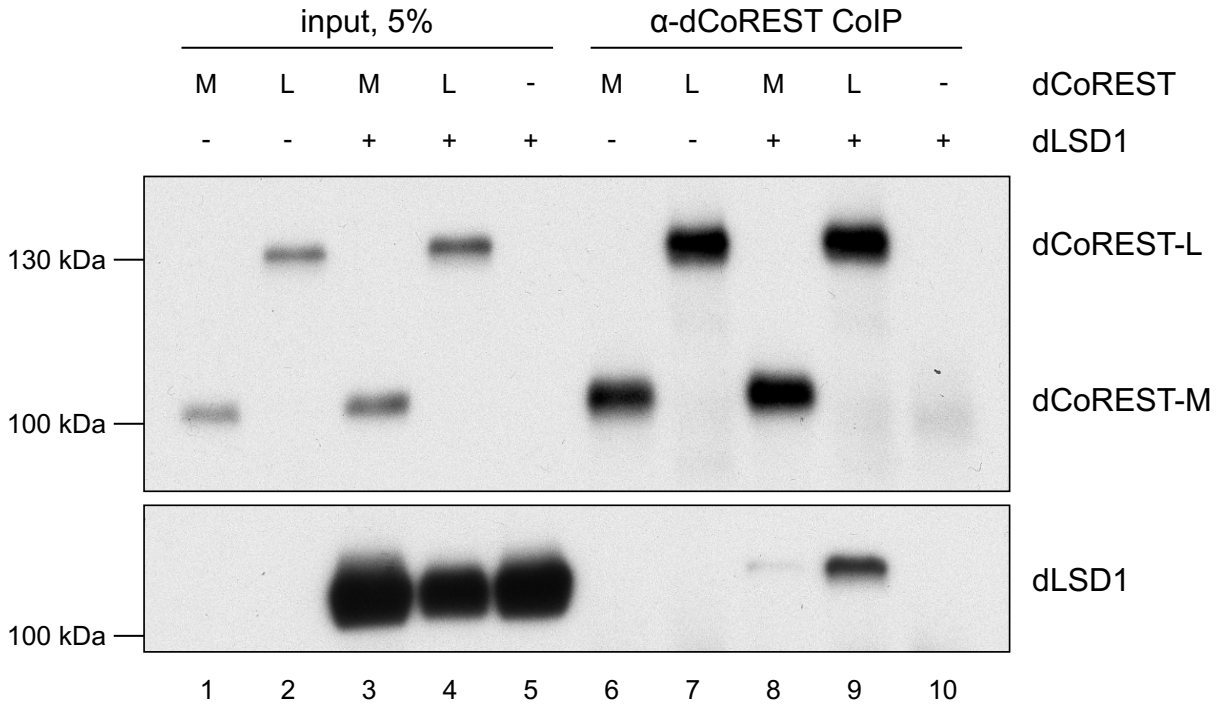

Supplementary Figure S2. dLSD1 preferentially interacts with dCoREST-L. Sf9 cells were co-infected with recombinant baculoviruses directing the expression of dLSD1, dCoREST-L and/or dCoREST-M, as indicated on top. Extracts were immunoprecipitated with anti-CoREST antibody and analysed by Western blot using the antibodies indicated on the right. Lanes 1-5: 5% input.

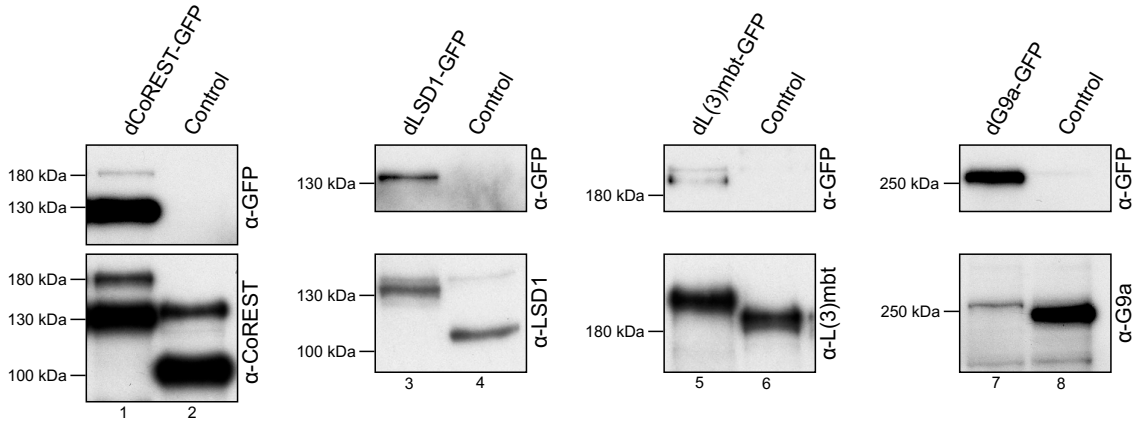

Supplementary Figure S3. Endogenously tagged cell lines were analysed by Western blot using anti-GFP antibody or antibody corresponding to the analysed protein. Note that in the dCoREST-GFP cell line both dCoREST isoforms are present.

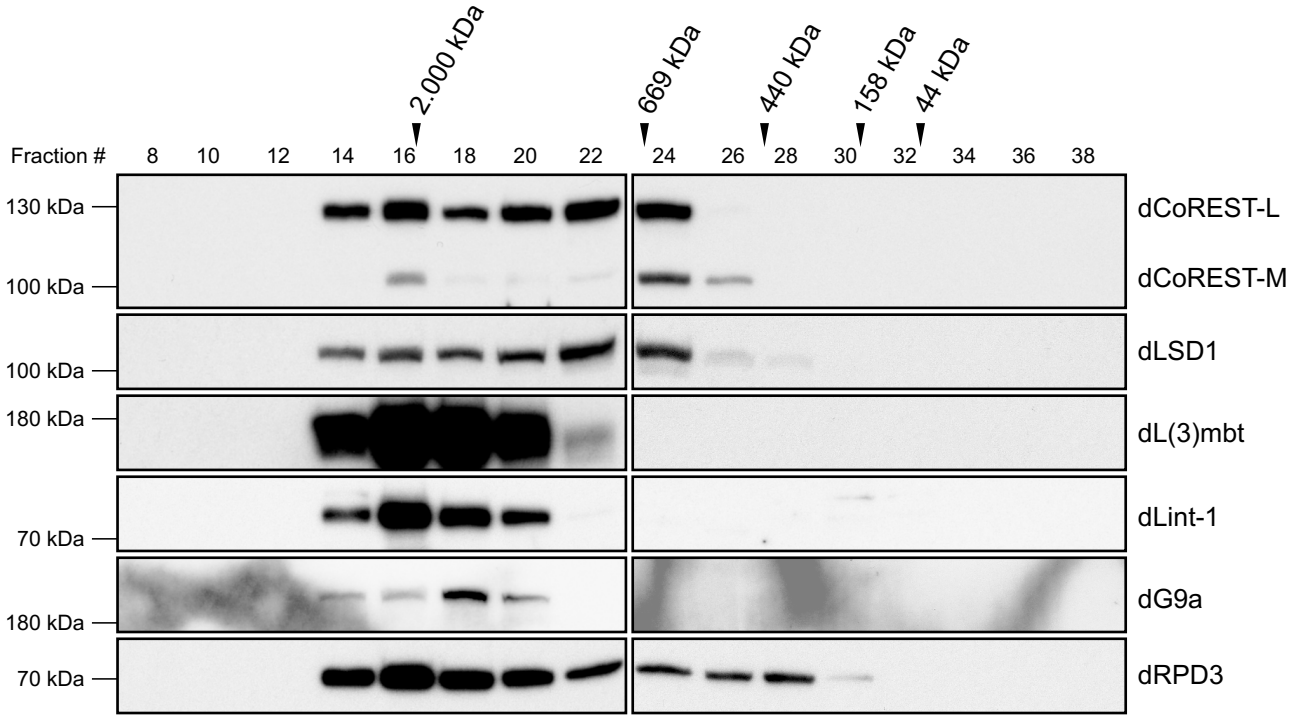

Supplementary Figure S4. Nuclear extract from *Drosophila* embryos (1 mg) was fractionated over a Superose 6 column. Fractions were analysed by Western blot using the antibodies indicated on the right. Fraction numbers and molecular mass standards are denoted on top.

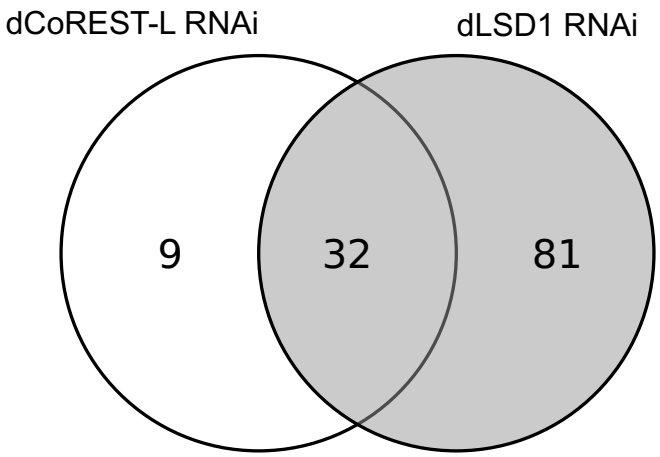

Supplementary Figure S5. Comparison of dCoREST-L and dLSD1 upregulated genes in S2 cells that are changed by a factor of 1.5 or more. Venn diagram comparing dCoREST-L and dLSD1 upregulated genes with fold change of 1.5 (log2FC≥0.58, adj. p≤0.05).

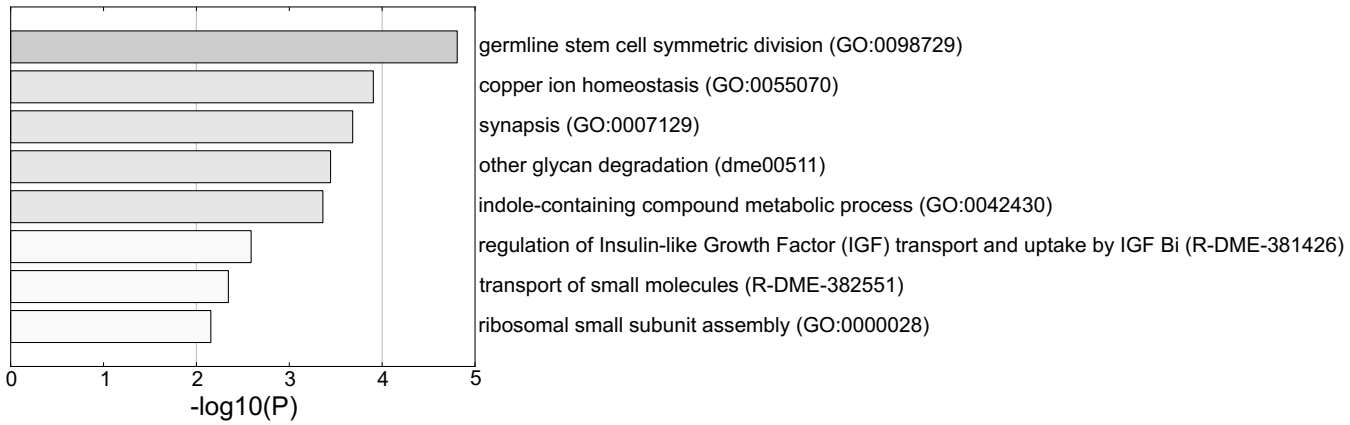

Supplementary Figure S6. Gene Ontology term enrichment analysis of LINT-repressed genes. GO analysis was performed using the Metascape tool.

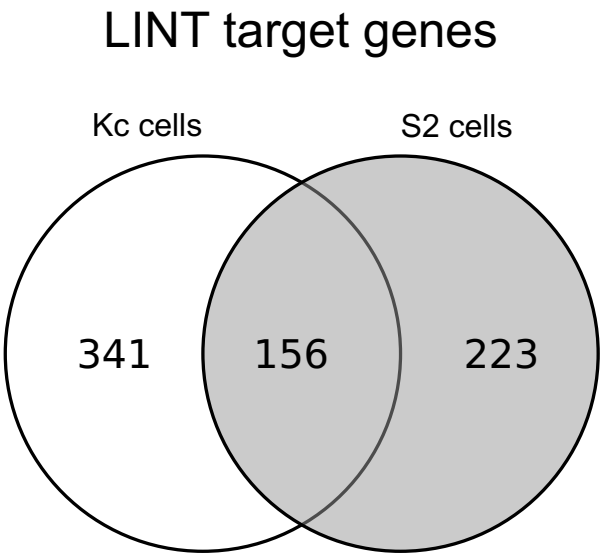

Supplementary Figure S7. Overlap of LINT target genes in Kc and S2 cells. Venn diagram of LINT target genes in Kc cells (microarray; (15)) and S2 cells (RNA-seq; this study) (fold change ≥2.0, adj. p≤0.05).

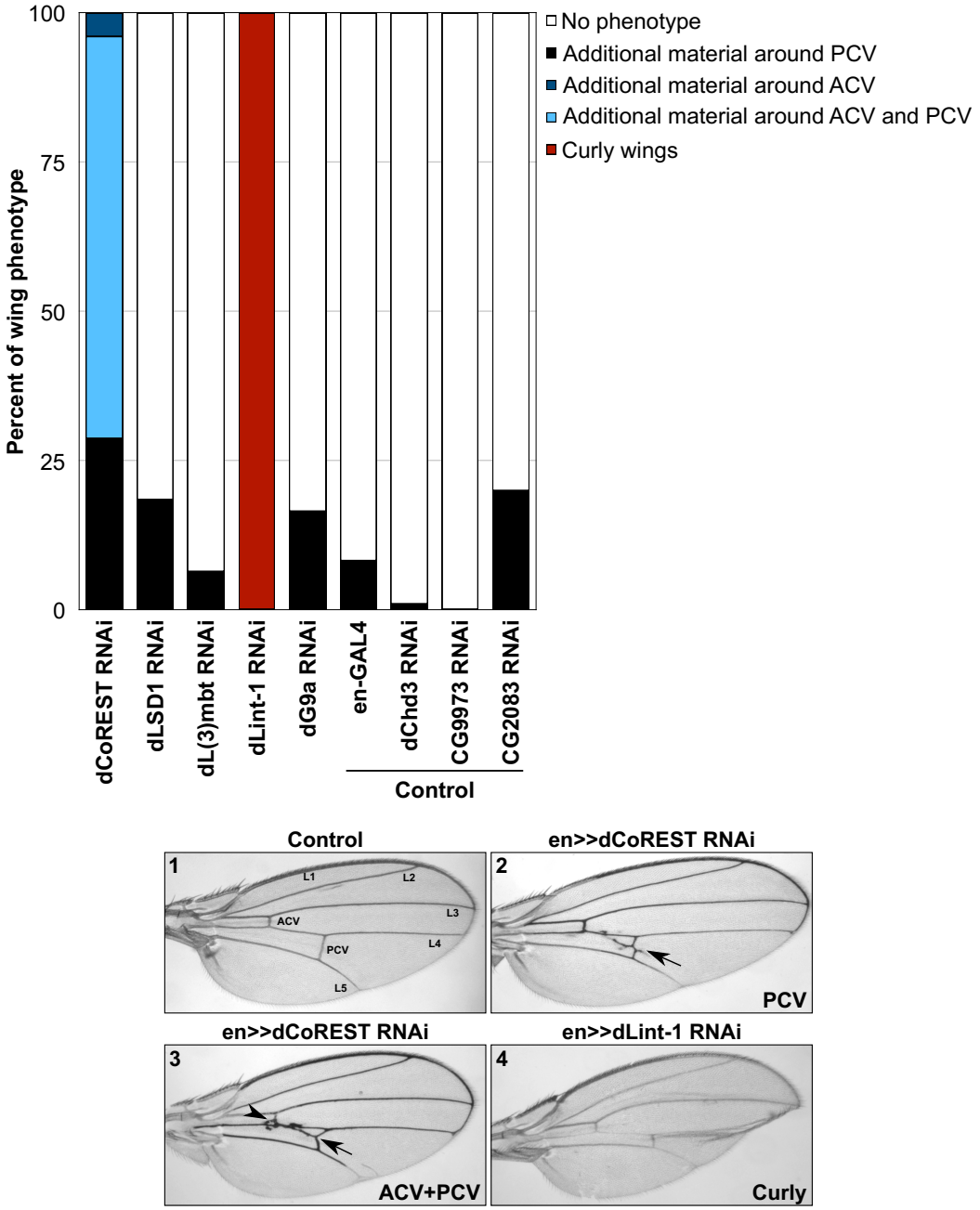

Supplementary Figure S8. Depletion of dCoREST disrupts wing vein differentiation. Upper panel: Graph showing the distribution (in %) of posterior crossvein (PCV, black), anterior crossvein (ACV, dark blue), combined ACV and PCV (light blue), and Curly (red) phenotypes upon depletion of dCoREST, dLSD1, dL(3)mbt, dLint-1, and dG9a in fly wing discs. Depletion of dChd3, CG9973, CG2083 as well as en-GAL4 driver flies served as controls. Lower panels: Examples of phenotypes: The positions of longitudinal veins (L1 to L5), ACV and PCV in wild type wings are shown in panel 1. PVC phenotypes are characterised by formation of additional PCV material around the PCV vein (panel 2; arrow). ACV and L4 phenotypes are characterised by formation of additional vein material around ACV and L4 (panel 3; arrow head). A combined ACV, L4 and PCV phenotype is shown in panel 3. The characteristic dLint-1 RNAi curly wing phenotype is shown in panel 4.

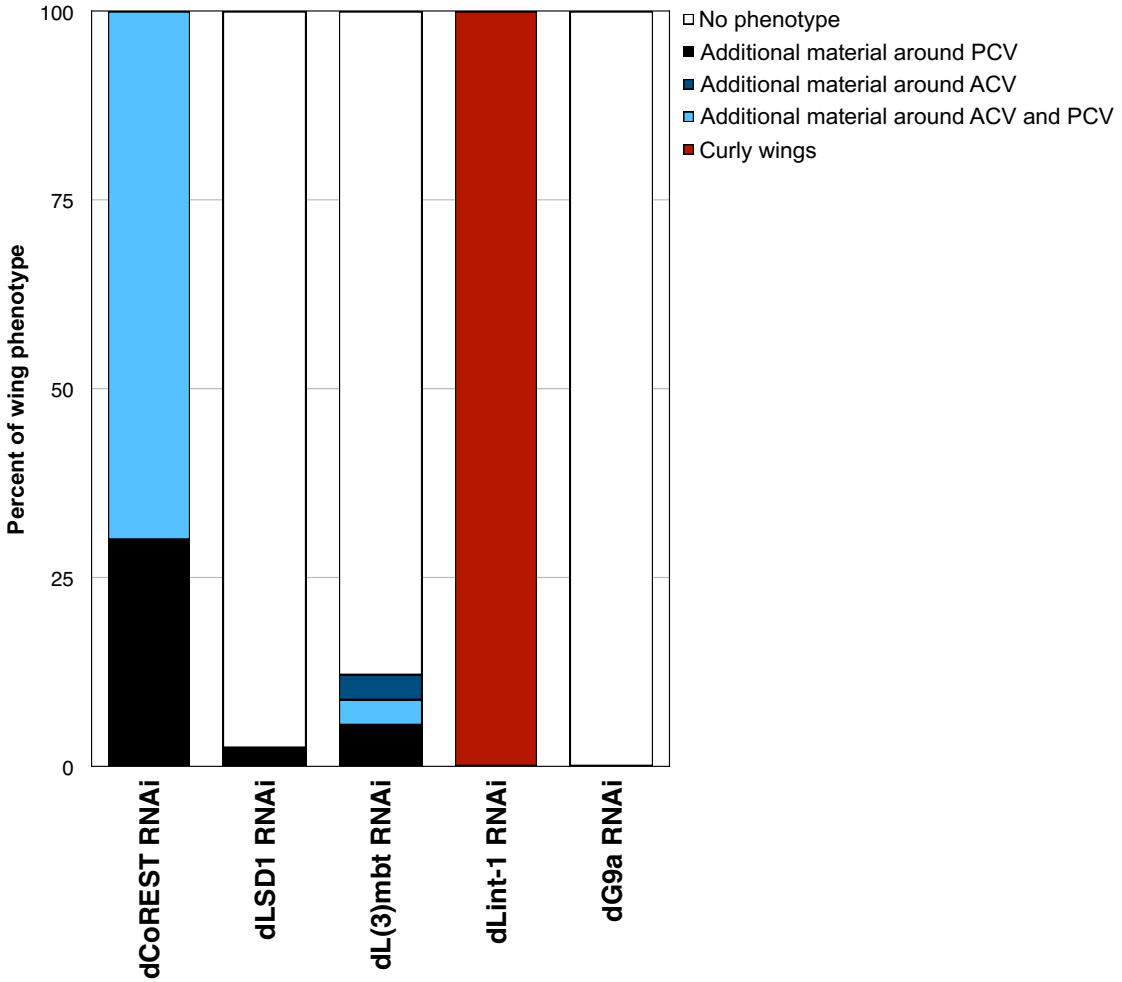

Supplementary Figure S9. Distribution of phenotypes in fly wings of flies raised at an elevated temperature of 30 °C. Graph showing the distribution (in %) of PCV (black), ACV (dark blue), combined ACV and PCV (light blue), and Curly (red) phenotypes upon depletion of dCoREST, dLSD1, dL(3)mbt, dLint-1, and dG9a in fly wing discs at 30 °C.

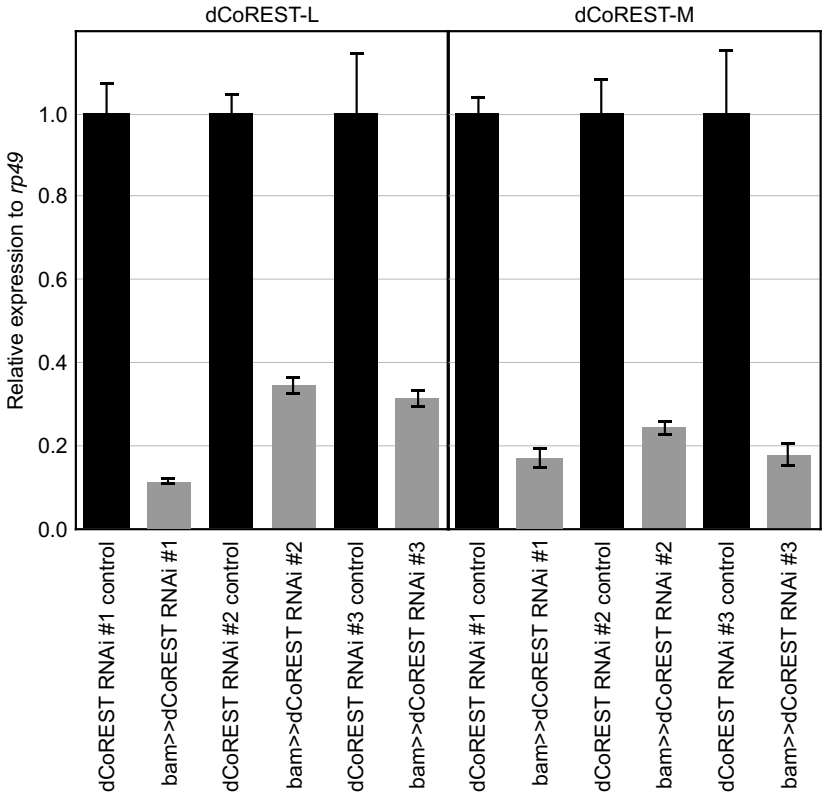

Supplementary Figure S10. Efficiency of RNAi knockdowns of dCoREST in fly testes. (A) qPCR analysis of dCoREST-L and dCoREST-M expression in three bam-GAL4 driven dCoREST RNAi fly lines. RNA levels in control testes were set to 1 and RNA levels in RNAi-depleted testes are depicted relative to the level in corresponding controls.

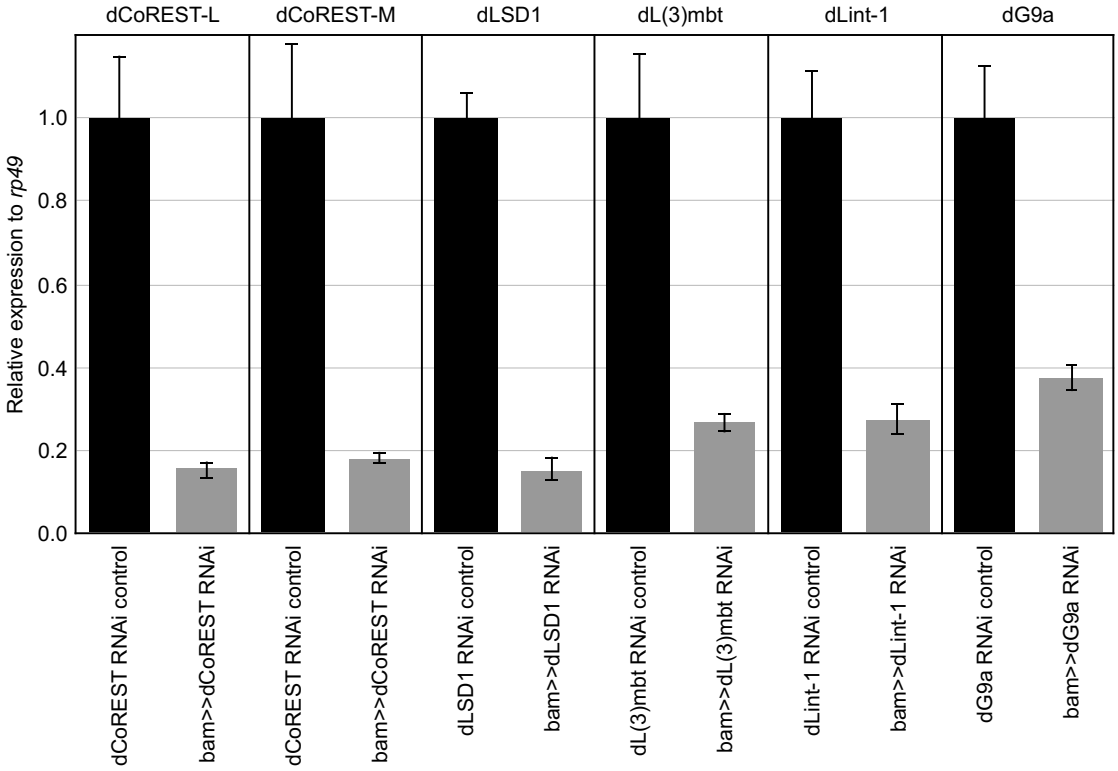

Supplementary Figure S11. qPCR analysis of dCoREST-L, dCoREST-M, dLSD1, dL(3)mbt, dLint-1 and dG9a expression in bam>>RNAi fly lines. RNA levels in control testes were set to 1 and RNA levels in RNAi-depleted testes are depicted relative to the level in corresponding controls.

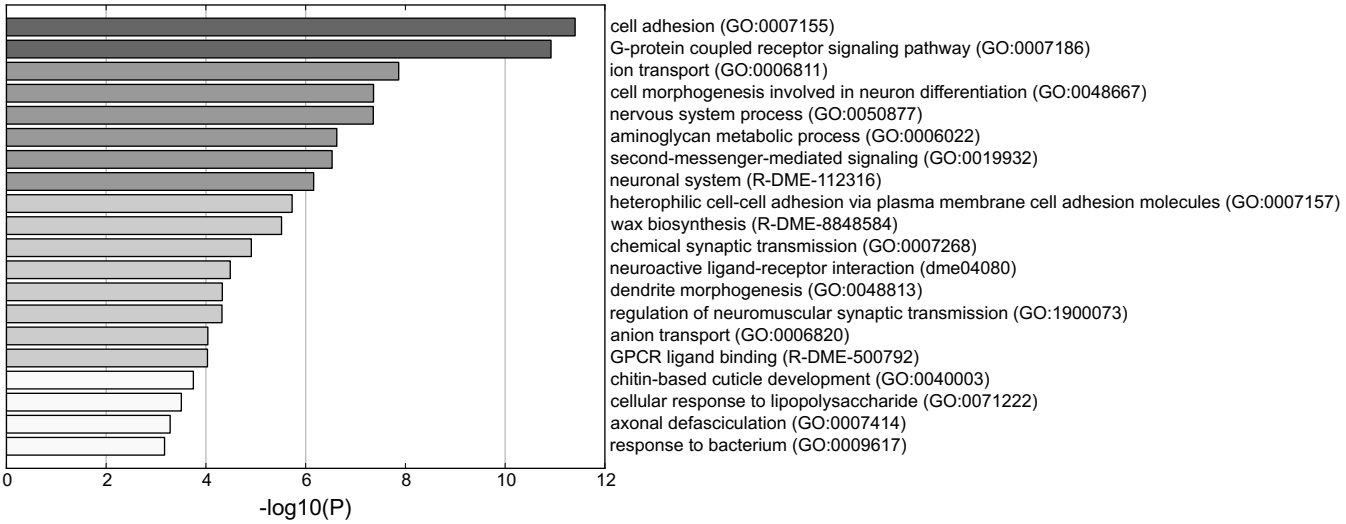

Supplementary Figure S12. Gene Ontology term enrichment analysis of dCoREST and dLSD1 co-repressed genes. GO analysis was performed using the Metascape tool.

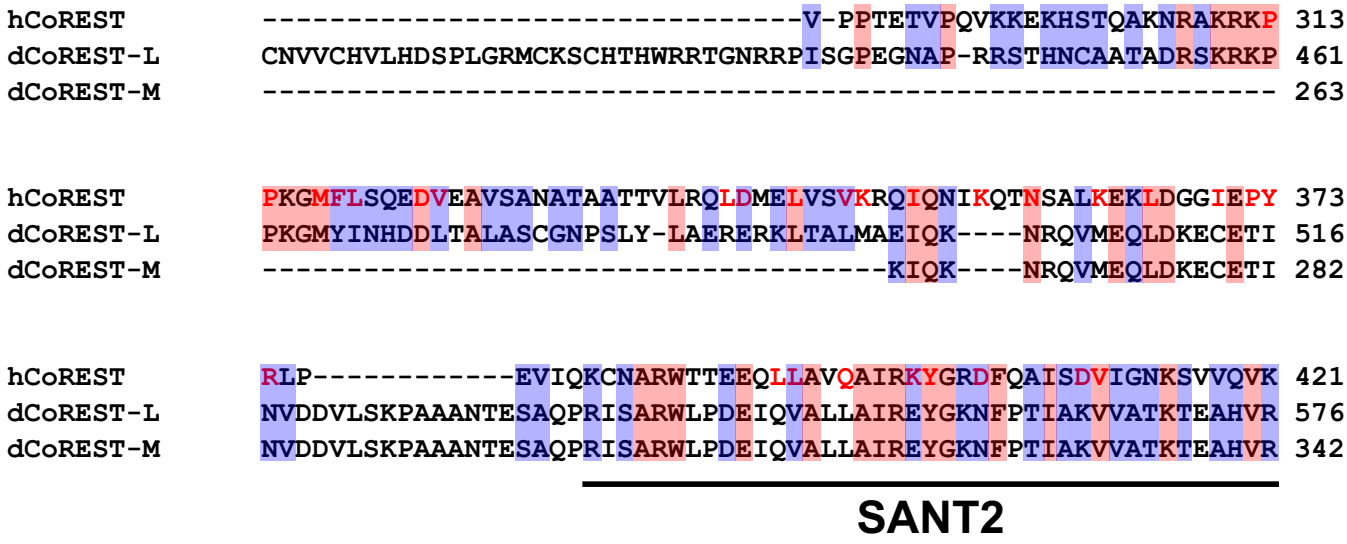

Supplementary Figure S13. Alignment of LSD1 binding interface of human CoREST with dCoREST-L and dCoREST-M. Multiple sequence alignment of hCoREST, dCoREST-L and dCoREST-M was generated with the ClustalW program. hCoREST amino acids that directly interact with LSD1 are in red (according to (39)). Identical residues are highlighted in yellow, similar residues are highlighted in blue.

Supplementary Table S1

Difference	-LOG(P-value)	Protein IDs	Majority protein IDs	Uniprot	GN	Peptides	Razor + unique peptides	Unique peptides	Sequence coverage [%]	Unique + razor sequence coverage [%]	Unique sequence coverage [%]	Mol. weight [kDa]	Q-value	Score	Intensity	MS/MS Count	iBAQ dCoREST_r1	iBAQ dCoREST_r2	iBAQ dCoREST_r3	iBAQ dCoREST_r4	iBAQ IgG_r1	iBAQ IgG_r2	iBAQ IgG_r3	iBAQ IgG_r4
12.21399021148	3.2267119338	tr|A0A126GUZ1|A0A126GUZ1_DROME;t	tr|A0A126	A0A126G	pre-mod(md	20	20	20	63.4	63.4	63.4	18.815	0	323.31	27791000	118	25.751363	26.705169	26.319602	25.805307	13.310139	18.915874	10.012382	13.487086
12.20592093467	3.1847790715	sp|Q8SY33|GAWKY_DROME	sp|Q8SY3	Q8SY33	gw	55	55	55	46.9	46.9	46.9	142.97	0	323.31	89138000	285	25.024705	26.306346	26.125852	25.384822	11.421276	18.606029	13.845097	10.145641
11.98284864425	3.2929279997	tr|B7Z0G7|B7Z0G7_DROME;sp|Q9VW97	tr|B7Z0G7	Q9VW97	Su(var)3-3	71	71	71	65.3	65.3	65.3	98.388	0	323.31	96178000	365	25.250282	25.846683	25.977514	25.338649	10.251482	18.186840	14.494543	11.548870
11.55669283866	6.2722545026	tr|A0A0B4LGA2|A0A0B4LGA2_DROME	tr|A0A0B4	A0A0B4L	CG44249	14	14	14	36.9	36.9	36.9	45.388	0	160.93	44516000	51	21.759794	22.578168	22.688228	22.140584	11.846201	11.194018	9.9967555	9.9030294
11.21490716934	5.5922180483	tr|D5SHR0|D5SHR0_DROME;tr|Q9W2F9	tr|D5SHR(	D5SHR0	twz	16	16	16	36.2	36.2	36.2	40.145	0	254.29	42340000	47	22.202606	22.676891	22.525209	22.503246	10.800995	13.123652	10.99945	10.124220
10.87461471557	5.7945420695	tr|Q9VBU6|Q9VBU6_DROME;tr|A0A140S	tr|Q9VBU(	Q9VBU6	Dmel\CG118	4	4	4	19.7	19.7	19.7	23.721	0	61.464	11451000	13	21.890039	22.192016	22.029617	21.696891	9.6334848	11.836007	12.166974	10.673640
10.72923541069	3.1288032705	tr|C7LAG1|C7LAG1_DROME	tr|C7LAG1	C7LAG1	CoRest	89	89	22	60.4	60.4	15.7	87.314	0	323.31	40424000	516	27.824869	28.334878	28.373973	27.954380	13.978442	22.087123	16.636651	16.868942
10.61815047264	6.0863651827	tr|A4UZ51|A4UZ51_DROME;tr|E1JGY2|E	tr|A4UZ51	P34021	EcR	1	1	1	2.6	2.6	2.6	91.181	0.0096618	6.6211	46048000	2	21.257761	22.847089	21.929040	20.806089	10.714219	11.842573	10.836870	10.973716
10.38192462921	4.0934669203	tr|Q9VB52|Q9VB52_DROME	tr|Q9VB52	Q9VB52	l(3)mbt	139	139	139	65	65	65	162.96	0	323.31	59015000	740	27.557277	27.957427	27.766103	27.317173	16.788640	20.470205	16.137990	15.673446
10.31998848915	4.2190796561	tr|Q32KD4|Q32KD4_DROME;tr|Q7KY08|(	tr|Q32KD4	Q32KD4	AGO1	20	20	20	24.2	24.2	24.2	109.83	0	207.87	60283000	60	21.281612	21.846937	22.056459	21.660404	10.875032	14.408329	10.413469	9.8686275
10.26388955116	3.7939431230	tr|Q9W4W7|Q9W4W7_DROME	tr|Q9W4W	Q9W4W7	EG:100G10.	52	52	52	69.7	69.7	69.7	49.227	0	323.31	18494000	252	27.445453	28.077398	27.980926	27.517433	18.213426	20.205383	17.196525	14.350317
9.911900758743	5.5298787186	tr|Q9VQK1|Q9VQK1_DROME	tr|Q9VQK(	Q9VQK1	Dmel\CG172	17	17	17	31.6	31.6	31.6	67.43	0	253.61	27950000	45	20.405927	21.667177	21.413228	20.783166	10.536744	11.846076	10.030529	12.208547
9.722523689270	2.9979551114	tr|Q9VZ22|Q9VZ22_DROME;tr|C6SV09|C	tr|Q9VZ22	Q9VZ22	Lint-1	71	71	71	83.9	83.9	83.9	67.899	0	323.31	29021000	507	27.648284	28.428422	28.395133	27.767240	15.053586	22.796319	17.481327	18.017753
9.718526601791	3.4289689908	sp|Q59E36|RCOR_DROME;tr|M9PJR2|M	sp|Q59E3(	Q59E36	CoRest	70	3	3	67.5	4.9	4.9	62.695	0	323.31	77715000	15	22.328550	23.186571	23.146486	22.431911	11.234335	17.027452	11.863021	12.094602
9.641425132751	4.1928858059	tr|Q9VZ30|Q9VZ30_DROME	tr|Q9VZ30	Q9VZ30	Dmel\CG111	104	104	104	36.8	36.8	36.8	384.99	0	323.31	32269000	337	22.070283	23.090938	22.755012	22.290386	12.860330	15.624995	11.522827	11.632767
9.637484550476	3.1270652238	sp|P26017|PC_DROME	sp|P26017	P26017	Pc	6	6	6	23.3	23.3	23.3	43.976	0	58.654	13103000	19	20.819328	21.632230	21.433389	21.010929	12.450833	15.027085	7.7278127	11.140208
9.532261133193	3.2330369510	tr|Q9VL20|Q9VL20_DROME	tr|Q9VL20	Q9VL20	Dmel\CG569	48	48	48	52.5	52.5	52.5	71.859	0	323.31	22029000	180	23.890039	24.190841	24.177520	23.830066	16.929605	16.882261	11.173052	12.974504
9.519985675811	4.8626637114	tr|Q0E8X8|Q0E8X8_DROME	tr|Q0E8X8	Q0E8X8	CG13551	2	2	2	32.7	32.7	32.7	11.948	0	15.391	13922000	9	20.606662	22.368423	22.738758	21.686584	11.665682	11.424750	12.256804	13.973248
9.379766225814	2.6579273686	tr|X2J8Z1|X2J8Z1_DROME;tr|X2J6P6|X2	tr|X2J847|	Q9VJ79	Pde11	24	24	24	25.4	25.4	25.4	155.62	0	323.31	15838000	86	22.240482	23.201333	22.686285	22.325313	14.128639	17.736083	9.0843544	11.985272
8.949820756912	6.0798694871	tr|Q9V9U6|Q9V9U6_DROME	tr|Q9V9U(	Q9V9U6	Dmel\CG189	3	3	3	23.6	23.6	23.6	28.291	0	56.841	50284000	11	19.544195	20.409141	20.440301	19.919210	11.480751	11.239542	10.044414	11.748857
8.947867631912	4.5256816318	tr|Q9VWH9|Q9VWH9_DROME	tr|Q9VWH	Q9VWH9	Dmel\CG122	8	8	8	27.9	27.9	27.9	39.066	0	64.316	10417000	23	20.216911	21.250839	21.114515	20.458538	11.090837	13.876420	10.371126	11.910948
8.918803215026	5.2590538204	tr|Q9VF92|Q9VF92_DROME;tr|A0A0B4K(	tr|Q9VF92	Q9VF92	ear	25	25	25	31.9	31.9	31.9	100.23	0	323.31	13213000	99	22.717329	23.990404	23.533977	22.973022	14.315219	15.640922	14.488969	13.094408
8.918714046478	5.3463425698	tr|Q9VIY9|Q9VIY9_DROME	tr|Q9VIY9|	Q9VIY9	Dmel\CG175	1	1	1	2.9	2.9	2.9	58.739	0.0050251	7.0656	17286000	5	20.989538	20.434204	20.503488	20.180589	12.560657	10.433605	12.525945	10.912755
8.763730287551	3.5495507645	tr|Q9VEB1|Q9VEB1_DROME	tr|Q9VEB1	Q9VEB1	Mdh2	6	6	6	19.3	19.3	19.3	35.318	0	45.567	10291000	23	19.574354	20.878747	20.622030	20.028100	11.515085	10.720220	14.574357	9.2386493
8.682967662811	4.3280376348	tr|M9NHB6|M9NHB6_DROME	tr|M9NHB(	M9NHB6	CoRest	27	2	2	44.6	4.5	4.5	34.351	0	160.14	68415000	5	20.769834	20.590488	18.160049	19.781791	10.578525	12.704862	9.9731979	11.313707
8.620313405990	4.8383891924	tr|Q9W0N9|Q9W0N9_DROME	tr|Q9W0N(	Q9W0N9	ebd1	9	9	9	17.7	17.7	17.7	65.419	0	77.701	16173000	24	20.040460	20.867782	20.593500	20.415552	13.769424	11.645748	11.107069	10.913795
8.615149021148	4.0497008262	tr|Q0E9E2|Q0E9E2_DROME;tr|Q7KN97|(	tr|Q0E9E2	Q0E9E2	PCB	109	109	109	70.8	70.8	70.8	132.67	0	323.31	11407000(	489	24.734588	25.725412	25.727310	25.090833	16.335739	19.216958	16.301729	14.963121
8.507410526275	4.7991310658	tr|X2J847|X2J847_DROME;sp|Q24523|BU	tr|X2J847|	Q24523	bun	6	6	6	6.8	6.8	6.8	118.47	0	66.698	10436000	13	19.315353	20.799465	20.186645	19.724740	10.878059	11.793764	10.284557	13.040182
8.325563192367	5.8770947753	sp|Q9VNI3|HPF1_DROME	sp|Q9VNI3	Q9VNI3	CG1218	6	6	6	9.6	9.6	9.6	51.099	0	45.823	80090000	17	19.165113	19.923480	19.944494	19.508409	10.987171	11.299923	10.553606	12.398543
8.143461704254	3.7906395902	sp|Q9VCH5|NUP98_DROME	sp|Q9VCH5	Q9VCH5	Nup98-96	21	21	21	12.4	12.4	12.4	210.14	0	269.39	41185000(	52	19.488718	20.943778	20.748455	19.855699	13.624795	9.7993459	13.524786	11.513875
8.128606796264	3.8826135893	sp|Q94517|HDAC1_DROME	sp|Q9451(	Q94517	Rpd3	57	57	57	77.7	77.7	77.7	58.33	0	323.31	39460000	392	28.174457	28.951158	29.165618	28.412319	19.709356	23.203979	20.153013	19.122777
8.117201089859	6.8338484422	tr|Q8IQ82|Q8IQ82_DROME;tr|Q8IQ80|Q8	tr|Q8IQ82|	Q8IQ82	pst	6	6	6	12	12	12	74.627	0	50.415	68579000	13	19.131998	19.378376	18.987041	18.723506	11.324743	11.293599	10.210184	10.923591
8.104497432708	1.6139441609	tr|Q9W0U4|Q9W0U4_DROME	tr|Q9W0U(	Q9W0U4	Dmel\CG138	1	1	1	2.5	2.5	2.5	55.577	0.005102	7.2621	34403000	3	11.858774	22.549266	22.297513	21.235378	10.300285	13.967292	10.053962	11.201402
8.019451379776	3.7144134478	tr|D0Z760|D0Z760_DROME;sp|P35820|P	tr|D0Z760|	P35820	Psc	27	27	27	22.5	22.5	22.5	169.83	0	269.49	43066000	68	19.985513	20.830589	20.605033	20.016313	14.058075	10.713844	10.606960	13.980764
8.001048803329	1.5949175500	tr|A0A0B4LFB3|A0A0B4LFB3_DROME;sp	tr|A0A0B4	Q7JVI3	eIF3m	2	2	2	9.8	9.8	9.8	44.086	0	12.18	21786000	2	13.889297	24.971715	24.790046	24.157846	14.023060	13.170093	14.344989	14.266567
7.98510169982	6.7635394688	tr|A0A0B4K6B8|A0A0B4K6B8_DROME;tr	tr|A0A0B4	Q86B87	mod(mdg4)	11	11	11	25.9	25.9	25.9	52.406	0	212.13	42556000	55	25.547925	26.660034	25.998476	25.352993	17.802213	18.042867	17.967756	17.806184
7.958374500274	3.3300490824	sp|Q9VB08|RING1_DROME	sp|Q9VB0	Q9VB08	Sce	12	12	12	38.4	38.4	38.4	47.255	0	274.61	40333000	48	21.660055	22.885019	22.484388	21.971584	14.739148	17.292123	12.744402	12.391874
7.894909381866	5.0864467843	tr|Q9W482|Q9W482_DROME	tr|Q9W482	Q9W482	lin-52	3	3	3	19.7	19.7	19.7	17.796	0	25.76	30153000	8	18.589189	19.637891	19.893280	19.087862	11.846750	10.133051	12.381690	11.267093
7.885422229766	6.1441110913	tr|Q9W0T7|Q9W0T7_DROME;tr|Q8IRJ7|(	tr|Q9W0T7	Q9W0T7	Dis3l2	21	21	21	27	27	27	116.84	0	285.61	60521000	63	21.028234	21.534357	21.642490	21.255918	12.827124	14.345197	13.713601	13.033388
7.879450082778	3.3465383619	tr|A0A0B4KGD8|A0A0B4KGD8_DROME;	tr|A0A0B4	Q01617	cpo	3	3	3	5.8	5.8	5.8	63.296	0	21.535	23793000	5	18.326719	19.458858	19.458358	19.168226	11.329178	14.316210	9.5852622	9.6637105
7.850336074829	4.5004402038	tr|Q9W543|Q9W543_DROME	tr|Q9W543	Q9W543	Rbcn-3B	15	15	15	13.4	13.4	13.4	168.47	0	182.3	24529000	39	19.199739	19.904600	19.959571	19.678380	11.336571	13.617696	10.363856	12.022823
7.819866657257	2.7314169031	tr|Q9VNP3|Q9VNP3_DROME;tr|Q8IG95|(	tr|Q9VNP3	Q9VNP3	Mes2	53	53	53	76.9	76.9	76.9	47.958	0	323.31	15838000	323	27.461702	28.432371	28.158750	27.471115	19.210172	24.379808	18.607835	18.046655
7.793529510498	3.8401570512	tr|Q9VXQ3|Q9VXQ3_DROME	tr|Q9VXQ3	Q9VXQ3	Mvd	5	5	5	19.3	19.3	19.3	42.832	0	43.785	47000000	14	18.478879	19.606861	19.697187	19.187974	10.849402	13.263781	9.2996587	12.383942
7.718215465545	9.0023503030	tr|Q9W0P0|Q9W0P0_DROME	tr|Q9W0P(	Q9W0P0	Dmel\CG338	3	3	3	11.1	11.1	11.1	33.748	0	26.159	30137000	8	19.042467	18.717929	18.838705	19.118551	11.022720	11.403094	11.181056	11.237919
7.717666625976	5.3540380202	sp|O76878|RIPL_DROME;tr|M9PG81|M9(	sp|O7687(	O76878	CG11448	3	3	3	13.3	13.3	13.3	50.147	0	26.497	41636000	7	18.379497	20.289964	19.383214	18.838951	11.569116	11.738663	11.996317	10.716863
7.702103614807	5.9053844186	tr|A8DZ10|A8DZ10_DROME	tr|A8DZ10	A8DZ10	Dmel\CG343	4	4	4	21	21	21	32.811	0	84.048	75449000	9	20.043802	20.807506	21.007717	20.245975	12.936454	13.131422	13.352319	11.876389
7.607298612594	5.0763748675	tr|A0A0B4KFZ8|A0A0B4KFZ8_DROME;tr	tr|A0A0B4	A0A0B4KI	nvy	13	13	13	24.4	24.4	24.4	76.366	0	323.31	22470000	33	20.215255	21.465082	21.014202	20.492382	12.864805	14.189901	13.657429	12.045589
7.560611248016	4.6253884652	sp|Q9VVE2|ROGDI_DROME	sp|Q9VVE(	Q9VVE2	rogdi	2	2	2	6.7	6.7	6.7	30.495	0.0055046	11.038	51057000	2	18.614105	19.558465	19.709558	19.324436	12.036609	10.122035	13.008787	11.796688
7.547646045684	2.9877677161	tr|Q9VMC7|Q9VMC7_DROME;tr|A8DYW	tr|Q9VMC	Q9VMC7	Dmel\CG316	14	14	14	26.7	26.7	26.7	79.784	0	323.31	27456000	44	20.051529	21.124773	20.997140	20.486402	12.623498	16.677417	12.329643	10.838695
7.520314455032	4.9254892167	tr|O46048|O46048_DROME;tr|Q7KW02|(	tr|O46048|	O46048	east	121	121	121	43.8	43.8	43.8	250.16	0	323.31	67896000	419	23.686990	24.573749	24.239797	23.514003	15.799686	18.015415	15.954218	16.163963
7.452577114105	3.9611045562	sp|Q7K1U0|ARC1_DROME	sp|Q7K1U(	Q7K1U0	Arc1	15	15	15	49.2	49.2	49.2	28.877	0	323.31	48195000	44	21.748987	22.912508	22.960172	22.414649	15.750079	16.646389	14.855987	12.973553
7.403163433074	6.1045116506	tr|Q9W425|Q9W425_DROME	tr|Q9W425	Q9W425	Rbcn-3A	47	47	47	16.7	16.7	16.7	377.32	0	323.31	75656000	117	19.857643	20.556465	20.588476	20.136835	13.162391	12.064270	13.501712	12.798390
7.396907806396	3.0905287919	tr|Q7KMP8|Q7KMP8_DROME	tr|Q7KMP(	Q7KMP8	Rpn9	4	4	4	21.2	21.2	21.2	43.766	0	68.137	80669000	12	18.921230	19.909515	19.903598	20.545194	9.8730459	15.331511	12.838756	11.648593
7.365468025207	4.8703895850	tr|M9PBZ3|M9PBZ3_DROME;tr|M9PBJ8|(	tr|M9PBZ3	M9PBZ3	spen	87	87	1	24.4	24.4	0.4	588.49	0	323.31	22643000	266	20.857036	22.012430	21.467571	21.077833	14.354043	15.218449	13.532842	12.847663
7.321277379989	5.8481169492	tr|A0A0B4KHE1|A0A0B4KHE1_DROME;t	tr|A0A0B4	A0A0B4KI	Dmel\CG155	11	11	11	25.8	25.8	25.8	34.676	0	142	29882000	35	21.251647	22.300392	22.133108	21.682432	14.344504	14.956331	15.053289	13.728345
7.320354461669	4.5513607459	tr|M9MRG5|M9MRG5_DROME;tr|Q9VLD5	tr|M9MRG	M9MRG5	tai	11	11	11	8.8	8.8	8.8	201.63	0	154.72	92409000	22	18.261690	19.372882	18.783727	18.860025	12.252695	11.841032	12.194979	9.7082004
7.282853603363	5.9459931107	tr|O44434|O44434_DROME	tr|O44434|	O44434	qkr58E-3	4	4	2	15.1	15.1	12	36.683	0	24.669	24262000	6	17.857688	18.587726	18.556707	18.335556	11.252656	11.895578	10.605766	10.452262

7.275157690048	3.4879123878	trIQ9W2E7IQ9W2E7_DROME	trIQ9W2E	Q9W2E7	Rae1	4	4	4	13.3	13.3	13.3	38.617	0	135.86	59644000	10	19.490875	20.075092	19.714715	19.569707	12.795411	12.953814	14.322562	9.6779727
7.220892190933	5.2928345274	trIQ8IPT9IQ8IPT9_DROME;trIQ8IPU0IQ8	trIQ8IPT9I	Q8IPT9	Dmel\CG105	6	6	6	24.1	24.1	24.1	37.955	0	37.239	35014000	12	17.831642	18.862964	19.320407	19.132875	11.608119	11.349329	10.841765	12.465106
7.191298007965	3.4469917308	trIA0A0B4LFS3IA0A0B4LFS3_DROME;sp	trIA0A0B4	Q8SX68	CG10915	9	9	9	22.2	22.2	22.2	65.421	0	90.566	15649000	23	19.241512	21.119653	20.600776	19.725988	10.497006	14.706226	13.758223	12.961282
7.156126022338	6.0635315088	trIQ9VNP4IQ9VNP4_DROME	trIQ9VNP4	Q9VNP4	Dmel\CG127	30	30	30	47.8	47.8	47.8	47.708	0	323.31	15893000	118	24.457950	25.113307	25.193399	24.496374	17.791315	18.419013	17.23902	17.187177
7.135100841522	4.2742005879	splQ9VI58ITUTT_DROME;trIA0A0B4KGN	splQ9VI58	Q9VI58	Tailor	11	11	11	32.1	32.1	32.1	63.944	0	323.31	69230000	50	22.160110	23.012840	22.538389	22.327234	16.425592	16.344781	13.518038	15.209757
7.10884904861 4	5.2876954123	trIQ7JW66IQ7JW66_DROME	trIQ7JW66	Q7JW66	CG12129	2	2	2	9.1	9.1	9.1	40.319	0	26.774	23017000	4	16.970397	18.779951	18.134807	17.809265	11.064731	11.476254	10.449888	10.268151
7.091084241867	4.7484713093	trIM9PD95IM9PD95_DROME;splQ03017I	trIM9PD95	Q03017	cact	6	6	6	10.8	10.8	10.8	53.818	0	37.944	40787000	9	18.189109	19.256380	19.351020	18.731683	11.143373	13.318966	11.388945	11.312571
7.030675411224	3.7830554210	splP39769IPHP_DROME;trIQ5U0W8IQ5U	splP39769	P39769	ph-p	16	16	9	17.5	17.5	9.1	167.28	0	323.31	45559000	50	21.305633	21.801044	21.587560	21.566394	15.302389	16.503995	12.810069	13.521477
7.030261993408	6.5539681019	trIQ7K0X9IQ7K0X9_DROME	trIQ7K0X9	Q7K0X9	Syx7	3	3	3	12.8	12.8	12.8	31.841	0	18.79	19616000	4	18.456594	19.082803	19.073106	18.272985	11.771993	11.924901	11.936271	11.131275
6.861247301101	4.7930333065	trIQ9VPL5IQ9VPL5_DROME	trIQ9VPL5	Q9VPL5	Tbc1d15-17	20	20	20	34.5	34.5	34.5	81.804	0	226.05	36383000	52	20.990161	21.588247	21.477733	21.215785	13.148142	15.693160	14.208844	14.776792
6.860788822174	6.0013749548	trIQ9VK42IQ9VK42_DROME;trIM9PCU7I	trIQ9VK42	Q9VK42	Dmel\CG993	84	84	84	47.5	47.5	47.5	237.05	0	323.31	46057000	291	23.113386	24.012481	23.753583	23.008640	16.669134	17.245162	16.414701	16.115938
6.832124233245	4.9852834303	trIA0A0B4KGB8IA0A0B4KGB8_DROME;t	trIA0A0B4	A0A0B4K(	px	13	13	13	11.8	11.8	11.8	205.95	0	119.69	15239000	38	18.527378	19.961975	19.212524	18.620491	13.173692	12.535160	11.865501	11.419517
6.828459978103	4.5532810879	trIA0A023GPV6IA0A023GPV6_DROME;t	trIA0A023	A0A023GI	Dmel\CG363	3	3	3	2.9	2.9	2.9	124.36	0	20.376	50938000	10	17.599142	18.010942	17.546758	17.353025	11.286745	9.6714658	10.024037	12.213780
6.741905689239	6.6372118854	trIA0A0B4KH12IA0A0B4KH12_DROME;tr	trIA0A0B4	A0A0B4KI	bon	20	20	20	18.2	18.2	18.2	120.37	0	323.31	13929000	84	22.393018	23.312990	22.997898	22.442808	15.960613	16.446792	15.969296	15.802390
6.672775030136	4.1576930976	trIQ9VWC7IQ9VWC7_DROME	trIQ9VWC	Q9VWC7	lincRNA.10	4	4	4	6.2	6.2	6.2	97.172	0	52.873	51442000	12	18.012144	17.892436	18.318445	18.197582	12.960798	11.813952	9.6760501	11.278707
6.668281555175	3.6697235675	trIQ9VYJ7IQ9VYJ7_DROME;trIM9PH0I	trIQ9VYJ7	Q9VYJ7	Dmel\CG400	10	10	10	27.3	27.3	27.3	37.783	0	159.1	15626000	21	21.221698	22.117593	21.578237	21.379781	15.578432	16.218467	15.307911	12.519373
6.582294225692	5.6711951742	trIM9PH72IM9PH72_DROME;trIM9PEH1I	trIM9PH72	M9PH72	Dmel\CG423	5	5	5	5.7	5.7	5.7	100.23	0	96.351	86014000	14	17.979358	19.478248	18.668199	18.655677	11.703211	11.885238	12.186887	12.676969
6.287880182266	4.7621855650	trIA0A0B4KGQ7IA0A0B4KGQ7_DROME;	trIA0A0B4	A0A0B4K(	Dmel\CG331	2	2	2	6.8	6.8	6.8	38.748	0.0054645	10.933	15463000	2	17.069492	18.314910	17.743598	17.425052	11.792474	12.041319	10.089501	11.478238
6.259621858596	4.1345481026	trIQ9W0R7IQ9W0R7_DROME;trIM9NFF9	trIQ9W0R	Q9W0R7	Atac3	16	16	16	27.4	27.4	27.4	63.194	0	323.31	50305000	62	21.395296	22.426521	21.792531	21.278724	16.637361	13.796648	15.825232	15.595344
6.244045495986	6.3250172180	trIQ9Y128IQ9Y128_DROME;trIM9PEI8IM	trIQ9Y128	Q9Y128	cert	3	3	3	7.5	7.5	7.5	68.51	0	18.663	23673000	4	17.134204	17.604944	17.757598	17.219017	10.980904	11.841768	11.130043	10.786867
6.195767402648	5.2622100780	trIQ95RU8IQ95RU8_DROME;trIM9PGH7	trIQ95RU8	Q95RU8	G9a	99	99	99	58.9	58.9	58.9	181.24	0	323.31	11201000	458	24.621147	25.592092	25.104656	24.407497	18.385744	19.431451	19.080072	18.045055
6.115013122558	4.7821512856	trIA0A0B4K6G6IA0A0B4K6G6_DROME;t	trIA0A0B4	A0A0B4K(	Dmel\CG751	9	9	9	5.8	5.8	5.8	268.01	0	67.44	89648000	16	17.111562	18.243629	17.576734	17.104721	12.156335	11.195802	10.319559	11.904897
6.080166101455	4.5163606974	splQ9VRP5IUBP36_DROME	splQ9VRF	Q9VRP5	scny	1	1	1	1.7	1.7	1.7	114.09	0.01059	5.9169	63781000	1	18.179811	19.016992	18.397407	17.251647	12.702989	11.289966	12.924951	11.607287
6.078249931335	4.9732879834	trIE1JH51IE1JH51_DROME;splP25172IS	trIE1JH51	P25172	Su(z)2	37	37	37	31.5	31.5	31.5	146.39	0	323.31	98339000	126	21.453372	22.471694	22.023031	21.476696	16.899946	15.238068	15.612350	15.361430
6.075634717941	4.1410115509	trIA0A0B4KEI3IA0A0B4KEI3_DROME;trIA	trIA0A0B4	A0A0B4K(	CG1513	1	1	1	2.1	2.1	2.1	53.566	0.011024	6.4445	25739000	3	17.296791	18.785261	18.231962	17.522979	10.855799	12.049835	13.301067	11.327753
6.064789772033	4.8616448431	trIQ9VBA0IQ9VBA0_DROME;trIQ8IMQ8I	trIQ9VBA(	Q9VBA0	Dmel\CG633	6	6	6	20.9	20.9	20.9	41.331	0	46.78	70682000	18	18.570819	19.882066	20.080827	19.699850	12.576059	14.149906	13.620563	13.627876
6.010402202606	5.5286498801	trIQ7KV27IQ7KV27_DROME;trIQ9VYD9I	trIQ7KV27	Q7KV27	Dmel\CG164	3	3	3	7	7	7	63.128	0	17.083	30107000	4	16.805618	17.828298	18.473421	17.987874	11.868575	11.893071	11.761007	11.530950
6.002869844436	3.8740194178	trIA0A126GUQ3IA0A126GUQ3_DROME;	trIA0A126	Q9VNA8	hd	4	4	4	10	10	10	63.437	0	29.749	28443000	10	16.994684	18.181753	18.194555	17.948036	11.040244	12.468581	13.278153	10.520570
5.988596200942	4.3314124462	trIQ7K3B7IQ7K3B7_DROME	trIQ7K3B7	Q7K3B7	CG11208	4	4	4	11.1	11.1	11.1	62.264	0	25.187	42907000	6	17.638916	18.700054	19.151924	18.227033	11.493097	13.675626	12.660451	11.934367
5.949917078018	2.1758266064	trIQ9W569IQ9W569_DROME	trIQ9W56(	Q9W569	EG:171E4.4	2	2	2	15	15	15	14.703	0	29.901	21261000	5	19.755088	21.106996	20.870645	20.735786	17.321575	16.827863	13.107834	11.417575
5.873906135559	5.9861277502	trIQ9W1K4IQ9W1K4_DROME	trIQ9W1K4	Q9W1K4	egl	13	13	13	13.7	13.7	13.7	112.13	0	134.37	19160000	36	19.782047	20.061971	20.090810	19.899946	13.95846	13.625823	13.838613	14.916253
5.802194118499	3.9766434193	trIQ9VDQ3IQ9VDQ3_DROME	trIQ9VDQ3	Q9VDQ3	Dmel\CG493	8	8	8	18.4	18.4	18.4	58.753	0	84.606	12008000	23	19.741312	20.753931	20.697443	20.254766	12.981352	14.812327	14.553449	15.891546
5.800572633743	5.8577660039	splQ9VLN1IWDR82_DROME	splQ9VLN	Q9VLN1	Wdr82	4	4	4	10.7	10.7	10.7	35.355	0	24.324	55080000	8	18.988735	19.601829	20.183258	19.741476	13.997179	13.868050	14.136030	13.311748
5.788707733154	5.1614935166	splQ9VKQ9IDPY30_DROME	splQ9VKC	Q9VKQ9	Dpy-30L1	5	5	5	50	50	50	13.794	0	323.31	75308000	26	24.407949	25.730966	25.462202	24.509239	19.649639	19.473201	19.198228	18.634456
5.764960527420	4.2529581136	trIQ9VJ08IQ9VJ08_DROME	trIQ9VJ08	Q9VJ08	B1	1	1	1	2.5	2.5	2.5	89.092	0.0053957	9.8259	12735000	4	16.947408	18.043027	17.770174	16.978130	11.012143	13.111459	11.586430	10.968865
5.707932233810	4.3434838870	trIE4NKG1IE4NKG1_DROME;splQ9I7D3I	trIE4NKG1	Q9I7D3	Capr	3	3	3	5.3	5.3	5.3	103.59	0	18.264	32967000	4	20.946924	21.870418	21.103096	20.111843	15.713896	15.759836	15.658713	14.068106
5.705997467041	3.2972055406	trIQ9VMH1IQ9VMH1_DROME;trIQ6NL34	trIQ9VMH	Q9VMH1	WDR79	2	2	2	6	6	6	55.921	0	16.306	12615000	3	16.926944	17.857446	17.906949	17.830837	13.206702	11.697812	13.068791	9.7248830
5.627684116363	2.5984833769	trIX2JDI1IX2JDI1_DROME;splP23696IPP	trIX2JDI1I	P23696	mts	1	1	1	10.7	10.7	10.7	35.469	0.0052817	8.2468	13071000	2	14.158826	18.254695	18.759614	16.809265	12.163340	11.307367	11.918485	10.082472
5.517843961715	4.5314588777	trIQ9W0K9IQ9W0K9_DROME	trIQ9W0K9	Q9W0K9	Dmel\CG920	2	2	2	10.3	10.3	10.3	24.322	0.0037313	11.318	7734500	2	17.050806	16.430076	17.042707	17.561153	10.389625	12.474041	11.731832	11.417867
5.515492677688	4.7613775724	splQ7KQZ4ILOLA3_DROME;splP42284IL	splQ7KQZ	Q7KQZ4	lola	11	11	4	21.2	21.2	11.7	82.172	0	323.31	34241000	31	21.166683	22.142953	21.723756	21.481533	16.234891	17.175626	15.368438	15.673998
5.512268781661	3.6211003059	trIA0A0B4LG47IA0A0B4LG47_DROME;s	trIA0A0B4	Q24141	mei-S332	1	1	1	4.2	4.2	4.2	44.401	0.0082372	6.7658	5158800	1	15.790654	17.209339	16.257516	15.129765	9.8803796	12.253311	10.137867	10.066641
5.393944263458	4.4596309509	trIQ7K3J0IQ7K3J0_DROME	trIQ7K3J0	Q7K3J0	CCT8	35	35	35	74.7	74.7	74.7	59.432	0	323.31	12470000	129	22.469684	23.454252	23.346244	22.892433	17.548866	18.273485	18.321575	16.442911
5.362606287002	3.3913655623	splQ7K0E3IMOB4_DROME	splQ7K0E	Q7K0E3	Mob4	1	1	1	8.5	8.5	8.5	25.747	0.0095087	6.4799	5933000	1	15.649144	17.513605	17.550821	16.731981	12.800073	11.400943	11.926788	9.8673210
5.358611345291	3.8443166586	splQ9I7F7IACKL_DROME;trIA0A0B4KEY	splQ9I7F7	Q9I7F7	Ack-like	3	3	3	3.9	3.9	3.9	147.48	0	21.749	30184000	9	15.087960	17.431676	17.337604	16.264223	11.162802	10.430034	11.933179	11.161002
5.248490333557	3.4377421760	trIQ9VHL2IQ9VHL2_DROME	trIQ9VHL2	Q9VHL2	CCT7	32	32	32	63.8	63.8	63.8	59.386	0	323.31	81779000	105	21.651933	22.758981	22.793663	22.245540	17.176795	18.110340	17.993082	15.175939
5.241980075836	4.8741300828	trIQ8SWW4IQ8SWW4_DROME	trIQ8SWW	Q8SWW4	anon-WO014	7	7	7	7.1	7.1	7.1	191.08	0	62.582	59840000	14	17.061391	18.273576	17.891250	17.058012	12.902977	12.610263	11.690303	12.112765
5.229042530059	1.9723088125	trIM9NGE4IM9NGE4_DROME;trIM9NEG	trIM9NGE	M9NGE4	mud	1	1	1	0.9	0.9	0.9	242.82	0.010937	6.4267	19365000	1	18.221380	18.169572	18.592952	18.547964	11.716559	11.184007	12.339278	17.375854
5.151200771331	3.9768320605	trIQ53YG3IQ53YG3_DROME;splP04197I	trIQ53YG3	P04197	Myb	3	3	3	8.1	8.1	8.1	74.044	0	19.118	14927000	5	16.215457	17.728466	16.556087	15.592894	12.379990	10.913832	11.364409	10.829870
5.099399566650	4.3761967555	splP17917IPCNA_DROME	splP17917	P17917	PCNA	8	8	8	47.3	47.3	47.3	28.83	0	62.535	19361000	19	21.154867	21.847547	22.009119	21.966312	15.521324	17.008209	17.585929	16.464784
5.024633646011	4.0827329460	trIQ9W5A0IQ9W5A0_DROME;trIQ9W599	trIQ9W5A(	Q9W5A0	anon-WO015	2	2	2	4.7	4.7	4.7	59.159	0	11.616	7950600	3	16.490489	17.707588	17.325357	15.865346	12.478309	12.333612	11.212774	11.265555
4.971212387084	3.9089248817	splA1Z9E2ILIN54_DROME;trIE1JH59IE1	splA1Z9E2	A1Z9E2	mip120	11	11	11	17.3	17.3	17.3	100.02	0	70.682	11917000	26	18.606426	19.561117	19.196620	18.452699	14.497602	14.431040	14.537218	12.466153
4.966226100921	4.2874130627	trIQ7YU80IQ7YU80_DROME;trIQ963E5I	trIQ7YU8(	Q7YU80	par-1	12	12	1	13	13	0.9	113.69	0	193.86	18286000	36	18.994491	20.120729	19.464155	18.967136	14.191521	15.535700	14.350179	13.604206
4.937675952911	4.4557219854	trIX2JDP6IX2JDP6_DROME;splQ8T079I	trIX2JDP6	Q8T079	BEST:GH194	19	19	19	36.4	36.4	36.4	65.251	0	323.31	61340000	53	21.519989	22.835359	22.230989	21.830047	17.170648	18.095170	17.007444	16.392417
4.911803722381	3.4944661884	trIQ9VQ58IQ9VQ58_DROME	trIQ9VQ58	Q9VQ58	Dmel\CG153	2	2	2	2.6	2.6	2.6	108.14	0	22.073	12339000	6	15.739332	16.751073	16.136030	14.957147	11.196535	10.575046	12.387452	9.7773351
4.877828121185	5.1442136693	trIQ9VKF4IQ9VKF4_DROME;trIE1JHF9IE	trIQ9VKF4	Q9VKF4	Dmel\CG149	5	5	5	25.2	25.2	25.2	22.542	0	66.44	12739000	13	21.151899	22.283931	21.819522	21.285570	17.399160	16.665113	16.532356	16.432981
4.833208560943	4.5824682118	trIA4V391IA4V391_DROME;splP12613IT	trIA4V391	P12613	CCT1	18	18	18	45.8	45.8	45.8	59.556	0	189.89	22780000	48	20.138336	21.000377	20.983566	20.551404	15.334866	16.437101	16.492527	15.076355
4.831305027008	4.4789813209	trIQ9W392IQ9W392_DROME	trIQ9W392	Q9W392	CCT2	39	39	39	75.7	75.7	75.7	58.063	0	323.31	21245000	181	23.196960	24.328275	24.127861	23.642181	18.787462	19.758037	19.323886	18.100671
4.816068887710	3.3972893460	trIQ9VC08IQ9VC08_DROME	trIQ9VC08	Q9VC08	Mink	13	13	13	23.1	23.1	23.1	84.471	0	117.25	18039000	37	19.462299	20.886360	20.221048	19.611551	16.416616	15.792739	13.633109	15.074518
4.813616991043	3.7191394614	trIQ8IR25IQ8IR25_DROME;trIX2JFL9IX2	trIQ8IR25I	Q8IR25	sd	1	1	1	3.8	3.8	3.8	42.456	0.01087	6.3886	4268200	1	15.923954	16.820030	16.590499	14.789431	10.278107	11.622643	12.017532	10.951164
4.781615257263	4.6841897097	trIQ9VS37IQ9VS37_DROME	trIQ9VS37	Q9VS37	Cdc27	2	2	2	4.1	4.1	4.1	101.28	0	33.158	19828000	5	16.066341	17.270843	17.297508	16.977123	11.498983	12.266874	11.913039	12.806458
4.775907993316	5.0056204051	splQ9VAG4IVP16B_DROME	splQ9VAG	Q9VAG4	Vps16B	1	1	1	2.9	2.9	2.9	50.411	0.0053097	8.5494	10019000	3	15.934589	16.872314	16.772365	16.696559	11.261109	11.395609	12.428214	12.087264
4.761121273040	4.4725795806	trIM9PF42IM9PF42_DROME;trIQ9VLT9I	trIM9PF42	M9PF42	Cka	8	8	8	16.1	16.1	16.1	77.105	0	72.056	14388000	24	20.246091	21.286415	20.824542	20.274124	16.801202	16.074245	15.550896	15.160344
4.750610589981	5.5062623194	trIM9PG56IM9PG56_DROME;trIM9PFQ9	trIM9PG56	M9PG56	Dmel\CG426	2	2	2	4.5	4.5	4.5	93.292	0	14.042	17877000	4	16.531686	17.576883	17.087318	16.909353	12.12642	12.564911	12.599012	11.812453
4.750423192977	4.7971449139	splQ867Z4ILOLA4_DROME	splQ867Z4	Q867Z4	lola	9	2	2	10.3	2.6	2.6	105.81	0	14.011	50955000	8	17.842607	19.253820	18.782896	18.761888	14.330777	14.285618	13.355901	13.667222

4.731259346008	3.6709178410	trIQ9VXW2IQ9VXW2_DROME	trIQ9VXW	Q9VXW2	DmRH29	4	4	4	4.4	4.4	4.4	136.28	0	24.856	30474000	9	16.368932	17.416996	17.062446	16.653264	11.304723	13.738518	11.994461	11.538899
4.715348243713	3.8561616165	splQ04688IELG_DROME;trIA0A0B4KHY6	splQ0468	Q04688	Ets97D	7	7	7	19.2	19.2	19.2	52.644	0	100.88	16609000	21	20.852472	21.731857	21.052583	19.740159	16.606405	16.874357	15.348417	15.686500
4.703399181365	4.6706626208	trIA4V303IA4V303_DROME;splP48605IT	trIA4V303	P48605	CCT3	38	38	38	64.3	64.3	64.3	59.394	0	323.31	11822000	135	22.312492	23.400152	23.272415	22.748208	18.048358	18.938619	18.440057	17.492635
4.700443267822	3.4286157865	trIQ5BIC3IQ5BIC3_DROME	trIQ5BIC3	Q5BIC3	az2	2	2	2	3.7	3.7	3.7	68.823	0	11.687	6543800	3	16.800951	14.768644	14.195285	16.360143	10.252083	10.853729	11.168253	11.049184
4.696720838546	4.0701538329	trIQ9V474IQ9V474_DROME	trIQ9V474	Q9V474	dbr	3	3	3	4.9	4.9	4.9	110.58	0	23.485	19852000	6	15.397307	17.194795	16.659132	15.975288	11.752631	12.434706	11.047669	11.204632
4.695680141448	3.2180441797	trIQ9W1H5IQ9W1H5_DROME	trIQ9W1H5	Q9W1H5	DCP1	4	4	4	15.9	15.9	15.9	41.359	0	30.04	36876000	6	17.302335	19.558914	19.367815	17.994409	13.053874	14.807556	14.516130	13.063192
4.662091732025	3.4986349490	trIA0A0B4LIJ0IA0A0B4LIJ0_DROME;splF	trIA0A0B4	P48601	Rpt2	4	4	4	10.7	10.7	10.7	49.323	0	22.128	34225000	5	17.966291	18.843006	18.350955	17.939567	14.126624	14.437686	14.041573	11.845569
4.627550125122	1.9741161212	trIQ960V1IQ960V1_DROME;trIQ0E8G1IC	trIQ960V1	Q960V1	simj	5	5	5	13.2	13.2	13.2	95.382	0	37.381	55394000	9	18.000253	19.498081	19.002645	17.989982	15.802163	15.521508	14.112277	10.544814
4.613677978515	5.1012723987	trIQ9VK69IQ9VK69_DROME	trIQ9VK69	Q9VK69	CCT4	30	30	30	62.7	62.7	62.7	57.116	0	323.31	74323000	78	21.898958	22.992895	22.780826	22.301620	17.246091	18.197101	18.104312	17.972082
4.608286619186	1.4287995322	trIQ9VX77IQ9VX77_DROME	trIQ9VX77	Q9VX77	Chchd2	1	1	1	7.1	7.1	7.1	17.329	0.010448	5.8232	4541500	1	17.212192	17.929201	18.332456	17.206003	12.198311	12.109095	9.9922876	17.947008
4.597616672515	2.4572656677	trIA0A0B4KFX5IA0A0B4KFX5_DROME	trIA0A0B4	A0A0B4KI	CtBP	12	1	1	30.9	6.3	6.3	41.344	0.0096931	6.6242	6767400	1	16.196006	16.359422	16.818656	15.972979	10.352238	14.063141	12.605301	9.9359169
4.588566780090	5.1730537543	trIA0A0B4LFD2IA0A0B4LFD2_DROME;s	trIA0A0B4	P29845	Hsc70-5	27	27	27	35.9	35.9	35.9	74.065	0	323.31	17422000	103	22.662969	23.774848	23.659053	23.051174	18.555734	19.037460	18.934768	18.265815
4.586024284362	3.3703875680	trIM9PH19IM9PH19_DROME;trIQ9W002I	trIM9PH19	M9PH19	msn	4	4	4	3.9	3.9	3.9	152.55	0	22.545	14146000	3	15.728399	16.608774	14.989705	14.902469	10.830324	12.451648	10.592082	10.011195
4.576665401458	3.9135383043	trIQ9V9T9IQ9V9T9_DROME	trIQ9V9T9	Q9V9T9	betaGlu	3	3	3	4.5	4.5	4.5	79.301	0	19.899	28406000	8	17.018896	18.312963	18.031389	17.676246	12.663180	12.980479	14.483185	12.605988
4.553205728530	4.2529622050	trIQ7K159IQ7K159_DROME	trIQ7K159	Q7K159	mip40	3	3	3	13.1	13.1	13.1	30.101	0	59.923	56580000	11	19.231000	20.385007	19.967052	19.209981	15.423575	15.418313	14.110483	15.627847
4.551949024200	2.9388573463	trIQ0E931IQ0E931_DROME	trIQ0E931	Q0E931	Dgp-1	1	1	1	2.8	2.8	2.8	72.501	0.0081833	6.7332	13182000	2	15.689724	17.269657	17.326499	16.215002	10.647991	11.405182	13.740940	12.498973
4.549242973327	3.8586624758	splQ9VPC0IKP58_DROME;trID3PFF6ID3	splQ9VPC	Q9VPC0	PitsIre	4	4	4	5.3	5.3	5.3	108.84	0	34.684	14047000	9	18.810459	19.445806	19.430982	19.388353	14.357895	16.236183	14.160186	14.124363
4.536190271377	2.3382733143	trIQ9W542IQ9W542_DROME	trIQ9W542	Q9W542	mip130	3	3	3	2.8	2.8	2.8	110.43	0	28.805	33621000	8	17.236312	17.970510	17.377464	17.304655	13.803222	15.385053	11.585768	10.970136
4.533339023590	4.5101209131	trIQ7KKI0IQ7KKI0_DROME;trIA1Z8U4IA1	trIQ7KKI0I	Q7KKI0	CCT5	43	43	43	81.9	81.9	81.9	59.278	0	323.31	18859000	172	23.041431	24.176151	24.133359	23.762737	19.368349	19.595087	19.680459	18.336427
4.532071590423	2.5381782189	trIA0A0B4KEQ0IA0A0B4KEQ0_DROME;s	trIA0A0B4	Q24318	Dp	2	2	2	6.7	6.7	6.7	46.658	0	13.57	9405400	2	16.615831	17.680374	15.795582	15.443720	10.060059	11.619766	13.928518	11.798878
4.513685941696	2.6242483656	trIQ59E01IQ59E01_DROME;trIQ8IPM6IQ	trIQ59E01	Q59E01	Dmel\CG979	4	4	4	6.9	6.9	6.9	76.392	0	41.163	33888000	11	17.606389	18.585269	18.307769	17.776420	14.972576	14.527782	13.629584	11.091163
4.494550466537	1.3467300805	splQ9VR89IPNO1_DROME	splQ9VR8	Q9VR89	l(1)G0004	1	1	1	6.7	6.7	6.7	26.676	0.0052724	8.1254	11553000	2	12.355175	19.267784	13.235862	18.338779	10.835902	10.919420	11.291922	12.172159
4.492812156677	3.0899097654	trIM9PCK7IM9PCK7_DROME;splQ9VLJ8	trIM9PCK7	Q9VLJ8	Uba4	2	2	2	4.9	4.9	4.9	50.238	0	14.595	21909000	6	16.990369	18.170795	18.086229	17.631334	14.094078	13.742625	11.221274	13.849502
4.429667234420	4.1493951019	trIQ7K2Q8IQ7K2Q8_DROME	trIQ7K2Q8	Q7K2Q8	Trs31	4	4	4	28.4	28.4	28.4	22.339	0	25.28	25843000	6	18.058012	19.037460	19.129158	19.384016	14.832345	13.832529	15.296306	13.928795
4.428961277008	2.1493193221	trIA0A0B4KHY2IA0A0B4KHY2_DROME;s	trIA0A0B4	Q7KRY7	scrib	2	2	2	2.5	2.5	2.5	191.34	0	20.703	26874000	4	15.540067	17.195949	17.414024	13.412173	11.619376	11.887034	9.7522754	12.587683
4.369230985641	2.1738535307	trIQ9VSD6IQ9VSD6_DROME	trIQ9VSD6	Q9VSD6	msk	1	1	1	1	1	1	119.31	0	15.523	18111000	5	16.504461	16.690298	16.380004	16.160245	15.154461	10.681029	10.548981	11.873613
4.345490932464	2.6835055482	trIA0A0B4KFX4IA0A0B4KFX4_DROME;tr	trIA0A0B4	A0A0B4KI	Rcd1	3	3	3	4.9	4.9	4.9	112.86	0	17.428	9003800	5	15.382522	15.965559	15.446953	14.203348	12.622737	11.395612	10.564892	9.0331764
4.339768648147	2.7305628617	trIQ9VND7IQ9VND7_DROME	trIQ9VND7	Q9VND7	Dmel\CG293	2	2	2	10.6	10.6	10.6	33.644	0	11.593	6607100	2	14.869834	17.882440	16.770948	15.800394	12.690852	10.723476	12.916319	11.633894
4.252028942108	2.6769036515	trIQ9VT60IQ9VT60_DROME;trIQ7KUD4I(	trIQ9VT60	Q9VT60	iPLA2-VIA	10	10	10	14.9	14.9	14.9	96.862	0	239.68	10150000	21	17.615686	19.456554	18.554124	18.373603	14.858223	15.617812	14.315715	12.200101
4.242337703704	0.9966360149	splQ94524IDYLT_DROME	splQ9452	Q94524	Dlc90F	1	1	1	15.3	15.3	15.3	12.479	0	14.477	12689000	3	18.747472	19.039953	19.772010	12.885503	11.617115	17.875196	12.099765	11.883511
4.241802453994	3.4177247493	trIM9NEA5IM9NEA5_DROME;trIM9PGW9	trIM9NEA5	P10180	ct	3	3	3	1.9	1.9	1.9	233.36	0	21.777	23114000	5	16.053607	17.076814	16.691253	15.640414	13.317097	11.866158	12.390550	10.921073
4.220561504364	3.4867281995	trIB7Z0I8IB7Z0I8_DROME	trIB7Z0I8I	B7Z0I8	anon-EST:L	6	6	6	2.8	2.8	2.8	378.59	0	42.693	33035000	8	14.610101	16.449954	15.517853	14.748297	10.714331	10.675780	12.276677	10.777173

4.199868202209	4.0852768383	trIQ9W3Z4IQ9W3Z4_DROME	trIQ9W3Z4	Q9W3Z4	Dmel\CG334	10	10	10	24.1	24.1	24.1	50.354	0	138.16	17756000	28	19.831224	21.293954	20.524971	20.221048	16.255434	15.596830	17.137811	16.081649
4.176397800445	1.8783978182	splQ9VWY6ITAF8_DROME	splQ9VW	Q9VWY6	Taf8	1	1	1	6.7	6.7	6.7	36.649	0.010802	6.2647	6139300	1	16.191116	17.572967	17.089801	12.685173	12.856042	11.430844	11.955979	10.590601
4.147234201431	2.0822621133	trIQ9VRV5IQ9VRV5_DROME	trIQ9VRV5	Q9VRV5	D19A	3	3	3	3.8	3.8	3.8	96.195	0	21.766	26713000	3	15.591142	18.676315	16.993137	15.634669	11.846783	14.456739	13.164153	10.838651
4.130854606628	2.1903579300	splP48609ICDK5_DROME	splP4860	P48609	Cdk5	1	1	1	4.1	4.1	4.1	33.18	0.010386	5.7949	6140600	2	15.946472	17.138311	16.278285	15.930113	15.072593	11.560448	10.875477	11.261244
4.120416164398	3.4352131877	trIE1JGM9IE1JGM9_DROME;trIQ963E6I(	trIE1JGM9	E1JGM9	par-1	12	1	1	16.9	1.6	1.6	88.549	0.0053286	8.7639	11708000	4	15.914384	17.187177	16.059766	15.922026	12.210834	13.494367	11.538043	11.358446
4.120319843292	4.5332713363	trIA0A0B4LHL0IA0A0B4LHL0_DROME;sp	trIA0A0B4	Q9VC61	REPTOR	4	4	4	9.4	9.4	9.4	82.262	0	29.689	52024000	9	19.325950	19.970144	19.671089	19.069858	15.565935	15.786932	14.474656	15.728239
4.095619678497	3.9180425515	splO77459IKEN_DROME	splO7745	O77459	ken	4	4	4	13	13	13	67.032	0	55.742	93873000	7	18.913684	20.284553	19.482213	18.798706	15.901055	15.595024	14.425674	15.174925
4.087455272674	4.3022251089	splP05205IHP1_DROME	splP0520	P05205	Su(var)205	7	7	7	36.4	36.4	36.4	23.185	0	94.249	25701000	28	21.567276	22.695850	22.768195	22.257932	18.149122	18.795665	18.524166	17.470483
4.044576168060	4.5624308639	trIQ9VXQ5IQ9VXQ5_DROME	trIQ9VXQ5	Q9VXQ5	CCT6	32	32	32	55	55	55	58.246	0	323.31	95203000	105	22.076398	23.123193	22.889019	22.481040	17.909587	18.825691	18.480222	19.175846
4.023383140563	3.7481015005	trIQ2MGP0IQ2MGP0_DROME;trIQ9W3U	trIQ2MGP	Q2MGP0	CG32737 OR	1	1	1	2	2	2	71.578	0.011076	6.4589	2913100	1	13.693160	15.588802	15.553929	14.777614	10.547897	10.520772	11.076644	11.374658
4.009383201599	3.7104340166	trIM9PDL9IM9PDL9_DROME;splP16568I	trIM9PDL9	P16568	BicD	25	25	25	47.2	47.2	47.2	88.953	0	323.31	69377000	73	20.728414	21.743080	22.453222	21.618001	17.673694	18.076763	18.130590	16.624137
3.991847753524	1.8860075929	trIM9NDL7IM9NDL7_DROME;trIQ8MQS4	trIM9NDL7	M9NDL7	Reps	3	3	3	4.8	4.8	4.8	93.383	0	23.902	29544000	9	16.389883	18.104312	17.754144	17.286809	10.285376	14.681183	15.039433	13.561765
3.987170696258	2.8933795750	trIQ59E33IQ59E33_DROME	trIQ59E33	Q59E33	scaf6	1	1	1	2	2	2	107.57	0.011041	6.4458	7281300	2	12.998632	15.847938	15.786116	15.499347	10.680360	11.125797	10.927975	11.449218
3.964599847793	1.3239701944	trIQ9V436IQ9V436_DROME	trIQ9V436	Q9V436	Rpn12	3	3	3	14.4	14.4	14.4	30.225	0	20.318	24459000	4	18.011485	18.622888	18.903717	17.974044	15.712956	15.247668	16.898176	9.7949399
3.878841876983	3.8104143988	trIQ9V3Z4IQ9V3Z4_DROME	trIQ9V3Z4	Q9V3Z4	Rpn5	7	7	7	15.5	15.5	15.5	57.747	0	84.336	61709000	10	18.884588	18.022859	19.619991	18.950231	14.959277	15.896521	14.734656	14.371844
3.855873823165	2.4922544213	trIM9PDG3IM9PDG3_DROME;trIM9PD57	trIM9PDG3	P40798	stc	1	1	1	1.3	1.3	1.3	121.91	0.0052448	7.7529	5672800	2	15.347932	13.895739	15.531655	14.573529	9.9607114	12.958340	9.8464269	11.159882
3.845554828643	3.6558462910	trIA0A0B4K7Z5IA0A0B4K7Z5_DROME;sp	trIA0A0B4	Q7KLV9	Rpn6	15	15	15	40.8	40.8	40.8	47.263	0	117.99	24633000	45	20.234560	21.510265	21.471397	20.420186	17.134906	17.605016	17.463716	16.050550
3.845453500747	1.8564138759	trIO61444IO61444_DROME	trIO61444	O61444	Mkk4	2	2	2	5.2	5.2	5.2	47.533	0	51.777	27234000	4	18.707284	19.350135	16.536642	16.403278	15.082773	14.938017	14.098361	11.496375
3.844643592834	4.6690254821	trIA0A0B4LFE2IA0A0B4LFE2_DROME;tr	trIA0A0B4	A0A0B4LI	CG8079	2	2	2	2.2	2.2	2.2	55.637	0	12.492	42725000	3	18.289018	19.596052	19.008647	18.472032	15.254586	15.084559	15.026436	14.621594
3.838787078857	6.2650741947	trIA0A0B4K7P1IA0A0B4K7P1_DROME;tr	trIA0A0B4	A0A0B4K	p53	6	6	6	21.9	21.9	21.9	38.185	0	46.438	79573000	11	19.493339	19.930919	19.871847	19.684694	16.312438	15.702957	15.722273	15.887982
3.838112592697	1.9282510425	trIQ9VY91IQ9VY91_DROME	trIQ9VY91	Q9VY91	Pdcd4	2	2	2	3.5	3.5	3.5	56.354	0	12.598	25755000	3	15.327622	18.948463	18.215372	17.853431	13.431105	15.713306	13.676287	12.171739
3.833173274993	3.8423002729	trIQ9VGQ8IQ9VGQ8_DROME	trIQ9VGQ	Q9VGQ8	Arfip	5	5	5	20.3	20.3	20.3	38.786	0	43.754	51188000	10	18.727567	19.806404	20.633338	19.458658	16.183227	15.585666	16.186481	15.337900
3.806982040405	2.6085053940	trIM9PGG0IM9PGG0_DROME;trIM9PG8	trIM9PGG	M9PGG0	ArfGAP3	2	2	2	7.4	7.4	7.4	54.454	0	21.448	18871000	3	16.696289	17.935256	17.468019	17.269838	14.075311	14.340892	14.334622	11.390648
3.800863742828	4.9729273229	trIX2JKZ0IX2JKZ0_DROME;trIX2JE83IX2	trIX2JKZ0	Q8T498	Dmel\CG426	2	2	2	2.6	2.6	2.6	171.58	0	14.406	25029000	6	15.760953	16.981477	16.512308	16.219339	12.672539	12.655530	12.734688	12.207868
3.797534942626	3.9389015556	trIQ9V4D4IQ9V4D4_DROME	trIQ9V4D4	Q9V4D4	bip2	1	1	1	0.9	0.9	0.9	154.5	0.005137	7.3983	9929800	4	14.479654	15.716926	15.703335	14.998061	10.865885	11.600326	12.215572	11.026053
3.756995439529	2.7718881033	trIQ9VX15IQ9VX15_DROME	trIQ9VX15	Q9VX15	DmRFC2	1	1	1	4.5	4.5	4.5	39.554	0.010622	5.9786	2930500	1	15.206403	15.988995	15.033079	14.690052	13.290732	11.458157	10.514739	10.626919
3.751716136932	3.1935175639	splQ9V3G7IPSMD6_DROME	splQ9V3G	Q9V3G7	Rpn7	14	14	14	45	45	45	45.38	0	140.2	25080000	40	20.549995	21.824115	21.767614	20.739418	17.753751	17.637784	18.350784	16.131958
3.712603092193	3.9245020746	splQ9VXG1IHANG_DROME;trIB7Z0Z1IB	splQ9VXG	Q9VXG1	hang	9	9	9	6.9	6.9	6.9	213.79	0	112.39	72855000	21	17.144195	18.529590	17.912691	17.382623	14.736296	13.979782	14.075060	13.327552
3.705517292022	2.0308448954	splQ7JVL3IPRP38_DROME	splQ7JVL3	Q7JVL3	Prp38	1	1	1	4.5	4.5	4.5	40.087	0.0051195	7.3199	4876300	4	15.472405	16.749502	16.036581	15.239710	14.625937	12.518815	10.488681	11.042695
3.701383590698	2.5485496300	trIQ9VBR1IQ9VBR1_DROME	trIQ9VBR1	Q9VBR1	Vps33B	3	3	3	5.8	5.8	5.8	71.213	0	18.71	15374000	5	15.753790	16.637077	17.245441	16.969049	14.093005	13.941414	12.637055	11.128349
3.700640439987	1.6553862143	trIA0A0B4KHB2IA0A0B4KHB2_DROME;s	trIA0A0B4	O46036	CtBP	12	1	1	24.5	4.9	4.9	50.362	0	30.264	8911000	2	15.970712	17.256448	16.600725	16.043689	10.937815	14.410915	15.137471	10.582812
3.659687042236	2.5834850640	trIQ9XYZ4IQ9XYZ4_DROME	trIQ9XYZ4	Q9XYZ4	mre11	2	2	2	2.6	2.6	2.6	69.284	0	11.898	9106900	2	15.339015	16.816408	16.327009	15.293867	13.827243	11.293016	11.178115	12.839175

3.651740789413	2.9421860459	splQ9V3H2lPSDE_DROME	splQ9V3H	Q9V3H2	Rpn11	6	6	6	22.1	22.1	22.1	34.4	0	44.337	69813000	15	19.619739	20.327070	20.942491	20.669946	17.924104	15.837529	17.462278	15.728372
3.648153066635	2.9995720103	trlQ8MMD2lQ8MMD2_DROME;trlQ9W11	trlQ8MMD	Q8MMD2	Eps-15	11	11	11	10.3	10.3	10.3	132.11	0	214.55	14319000	31	18.460800	19.749208	19.330751	18.999923	15.201128	15.795886	16.785835	14.165221
3.641528606414	2.1091099347	splP53034lRFC2_DROME	splP53034	P53034	RfC4	2	2	2	7.6	7.6	7.6	37.173	0.0018904	11.43	9922700	2	15.983616	16.744649	17.135608	16.633676	15.089657	13.368097	12.727580	10.746102
3.613619327545	3.1930546444	splP20028lRPA2_DROME	splP20028	P20028	Rpl135	1	1	1	0.8	0.8	0.8	128.44	0.0066556	6.9066	6291600	2	14.559556	15.112113	14.233919	14.009828	11.916505	10.904317	9.5009479	11.139168
3.558002233505	3.7370661378	trlA0A0B4LEV8lA0A0B4LEV8_DROME;s	trlA0A0B4	A1Z7A8	coil	5	5	5	11.4	11.4	11.4	70.458	0	44.065	13042000	14	19.102748	20.559736	19.956880	19.286043	16.244419	16.452594	15.354249	16.622137
3.555762290954	1.5525481900	trlQ8T6I0lQ8T6I0_DROME	trlQ8T6I0l	Q8T6I0	Past1	1	1	1	1.3	1.3	1.3	61.004	0.01072	6.1301	7628500	3	15.954218	16.306488	16.080421	13.002985	11.408705	14.584081	10.569038	10.559238
3.542491674423	4.0178393501	splQ03427lLAMC_DROME;trlA0A0B4KF	splQ0342	Q03427	LamC	2	2	2	5.6	5.6	5.6	69.859	0	11.79	6262600	3	15.103984	14.741150	15.549513	15.056552	11.432099	11.103943	11.148794	12.596398
3.526466846466	4.5608356212	trlQ9VAA9lQ9VAA9_DROME	trlQ9VAA9	Q9VAA9	Dmel\CG794	3	3	3	6.5	6.5	6.5	52.838	0	20.167	16373000	7	16.692070	17.807945	17.217693	16.522197	13.838416	13.326429	13.459047	13.510146
3.505920410156	1.0292388121	trlX2JGG6lX2JGG6_DROME;splP02517l	trlX2JGG6	P02517	Hsp26	2	2	2	14.9	14.9	14.9	22.994	0	323.31	41798000	6	18.548490	19.515857	19.884349	17.496541	17.390287	12.338068	12.682943	19.010259
3.501209259033	1.4357693791	trlQ9VPF1lQ9VPF1_DROME	trlQ9VPF1	Q9VPF1	Dmel\CG519	1	1	1	3.7	3.7	3.7	42.348	0.0053004	8.5244	4225500	1	15.297525	16.547164	16.779821	12.143554	13.159861	11.324463	12.546326	9.7325773
3.494295358657	2.0365369962	trlQ9VEN9lQ9VEN9_DROME	trlQ9VEN9	Q9VEN9	Patr-1	3	3	3	6.9	6.9	6.9	108.22	0	19.394	17317000	4	14.897183	16.550926	17.602336	14.345613	12.227683	13.654904	12.520878	11.015412
3.469472885131	2.5949803593	trlQ7JX95lQ7JX95_DROME	trlQ7JX95	Q7JX95	CG11123	1	1	1	1.7	1.7	1.7	75.735	0.010294	5.7388	7846100	1	15.716899	16.181230	15.842694	15.450824	12.159864	13.786576	12.823625	10.543691
3.462613105773	1.3566033799	trlQ9NF31lQ9NF31_DROME;trlQ9W523l	trlQ9NF31	Q9NF31	ph-d	8	1	1	12.6	2.7	2.7	143.15	0.0053763	9.0711	10511000	1	13.464434	13.967682	16.878913	18.036012	14.000405	12.126957	12.232305	10.136922
3.438395261764	2.6209882216	splQ24472lRBF_DROME	splQ24472	Q24472	Rbf	1	1	1	2.1	2.1	2.1	96.825	0.0081566	6.7128	7979500	2	14.694738	15.865322	15.341623	14.442424	13.230140	11.399027	10.301006	11.660352
3.400121688842	4.9010285154	trlA0A0B4JD39lA0A0B4JD39_DROME;sp	trlA0A0B4	P17789	ttk	4	4	4	10.7	10.7	10.7	68.77	0	24.507	56847000	13	18.705463	19.500593	18.784461	18.801456	15.873588	15.833507	15.120804	15.363587
3.396194696426	5.1183365806	trlQ9W2D0lQ9W2D0_DROME;trlQ9W24(	trlQ9W2D(	Q9W2D0	CG4021	3	1	1	7.5	4.4	4.4	36.979	0.0053381	8.7704	8648100	1	16.938707	17.107583	16.893325	16.664836	13.734815	13.567005	12.865520	13.852334
3.349175453186	2.3830807348	trlM9PFS7lM9PFS7_DROME;splQ9VK33	trlM9PFS7	Q9VK33	Sfmbt	2	2	2	3	3	3	133.67	0.0018939	11.441	3689500	2	15.349696	14.819580	14.957465	12.712416	12.279948	10.903276	10.093202	11.166028
3.342370510101	1.6604223007	trlQ9VX34lQ9VX34_DROME	trlQ9VX34	Q9VX34	DmRH14	3	3	3	5.8	5.8	5.8	92.844	0	36.426	28580000	7	16.522459	17.791767	17.042707	16.591609	14.311393	14.787800	14.951740	10.528120
3.337423801422	1.3281046061	trlQ9W3J4lQ9W3J4_DROME	trlQ9W3J4	Q9W3J4	Dmel\CG212	1	1	1	3.7	3.7	3.7	53.308	0.010703	6.1095	5909200	1	16.153671	16.821151	16.500234	12.354741	11.189979	14.597669	11.698399	10.994054
3.324390411376	1.9743785899	trlQ9VB49lQ9VB49_DROME	trlQ9VB49	Q9VB49	mrt	1	1	1	2.3	2.3	2.3	85.776	0.0083056	6.8552	12727000	3	15.760226	17.156202	16.548265	15.474593	14.357002	13.795735	12.877360	10.611627
3.311282396316	1.3320656775	splQ9U9Q4lEIF3H_DROME	splQ9U9C	Q9U9Q4	eIF3h	1	1	1	5	5	5	38.407	0.010511	5.8853	5600200	1	15.862686	16.802213	16.833433	14.734018	10.218751	14.723927	11.065206	14.979335
3.310178518295	3.1380233762	trlQ6NP69lQ6NP69_DROME;trlQ8INS9lC	trlQ6NP69	Q6NP69	gfzf	7	7	7	10.1	10.1	10.1	119.28	0	65.152	78464000	18	18.438312	18.714479	18.740966	18.365682	13.770870	16.097846	15.407832	15.742177
3.305727243423	4.5502698205	trlQ9VZ27lQ9VZ27_DROME;trlM9PEA2lM	trlQ9VZ27	Q9VZ27	CDK2AP1	2	2	2	14.6	14.6	14.6	29.26	0	11.957	10865000	2	17.569410	18.524663	17.869606	17.441761	14.066929	14.767615	14.735291	14.612695
3.299454927444	2.8110580182	splP23128lDDX6_DROME	splP23128	P23128	me31B	2	2	2	8.1	8.1	8.1	51.945	0	66.334	10549000	8	19.379665	20.311855	19.901243	19.322544	16.994132	17.714580	15.422492	15.586282
3.285538673400	2.4633244090	trlQ7KU01lQ7KU01_DROME	trlQ7KU01	Q7KU01	PNUTS	1	1	1	1.1	1.1	1.1	120.63	0.0098315	5.346	6848800	0	14.975355	16.236986	15.383502	13.417175	12.331768	12.367054	11.374565	10.797474
3.280791521072	4.5728715381	trlQ7JWH6lQ7JWH6_DROME	trlQ7JWH(	Q7JWH6	CG1888	2	2	2	9.9	9.9	9.9	42.274	0	12.3	13446000	3	17.127470	17.794618	17.100622	17.332717	14.444108	13.398476	14.361944	14.027732
3.275403738021	1.9980773094	trlA1Z9I5lA1Z9I5_DROME	trlA1Z9I5l	A1Z9I5	tum	2	2	2	1.8	1.8	1.8	69.762	0	12.442	6922800	5	15.696805	16.485734	13.654251	15.985841	11.870633	13.975757	11.039714	11.834912
3.263840913772	3.9531500198	trlM9PEL3lM9PEL3_DROME;trlQ9VS54l(	trlM9PEL3	M9PEL3	qm	3	3	3	13.2	13.2	13.2	37.385	0	65.366	42649000	9	18.159063	19.194145	19.034158	18.636299	14.657932	15.926875	15.639029	15.744465
3.263477325439	2.9130840472	trlA8DYB0lA8DYB0_DROME	trlA8DYB0	A8DYB0	CG13185	1	1	1	0.2	0.2	0.2	631.32	0.0066667	6.9159	2285800	1	14.476592	11.916214	13.325895	13.245399	10.556218	9.7917652	9.5062484	10.055960
3.258956909179	4.2192764329	trlE1JHK1lE1JHK1_DROME;splP98149lD	trlE1JHK1	P98149	Dif	1	1	1	1.6	1.6	1.6	73.934	0.010989	6.4405	10808000	1	16.252943	17.428327	17.416170	16.434839	13.526132	13.915785	13.518529	13.536004
3.238141536712	4.4793766970	splQ94527lNFKB1_DROME	splQ9452	Q94527	Rel	1	1	1	1	1	1	109.77	0.0050505	7.0976	10488000	1	15.361018	16.021566	16.005338	15.481168	12.679018	13.021205	12.293011	11.923290
3.147836446762	2.9940159885	trlE1JJ72lE1JJ72_DROME;trlA0A0B4LGl	trlE1JJ72l	E1JJ72	Taf1	6	6	6	5.1	5.1	5.1	235.56	0	44.854	46796000	9	16.535200	17.160146	16.812904	16.517745	14.266493	13.591755	14.396337	12.180064

3.125924348831	2.5044834594	trlX2JJ32lX2JJ32_DROME;trlB7Z134lB7Z	trlX2JJ32l	X2JJ32	Dmel\CG7766	1	1	1	1.7	1.7	1.7	136.66	0.0096	6.5839	4820100	2	14.475669	15.627562	13.591540	14.098196	11.690671	12.527214	10.764208	10.307177
3.117255210876	3.4977662514	trlQ0E8J0lQ0E8J0_DROME	trlQ0E8J0	Q0E8J0	MEP-1	4	4	4	6.8	6.8	6.8	124.06	0	28.605	34130000	9	17.115531	17.759874	16.877836	16.486505	14.507670	14.460200	13.640244	13.162611
3.110963344573	3.2241678878	trlX2JGE9lX2JGE9_DROME;trlX2JLN4lX	trlX2JGE9	X2JGE9	l(1)G0196	2	2	2	1.9	1.9	1.9	130.72	0.0018975	11.453	13018000	6	15.215608	15.626935	15.496198	15.162076	12.730873	13.274305	11.198322	11.853465
3.099744558334	2.1598410716	trlB7Z0X1lB7Z0X1_DROME;trlQ9W457lC	trlB7Z0X1	B7Z0X1	Shmt	5	5	5	16.9	16.9	16.9	50.984	0	39.985	40905000	9	16.971633	18.742940	18.353887	18.532789	15.698379	14.592632	16.462629	13.448632
3.094651222229	3.5262708094	trlM9PG62lM9PG62_DROME;splP25161l	trlM9PG62	P25161	Rpn3	9	9	9	28.5	28.5	28.5	56.003	0	93.722	15118000	23	19.353500	20.400934	20.255342	19.583398	16.936178	17.369647	17.047294	15.861450
3.093763351440	5.2015494141	trlQ9VZF5lQ9VZF5_DROME	trlQ9VZF5	Q9VZF5	pav	12	12	12	16.2	16.2	16.2	100.67	0	84.893	95465000	24	18.391714	19.198038	18.945753	18.503234	15.937626	15.527690	15.641204	15.557164
3.091913461685	3.0968103072	trlQ8IPN8lQ8IPN8_DROME;trlA0A0B4KF	trlQ8IPN8	Q8IPN8	mtd	1	1	1	0.9	0.9	0.9	94.449	0.0095694	6.582	5464800	4	14.658100	15.404742	14.762278	14.730045	10.491488	12.467635	11.758827	12.469561
3.087756633758	4.2426408339	trlA4V1Y7lA4V1Y7_DROME;trlQ2PDY2lC	trlA4V1Y7	Q08605	Trl	6	6	6	11.8	11.8	11.8	54.815	0	198.49	18752000	18	21.888776	22.888721	22.511882	21.709608	18.823392	19.497341	19.083297	19.243930
3.072094678878	3.4767888833	trlQ9V3V6lQ9V3V6_DROME;trlQ9VA54lC	trlQ9V3V6	Q9V3V6	Rpt5	5	5	4	15.7	15.7	12.9	47.806	0	31.619	46988000	6	18.422590	18.882141	18.896463	17.790489	15.232908	16.306594	15.439181	14.724620
3.052973270416	3.7753132128	trlQ9V406lQ9V406_DROME	trlQ9V406	Q9V406	crp	20	20	20	40.1	40.1	40.1	67.163	0	292.51	56515000	62	21.637237	22.955640	22.662425	22.233770	19.873981	19.527187	18.888666	18.987346
3.035366058349	1.2228610729	splQ9VN50lEI3F1_DROME	splQ9VN5	Q9VN50	eIF3f1	1	1	1	3.9	3.9	3.9	31.104	0.0096154	6.5924	4317200	2	14.096743	16.544572	16.784940	13.544700	11.686894	12.488310	14.774838	9.8794498
3.007941722869	3.3782729459	splP28166lZFH1_DROME	splP28166	P28166	zfh1	2	2	2	2.1	2.1	2.1	116.6	0.0037523	11.334	13797000	2	15.613501	17.032196	15.681732	16.116952	13.583905	13.551227	12.815543	12.461939
2.970137357711	5.3314524396	trlQ9VUB5lQ9VUB5_DROME	trlQ9VUB5	Q9VUB5	upSET	2	2	2	0.8	0.8	0.8	336.44	0	12.756	15069000	5	14.820577	15.161052	14.597586	14.599738	11.497452	11.851436	11.775651	12.173864
2.963312149047	0.8420671441	trlQ9VD81lQ9VD81_DROME	trlQ9VD81	Q9VD81	Rpl12	1	1	1	11.7	11.7	11.7	13.63	0.0081301	6.7029	5461400	1	17.582553	17.892732	13.615485	17.601902	16.185728	12.241914	16.033744	10.378037
2.963305950164	2.0646700722	trlA4V3G8lA4V3G8_DROME;splQ7KRY6	trlA4V3G8	Q7KRY6	ball	1	1	1	3.3	3.3	3.3	65.993	0.0051993	7.5964	3492200	1	13.030281	16.190809	13.392479	14.921004	11.751540	11.824390	11.410320	10.695095
2.960730075836	3.9266317780	trlQ960S0lQ960S0_DROME;trlM9PH51lN	trlQ960S0	Q960S0	BtbVII	7	7	7	8.7	8.7	8.7	78.417	0	70.891	15743000	19	20.748615	21.884908	21.457838	21.084529	18.757272	18.697103	18.023342	17.855257
2.959474802017	4.0870010211	trlA0A0B4KF23lA0A0B4KF23_DROME;tr	trlA0A0B4	Q7PLI2	Nipped-B	1	1	1	0.6	0.6	0.6	223.3	0.010654	6.0211	9133400	1	14.385390	14.714674	14.430126	14.059429	11.240314	12.280278	11.200531	11.030597
2.948697566986	3.0646710997	trlM9PBH6lM9PBH6_DROME;splQ9W0K	trlM9PBH6	Q9W0K4	bab2	6	6	6	9.1	9.1	9.1	114.59	0	45.513	76996000	15	17.764547	19.409141	18.513410	18.168888	16.356039	15.602148	15.334308	14.768701
2.939001321792	3.8346416331	trlQ9VIP9lQ9VIP9_DROME	trlQ9VIP9	Q9VIP9	barr	1	1	1	1.6	1.6	1.6	82.761	0.0051724	7.4652	8017400	4	15.703335	16.444917	15.495387	15.298170	12.717076	13.210717	13.104238	12.153773
2.928166389465	1.3075936439	trlQ8IQV5lQ8IQV5_DROME;trlM9NG75lN	trlQ8IQV5	Q8IQV5	Dmel\CG172	2	2	2	3.6	3.6	3.6	83.51	0	12.13	12193000	2	17.814470	18.272483	17.635732	16.512432	15.473578	16.328130	11.294643	15.426100
2.910745620727	1.5645145775	trlM9NEL3lM9NEL3_DROME;trlM9NDB7l	trlM9NEL3	M9NEL3	kis	12	12	12	5.2	5.2	5.2	560.92	0	214.42	23082000	33	17.388185	18.662126	18.156793	17.468734	17.167320	13.701522	16.038940	13.125074
2.902949571609	1.7120583885	splP49906lTAF11_DROME	splP49906	P49906	Taf11	2	2	2	15.3	15.3	15.3	22.091	0	12.834	19486000	3	18.300458	18.748912	18.550708	18.339607	17.168985	15.561586	16.560855	13.036461
2.889081478118	2.3441515610	trlA0A0B4LFQ2lA0A0B4LFQ2_DROME;tr	trlA0A0B4	A0A0B4LF	Incenp	2	2	2	5	5	5	83.408	0	12.699	7862900	2	16.082523	16.790042	14.089615	14.448955	12.415821	12.781360	12.285662	12.371967
2.863704919815	2.2028906204	splQ9XZ06lNU931_DROME	splQ9XZ0	Q9XZ06	Nup93-1	2	2	2	3.3	3.3	3.3	93.851	0	15.244	13756000	5	14.720297	16.273031	16.654245	16.257497	13.561526	14.356520	11.801332	12.730873
2.850718259811	1.9444261514	trlQ7KMQ0lQ7KMQ0_DROME	trlQ7KMQ	Q7KMQ0	Rpt1	3	3	3	7.9	7.9	7.9	48.541	0	17.632	14834000	4	15.888410	16.528652	17.459878	16.878793	14.034541	15.031313	14.521906	11.765100
2.842562437057	5.8058437788	trlQ9VSY2lQ9VSY2_DROME;trlQ0E8G6l	trlQ9VSY2	Q9VSY2	Dmel\CG368	1	1	1	7.4	7.4	7.4	23.03	0	29.595	30975000	4	19.108121	19.273077	18.717494	18.821369	15.919608	16.313838	16.207147	16.109218
2.836247920989	2.8823180693	trlQ9V405lQ9V405_DROME;trlQ9VH79lC	trlQ9V405	Q9V405	Rpt3	4	4	4	11.1	11.1	11.1	46.998	0	23.386	31670000	7	17.571115	18.262424	18.324523	17.971015	15.107380	15.715345	16.051187	13.910174
2.825666427612	3.5083316046	splQ9VKJ1lMPND_DROME	splQ9VKJ	Q9VKJ1	CG4751	6	6	6	5.9	5.9	5.9	149.95	0	39.607	44752000	15	16.910526	18.108554	17.620204	17.025398	15.254032	14.000440	14.663113	14.444432
2.811228275299	1.3903818952	trlQ8INN5lQ8INN5_DROME;trlA0A126GU	trlQ8INN5	Q8INN5	Unc-115b	1	1	1	3.9	3.9	3.9	82.142	0.0095541	6.5551	6975900	1	13.621877	16.721206	13.082394	15.725791	11.823153	13.594032	12.093086	10.396085
2.810094833374	3.5374176205	trlX2JC82lX2JC82_DROME;splP02518lH	trlX2JC82	P02518	Hsp27	5	5	5	25.4	25.4	25.4	23.616	0	68.612	10896000	17	20.692342	20.694299	20.206457	20.690809	17.172700	18.428573	17.124647	18.317607
2.792106151580	2.9262883132	splQ7KQM6lGGYF1_DROME	splQ7KQM	Q7KQM6	CG11148	3	3	3	4.4	4.4	4.4	173.73	0	21.14	34907000	4	15.968419	17.394563	16.860116	15.945558	14.586429	13.931660	13.396604	13.085538
2.788928031921	2.1718597345	trlE1JIM1lE1JIM1_DROME;trlA0A0B4K6	trlE1JIM1l	E1JIM1	nsl1	1	1	1	1.9	1.9	1.9	99.089	0.0099857	5.4455	0	1	13.881622	15.664421	14.409463	13.134922	11.477663	10.566043	11.231062	12.659948

2.788026571273	2.1596967630	trIQ9VAW3IQ9VAW3_DROME	trIQ9VAW3	Q9VAW3	Gfat2	1	1	1	2	2	2	76.538	0.005059	7.1127	6722100	2	14.822669	15.296629	15.556027	15.187004	10.584917	13.239031	12.273868	13.612407
2.783594131469	1.1041104592	trIA0A0B4KG68IA0A0B4KG68_DROME;t	trIA0A0B4	A0A0B4K(	Tm1	1	1	1	6	6	6	29.105	0.0050336	7.0656	11671000	2	16.865806	16.818782	17.567628	16.482303	11.176361	16.016199	16.600957	12.806627
2.778891563415	2.7446265849	splQ9XZT7ITAFAB_DROME	splQ9XZT	Q9XZT7	Taf10b	5	5	5	30.8	30.8	30.8	15.784	0	64.586	54138000	9	20.689445	22.137086	21.668172	21.024316	19.311079	18.617231	19.028045	17.447099
2.773900032043	2.8040465847	trIM9PG55IM9PG55_DROME;trIQ9VJ42I(	trIM9PG55	M9PG55	Dmel\CG106	1	1	1	1.7	1.7	1.7	150.42	0.0081967	6.7385	4907500	3	13.820378	14.943614	14.795024	14.285474	11.352893	12.713443	12.014133	10.668420
2.763601541519	1.6321662787	trIA8DYJ0IA8DYJ0_DROME;trIQ8T389IQ	trIA8DYJ0	A8DYJ0	EndoB	1	1	1	3.3	3.3	3.3	41.336	0.0096308	6.6119	3602100	2	14.698759	15.374768	16.223869	15.014107	10.559094	11.896695	13.310896	14.490411
2.761202335357	4.9474948259	trIM9PID3IM9PID3_DROME;trIM9PG82IM	trIM9PID3	M9PID3	HIPP1	1	1	1	1.4	1.4	1.4	99.652	0.0052356	7.7303	13068000	7	15.704389	16.348295	15.709191	15.531563	13.354800	12.992495	12.86190	13.039433
2.758350133895	2.8163166597	trIP91638IP91638_DROME;trIQ7KU82IQ	trIP91638I	P91638	smid	6	6	6	8.5	8.5	8.5	104.28	0	38.646	78852000	16	18.057537	18.904981	18.550033	17.697782	16.545190	15.814983	15.291422	14.525337
2.752583026885	2.0454568761	splQ9VBZ5IYTHDF_DROME	splQ9VBZ	Q9VBZ5	Ythdf	2	2	2	3.4	3.4	3.4	78.915	0	13.379	2394700	2	13.190075	16.021478	14.338432	13.848064	12.758922	10.941624	11.275717	11.411454
2.734569549560	1.8958406769	trIX2JA43IX2JA43_DROME;splQ9W590IL	trIX2JA43I	Q9W590	Ns3	1	1	1	2	2	2	70.245	0.010145	5.6068	8187000	1	14.847351	16.478090	15.351111	15.053034	11.545578	14.261286	11.530145	13.454298
2.725233078002	3.7437549261	trIE1JGK7IE1JGK7_DROME;splQ7KRI2IL	trIE1JGK7	Q7KRI2	lolal	8	8	8	49.6	49.6	49.6	14.489	0	162.69	36944000	35	22.715717	23.793027	23.711143	23.352455	20.403327	20.914443	21.167234	20.186405
2.713713884353	3.8779556743	splO18413IPRS8_DROME	splO18413	O18413	Rpt6	2	1	1	6.2	3.2	3.2	45.857	0.010014	5.4607	8706400	1	15.578284	16.696832	16.588113	15.928865	13.599448	13.813880	13.491727	13.032183
2.702497005462	3.3536706408	trIQ86PF3IQ86PF3_DROME;trIA0A0B4KI	trIQ86PF3	Q86PF3	cindr	11	11	11	21.7	21.7	21.7	67.101	0	95.82	22983000	37	20.076267	21.167968	20.784845	20.136461	18.351690	18.286720	17.533740	17.183403
2.699293375015	1.6177979922	splQ9VL18IEF1D_DROME	splQ9VL1(	Q9VL18	eEF1delta	1	1	1	9	9	9	28.934	0.010836	6.3519	3087500	1	14.854381	16.246833	12.923763	15.620449	11.531904	13.748507	12.175240	11.392601
2.689694881439	2.6678117472	trIE8NHB1IE8NHB1_DROME;splQ24325I	trIE8NHB1	Q24325	Taf2	1	1	1	1.4	1.4	1.4	139.5	0	15.605	0	1	14.102590	14.948700	12.925512	13.373331	10.510453	11.741074	10.867948	11.471879
2.682710647583	3.9116881032	splP46863IKL61_DROME;trIQ7KVC2IQ7I	splP46863	P46863	Klp61F	4	4	4	4.7	4.7	4.7	121.16	0	28.375	83723000	12	17.901479	18.955207	18.386796	17.795633	15.951717	15.643658	15.497290	15.215608
2.675022602081	4.6609069222	trIA4V201IA4V201_DROME;trIE1JI11IE1J	trIA4V201I	P47825	Taf4	6	6	6	11.8	11.8	11.8	92.06	0	79.014	91051000	16	18.904188	19.660072	19.263710	18.761013	16.674522	16.485435	16.540945	16.187990
2.671746253967	3.2642058054	splO02649ICH60A_DROME;splQ9VMN5I	splO02649	O02649	Hsp60A	43	43	43	63.2	63.2	63.2	60.808	0	323.31	29075000	217	23.197795	24.582389	24.623493	23.930034	21.258623	21.695871	21.824153	20.868083
2.663576602935	2.4513452257	trIM9PBH8IM9PBH8_DROME;splQ8IRH5	trIM9PBH8	Q8IRH5	FBpp007260	1	1	1	2.1	2.1	2.1	80.904	0.005291	8.5004	5482300	1	14.331196	15.846371	15.360915	14.665557	12.645568	12.821195	11.025774	13.057195
2.661242961883	3.2368556002	trIQ9VUR2IQ9VUR2_DROME	trIQ9VUR2	Q9VUR2	Dmel\CG123	10	10	10	18.9	18.9	18.9	88.727	0	107.49	15954000	28	19.668424	20.682346	20.029582	19.447443	17.324567	16.511737	17.378650	17.967868
2.633003950119	2.2832086267	trIX2JE07IX2JE07_DROME;trIQ9W3R9IC	trIX2JE07I	X2JE07	Dmel\CG167	1	1	1	1.7	1.7	1.7	108.98	0.010401	5.7996	6196100	2	14.848671	15.486552	14.832939	14.511444	13.651275	11.853254	10.938461	12.704600
2.625190496444	2.2671410656	trIB5RIU6IB5RIU6_DROME;splQ8T390IS	trIB5RIU6I	Q8T390	EndoA	2	2	2	13.8	13.8	13.8	41.408	0	15.93	12849000	3	16.294136	18.648883	17.140609	16.186635	14.500281	14.840384	14.684529	13.744308
2.623155593872	2.7727508940	trIA0A0B4KGP6IA0A0B4KGP6_DROME;t	trIA0A0B4	A0A0B4K(	Fmr1	3	3	3	5.4	5.4	5.4	64.917	0	16.821	15370000	3	16.165966	17.318666	16.506525	16.282436	14.551948	14.649930	13.684748	12.894344
2.609766006469	2.7578314569	trIQ9VE85IQ9VE85_DROME	trIQ9VE85	Q9VE85	Nup43	3	3	3	11.5	11.5	11.5	40.148	0	31.132	17662000	7	17.104209	18.453382	16.587484	17.348451	14.481421	15.334517	15.144777	14.093748
2.603446960449	1.6862061279	splP12982IPP12_DROME	splP12982	P12982	Pp1-87B	1	1	1	4	4	4	34.542	0.0098731	5.346	1115800	0	12.426476	15.183982	16.089677	13.642671	11.575680	12.186641	11.867112	11.299586
2.545866489410	3.7847296604	trIM9NF33IM9NF33_DROME;splQ9VSH4	trIM9NF33	Q9VSH4	CFlm-68k	4	4	4	7.8	7.8	7.8	66.125	0	26.592	61573000	8	18.578468	19.764093	19.501117	18.911228	16.701442	16.697103	16.928680	16.244215
2.533439636230	3.8078728809	trIQ9VXR5IQ9VXR5_DROME	trIQ9VXR5	Q9VXR5	BEST:LD382	1	1	1	1.8	1.8	1.8	69.501	0.0098177	5.346	3433400	0	14.884408	14.770354	14.358994	13.871712	12.319361	11.493924	12.210275	11.728150
2.533068895339	1.9504333110	trIQ9VTH2IQ9VTH2_DROME;trIX2J8Y9IX	trIQ9VTH2	Q9VTH2	Dmel\CG426	2	2	2	3.2	3.2	3.2	133.05	0	12.645	8582900	2	13.305634	16.231746	14.505811	15.385289	12.471522	13.159761	11.846117	11.818805
2.529572486877	2.0172067833	trIQ9VJD1IQ9VJD1_DROME	trIQ9VJD1	Q9VJD1	GCS2beta	5	5	5	6.8	6.8	6.8	61.539	0	62.35	54486000	12	18.901361	19.168323	19.072896	19.186622	16.507360	17.731386	17.290325	14.681842
2.501086235046	3.5778229499	trIA0A0B4JD11IA0A0B4JD11_DROME;sp	trIA0A0B4	Q9NJH0	eEF1gamma	25	25	25	44.3	44.3	44.3	48.967	0	323.31	13127000	104	22.742403	23.786861	23.947887	23.392442	21.084270	21.201021	21.173408	20.406549
2.494210720062	2.0045264866	splQ7KNA0IDYM_DROME	splQ7KNA	Q7KNA0	CG8230	1	1	1	1.7	1.7	1.7	79.124	0.010955	6.4311	0	1	14.690466	14.959958	13.674166	13.516905	11.452693	12.545244	12.643324	10.223394
2.481398820877	3.2041154296	trIB7Z0V1IB7Z0V1_DROME;splQ9VHY5I	trIB7Z0V1	Q9VHY5	Taf7	3	3	3	7.6	7.6	7.6	51.376	0	18.685	24817000	10	17.085451	18.269062	17.746553	17.066972	15.089822	15.432117	15.369495	14.351008
2.479095220565	2.5559291253	splQ9VXE6INU153_DROME;trIA8JV18IA	splQ9VXE	Q9VXE6	Nup153	5	5	5	3.7	3.7	3.7	196.58	0	77.996	50940000	10	17.038747	18.186695	16.918350	16.332859	15.279102	14.959141	14.566826	13.755200
2.478653669357	3.1741772959	trIA1Z8M2IA1Z8M2_DROME;trIA0A0B4K	trIA1Z8M2	A1Z8M2	tou	4	4	4	1.9	1.9	1.9	322.21	0	25.502	31990000	8	15.917139	16.912631	16.191541	15.395165	13.968397	13.527843	13.040289	13.965332
2.471868515014	3.8234645827	trIA0A0B4KGE6IA0A0B4KGE6_DROME;s	trIA0A0B4	P26270	Rpn8	12	12	12	46.2	46.2	46.2	38.089	0	164.23	14872000	31	20.244466	21.108911	21.408002	21.031873	18.131395	18.850137	18.581817	18.342430
2.455039024353	1.5680490453	splP13709IFSH_DROME;trIM9PJC7IM9P	splP13709	P13709	fs(1)h	1	1	1	1.6	1.6	1.6	205.34	0.0098592	5.346	2324200	0	13.047904	13.245343	13.755911	15.533603	12.367772	12.627305	10.063822	10.703707
2.401970386505	2.9703026309	trIQ9VJZ5IQ9VJZ5_DROME	trIQ9VJZ5	Q9VJZ5	Tap42	2	2	2	2.6	2.6	2.6	43.319	0	12.208	25585000	7	17.593391	18.784685	18.274715	17.785963	16.433406	15.825778	15.639934	14.931753
2.394500255584	2.9985943042	trIL0MLQ9IL0MLQ9_DROME;trIQ8IH18IC	trIL0MLQ9	L0MLQ9	4E-T	12	12	12	20.2	20.2	20.2	110.58	0	89.826	12803000	23	18.629199	19.848335	18.994878	18.669065	17.447664	16.402112	16.590469	16.123231
2.382647037506	3.4655948250	splP52172ISRP_DROME;trIA0A0B4K6J1	splP52172	P52172	srp	8	8	8	9.5	9.5	9.5	134.16	0	104.8	32669000	44	21.520805	22.560972	21.961410	21.463136	19.956171	19.724773	19.199930	19.094861
2.377527475357	5.0272031180	splQ9XYP8IGCP3_DROME	splQ9XYP	Q9XYP8	Grip91	1	1	1	1.5	1.5	1.5	103.71	0.0053476	8.9849	9754300	4	15.312280	15.950692	15.785580	15.461479	13.275599	12.978241	13.382083	13.363997
2.360375404357	3.4726876952	trIQ8SX89IQ8SX89_DROME	trIQ8SX89	Q8SX89	kuk	16	16	16	29.3	29.3	29.3	60.159	0	196.24	53728000	74	21.622209	22.613332	22.218687	21.725963	20.122751	20.031738	19.293853	19.290348
2.356244087219	3.2396927867	trIQ9V455IQ9V455_DROME	trIQ9V455	Q9V455	Kap-alpha3	5	5	5	12.1	12.1	12.1	56.989	0	89.392	67103000	13	18.782703	20.051124	19.879077	18.882619	17.217220	17.138412	17.176990	16.637926
2.353933334350	4.5252046678	trIM9PIA6IM9PIA6_DROME;trIE1JI46IE1	trIM9PIA6	O97159	Mi-2	7	7	7	4.9	4.9	4.9	223.13	0	46.972	40026000	10	16.194314	16.812276	16.735027	16.164808	14.100252	14.467287	13.966415	13.956739
2.352618217468	3.1199785649	trIM9PFM9IM9PFM9_DROME;trIO61362I	trIM9PFM9	M9PFM9	crol	1	1	1	2.8	2.8	2.8	75.059	0	18.114	54324000	6	18.721406	19.872344	18.979442	18.124898	16.817783	16.489534	16.385862	16.594440
2.350370645523	1.7831967243	trIQ9V3Y5IQ9V3Y5_DROME	trIQ9V3Y5	Q9V3Y5	BcDNA:LD23	1	1	1	2	2	2	112.7	0.009887	5.3592	4897400	1	15.134346	15.457925	15.120804	12.968458	11.319327	12.549654	13.343105	12.067964
2.336878299713	4.3584711036	trIM9PB68IM9PB68_DROME;splQ9VLT5I	trIM9PB68	Q9VLT5	poe	1	1	1	0.3	0.3	0.3	590.7	0.0082508	6.771	8134400	1	12.432098	12.987442	12.851553	12.808963	10.404929	10.950993	10.322153	10.054469
2.328176498413	1.2672968510	trIQ9VWG1IQ9VWG1_DROME;trIQ8IQW	trIQ9VWG1	Q9VWG1	Dmel\CG142	7	7	7	48.1	48.1	48.1	20.841	0	49.404	79629000	14	18.050273	21.649436	22.048997	20.937112	18.577066	17.651933	19.263526	17.880588
2.305707693099	1.0880768308	trIQ9VGA4IQ9VGA4_DROME	trIQ9VGA4	Q9VGA4	MBD-R2	1	1	1	0.9	0.9	0.9	130.15	0.010249	5.7088	2007400	1	13.814282	10.057991	13.890454	14.607341	9.9329824	11.767977	11.076682	10.369597
2.299894332885	2.1974523396	splP49847ITAF6_DROME;trIM9PG32IM9	splP49847	P49847	Taf6	10	10	10	24.4	24.4	24.4	65.653	0	132.53	90532000	17	18.417819	19.805067	18.852487	18.543516	17.756425	16.737802	16.422657	15.502428
2.295595407485	2.8593906395	splQ7K0D8INUP50_DROME	splQ7K0D	Q7K0D8	Nup50	2	2	2	5.5	5.5	5.5	59.434	0	14.044	33703000	8	17.136610	18.381568	17.972419	17.302959	15.511783	15.804786	15.738698	14.555907
2.288678646087	1.6953065238	splQ9VZE6IBRX1_DROME	splQ9VZE	Q9VZE6	CG11583	1	1	1	4.7	4.7	4.7	41.618	0.01	5.4508	0	1	13.583374	13.673192	13.031205	13.048423	10.333294	12.857631	11.402001	9.5885524
2.281475305557	2.2914154571	trIA0A0B4K8B2IA0A0B4K8B2_DROME;tr	trIA0A0B4	O44081	Nop60B	2	2	2	11	11	11	25.787	0	12.547	9514500	2	16.544677	16.194622	17.654033	16.770174	13.825455	15.180764	15.322949	13.708436
2.268779277801	1.4303298248	splP14199IREF2P_DROME	splP14199	P14199	ref(2)P	4	4	4	12.5	12.5	12.5	65.302	0	24.005	23148000	4	17.417901	18.797693	18.339431	15.218601	15.213673	15.545567	15.628018	14.311251
2.263165473937	4.0183354095	trIQ961C3IQ961C3_DROME;trIQ9VH75IC	trIQ961C3	Q961C3	Dmel\CG847	10	10	10	20.5	20.5	20.5	62.427	0	75.283	15474000	28	19.694129	20.607475	20.223289	19.808856	17.908298	18.158422	17.605089	17.609279
2.261735439300	2.2431209669	trIQ9NCC3IQ9NCC3_DROME	trIQ9NCC3	Q9NCC3	SH3PX1	2	2	2	4.2	4.2	4.2	63.166	0.0055453	11.192	10901000	2	15.794466	16.773654	16.440349	16.078025	14.538613	13.936178	14.912187	12.652576
2.252473831176	2.8268237699	splQ9V9A7IMCCB_DROME	splQ9V9A	Q9V9A7	l(2)04524	7	7	7	20.8	20.8	20.8	62.648	0	69.907	13385000	20	19.080905	20.227291	20.414106	19.576089	17.734563	18.161132	17.527721	16.865079
2.249722003936	2.4733671015	trIQ9VWQ3IQ9VWQ3_DROME;trIQ9VWC	trIQ9VWQ	Q9VWQ3	Dmel\CG696	13	13	13	31.9	31.9	31.9	53.015	0	113.07	20696000	39	20.097513	21.533977	20.872295	20.032680	19.019140	18.858720	17.865926	17.793794
2.234269142150	2.6755477701	trIA0A0B4KGG9IA0A0B4KGG9_DROME;	trIA0A0B4	A0A0B4K(	CtBP	12	12	1	26.6	26.6	2.3	41.877	0	89.837	26671000	28	20.625780	21.980989	21.652109	20.911958	19.165603	19.427917	19.453544	18.186695
2.231971025466	2.2551464330	trIA0A0B4KHE9IA0A0B4KHE9_DROME;s	trIA0A0B4	Q9V3P6	Rpn2	3	3	3	5.1	5.1	5.1	113.2	0	31.557	57439000	5	16.941345	18.270523	17.646951	17.919107	15.035529	15.675046	16.607416	14.532051
2.228800296783	2.4115257262	splQ7YZA2IY7065_DROME	splQ7YZA	Q7YZA2	CG7065	3	3	3	3.8	3.8	3.8	136.77	0	18.623	17163000	4	14.940864	16.527507	16.162607	15.333714	14.264076	13.396604	13.690216	12.698596
2.188009738922	4.3032000820	trIQ8MZI3IQ8MZI3_DROME;trIQ7KU78IC	trIQ8MZI3	Q8MZI3	BcDNA:HL01	3	3	3	6.1	6.1	6.1	88.209	0	18.365	66517000	9	18.021717	18.883573	18.392677	18.073575	16.349454	16.145772	16.159732	15.964544
2.179436206817	4.1645869769	trIM9MQH9IM9MQH9_DROME;splP3617	trIM9MQH	P36179	Pp2A-29B	5	5	5	9	9	9	65.423	0	34.094	61285000	15	18.614681	19.003990	19.050910	18.556596	16.831331	16.821895	16.779180	16.076023
2.176415920257	3.3029218386	trIX2JEU3IX2JEU3_DROME;trIQ9VZ00IC	trIX2JEU3	X2JEU3	Dmel\CG173	18	18	18	25.8	25.8	25.8	100.09	0	190.72	21181000(	36	19.070331	20.317386	19.797725	19.045642	17.516530	17.530239	17.329481	17.149171
2.170649528503	3.3819837245	trIM9PE74IM9PE74_DROME;trIQ9W2U7I	trIM9PE74	M9PE74	nocte	17	17	17	11.5	11.5	11.5	235.04	0	125.57	17687000	35	18.381273	19.710163	19.025695	18.563501	16.797534	16.838485	16.871833	16.490177
2.164488792419	2.9496473776	trIE1JH57IE1JH57_DROME;splQ7K3L1IN	trIE1JH57(	Q7K3L1	mars	12	12	12	17.9	17.9	17.9	101.94	0	88.547	14525000	26	18.845705	19.685943	19.412330	18.629911	17.303495	17.592880	16.592704	16.426855

2.157957553863	2.9312555374	trIQ9VHI7IQ9VHI7_DROME	trIQ9VHI7	Q9VHI7	Dmel\CG119	3	3	3	12.9	12.9	12.9	40.319	0	23.525	13479000	6	16.929605	17.854284	18.158964	17.060232	15.660831	15.460935	15.562660	14.686828
2.131818771362	1.4310052962	spIP48592IRIR2_DROME	spIP48592	P48592	RnrS	1	1	1	2.5	2.5	2.5	45.114	0.009539	6.5033	0	2	13.183978	13.153052	15.017714	11.222967	11.023098	10.956769	11.508366	10.562201
2.119361162185	2.8836107458	trIA0A0B4KHR8IA0A0B4KHR8_DROME;s	trIA0A0B4	Q9VCA8	mask	11	11	11	4.5	4.5	4.5	423.07	0	141.78	14429000	34	17.371265	18.349056	18.060178	17.182723	15.979425	16.061834	14.975355	15.469164
2.118299484252	2.8484144502	trIQ9VW54IQ9VW54_DROME	trIQ9VW54	Q9VW54	Rpn1	2	2	2	3.6	3.6	3.6	102.28	0	14.458	18009000	7	15.359990	15.685707	16.924394	16.349435	14.058921	13.678930	14.344642	13.763834
2.108922243118	1.4955448982	trIM9NE89IM9NE89_DROME;spIP08928I	trIM9NE89	P08928	Lam	1	1	1	2.1	2.1	2.1	71.299	0.01037	5.7813	1941800	1	13.481925	15.452473	14.733757	13.210935	13.023871	13.082631	11.170987	11.165913
2.096563339233	3.0933190553	spIQ9V4C8IHCF_DROME	spIQ9V4C8	Q9V4C8	Hcf	7	7	7	6.7	6.7	6.7	160.18	0	50.677	11340000	8	18.153581	18.942749	18.123434	17.520065	16.455230	16.251501	15.975690	15.671154
2.090487480163	3.7025829095	spIQ27268IDX39B_DROME;trIM9PC90IM	spIQ27268	Q27268	Hel25E	6	6	6	25.7	25.7	25.7	48.651	0	110.9	11796000	12	20.022014	19.817283	20.420597	20.382793	18.592952	18.244373	17.646320	17.797092
2.082065343856	2.6579052218	trIM9PH75IM9PH75_DROME;trIX2JEC4I	trIM9PH75	M9PH75	BcDNA:GH23	4	4	4	1.8	1.8	1.8	357.39	0	23.632	38253000	6	14.919185	16.197542	15.636313	14.800040	13.637643	13.607095	13.383028	12.597051
2.081638813018	2.3999253391	spIO62621ICOPB2_DROME	spIO62621	O62621	betaCOP	1	1	1	1.1	1.1	1.1	102.71	0.010101	5.5563	7986600	1	14.576185	15.675046	15.553599	14.766425	12.957246	12.165543	13.953650	13.168264
2.081400632858	1.9360588176	trIM9NDM3IM9NDM3_DROME;trIM9PEJ8	trIM9NDM	M9NDM3	rhea	1	1	1	0.8	0.8	0.8	235.28	0.009929	5.4021	3418600	1	12.706906	13.522213	12.783960	14.034680	11.953941	10.850133	9.9490365	11.969046
2.071228027343	2.8948161967	spIQ9W1V3IFBRL_DROME	spIQ9W1V3	Q9W1V3	Fib	7	7	7	31.1	31.1	31.1	34.636	0	70.917	40104000	31	22.727481	21.952587	21.639667	21.443998	20.436647	20.050991	19.510883	19.480300
2.050820350646	2.6460791942	trIQ9VUE5IQ9VUE5_DROME;trIM9PI58IM	trIQ9VUE5	Q9VUE5	stwl	14	14	14	24.7	24.7	24.7	112.87	0	153.73	26214000	47	19.351324	20.692598	20.064737	19.419589	18.496191	17.927234	17.335250	17.566291
2.046130657196	1.5716862819	trIQ7KND8IQ7KND8_DROME	trIQ7KND8	Q7KND8	Mad1	1	1	1	1.2	1.2	1.2	85.017	0.010174	5.6628	4647500	1	14.232271	14.541035	14.630551	14.658601	12.888933	13.646446	12.888477	10.454080
2.015537738800	1.8888180626	trIQ9VNF7IQ9VNF7_DROME;trIQ9VNF6I	trIQ9VNF7	Q9VNF7	MTA1-like	6	6	6	9.4	9.4	9.4	92.773	0	38.001	47346000	12	17.293291	17.921085	18.087629	16.848304	16.576646	16.177108	14.719923	14.614480
2.009912252426	1.3534190833	trIQ9W061IQ9W061_DROME;trIA2VEF9I	trIQ9W061	Q9W061	mu2	2	2	2	3	3	3	138.3	0.0054845	10.948	19393000	3	15.903011	16.423034	16.270751	14.384243	12.582847	15.348209	14.171958	12.838376
2.008992195129	2.1945664782	trIQ7JQN4IQ7JQN4_DROME	trIQ7JQN4	Q7JQN4	Rs1	2	2	2	2.9	2.9	2.9	87.839	0	12.834	14030000	5	15.557403	16.734895	16.237266	15.815558	14.841613	14.286629	12.887296	14.293615
2.004975318908	2.6475087612	trIA0A0B4KFN0IA0A0B4KFN0_DROME;s	trIA0A0B4	P49905	Taf12	3	3	3	29.4	29.4	29.4	17.63	0	18.828	35716000	9	19.193521	20.601774	20.715150	19.805019	18.126613	18.366449	18.200889	17.601612
1.997773647308	3.6794605866	trIQ9W526IQ9W526_DROME	trIQ9W526	Q9W526	EG:67A9.2	1	1	1	3	3	3	62.323	0.010309	5.7472	5737800	1	15.298670	15.583993	15.914805	15.270586	13.423509	14.002375	13.614594	13.036482
1.993981122970	1.5017840178	trIM9PJN8IM9PJN8_DROME;spIP07487(	trIM9PJN8	P07487	Gapdh2	2	2	2	5.7	5.7	5.7	35.369	0.0055249	11.106	8642700	2	16.006633	16.598226	16.822645	16.101524	15.150422	14.990237	15.082149	12.330296
1.985302448272	2.1067791474	trIM9PIG8IM9PIG8_DROME;spIP55035IF	trIM9PIG8	P55035	Rpn10	9	9	9	28.5	28.5	28.5	42.618	0	133.95	80579000	25	19.311212	19.888442	21.076463	20.579666	18.726936	18.231164	18.652355	17.304119
1.983525276184	1.4727756795	trIQ8SXM8IQ8SXM8_DROME;trIQ9W327	trIQ8SXM8	Q8SXM8	LysRS	4	4	4	6.6	6.6	6.6	64.66	0	32.455	37130000	8	17.800065	18.577768	18.291540	16.253349	14.741203	16.763185	16.455551	15.028682
1.973823547363	2.2434340064	trIA0A0B4LFX4IA0A0B4LFX4_DROME;tr	trIA0A0B4	Q9V8R9	cora	2	2	2	2	2	2	173.91	0	13.905	10591000	2	14.593445	15.236125	14.828582	13.457124	13.294477	12.139903	12.657742	12.127865
1.972930431365	2.8968162785	spIQ24478ICP190_DROME	spIQ24478	Q24478	Cp190	10	10	10	14.9	14.9	14.9	121.68	0	77.372	12522000	20	18.154422	19.369819	18.976535	18.373180	17.067182	16.955717	16.814281	16.145055
1.968966007232	2.5627440499	trIM9PBZ9IM9PBZ9_DROME;spIP48598I	trIM9PBZ9	P48598	eIF4E1	7	7	7	30.9	30.9	30.9	29.223	0	84.275	22278000	24	21.261093	22.241443	22.265707	21.739376	19.300704	20.420700	20.514991	19.395359
1.965691089630	2.8611649090	spIQ9NBD7ICLASP_DROME	spIQ9NBD7	Q9NBD7	chb	5	5	5	5.5	5.5	5.5	165.57	0	65.531	14110000	27	18.079891	19.081893	18.485616	17.904481	16.836519	16.735424	15.810722	16.306453
1.948189258575	2.0526083604	trIQ9U9Q1IQ9U9Q1_DROME	trIQ9U9Q1	Q9U9Q1	RfC38	2	2	2	5.9	5.9	5.9	40.815	0	13.059	15905000	4	16.565965	17.927522	17.029718	16.837381	15.627533	15.606347	15.438564	13.895385
1.938957214355	3.8899628315	spIQ7K2G1IADRM1_DROME;trIA0A0B4L	spIQ7K2G1	Q7K2G1	Rpn13	5	5	5	19.5	19.5	19.5	42.012	0	62.628	54153000	11	19.064264	19.701679	19.365575	19.204595	17.430370	17.677003	17.584096	16.888814
1.936522960662	4.6338007343	trIQ9VUM1IQ9VUM1_DROME	trIQ9VUM1	Q9VUM1	Prp31	2	2	2	4	4	4	55.544	0.0018868	11.413	16495000	5	17.415098	17.533740	17.452899	17.127672	15.730947	15.639623	15.200745	15.212002
1.928265333175	3.3039542292	spIP35600IRFC1_DROME	spIP35600	P35600	Gnf1	3	3	3	4	4	4	108.61	0	16.052	35098000	1	16.586664	17.498178	17.099697	16.755382	15.565220	14.959775	14.600667	15.101196
1.920125484466	3.5028369064	trIC9QP42IC9QP42_DROME;spIQ02748I	trIC9QP42	Q02748	eIF4A	4	4	4	15.9	15.9	15.9	45.878	0	64.17	13099000	19	19.780414	20.369647	20.066841	20.101749	18.676588	19.390539	17.916776	17.654245
1.919672966003	2.9269479416	trIQ8IRX4IQ8IRX4_DROME;trID8FT05ID8	trIQ8IRX4	Q8IRX4	br	1	1	1	3.1	3.1	3.1	55.459	0	16.001	36409000	1	18.143951	19.203710	18.473936	17.643293	16.572492	16.523117	16.369102	16.321487
1.916090011596	3.0834392417	trIQ9VU35IQ9VU35_DROME	trIQ9VU35	Q9VU35	anon-WO011	1	1	1	13.6	13.6	13.6	11.016	0.0055147	11.101	11982000	1	17.525047	18.793031	18.736515	18.138610	16.374631	16.512462	16.506120	16.135629
1.915842533111	2.4053865513	trIQ9VQ76IQ9VQ76_DROME;trIM9PE28I	trIQ9VQ76	Q9VQ76	tho2	4	4	4	4.4	4.4	4.4	188.51	0	76.555	62128000	9	16.623710	18.070016	17.479274	16.743598	16.004373	15.373612	14.962308	14.912936
1.912287473678	3.8599849151	trIX2JAX3IX2JAX3_DROME;spIP52486IU	trIX2JAX3	P52486	Ubc4	1	1	1	6	6	6	22.51	0.0099715	5.4198	7779000	1	16.729461	16.679067	17.305456	16.575656	15.193179	15.109381	14.805088	14.532842
1.890087127685	2.0851060971	spIP23257ITBG1_DROME	spIP23257	P23257	gammaTub23	8	8	8	22.5	22.5	22.5	53.339	0	56.899	10048000	19	18.549243	20.206336	19.963386	19.412267	17.809516	17.912397	18.145095	16.703876
1.889673709869	3.2035416332	trIM9NE68IM9NE68_DROME;spIP02516I	trIM9NE68	P02516	Hsp23	8	8	8	75.8	75.8	75.8	20.629	0	90.256	31142000	37	21.559549	22.332735	22.472091	22.150876	19.938907	20.629697	20.568298	19.819654
1.877825736999	3.9791704204	spIP08841ITBB3_DROME;trIA0A0B4LGH	spIP08841	P08841	betaTub60D	21	8	8	44.5	25.6	25.6	50.849	0	96.075	33093000	39	21.470405	21.797447	21.723257	21.485076	20.094423	20.049661	19.398763	19.422035
1.877626419067	2.1516773708	trIQ9VPR5IQ9VPR5_DROME	trIQ9VPR5	Q9VPR5	Sf3b1	1	1	1	1.6	1.6	1.6	149.64	0.0097087	6.6455	10692000	1	14.310967	15.385154	15.607388	13.972082	13.596539	12.929184	12.420460	12.818902
1.875938415527	2.4452275416	trIQ86BS3IQ86BS3_DROME	trIQ86BS3	Q86BS3	Chro	9	9	9	16.1	16.1	16.1	101.05	0	74.209	11547000	14	18.369009	19.961692	19.414602	18.311100	17.155410	17.126260	17.174263	17.096715
1.857012033462	3.2597174822	trIM9PH10IM9PH10_DROME;spIP46461I	trIM9PH10	P46461	comt	3	3	3	5.8	5.8	5.8	82.555	0	22.451	17322000	6	16.134225	15.981366	16.056213	15.949530	14.959186	13.850968	14.142825	13.740307
1.845738887786	2.4949299450	trIM9NCM6IM9NCM6_DROME;trIM9PDR	trIM9NCM	Q8SX83	spen	87	1	1	24.2	0.4	0.4	593.52	0.0050847	7.192	14297000	4	13.875749	14.633563	14.006325	13.759888	12.393570	12.077316	11.399902	13.021781
1.841884851455	2.6963399739	spIP15348ITOP2_DROME	spIP15348	P15348	Top2	7	7	7	6.6	6.6	6.6	164.39	0	91.783	11173000	18	17.197965	18.679342	18.329393	17.749305	16.544813	16.112071	15.921120	16.010461
1.825339078903	2.1489283477	trIA0A0B4K7Y7IA0A0B4K7Y7_DROME;s	trIA0A0B4	Q9VAW5	larp	5	5	5	4.2	4.2	4.2	178.14	0	30.511	37742000	10	16.620992	17.754077	16.381137	15.769062	14.808058	15.289658	14.367141	14.759056
1.819553852081	4.0098297859	spIP06605ITBA3_DROME;spIP06603ITB	spIP06605	P06605	alphaTub84	27	27	27	53.1	53.1	53.1	49.89	0	323.31	50481000	173	25.283056	25.668823	25.653816	25.251186	24.008384	23.834703	23.372520	23.363058
1.817770957946	2.2206757899	trIA0A0B4LH25IA0A0B4LH25_DROME;tr	trIA0A0B4	A0A0B4LH	CG4266	1	1	1	1.1	1.1	1.1	130.07	0.010671	6.0218	3703400	1	12.998455	14.796799	14.755200	14.043283	12.667178	12.114330	12.187382	12.353763
1.815828800201	2.2101742289	trIX2JAA8IX2JAA8_DROME;spIQ9W517I	trIX2JAA8	Q9W517	wapl	1	1	1	0.9	0.9	0.9	185.15	0.010355	5.7516	6546500	1	14.346721	15.343879	14.381340	13.745950	12.653046	12.258600	12.413654
1.814100980758	2.8385703154	spIQ7KKH3ISDA1_DROME	spIQ7KKH3	Q7KKH3	Mys45A	1	1	1	2.1	2.1	2.1	81.983	0	13.007	13577000	1	15.913052	17.043134	16.075563	16.018526	15.014194	14.323054	14.116912	14.339711
1.770941972732	3.0582962057	trIQ9W1N1IQ9W1N1_DROME;trIQ95RQ8	trIQ9W1N1	Q9W1N1	pita	2	2	2	3.7	3.7	3.7	71.633	0	13.988	18066000	6	16.634811	17.096097	16.837873	16.226732	15.006325	15.262572	15.168397	14.274451
1.769822597503	3.7314406556	trIR9PY26IR9PY26_DROME;trIQ9VWP5I	trIR9PY26	R9PY26	htk	2	2	2	1.7	1.7	1.7	192.57	0	16.454	21770000	4	15.468688	16.213008	16.169769	15.607677	14.316705	13.920818	14.229720	13.912609
1.758592605590	2.4880045614	trIO61380IO61380_DROME;trIA8DZ29IA8	trIO61380	O61380	eIF4G1	24	24	24	19.6	19.6	19.6	183.94	0	191.79	39983000	71	19.368476	20.396654	20.042600	19.350158	18.734497	18.162557	17.618844	17.607620
1.711244106292	2.8202187317	trIQ9W0S7IQ9W0S7_DROME	trIQ9W0S7	Q9W0S7	Tudor-SN	3	3	3	6	6	6	103.1	0	32.139	31941000	5	16.872314	17.046228	16.649480	16.226713	15.372184	15.277832	14.246963	15.052780
1.699691772460	2.6297165943	trIA0A0B4LF82IA0A0B4LF82_DROME;trI	trIA0A0B4	A0A0B4LF	Sin3A	6	6	6	3.5	3.5	3.5	220.36	0	38.398	82043000	13	17.167907	17.893207	17.871292	17.185920	16.552984	15.615715	15.287279	15.863581
1.693608760833	2.7267958076	trIQ8IPX7IQ8IPX7_DROME	trIQ8IPX7	Q8IPX7	Rrp40	4	4	4	18.1	18.1	18.1	25.026	0	24.94	48367000	5	18.794427	19.625833	19.383298	18.941316	16.984706	17.768753	18.072582	17.144399
1.649255752563	3.8309091524	spIQ24560ITBB1_DROME;trIA1ZBL0IA1Z	spIQ24560	Q24560	betaTub56D	40	40	27	74.7	74.7	59.5	50.147	0	323.31	77738000	303	25.927143	26.160945	26.379985	26.011714	24.820749	24.662969	24.321479	24.077571
1.635329723358	2.8075049087	trIQ8I0S9IQ8I0S9_DROME;trIQ9V9T5IQ9	trIQ8I0S9I	Q8I0S9	Mccc1	11	11	11	25.2	25.2	25.2	69.41	0	86.909	94733000	21	18.402578	19.224586	19.353780	19.046709	17.690298	17.149370	17.760589	16.886077
1.634600162506	3.9585752632	spIQ9VN25IEIF3A_DROME	spIQ9VN25	Q9VN25	eIF3a	3	3	3	4	4	4	133.88	0	20.201	28235000	4	16.501169	16.801202	16.862661	16.239206	15.265358	14.876996	14.732538	14.990945
1.624506473541	3.2755884938	trIQ9VN21IQ9VN21_DROME	trIQ9VN21	Q9VN21	lost	3	3	3	5.1	5.1	5.1	59.742	0	45.803	59513000	9	18.490051	18.850870	18.831951	18.172212	17.376194	16.994243	16.494808	16.981813
1.599863052368	3.1098691663	trIM9NG39IM9NG39_DROME;spIP41073	trIM9NG39	P41073	Pep	7	7	7	15.4	15.4	15.4	75.598	0	88.624	15545000	24	19.753490	20.495019	20.023235	19.778972	18.403577	18.782640	18.571189	17.893857
1.594147920608	3.2130492131	trIE2QCG7IE2QCG7_DROME;spIQ0E940	trIE2QCG7	Q0E940	eIF3b	2	2	2	3	3	3	80.44	0	11.967	13189000	3	15.865467	16.630125	16.175062	15.988662	14.626336	14.982726	14.553745	14.119914
1.574131011962	4.0711477350	trIQ9VBU9IQ9VBU9_DROME	trIQ9VBU9	Q9VBU9	RpS27	4	4	4	31	31	31	9.364	0	30.751	77137000	13	21.785484	21.816322	21.825706	21.671934	19.904628	20.639623	20.260978	19.997692

Supplementary Table S2

Difference	-LOG(P-value)	Protein IDs	Majority protein IDs	Uniprot	GN	Peptides	Razor + unique peptides	Unique peptides	Sequence coverage [%]	Unique + razor sequence coverage [%]	Unique sequence coverage [%]	Mol. weight [kDa]	Q-value	Score	Intensity	MS/MS Count	iBAQ dCoREST-L_r1	iBAQ dCoREST-L_r2	iBAQ dCoREST-L_r3	iBAQ dCoREST-L_r4	iBAQ mock_r1	iBAQ mock_r2	iBAQ mock_r3	iBAQ mock_r4
7.4381184	3.56244516	trIC7LAG1	trIC7LAG1	C7LAG1	CoRest	48	48	48	55.3	55.3	55.3	87.314	0	323.31	39818000	151	24.860033	24.552564	25.463230	23.820360	18.563837	16.749502	18.789596	14.840778
6.3387651	1.53967912	trIA0A0B4	trIA0A0B4	Q9W5N2	RpL38	3	3	3	32.9	32.9	32.9	8.1996	0	18.271	32648000	4	22.370340	22.090518	22.165395	19.144001	17.190364	12.011115	19.937040	11.276675
5.7645156	1.99698493	spIQ9VB1	spIQ9VB1	Q9VB14	RpS10a	3	2	2	10.4	10.4	10.4	18.23	0	11.577	29207000	2	19.930110	19.880393	19.800998	17.657249	14.931014	10.851109	16.984373	11.444193
5.3571152	2.00261755	trIQ9W4W	trIQ9W4W	Q9W4W7	EG:100G1	5	5	5	18.8	18.8	18.8	49.227	0	31.06	36502000	8	18.851968	18.384057	19.212524	18.129081	15.126462	11.191288	16.286125	10.545294
5.2770605	1.58648940	trIM9PB84	trIM9PB84	P31009	RpS2	4	4	4	22.5	22.5	22.5	28.899	0	28.79	14628000	12	21.417047	20.738676	21.221521	19.788307	15.924371	11.832995	20.148054	14.151888
5.1406891	2.01322631	trIM9NEQ	trIM9NEQ	Q9VWG3	RpS10b	10	10	9	63.8	63.8	63.8	17.878	0	190.45	18410000	27	22.480499	22.026243	22.378168	20.309413	15.228443	14.849356	20.413177	16.140590
5.0595247	2.29497073	trIM9PFR5	trIM9PFR5	Q9VW	Su(var)3-3	6	6	6	8.5	8.5	8.5	95.946	0	46.151	62953000	7	18.572669	18.541587	19.233787	14.952058	13.436711	11.600957	14.305022	11.719313
4.7373363	1.91506908	trIQ9VR42	trIQ9VR42	Q9VR42	DmelCG3	1	1	1	2.3	2.3	2.3	69.277	0.0016639	6.8667	30350000	2	18.426977	18.018787	18.279029	16.698459	12.085806	11.967126	16.930183	11.490791
4.6381170	2.12595944	spIP04359	spIP04359	P04359	RpL32	8	8	8	44	44	44	16.02	0	104.91	18154000	31	22.945924	22.569410	23.170415	21.900764	18.558053	16.687976	20.965221	15.822794
4.6184513	1.32582177	trIE1JJM9	trIE1JJM9	P48149	RpS15Aa	5	5	5	57.7	57.7	57.7	14.771	0	42.894	63134000	13	21.444654	20.092617	20.625869	18.803033	16.377904	15.339675	19.680906	11.093882
4.3827052	2.33827626	trIM9PEA6	trIM9PEA6	O76927	RpS21	12	12	12	86.7	86.7	86.7	9.1672	0	323.31	33659000	33	24.210519	24.231691	24.917297	22.879758	17.727933	18.674039	21.694129	20.612342
4.3427455	1.33904863	trIQ9VB52	trIQ9VB52	Q9VB52	l(3)mbt	16	16	16	13.7	13.7	13.7	162.96	0	204.63	24316000	28	19.283603	19.137987	19.637218	19.894628	17.593610	13.938385	18.220293	10.830166
4.3319993	1.84249301	trIA8Y560	trIA8Y560	O17445	RpL15	6	6	6	19.6	19.6	19.6	24.325	0	40.146	12397000	14	22.097545	21.659358	22.152393	20.292776	17.322368	16.080297	20.501934	14.969476
4.2625131	2.21506899	trIM9MRF7	trIM9MRF7	Q9VMU4	RpL37A	6	6	6	46.7	46.7	46.7	10.311	0	38.367	11779000	14	22.718248	22.652612	22.916231	22.246496	16.788768	18.441883	21.229757	17.023126
4.1400361	2.06898085	trID1Z3A1	trID1Z3A1	Q9VZS5	RpL28	12	12	12	61.1	61.1	61.1	16.029	0	323.31	58007000	32	24.010007	24.015121	24.539194	22.839517	19.565586	17.267829	22.237947	19.772333
4.1286342	2.00627726	trIQ9V9W2	trIQ9V9W2	Q9V9W2	RpL6	12	12	12	53.5	53.5	53.5	27.697	0	108.66	22310000	31	22.457761	21.988740	22.505233	21.083946	17.894628	15.641713	20.723756	17.261047
4.1043829	2.17464633	trIQ9VJ19	trIQ9VJ19	Q9VJ19	RpL30	8	8	8	66.7	66.7	66.7	12.234	0	85.342	11747000	25	22.699647	22.401115	22.808408	20.680631	17.046867	17.441841	20.673057	17.010505
4.0175285	3.18852268	spIP38979	spIP38979	P38979	sta	15	15	15	64.8	64.8	64.8	30.228	0	323.31	85000000	51	24.053329	23.885112	24.535461	23.055202	19.313982	19.409826	21.479610	19.255573
4.0140333	1.37546915	trIQ9VBN5	trIQ9VBN5	Q9VBN5	RpL27	9	9	9	55.6	55.6	55.6	15.903	0	64.095	25078000	32	23.440883	23.297260	23.755216	21.611171	18.444473	16.595708	23.314512	17.693704
3.9474582	2.59753559	spIP48588	spIP48588	P48588	RpS25	8	8	8	51.3	51.3	51.3	13.201	0	110.33	26935000	25	24.001098	23.886787	24.282701	23.052202	18.592332	18.966545	21.938045	19.936033
3.9238386	1.62885287	spIP80455	spIP80455	P80455	RpS12	8	8	8	51.1	51.1	51.1	15.168	0	116.13	21865000	29	23.364795	22.435628	23.311744	20.116800	16.531152	17.217977	21.310192	18.474292
3.8031029	2.49512008	trIX2JDU0	trIX2JDU0	P50882	RpL9	15	15	15	65.3	65.3	65.3	21.392	0	98.259	29921000	37	23.150892	22.698947	23.289684	21.811195	18.297864	18.213901	21.121614	18.104927
3.6913208	2.07461802	trIX2J5G6	trIX2J5G6	P32100	RpL7	21	21	21	50.4	50.4	50.4	29.552	0	323.31	41721000	62	22.883827	22.732727	23.309108	21.588888	18.755514	17.783472	21.493555	17.716726
3.5933165	1.91020285	spIQ24154	spIQ24154	Q24154	RpL29	4	4	4	26.3	26.3	26.3	8.9202	0	322.01	18163000	11	24.383899	24.300895	24.850812	22.661708	19.287080	19.351947	23.090728	20.094293
3.4912643	1.82079906	trIQ9VHE5	trIQ9VHE5	Q9VHE5	RpL34b	9	9	9	33.9	33.9	33.9	18.431	0	74.712	43652000	38	25.081071	24.739953	25.285209	24.144292	21.328659	19.339693	24.080909	20.536209
3.4457364	2.36308795	spIQ9VNE	spIQ9VNE	Q9VNE9	RpL13A	9	9	9	36.6	36.6	36.6	23.647	0	106.94	21908000	26	22.166254	21.814601	22.528646	21.530124	18.178743	17.244419	20.699815	18.133703
3.4216284	2.45985769	spIP55841	spIP55841	P55841	RpL14	15	15	15	59	59	59	19.173	0	323.31	46708000	42	23.490203	23.212583	23.785264	23.180786	19.645263	18.753458	22.076005	19.507596
3.3779473	2.27779818	trIM9PCC1	trIM9PCC1	O18640	Rack1	15	15	15	51.9	51.9	51.9	35.618	0	154.16	34063000	33	21.940162	22.039758	22.616544	19.709390	17.120601	18.273530	19.382560	18.017374
3.3707032	1.96480391	spIQ94517	spIQ94517	Q94517	Rpd3	20	20	20	35.7	35.7	35.7	58.33	0	244.87	64486000	84	23.033386	22.173835	22.748291	22.246206	20.144449	18.208244	21.172187	17.194025
3.3578033	2.81636253	trIQ9VNB9	trIQ9VNB9	Q9VNB9	RpL35A	11	11	11	51.6	51.6	51.6	17.655	0	121.58	38473000	44	23.109008	22.633804	23.522409	23.321960	19.487129	18.514335	21.315784	19.838720
3.3460278	1.72419574	trIX2JCS6	trIX2JCS6	P46223	RpL7A	15	15	15	45.8	45.8	45.8	30.731	0	117.06	46982000	35	23.451740	23.099569	23.691150	22.306024	19.738231	17.783727	22.547784	19.094629
3.3258194	2.40484189	trIE2QD65	trIE2QD65	P39018	RpS19a	19	19	19	75.6	75.6	75.6	17.291	0	323.31	85495000	73	24.240234	23.625333	24.275047	23.164014	20.237596	19.513950	22.497554	19.752250
3.2405028	2.69068731	trIQ9VDH8	trIQ9VDH8	Q9VDH8	RpS30	3	3	3	9.1	9.1	9.1	14.585	0	58.801	27200000	19	23.971496	23.115943	24.115055	23.941184	20.065790	20.035905	22.282405	19.797567
3.1435422	2.06333737	trIM9PHM1	trIM9PHM1	Q9VS34	RpL18	13	13	13	46.8	46.8	46.8	21.664	0	96.117	35704000	44	23.496435	23.067020	23.648448	22.107635	19.492576	18.643186	22.080989	19.528617
3.1364574	2.17445821	spIP41093	spIP41093	P41093	RpL18A	13	13	13	61	61	61	21.029	0	180.29	69679000	56	24.006416	23.671417	24.296981	23.091665	20.042064	19.268377	22.671913	20.538295
3.1044521	2.51767175	trIQ9V9M7	trIQ9V9M7	Q9V9M7	RpL21	13	13	13	67.9	67.9	67.9	18.476	0	115.98	50224000	37	24.219558	23.551334	24.406457	23.053661	20.242723	20.319042	22.383609	19.867828
3.0573987	2.24005472	spIQ9V3G1	spIQ9V3G1	Q9V3G1	RpL8	16	16	16	52	52	52	27.892	0	163.67	51464000	58	23.204278	22.899051	23.622879	23.154357	19.700866	18.790042	22.161956	19.998106
3.0462942	1.65489582	trIQ9VLT7	trIQ9VLT7	Q9VLT7	RpL36A	4	4	4	23.1	23.1	23.1	12.501	0	25.202	64626000	9	22.656698	21.851900	22.339899	20.957590	18.645862	17.063920	21.465280	18.445846
3.0122733	1.64580995	trIX2JC35	trIX2JC35	P49630	RpL36	6	6	6	45.2	45.2	45.2	13.502	0	55.059	16761000	21	23.538484	23.412221	23.827646	22.589895	19.932722	19.183862	23.128993	19.073575
2.9832210	1.84227932	spIP41094	spIP41094	P41094	RpS18	10	10	10	52.6	52.6	52.6	17.611	0	81.816	24585000	27	22.688869	21.838113	22.814817	22.162416	18.815685	17.661916	21.683631	19.410095
2.9828572	1.89033232	trIQ9W1B9	trIQ9W1B9	Q9W1B9	RpL12	5	5	5	30.3	30.3	30.3	17.673	0	37.194	19437000	25	22.186798	22.043100	22.387113	21.552951	18.729892	17.912281	21.506299	18.090061
2.9404351	2.52531918	trIX2JC82	trIX2JC82	P02518	Hsp27	5	5	5	28.6	28.6	28.6	23.616	0	37.404	65899000	12	20.611442	19.786281	19.623764	18.986320	16.090608	17.111156	18.129333	15.914969
2.9377923	2.42185873	spIQ9VTP4	spIQ9VTP4	Q9VTP4	RpL10Ab	10	10	10	41.5	41.5	41.5	24.273	0	130.58	18360000	20	21.914699	21.811273	22.344701	21.355093	18.605125	18.161180	20.720003	18.188289
2.8787989	4.25728650	trIX2JEM4	trIX2JEM4	Q9W334	RpS28b	6	6	6	84.6	84.6	84.6	7.4766	0	64.378	57576000	26	25.491212	25.004659	25.370958	25.384691	21.940341	22.556465	23.127420	22.112098
2.7117791	1.84239696	trIM9NE68	trIM9NE68	P02516	Hsp23	8	8	8	63.4	63.4	63.4	20.629	0	59.397	17228000	21	22.154188	20.798673	21.573345	20.406965	17.372541	18.113142	20.538768	18.061603
2.6749277	2.23916757	spIP09180	spIP09180	P09180	RpL4	33	33	33	65.8	65.8	65.8	45.025	0	323.31	84496000	101	23.020626	22.851308	23.337287	22.302513	19.906244	19.477161	21.978374	19.450244
2.6012005	1.88821035	spIO16797	spIO16797	O16797	RpL3	20	20	20	42.8	42.8	42.8	46.915	0	158.29	48265000	41	22.354475	21.875976	22.744396	21.251070	18.743303	18.668891	21.462139	18.946781

Supplementary Table S3

Difference	-LOG(P-value)	Protein IDs	Majority protein IDs	Uniprot	GN	Peptides	Razor + unique peptides	Unique peptides	Sequence coverage [%]	Unique + razor sequence coverage [%]	Unique sequence coverage [%]	Mol. weight [kDa]	Q-value	Score	Intensity	MS/MS Count	iBAQ dCoRES T-M_r1	iBAQ dCoRES T-M_r2	iBAQ dCoRES T-M_r3	iBAQ dCoRES T-M_r4	iBAQ mock_r1	iBAQ mock_r2	iBAQ mock_r3	iBAQ mock_r4
7.9690585	3.1476717	splQ59E3(	splQ59E3(	Q59E36	CoRest	47	47	47	65.4	65.4	65.4	62.695	0	323.31	65907000	165	26.056062	26.488059	24.988151	25.699594	19.681367	17.731121	19.496385	14.446760
6.5887227	1.9910980	trlQ9W4W	trlQ9W4W	Q9W4W7	EG:100G1	7	7	7	20.9	20.9	20.9	49.227	0	53.265	11029000(	18	19.208005	20.672021	20.050458	20.873950	15.299279	9.5954017	17.504711	12.050154
6.1213052	1.9399749	splQ9VB1	splQ9VB1	Q9VB14	RpS10a	3	2	2	10.4	10.4	10.4	18.23	0	12.423	23620000	3	19.434185	19.271299	19.110391	19.085685	14.931014	10.472905	16.984373	10.028048
5.8458931	2.1257367	splP02515	splP02515	P02515	Hsp22	5	5	5	36.2	36.2	36.2	19.763	0	29.857	78276000	10	20.149047	19.696933	21.285230	21.095067	17.966178	15.659939	14.046899	11.169689
5.8163092	1.8352298	trlQ9VR42	trlQ9VR42	Q9VR42	Dmel\CG3	1	1	1	2.3	2.3	2.3	69.277	0.005772	5.5766	37691000	2	18.777929	18.364997	18.358488	17.621065	11.018045	8.9590969	16.930183	12.949917
5.5395777	2.3160678	trlM9NEQ9	trlM9NEQ9	Q9VWG3	RpS10b	9	9	8	56.9	56.9	56.9	17.878	0	73.727	20768000	25	22.298744	22.475955	21.891263	22.069269	15.228443	14.849356	20.358531	16.140590
5.4588608	1.5171671	splQ9XZT	splQ9XZT	Q9XZT7	Taf10b	4	4	4	30.8	30.8	30.8	15.784	0	25.754	37767000	5	21.582471	21.684188	19.660873	20.379940	18.350093	13.508403	18.624780	10.988752
5.4464094	2.3831526	splP04359	splP04359	P04359	RpL32	11	11	11	70.9	70.9	70.9	16.02	0	119.52	31119000(	39	23.841150	24.002902	22.820457	23.265707	19.119817	16.687976	20.788354	15.548430
5.3123750	4.4137076	splP38979	splP38979	P38979	sta	17	17	17	60.4	60.4	60.4	30.228	0	150.91	17563000	65	25.349388	25.230630	24.877643	24.796398	19.345163	19.225786	21.178037	19.255573
5.1887016	1.6698311	trlQ9VB52	trlQ9VB52	Q9VB52	l(3)mbt	21	21	21	17.5	17.5	17.5	162.96	0	192.04	50094000	48	18.773750	21.362388	20.496580	21.040796	17.555248	13.938385	18.046920	11.378154
5.1053001	2.1175532	trlM9PB84	trlM9PB84	P31009	RpS2	9	9	9	31.8	31.8	31.8	28.899	0	89.899	26886000	28	21.954504	22.203323	21.379993	21.795824	16.434074	14.514159	20.396759	15.567451
5.0732688	2.1334251	trlA8Y560	trlA8Y560	O17445	RpL15	17	17	17	39.7	39.7	39.7	24.325	0	118.02	34286000	40	23.618068	23.833353	22.359174	22.617755	18.245487	16.657178	21.389057	15.843553
4.9212598	3.2103376	trlX2JC82	trlX2JC82	P02518	Hsp27	11	11	11	62.4	62.4	62.4	23.616	0	102.61	55519000	30	24.098926	23.355550	21.335435	22.134363	17.277667	17.943864	18.976173	17.041530
4.8843352	2.9841150	trlA0A0B4	trlA0A0B4	P29845	Hsc70-5	4	4	4	8.6	8.6	8.6	74.065	0	26.318	26818000	11	17.698392	17.608846	16.921607	17.065500	13.749031	12.056365	13.624182	10.327427
4.7148222	3.6923097	trlQ9VDH8	trlQ9VDH8	Q9VDH8	RpS30	4	4	4	12.9	12.9	12.9	14.585	0	82.806	67951000	24	25.421592	25.383373	25.024284	25.211708	20.065790	20.035905	22.282405	19.797567
4.6407394	2.8668020	trlM9NE68	trlM9NE68	P02516	Hsp23	12	12	12	63.4	63.4	63.4	20.629	0	127.4	59130000	40	23.923612	23.872392	22.491403	22.501327	17.372541	18.137161	20.654472	18.061603
4.6341967	3.5887694	trlQ9VNB9	trlQ9VNB9	Q9VNB9	RpL35A	18	18	18	67.5	67.5	67.5	17.655	0	193.73	10948000	72	25.013631	25.247316	24.196556	24.460702	19.743268	18.889200	21.540945	20.208005
4.5696258	3.1137010	splP55841	splP55841	P55841	RpL14	16	16	16	68.1	68.1	68.1	19.173	0	206.52	10024000	53	25.179647	24.950914	23.926691	24.180330	19.689888	18.812496	21.898958	19.557737
4.5291905	2.5173194	trlX2J5G6	trlX2J5G6	P32100	RpL7	25	25	25	67.9	67.9	67.9	29.552	0	323.31	67150000	77	23.939481	23.909122	22.829095	23.023149	18.634031	17.783472	21.516195	17.650392
4.4706711	3.7681831	trlM9PEA6	trlM9PEA6	O76927	RpS21	15	15	15	100	100	100	9.1672	0	288.75	49246000	42	24.881057	25.028757	24.762229	24.465942	19.149196	19.842945	21.595550	20.667610
4.4502329	2.5721054	trlQ9VJ19	trlQ9VJ19	Q9VJ19	RpL30	8	8	8	55	55	55	12.234	0	75.919	13255000	22	22.839536	22.908609	21.883565	22.306024	17.046867	17.441841	20.637590	17.010505
4.3832354	5.6102488	trlX2JEM4	trlX2JEM4	Q9W334	RpS28b	10	10	10	96.9	96.9	96.9	7.4766	0	261.62	18764000	38	27.354391	27.319328	26.947484	26.927053	22.316419	22.897130	23.326082	22.475683
4.3540034	2.4390480	trlQ9V9W3	trlQ9V9W3	Q9V9W3	RpL6	20	20	20	53.4	53.4	53.4	29.736	0	206.86	52734000	50	23.653707	23.907657	22.698545	22.990959	18.812654	17.255065	21.480596	18.286539
4.3530132	1.3700064	trlB7YZQ7	trlB7YZQ7	B7YZQ7	Nurf-38	3	3	3	21.4	21.4	21.4	32.646	0	41.53	18239000	4	18.281612	17.551723	17.443138	16.677692	11.277962	11.092563	18.090318	12.081268
4.2818336	2.7658026	trlM9MRF2	trlM9MRF2	Q9VMU4	RpL37A	7	7	7	65.2	65.2	65.2	10.311	0	47.131	25536000	26	23.773944	24.295299	23.022472	23.899843	18.525047	18.818220	21.712635	18.808322
4.2497868	3.6549067	splO16130	splO16130	O16130	RpL39	5	5	5	39.2	39.2	39.2	6.2985	0	36.198	34796000	19	26.573129	26.518047	25.802993	26.112392	21.568250	21.508960	23.522409	21.407794
4.1809554	1.3798108	trlQ9VWG	trlQ9VWG	Q9VWG1	Dmel\CG1	7	7	7	36.1	36.1	36.1	20.841	0	55.585	94432000	15	22.565301	22.102903	19.552061	19.610307	13.310564	18.410467	19.621082	15.764637
4.1601529	1.9932390	trlE1JJM9	trlE1JJM9	P48149	RpS15Aa	3	3	3	27.7	27.7	27.7	14.771	0	30.923	54851000	9	20.661708	20.411626	20.066841	20.248641	16.909118	14.075980	19.012662	14.750445
4.1566104	2.1592457	trlD1Z3A1	trlD1Z3A1	Q9VZS5	RpL28	20	20	20	66.7	66.7	66.7	16.029	0	230.45	79073000	55	24.489101	25.000711	23.421882	24.391000	20.667783	17.707117	22.428543	19.872810
4.1270356	2.9890711	trlX2JDU0	trlX2JDU0	P50882	RpL9	11	11	11	48.9	48.9	48.9	21.392	0	82.121	33537000	36	23.334699	23.253223	22.550371	22.875207	18.297864	18.213901	20.888666	18.104927
4.1228022	2.2828622	trlQ9VHE5	trlQ9VHE5	Q9VHE5	RpL34b	13	13	13	51.8	51.8	51.8	18.431	0	232.74	73493000	59	25.995307	26.176511	24.981504	25.447141	21.495410	19.731103	24.078304	20.804437
4.1023001	2.2096674	trlX2JC35	trlX2JC35	P49630	RpL36	6	6	6	53.9	53.9	53.9	13.502	0	50.026	32188000	28	24.790096	25.045768	23.763242	24.115371	19.932722	19.183862	23.115118	19.073575
4.0834226	3.0147901	splP48588	splP48588	P48588	RpS25	10	10	10	53	53	53	13.201	0	93.435	30952000	34	24.007272	24.136022	24.030694	24.165687	18.925642	19.206266	21.938045	19.936033
4.0370516	2.4268265	trlQ9W1B9	trlQ9W1B9	Q9W1B9	RpL12	6	6	6	27.3	27.3	27.3	17.673	0	101.73	34249000	26	23.365596	23.465007	22.404029	22.628896	18.564990	17.765712	21.396080	17.988540
4.0354247	2.9630474	trlE2QD65	trlE2QD65	P39018	RpS19a	24	24	24	91.7	91.7	91.7	17.291	0	323.31	13134000	111	24.742218	24.755929	24.247497	24.528682	20.305189	19.573575	22.512172	19.741691
4.0180296	2.5882414	splQ24154	splQ24154	Q24154	RpL29	6	6	6	36.8	36.8	36.8	8.9202	0	323.31	23093000	20	24.808723	24.887672	24.357498	24.421239	19.652511	19.672677	22.983531	20.094293
4.0101423	2.8286190	splQ9V3G	splQ9V3G	Q9V3G1	RpL8	20	20	20	60.2	60.2	60.2	27.892	0	172.04	99319000	62	24.537063	24.777912	23.663837	23.989971	19.697799	19.076658	22.196735	19.957021
3.9855768	1.2760206	splQ7KBL	splQ7KBL	Q7KBL8	ix	1	1	1	9	9	9	21.147	0	12.846	9807300	1	17.828111	18.307947	17.420618	17.067287	15.385660	11.015504	17.432575	10.847916
3.9771389	2.6782777	splQ9VNE	splQ9VNE	Q9VNE9	RpL13A	10	10	10	37.1	37.1	37.1	23.647	0	112.79	32710000	33	22.855155	23.209955	21.838806	22.564767	18.235378	17.400161	20.699815	18.224773
3.9414031	2.6731539	splQ9V53	splQ9V53	Q9V535	tsu	1	1	1	10.3	10.3	10.3	19.01	0.0056818	5.4341	2347900	1	16.323301	16.661495	15.080609	15.308018	10.763236	12.347524	13.577933	10.919121
3.9220829	1.9587586	trlX2JCS6	trlX2JCS6	P46223	RpL7A	19	19	19	60.5	60.5	60.5	30.731	0	226.72	69563000	57	24.106054	24.418861	23.081121	23.479881	19.824293	17.783727	22.694936	19.094629
3.8842282	3.1704361	trlQ9V9M7	trlQ9V9M7	Q9V9M7	RpL21	11	11	11	61.6	61.6	61.6	18.476	0	179.16	79358000	52	25.008768	24.895366	24.190238	24.272701	20.242723	20.336580	22.383029	19.867828
3.8393616	1.9778024	splP80455	splP80455	P80455	RpS12	6	6	6	49.6	49.6	49.6	15.168	0	45.623	12150000	18	21.841802	21.888702	21.651803	21.930955	16.531152	16.403295	20.899400	18.121969
3.8126707	2.8257747	splQ9VTP	splQ9VTP	Q9VTP4	RpL10Ab	10	10	10	43.8	43.8	43.8	24.273	0	291.9	32701000	26	23.185239	23.233974	22.059169	22.539266	18.605125	18.161180	20.812372	18.188289
3.7867412	2.4079541	trlQ9VLT7	trlQ9VLT7	Q9VLT7	RpL36A	5	5	5	32.7	32.7	32.7	12.501	0	53.836	14639000	23	23.660251	23.628896	22.814954	23.244583	18.999839	18.114414	21.869892	19.217575
3.7862987	1.8633958	trlX2JKU5	trlX2JKU5	Q24186	RpS5a	8	8	8	26.3	26.3	26.3	25.434	0	202.74	20520000	25	22.577131	22.426445	21.767936	22.013793	18.900918	17.467861	21.169437	16.101894
3.7673525	2.7834864	trlQ9VVU2	trlQ9VVU2	Q9VVU2	RpL26	13	13	13	62.4	62.4	62.4	17.281	0	125.73	11921000(	52	25.390737	25.401975	24.888740	25.042057	21.317937	20.247251	23.358503	20.730407

3.7070574	2.4332834	trIM9PHM	trIM9PHM	Q9VS34	RpL18	18	18	18	55.3	55.3	55.3	21.664	0	121.9	49537000	62	23.962257	24.246772	23.068941	23.312990	19.479175	18.597652	22.115657	19.570245
3.6793076	2.4817448	trIQ9VZJ3	trIQ9VZJ3	Q9VZJ3	Rcd5	5	5	5	8.3	8.3	8.3	63.537	0	32.536	14646000	9	20.478525	20.358209	21.035905	19.578559	16.867616	15.406071	18.641424	15.818857
3.6692976	1.6962792	splO97125	splO97125	O97125	Hsp68	3	2	2	5.5	3.8	3.8	69.743	0	11.023	12947000	3	17.168201	16.975221	15.109177	15.834841	11.060481	11.873028	15.748137	11.728604
3.6692638	2.3917531	trIM9PH59	trIM9PH59	Q9VXX8	RpL37a	11	11	11	54.8	54.8	54.8	10.643	0	75.163	56065000	35	25.191293	25.095348	24.287078	24.815874	20.885988	20.349489	23.477167	19.999895
3.6143002	2.3341741	trIA0A0B4	trIA0A0B4	P46222	RpL11	10	10	10	37.5	37.5	37.5	21.112	0	104.82	28196000	30	23.083719	22.924373	22.259025	22.478796	19.119588	17.497087	21.259830	18.412206
3.5909454	0.6822970	trIQ8IG95I	trIQ8IG95I	Q8IG95	Mes2	10	10	10	39	39	39	41.128	0	173.15	45354000	27	18.859510	23.368795	24.021999	20.512870	21.539573	18.599288	20.612882	11.647648
3.5858240	2.4820545	splP41093	splP41093	P41093	RpL18A	12	12	12	62.7	62.7	62.7	21.029	0	202.63	92539000	64	24.596221	24.667144	23.678741	24.023691	20.081478	19.312431	22.690298	20.538295
3.5609350	2.2525431	splP41094	splP41094	P41094	RpS18	12	12	12	58.6	58.6	58.6	17.611	0	144.82	37667000	35	23.706302	22.982940	23.120143	22.473728	19.022800	17.883096	21.723382	19.410095
3.5603990	0.9455069	trIX2JA05I	trIX2JA05I	Q9W5E1	Roc1a	1	1	1	15.7	15.7	15.7	12.538	0	7.6205	10011000	3	19.426527	19.080776	19.318666	18.929922	18.080047	10.851256	14.278672	19.304319
3.5543689	0.8479612	trIQ9VZ22	trIQ9VZ22	Q9VZ22	Lint-1	17	17	17	29.2	29.2	29.2	67.899	0	244.8	38022000	48	18.564022	22.574592	22.136522	20.624263	20.096097	17.634881	19.965080	11.985864
3.5437078	1.3743754	trIM9PG76	trIM9PG76	P19889	RpLP0	13	13	13	41.3	41.3	41.3	34.202	0	215.37	22264000	41	22.228202	22.133390	20.947208	21.266651	17.859085	16.299602	21.966136	16.275796
3.5376911	2.7297479	splP09180	splP09180	P09180	RpL4	42	42	42	69.8	69.8	69.8	45.025	0	323.31	14690000	145	24.108449	24.378085	23.014015	23.494848	19.697952	19.503351	21.993240	19.650094
3.5199871	1.3808910	trIQ7JZW2	trIQ7JZW2	Q7JZW2	RpS15	7	7	7	38.5	38.5	38.5	17.037	0	174.2	29721000	20	22.428030	23.530767	22.907527	22.576763	19.080568	17.278305	23.199085	17.805177
3.5196032	1.4017447	trIQ9VBN5	trIQ9VBN5	Q9VBN5	RpL27	10	10	10	60.7	60.7	60.7	15.903	0	111.35	22320000	33	23.231267	23.711353	22.222141	22.507413	19.219301	17.549093	23.131664	17.693704
3.4227499	2.4210428	splQ9VKC	splQ9VKC	Q9VKQ9	Dpy-30L1	2	2	2	26.9	26.9	26.9	13.794	0	13.299	37035000	5	20.843681	20.970916	20.401975	20.140958	16.553493	16.398042	19.332389	16.382606
3.3875231	2.2112875	splP55828	splP55828	P55828	RpS20	9	9	9	58.3	58.3	58.3	13.488	0	102.81	42753000	34	23.481607	23.437332	24.318655	24.088611	20.363458	19.703386	22.671243	19.038024
3.3815388	1.5281923	trIQ9W499	trIQ9W499	Q9W499	RpL35	8	8	8	38.2	38.2	38.2	14.449	0	58.143	15880000	22	23.576232	23.489101	22.724632	23.280366	19.656812	18.651058	23.258680	17.977626
3.3129909	1.0402779	trIQ9V455	trIQ9V455	Q9V455	Kap-alpha	2	2	2	7.2	7.2	7.2	56.989	0	24.468	17570000	9	17.319900	17.324831	17.183984	17.403245	15.774838	11.497958	17.738328	10.968873
3.2618422	2.5714183	splO16797	splO16797	O16797	RpL3	28	28	28	49	49	49	46.915	0	253.85	82031000	69	23.343944	23.419826	22.475856	22.650774	19.149940	18.904247	21.557867	19.230978
3.2231302	0.8178335	trIE1JGK7	trIE1JGK7	Q7KRI2	lolal	1	1	1	10.2	10.2	10.2	14.489	0.0044577	5.8855	10129000	2	18.520412	18.675212	16.880109	16.502986	17.202468	11.119742	18.136060	11.227929
3.1708245	3.3197052	trIM9PCC	trIM9PCC	O18640	Rack1	14	14	14	44.7	44.7	44.7	35.618	0	91.127	29122000	42	21.695745	21.942062	21.271446	21.503099	17.418889	18.431594	19.568668	18.309902
3.1598768	1.8699598	splQ94517	splQ94517	Q94517	Rpd3	16	16	16	26.7	26.7	26.7	58.33	0	218.52	58493000	70	21.757110	22.867179	22.778081	22.044467	20.210861	18.292663	21.058738	17.245069
3.0569870	1.0816925	trIQ7K180	trIQ7K180	Q7K180	Map60	8	8	8	24.8	24.8	24.8	47.589	0	69.287	44597000	13	19.534215	19.803333	16.247390	16.290216	14.531925	12.623495	17.890419	14.601364
3.0095725	1.7114928	trIC7LA75	trIC7LA75	P11147	Hsc70-4	34	34	30	43.3	43.3	40.4	71.131	0	323.31	19590000	130	24.228025	24.331422	22.322237	22.548397	19.902246	19.483236	22.677946	19.328363
2.9741806	1.7310918	trIQ9W0A8	trIQ9W0A8	Q9W0A8	RpL23A	20	20	20	50.9	50.9	50.9	29.463	0	263.85	11637000	72	24.522529	24.752002	23.896705	24.042766	21.253957	19.943206	23.914972	20.205144
2.9368672	1.6573632	trIC6SUW	trIC6SUW	P55935	RpS9	18	18	18	70.8	70.8	70.8	22.623	0	262.02	51224000	55	23.229009	23.157337	22.733657	22.860773	20.108274	18.858022	22.722402	18.544609
2.8706374	2.1539461	trIQ7K1Q7	trIQ7K1Q7	Q7K1Q7	RpLP0-like	6	6	6	28.1	28.1	28.1	29.441	0	38.744	97122000	12	21.407690	21.446474	20.654996	20.750173	18.160392	17.614753	20.095453	16.906185
2.7971079	1.4679524	splP15357	splP15357	P15357	RpS27A	3	3	2	27.6	27.6	16	17.94	0	36.11	55944000	11	20.833681	20.827180	20.404888	20.917797	15.927384	17.805618	20.757190	17.304922
2.7794477	1.3074627	trIQ95RU8	trIQ95RU8	Q95RU8	G9a	5	5	5	6.2	6.2	6.2	181.24	0	31.462	16518000	8	12.963167	15.952149	16.426576	15.139870	12.517201	11.368827	14.609962	10.867980
2.7636289	1.4076259	trIX2J950I	trIX2J950I	Q03334	RpS13	13	13	13	62.3	62.3	62.3	17.178	0	171.88	28131000	49	22.915592	22.929836	22.138961	22.467098	19.739368	18.720571	22.789152	18.147880
2.7545733	3.6712298	trIA0A0C4	trIA0A0C4	Q9VH69	RpS29	6	6	6	73.2	73.2	73.2	6.5906	0	82.487	29972000	35	24.519952	24.393621	24.319757	24.187673	20.737192	21.426240	22.312297	21.926980
2.7425961	1.1028844	trIQ9W229	trIQ9W229	Q9W229	RpS24	7	7	7	51.1	51.1	51.1	15.048	0	50.631	11493000	15	22.052583	22.130596	20.705226	21.271959	18.827770	16.810522	22.320337	17.231351
2.7334952	1.7198088	trIM9PBK9	trIM9PBK9	P08570	RpLP1	4	4	4	58.9	58.9	58.9	11.513	0	32.031	27784000	12	24.241472	24.095148	23.058525	23.160833	20.012226	19.800792	23.266994	20.541984
2.6616706	1.4629569	trIG3M3A2	trIG3M3A2	Q06559	RpS3	12	12	12	43.1	43.1	43.1	27.471	0	91.733	26521000	42	21.515039	21.623460	20.383531	21.241327	18.056478	17.295356	21.293561	17.471279
2.5884184	1.6132671	splQ9V597	splQ9V597	Q9V597	RpL31	12	12	12	69.4	69.4	69.4	14.532	0	85.143	28778000	29	23.074880	23.227981	22.523797	22.753238	20.211931	18.928737	22.732271	19.353284
2.5806982	0.8553419	splQ9V4C8	splQ9V4C8	Q9V4C8	Hcf	7	7	7	7.1	7.1	7.1	160.18	0	46.083	35121000	8	16.163295	17.241163	14.893301	15.158452	12.820195	11.863257	17.398075	11.051888
2.5744304	1.5225378	trIR9Q794	trIR9Q794	Q9W5R8	RpL5	17	17	17	44.1	44.1	44.1	34.036	0	176.55	66094000	67	23.911685	23.940105	22.588705	23.055564	20.667264	19.565008	23.234983	19.731086
2.5385422	1.6361976	trIQ8IMI7I	trIQ8IMI7I	Q9VA91	RpS7	12	12	12	60.8	60.8	60.8	22.17	0	84.53	32909000	33	22.541204	22.688976	22.044601	22.501399	19.948350	18.698629	22.227790	18.747241
2.4557931	1.3876177	splP25007	splP25007	P25007	Cyp1	3	3	3	15.4	15.4	15.4	24.666	0	16.912	17996000	4	17.838859	17.877176	18.149419	18.205144	13.414386	14.574179	16.860116	17.398744
2.4429969	1.2882300	trIX2JE06I	trIX2JE06I	Q9VJY6	RpL24	9	9	9	53.5	53.5	53.5	17.52	0	90.448	51441000	37	23.909854	23.968687	23.194152	23.488489	21.437356	19.307458	23.863912	20.180467
2.4117026	1.3163547	splP36241	splP36241	P36241	RpL19	18	18	18	50.7	50.7	50.7	23.998	0	200.82	60781000	53	23.853956	24.257242	23.148458	23.353935	20.985374	19.955888	23.981983	20.043535
2.3622241	2.5869606	trIM9PFF0	trIM9PFF0	P41126	RpL13	17	17	17	51.4	51.4	51.4	24.951	0	168.97	93117000	61	24.271987	24.469486	23.445564	23.816556	20.808134	21.393045	22.798318	21.555200
2.3217911	1.2832012	trIA0A0B4	trIA0A0B4	Q8MLY8	RpS8	19	19	19	68.3	68.3	68.3	23.759	0	320.32	90545000	89	24.207395	24.396694	23.644714	24.096837	22.055698	20.466426	24.328823	20.207529
2.2837276	1.3070769	splP48159	splP48159	P48159	RpL23	12	12	12	58.6	58.6	58.6	14.936	0	227.48	52839000	45	23.677669	23.497653	22.880523	23.137351	20.956314	19.487010	23.594572	20.020387
2.2785305	1.3793984	splP29843	splP29843	P29843	Hsc70-1	4	2	2	6.1	3.1	3.1	70.686	0	12.603	65468000	4	19.630622	19.469152	16.819780	16.803602	15.597004	15.438402	17.074623	15.499005
2.2471518	1.3256827	trIA0A0B4	trIA0A0B4	Q9W237	RpS16	13	13	13	63.5	63.5	63.5	16.774	0	138.36	26080000	29	22.140304	22.477537	21.542362	21.837574	19.908254	18.681335	22.173164	18.246416
2.2232007	1.1218844	splP50887	splP50887	P50887	RpL22	10	10	10	35.8	35.8	35.8	30.61	0	143.14	26437000	41	22.032815	22.150629	21.357725	21.569410	19.111436	17.986207	22.532075	18.588056
2.2216539	1.9178197	trIM9PG47	trIM9PG47	P13008	RpS26	6	6	6	49.1	49.1	49.1	13.266	0	61.827	13407000	20	23.151588	23.306608	22.525495	23.136068	20.074831	19.761953	22.449222	20.947137
2.2192320	1.1685915	splP55830	splP55830	P55830	RpS3A	22	22	22	63.1	63.1	63.1	30.34	0	158.89	57917000	67	22.709209	22.829313	22.162786	22.528789	20.408002	18.461278	23.049480	19.434408
2.1776404	1.2565226	trIA0A0B4	trIA0A0B4	Q8T3U2	RpS23	12	12	12	60.8	60.8	60.8	16.016	0	120.87	48262000	47	23.731796	24.023775	23.443288	23.721923	21.266078	19.987041	24.166835	20.790266
2.1501679	2.5005191	trIQ7JYK1	trIQ7JYK1	P18101	RpL40	2	1	1	25	10.9	10.9	14.729	0	9.0069	45296000	7	20.637590	20.998657	19.878074	20.414520	17.965784	18.854345	19.084465	17.423576
2.1085834	1.1523329	splP29327	splP29327	P29327	RpS6	14	14	14	51.2	51.2	51.2	28.407	0	171.85	11680000	82	24.437015	24.571031	23.781667	24.144605	22.163923	20.308969	24.717956	21.309137
2.1003923	1.2420517	splP17704	splP17704	P17704	RpS17	12	12	12	63.4	63.4	63.4	15.285	0	198.15	48798000	51	24.055814	23.888740	23.394275	23.573345	21.306413	20.281839	24.198429	20.723924
2.0489516	1.0508818	splQ0E9B	splQ0E9B	Q0E9B6	RpS11	15	15	15	64.5	64.5	64.5	18.105	0	227.78	46426000	41	23.098911	23.448593	22.367544	22.980136	20.527072	19.189424	23.751951	20.230930
1.9994750	1.6858150	trIQ8T0Q2	trIQ8T0Q2	Q8T0Q2	Dmel\CG9	1	1	1	5.4	5.4	5.4	34.156	0.004644	6.347	7264300	3	17.397741	17.416336	16.367448	16.386720	16.574001	14.523868	14.084324	14.388152

II. List of academic teachers

My academic teachers at the Philipps-University Marburg were:

Adamkiewicz, Adhikary, Aigner, Arenz, Bartsch, Bauer, Bauer, Baum, Böhm, Brandt, Brehm, Bremmer, Buchholz, Daut, Decher, Dietrich, Einhäuser-Treyer, Ellenrieder, Elsässer, Fritz, Garten, Greiner, Grosse, Großmann, Grzeschik, Hagemann, Hänze, Heverhagen, Heyd, Jacob, Käuser, Kinscherf, Klingmüller, Lauth, Lill, Lillig, Lohöfer, Lohoff, Maisner, Mandic, Meißner, Milani, Mühlenhoff, Müller, Müller-Brüsselbach, Ocker, Oliver, Pfestroff, Plant, Preisig-Müller, Puccetti, Reinartz, Schäfer, Schmeck, Schütz, Steinhoff, Stiewe, Subtil, Suske, Voigt, Westermann, Wrocklage

III. Acknowledgements

This thesis would not have been possible without the contribution and support of many dear people.

First and foremost I want to thank Prof. Dr. Alexander Brehm for providing the financial and thematic framework and the infrastructure that made this thesis possible. But, more importantly, I want to say thank you for his continuing support and mentorship, his trust, and his brilliant ways of teaching!

Thanks to Prof. Dr. Sven Bogdan for his report on this thesis.

I am grateful to everyone who, over the years, added to the very nice working environment at the Brehm lab, especially Dr. Stephan Awe, Dr. Karim Bouazoune, Dr. Kristina Kovač, Dr. Igor Mačinković, Dr. Ikram Ullah, Joanna Brühl, Ulla Kopiniak, Karin Theis, Bernhard Groß, and Elisabeth Schneider. Thank you for every advise, practical help and our productive discussions.

I am thankful to Dr. Robert Liefke, Prof. Dr. Olalla Vazquez, Dr. Lea Albert, Dr. Hartmann Raifer, Prof. Dr. Nancy Fossett, Dr. Tsuyoshi Tokusumi, Prof. Dr. Klaus Förstemann and his lab staff, Prof. Dr. Thorsten Stiewe, and Dr. Andrea Nist for their contribution to the U-shaped publication and the very pleasant and fruitful cooperation.

Likewise, I want to thank everyone involved in publishing our results on dCoREST complexes, especially Dr. Igor Mačinković.

I want to thank all members and organizers of the TRR81 research network “Chromatin changes in differentiation and malignancies” for providing an excellent scientific environment with productive discussions and input.

A special thanks goes to my dear friends and lab colleagues, who all shared and shouldered my everyday lab life: Igor, Kristina, Sara, Lisa, Sabrina, Clara. Thank you for your support!

I also want to thank all students I had the pleasure of supervising during my thesis work. Especially Julia, Sam, and Laura, who brought me forward in critically reflecting on experiments, results, and approaches.

Finally, I want to thank my friends and family for keeping me grounded and for caringly distracting me from and encouraging my work in equal measures. Especially I want to thank my parents, who always support and believe in me. Thank you!